

# **Phase Behavior and Structural Transitions in The Mixtures of Cationic Surfactants and Hydrophobic Counterions**

**Dissertation  
zur Erlangung des Doktorgrades  
der Fakultät Biologie, Chemie und Geowissenschaften der  
Universität Bayreuth**

**vorgelegt von  
Rami Abdel-Rahem  
aus Jordanien**

**Juli 2003**

Die experimentellen Arbeit zur Dissertation wurden in der Zeit von Dezember 2000 bis Juli 2003 am Lehrstuhl physikalische Chemie I der Universität Bayreuth unter der Leitung von Prof.Dr. H. Hoffmann durchgeführt.

Vollständiger Abdruck der vom Fachbereich Biologie, Chemie und Geowissenschaft der Universität Bayreuth genehmigten Dissertation zur Erlangung des akademischen Grades eines Doktors der Naturwissenschaften.

Promotionsgesuch eingereicht am: 13.12.2000  
Zulassung durch die Promotionskommission: 16.07.2003  
Wissenschaftliches Kolloquium: 06.10.2003

#### Prüfungsausschuß

Prof. Dr. A. Müller (Vorsitzender)  
Prof. Dr. H. Hoffmann (Erstgutachter)  
Priv. Doz. Dr. V. Abetz (Zweitgutachter)  
Prof. Dr. K.H. Seifert  
Prof. Dr. G. Platz

*Devoted to everyone who has been able to reach their targets, cope with the difficulties of life and at the same time to keep following the correct rules of life.*

## Acknowledgment

It seems that I need a lot of pages to express my appreciation and respect for everyone I remember now and for those who are not in my mind at the moment but always in my heart. I am thankful to everyone who has helped me during the three years I have spent in Germany.

*When I was in Jordan three years ago, I had a chance to meet the well known scientist **Prof. Dr. Heinz Hoffmann**. Before meeting him I had read a lot of his publications, and I had used his illustrations to explain the results of my master work. At that time it was hard for me to understand everything he had reported about rheology, microstructure and surfactant mixtures, etc... Nowadays and after spending three years in his group, these things became clearer to me. There are still many questions in surfactant science and their novel mixtures. These questions need answering, which requires further work and researches. Since I have already started this work, I will continue with it, depart what I have learnt to people in my home country and take the help from other groups over the whole world, as the science develops due to the efforts of the whole humanity and is not limited to certain people or countries. I was not the only one to work hard to become a scientist. Prof. Dr. Heinz Hoffmann (my supervisor) is the first person who should be acknowledged for that, as well as for his very rich publications, his lectures, his proposals and discussions. Outside the university, he was not my supervisor anymore. He was one of my relatives, he and his wife (**Ms. Claudia Hoffmann**) were taking care of me. They were my second family in Germany. The kindness of this family started from the first day when I came to Germany, where I found that everything was arranged for my life. I don't forget the conferences and the visits to Düsseldorf, Würzburg, Ludwigshafen (BASF) and Heidelberg. These journeys were also arranged for me by him. If one wants to be a good researcher, she/he has to be self-dependent. I have also learned this in Prof. Dr. H. Hoffmann's group. I have got many things to say, but I hope that I will prove this by doing and not only by saying.*

***Prof. Dr. Gerhard Platz** deserves acknowledgment. Thank you very much for your help in answering the questions I asked, for your lectures, for your humanity and your friendship.*

***PD. Dr. Michael Gradzielski**: a young scientist, who is kind enough to break all bridges between himself and each one in the group. Even he is special in his abilities, but never has he made the others to feel that. He has always assumed that all the people are clever and equal. Thank you PD. Dr. Micheal Gradizalskie for your well-organized lectures, SANS measurements and your support.*

***Dr. Thomas Dürschmidt** helped me a lot in rheology, reading my thesis and making very nice suggestions. I was always asking him, but he never said "No" to me. This reflects his humanity and cooperation. These are usually the characteristics of a true scientist. **Ms. Olga Dürschmidt** (I hope soon Dr.) is also acknowledged for her support. She is like one of my relatives.*

***Dr. Klaus Horbaschek** was the first person to explain to me how to use freeze fracture electron microscopy. He spent a lot of time explaining the things to me, and he was very tolerant. He is also acknowledged for his continuous support.*

***Klaus Redlich, Dr. Matthias Nanninga, and Dieter Grübner** were always cooperative and kind, and they never told me "No" for any kind of help I was asking.*

*Thinking and doing scientific work are not enough to make progress. One needs also suitable environment, which will be made by the people in the group. So, I don't find representative words to express my emotions to my friend, brother and a very close person to my heart, **Mr. Karl-Heinz Lauterbach** (Abu Martin). To his wife **Ms. Friedel Lauterbach** for kindness and the private invitations.*

***Ms. Roswitha Hammel** and **Ms. Christa Bächer** are acknowledged for their help in explaining some techniques to me, their help in the practical work and their attempts to explain the things to me in German, so that I could learn more.*

*If anyone is asked about the way **Ms. Christine Thunig** deals with others, I think everybody will answer in the same way. She is very expert, cooperative, helpful and kind. **Ms. Astrid Göpfert** and **Ms. Carmen Kunert** are very similar to her (MCII, PCII). They were very helpful in electron microscopy work.*

*I don't forget the help I got from **Ms. Ute Meyer**. Thank you for our discussions in the Arabic language (with the Egyptian dialect). For your support, for Arabian on the whole. You are especially interested in the Arabians and their politics. I know that you have some friends in Egypt, so you have now a friend in Jordan as well.*

*My thanks are also addressed to my group members. **Mr. Stefan Schmölzer**, **Ms. Annette Fischer**, **Mr. Markus Meyer**, **Mr. Reiner Beck**, **Ms. Elham Egbal**, **Dr. Jing Liu**, **Dr. Shuji Fujii**, and **Ing. Yuji Yamashita**, **Platz's group** (**Ms. Amelie Zapf** and **Mr. Christian Fehn**) and **Gradslskie's group** (**Mr. Markus Burkhardt**, **Mr. Md. Ekramun Nabi**, **Mr. Christian Wolf**, **Ms. Stefka Kinzel**) are all acknowledged for the nice and funny environment we had together.*

***Dr. Jürgen Meyer** is greatly acknowledged for his help, e-mails, and support.*

*I also don't forget the help I got from **Dr. Pal** and **Dr. N.V. Sastry**, their support.*

*Outside the university I will surely start with my brother and friend **Dr. Akram Atalla**. Not only for his support and encouragement, but also for being my second soul. I hope that the god will give you more and more. What I feel to you can't be described by words.*

***Dr. Bassam Bitar** is the first person who helped me and has kept helping until now. He showed me the way. I hope he will get reward for that.*

*To : **Ms. Rehab Nahil**, **Ms. Menchu Lacsamana**, **Ms. Ludmila Kolesnikova** and **Mr. Radostin Simatev***

*and also to my family (**Mr. Abdel Majeed**, **Ms. Khadra**, **Ms. Arabia**, **Mr. Raed**, **Ms. Abeer**, **Dr. Rabah**, **Ms. Ola**, **Ms. Orayb**, **Mr. Rafat**, **Ms. Andleeb**, **Mr. Mohammad**, **Alia**, **Joad**, **Aya**, and **Mahdee**- all with the family name **Al-Shiyap**) also to **Cognis Company** for the financial support (**Dr. Michael Müller** and others),*

*and finally I use the German saying*

***‘Ende gut, alles gut’***

## Abbreviation

Ns	Packing Parameter
SANS	Small Angle Neutron Scattering
$\sigma$	Shear stress
$\eta$	Viscosity
$G'$	Loss modulus
$G''$	Storage modulus
$G^0$	Normal modulus
.	
$\dot{\gamma}$	Shear rate
$\gamma$	Deformation
*	
$\eta$	Complex viscosity
N1	First normal stress difference
$\nu$	Frequency
DSC	Differential scanning calorimetry
Cryo-TEM	Cryogenic temperature transmission electron microscopy
FF-TEM	Freeze fracture transmission electron microscopy
DICM	Differential interface contrast microscopy
CTAB, (C <sub>16</sub> )CTAOH	Cetyltrimethylammonium bromide, hydroxide
TTAB, (C <sub>14</sub> )TTAOH	Tetradecyltrimethylammonium bromide, hydroxide
DOTAB, (C <sub>12</sub> )DOTAOH	Dodecyltrimethylammonium bromide, hydroxide
DTAB, (C <sub>10</sub> )DTAOH	Decyltrimethylammonium bromide, hydroxide
OTAB, (C <sub>8</sub> )OTAOH	Ocyltrimethylammonium bromide, hydroxide
2,1 HNC	2-hydroxy-1-naphthoic acid
3,2 HNC	3-hydroxy-2-naphthoic acid
6,2 HNC	6-hydroxy-2-naphthoic acid
CTAHCN(3,2HCN)	Cetyltrimethylammonium-3-hydroxy-2-naphthoat
mM	Molar $\times 10^{-3}$
$\kappa$	Conductivity
I	Intensity
q	Angle
T	Temperature
$\tau_m$	Relaxation time
dH/dt	Heat flow
L1	Micellar solution
L $\alpha$	Lamellar phase

# ***Contents***

<b><i>Description</i></b>	<b><i>Page</i></b>
<b><i>1.Introduction and The aims of This Work</i></b>	<b>1</b>
1.1 Introduction	1
1.2 Electrostatic Interactions	5
1.3 Hydrophobic Counterions & Catanionic Surfactants	10
1.4 Aims of The Present Work	13
<b><i>2.Experimental Theory , Methods and Chemicals</i></b>	<b>14</b>
2.1 Birefringence	14
2.2 Conductivity	15
2.3 Differential Interference Contrast Microscopy	16
2.4 Freeze Fracture Electron Microscopy	17
2.5 Small Angle Neutron Scattering	19
2.6 Rheology	22
2.7 Differential Scanning Calorimetry	27
2.8 Surface Tension	28
2.9 Methods	28
2.10 Chemicals	30
<b><i>3. Results and Discussion</i></b>	<b>31</b>
3.1 The System 2,1 HNC/CTAOH/Water	31
3.1.1 Phase Behavior	31
3.1.2 Conductivity and pH Measurements	33
3.1.3 Differential Interference Contrast Microscopy	34
3.1.4 Freeze Fracture Electron Microscopy	36
3.1.5 Cryogenic Temperature Electron Microscopy	42
3.1.6 Small Angle Neutron Scattering	46
3.1.7 Rheological Behavior	49
3.2 The System 6,2 HNC/CTAOH/Water	70
3.2.1 Phase Behavior	70
3.2.2 Small Angle Neutron Scattering	71
3.2.3 Rheological Behavior	72
3.2.4 The Influence of The Substitution on Phase Behavior	75
3.3 The Systems 2,1 HNC/C <sub>x</sub> TAOH (x = 14,12,10,8)/Water	79

3.3.1 Phase Behavior of the systems	79
3.3.2 Conductivity and pH Measurements	83
3.3.3 Differential Interference Microscopy	85
3.3.4 Freeze Fracture Electron Microscopy	88
3.3.5 Small Angle Neutron Scattering	96
3.3.6 Rheological Behavior of the systems	99
3.4 Comparative Study	122
4. <i>Summary</i>	142
5. <i>Zusammenfassung</i>	145
6. <i>References</i>	149

### 1.1 Introduction:

Colloids are particles that have linear dimension between  $10^{-9}$  m (10 Å) -  $10^{-6}$  m (1 μm or 1 μ) [1]. Since there are many particles in nature which fall in this range, the chemistry of colloids is a very essential topic that has application in several areas of chemistry as well as biology and engineering. In modern terminology, colloidal science could be regarded as having control over synthesis and shape of small particles and their properties[2].

It is known that the science of surface active agents (Surfactants) is one of the important subtopics of the colloidal science. Surfactants are known as surface-active compounds that have the capability of adsorbing at the gas/liquid, liquid/liquid and solid/liquid interfaces. Surfactants with lower concentration greatly reduce the surface tension between two or more incompatible phases. In some sense, the structural features of surfactants are responsible for the surface activity. The structural features of a surfactant is characterized by the existence of a polar head and a non-polar tail. The polar head of the surfactant may be charged or uncharged (but polar). A charged polar head may carry a positive or a negative charge or both while the nonpolar (hydrophobic) tail is usually a flexible hydrocarbon chain (C<sub>8</sub>- C<sub>18</sub>) which may contain an aromatic ring. The four major types of surfactants are classified as anionic, cationic, amphoteric or zwitterionic and nonionic depending on the head [3-5].

Surfactants have gained great interest in recent years due to a huge benefit achieved in many industries producing detergent, cosmetics and pharmaceuticals which have surfactants as one of their constituent. This interest continues to grow because of the flexibility of the properties of these surfactants. For instance, surfactants can be used to enhance the viscosity of solutions or to solve difficulties encountered in the formation of solutions in the processes such as wetting, solubilization, dispersion or emulsion formation. The availability of natural resources, from which surfactants can be produced, makes a way for several experimental studies to learn interesting properties of these surfactants. In addition, there exists different ways to build the hydrophobic tail (aliphatic or aromatic) or hydrophilic head ( ionic or nonionic) of the surfactant molecule which determine the efficiency on the shape of the final products.

On the other hand, mixing different surfactant types is encountered in nearly all-practical applications of surfactants. This is due to the inherent difficulty of preparing chemically pure

## 1. Introduction and Aims of The Present Work

surfactants and the performance advantage or synergism that often results from deliberately mixing different surfactant types. This leads to considerable theoretical and experimental work to understand the properties and behavior of these complex systems [3]. A mixture of two distinct surfactants may have intermediate properties that are hard to realize by the use of any single species of a surfactant. Furthermore, synergism of anionic/nonionic and cationic/nonionic, anionic/amphoteric and anionic/cationic mixtures have also been observed for various systems. In fact synergism leads to mixing of the two-micelles into one involving both surfactant molecules [6-21]. The physical properties of surfactant solutions can also be changed by mixing with cosurfactant (defined as Amphiles which normally do not form micelles on their own in solution like aliphatic alcohols, amines, fatty acids etc.), electrolytes, additives, and by changing the temperature as well [22-27]. Surfactants have great importance also when they are used as additives to modify the properties of polymer solutions [28-30].

Surfactant molecules in aqueous media form micelles above their critical micelle concentration (cmc), accompanying striking changes in the various physical properties [28]. With increasing surfactant concentration the micelles undergo a special set of structural transitions, transforming from spherical shape into cylindrical, rodlike or long threadlike, disklike vesicles and other shapes. The shape of a micelle depends on the concentration of surfactant and the presence of additives for single systems, and is controlled by the spontaneous curvature of the micellar interface [23]. Since surfactant solutions can have certain aggregation structures which are responsible for giving the solution its physical properties, they are defined as complex fluids. More generally, complex fluids are defined as the fluids which have a mesoscopic length scale substances (Greek mesos middle, between  $10^{-9}$ m (10 Å) and  $10^{-6}$  m (1 μm) ) which necessarily plays a key role in determining the properties of the system[31]. A very interesting surfactant microstructure is that when the surfactants that are dispersed in water form closed multilayer aggregates capable of separating an internal compartment from the bulk solution. The foresaid microstructure is called a vesicle that is filled with the solvent in which a bilayer membrane is dispersed. Vesicles can be prepared as small unilamellar vesicles (SUV), large unilamellar vesicles (LUV) or large multilamellar vesicles (liposomes). Multilamellar vesicles can be large having diameter of several μms and they are also termed as onions [32-33]. Small micelle aggregates are useful in detergency applications, while rodlike micellar solutions have been used as drag-reduction agents in pipeline flow and thickening chemical formulations etc.[34]. Vesicles

have been found useful as agent in many practical applications and also a basis for several theoretical investigations. Some areas in which vesicles can be used are mentioned below:

- 1- Model system for biological membranes in order to study the permeability as a function of various additives.
- 2- Model system for studying shape fluctuations and formation of biological cells.
- 3- Prevention of photooxidation of metal ions by inserting them into vesicles [35].
- 4- Vesicles work as vehicles for drug delivery, cosmetics, immunoagents, herbicides, pesticides, imaging agents.[36-37].
- 5- Polymerisation in vesicle bilayer membranes - to control the architecture of the resulted polymer that are based on vesicles as matrix[38].
- 6- Micro-reactors - for production of ultrafine particles[39].
- 7- Used as components of artificial photosynthesis, metallic, magnetic, and semiconducting nanoparticles [37].

The formation of vesicles from binary systems or more-component-systems was observed for nonionic surfactants with hydrophobic chain or sugar surfactants with a small head group, nonionic surfactants with two hydrophobic chains, cationic or anionic surfactants with two long alkyl chain, mixtures of cationic and anionic single chain surfactants, mixtures of aminoacid surfactants or aminoacid surfactants at intermediate pH-values, perfluoro surfactants with two hydrophobic chains, mixtures of cationic perfluoro and anionic hydrocarbon surfactants, mixtures of cationic/anionic and zwitterionic perfluoro surfactants or nonionic perfluorosurfactants, mixtures of surfactants with cosurfactants, mixtures of perfluoro surfactants with cosurfactants or with perfluoro cosurfactants[40-47]. Unilamellar vesicles can be prepared also from defected lamellar phase by shear [48-52].

Since micelle exists in interesting structures, many theoretical models have been made to describe the formation of micelle structures. Depending on the geometry of the packing of surfactant molecules, Israelachvili [53] proposed a general theory for the aggregation of amphiphiles in aqueous solutions by introducing what is called a *packing parameter*  $N_s$ . The surfactant packing parameter  $N_s$ , also referred to as surfactant number or surfactant parameter or critical packing parameter which is calculated from the following equation:

$$N_s = v / la_h; \quad (1.1)$$

## 1. Introduction and Aims of The Present Work

$v$  is related to the volume of the hydrophobic portion of a surfactant,  $l$  is the length of the hydrophobic portion of the surfactant and  $a_h$  is the area occupied by a surfactant head group at an interface. The estimation of head group areas is less straightforward since this parameter depends strongly on the counterion adsorption and also the ionic strength. Counterion adsorption greatly modifies intermolecular head group repulsion which in turn affects  $a_h$  significantly. Similarly, ionic strength affects counterion adsorption as well as the shielding of intermolecular repulsion between head groups. The increase of ionic surfactant concentration increases the ionic strength of the system which minimizes the electrostatic repulsion between the head groups and the corresponding head area resulting a transition from one micellar shape to another [54]. The packing parameter is used to describe a variety of regular and axisymmetric structures pointed out by Israelachvili as critical packing shapes. These shapes may be related to assembly structures with characteristic curvatures. Table 1.1 shows a schematic surfactant structures and shapes derived from various packing parameters ( $Ns$ ).

Geometrical structure					
$Ns$	$Ns < 1/3$	$1/3 < Ns < 1/2$	$1/2 < Ns < 1$	$Ns \cong 1$	$Ns > 1$
Name of the structure	Cone	Truncated Cone	Truncated Cone	Cylinder	Reverse Truncated Cone
Corresponding micelle structure	Spherical	Rodlike	Vesicles	Bilayers	Reverse Micelles

*Table 1.1 : Schematic of surfactant structures and shapes derived from various packing parameters*

The surface of larger aggregates is highly irregular and convoluted. According to  **Helfrich's theory**  [55-57], the free energy per unit area of the bilayer associated with bilayer curvature is given by

$$E_a = F / A = 1/2k_c(c_1 + c_2 - c_0)^2 \quad (1.2)$$

where  $E_a$  is the free energy per unit area,  $k_c$  is the bending modulus, which is of the order of a few  $k_B T$  (here,  $k_B$  is the Boltzmann constant, and  $T$  is the temperature),  $C_1$  and  $C_2$  are the

principal curvatures of the bilayer surface and  $C_0$  is the spontaneous curvature. This equation implies that spontaneous curvature deviation raises the free energy level by an amount proportional to the square of the curvature deviation. The energy needed to deform the surface depends on the magnitude of  $k_c$ . The Helfrich theory originally derived for membranes has also been extended to the case of mixtures of surfactants by Safran who assumed different spontaneous curvature at each monolayer forming the bilayered vesicles leading to the following expression for  $E_a$ :

$$E_a = F / A = 1/2k[(C + C_0)^2 + (C - C_i)^2]. \quad (1.3)$$

Here,  $C$  is the curvature of the vesicle and  $C_i$  and  $C_o$  are the spontaneous curvatures of the inner and outer monolayers, respectively. This reveals a nonideal mixing of the surfactant molecules in the vesicle. In the particular case of two opposite charged surfactants, it may be assumed that the surfactant complexes with small area per head group are placed on the internal monolayer while the free surfactant is placed on the outer monolayer. From x-ray measurements, it was found that the value of  $k_c$  depends on the surfactant's chain length. It has been noted that  $k_c$  is a non-linear function of co-surfactant's chain length and the effect of replacing longer chain surfactants by shorter ones in a mixed membrane system is to reduce  $k_c$  dramatically (meaning thinning of the membrane). In this case, the system changes from a state of bounded membrane to the floppy unbound regime of fluctuating dilute membrane [58-59].

### 1.2 Electrostatic Interactions between Molecules and Particles in Colloidal Science.

Adsorption of electrolytes or ionic surfactants plays a critical role in self-assembled structures, such as monolayers, micelles, bilayers, vesicles, and emulsions apart from producing a charged interface, and polar interactions involving head groups and solvent. The adsorption of electrolyte due to electrostatic interactions also control the self-assembly and stability of charged latex particles, silica particles, clays, amongst other colloidal systems. Therefore, the study of electrostatic interactions between molecules and particles is central to colloidal science. Indeed, a knowledge of charged interface is a major step towards

understanding many phenomena in colloidal science [1,60]. For this reason, a theoretical basis for the electrostatic interactions between molecules and particles is provided below:

A molecule, in an electrostatic description, represents a charge distribution  $\rho(\vec{r})$  set up by its electron and nuclei. The corresponding charge distribution generates an electrostatic potential  $\Phi$  that obeys Poisson equation :

$$\epsilon_o \nabla^2 \Phi(\vec{r}) = -\rho(\vec{r}) \quad (1.4)$$

where  $\nabla^2 = \frac{\partial^2}{\partial X^2} + \frac{\partial^2}{\partial Y^2} + \frac{\partial^2}{\partial Z^2}$  is the Laplacian operator and  $\epsilon_o$  represents the dielectric permittivity of a vacuum. The potential generated by two charge distributions,  $\rho_1(\vec{r}) + \rho_2(\vec{r})$ , is the sum  $\Phi = \Phi_1 + \Phi_2$  of the potentials generated by  $\rho_1(\vec{r})$  and  $\rho_2(\vec{r})$  independently. Now, the Coulomb ion-ion electrostatic interaction energy  $E$  between molecules in the gas phase is given by

$$E_{coulomb} = \frac{q_1 q_2}{4\pi \epsilon_o R_{12}}, \quad (1.5)$$

where  $q_1$  and  $q_2$  are the charges of the first and second ions, and  $R_{12}$  is the distance between them. If there is a coulomb interaction between the charges  $q_1$  and  $q_2$  in a solvent with a relative dielectric permittivity  $\epsilon_r$ ,  $E_{coulomb}$  takes the form

$$E_{coulomb} = \frac{q_1 q_2}{4\pi \epsilon_r \epsilon_o R_{12}}. \quad (1.6)$$

Ion-ion interactions are stronger and longer than the other multipole interactions. As a consequence, they typically play a vital role in determining the interactions in the electrolyte or charged colloidal solutions. This fact suggests that one could write the interaction between free charges explicitly while averaging over the electrostatic interactions in a solvent. This averaging is effectively done by the use of poisson equation (1.4) to analyze a parallel plate capacitor gives us the simplest illustration of the principle for how to perform such an average.

In a parallel plate capacitor(parallel to X-Y plane), an applied potential  $\Phi$  leads to a potential drop  $\Delta\Phi$  (influenced by the distance between the plates in the Z-direction )and induces charge

density  $\sigma$  and  $-\sigma$  at the surface of the conducting planes. The capacitance  $C$  in this case is defined as

$$C = \frac{\sigma}{\Delta\Phi} \text{area} . \quad (1.7)$$

The quantity  $C$  according to Poisson equation is given by

$$\nabla^2 \Phi(\vec{r}) = \frac{d^2 \Phi}{dZ^2} = -\frac{\rho}{\epsilon_0}, \quad (1.8)$$

since the potential is a constant parallel to the plates.

Interactions between the fixed charges at the surface and the free charges in solution play an important role in colloidal systems. In this situation the solution adjacent to the plates will have an electrolyte characterized by the bulk concentration  $c_{io}$ , valency  $z_i$ , and the solvent dielectric constant. If one is interested in determining the relationship between  $\sigma$  and  $\Phi_0$  (the potential at the surface) and the variation of potential as well as the ionic distribution with the distance from the charged interface, one needs to solve the Poisson equation.

In the region of the electrolytic solution, the Poisson equation takes the form

$$\epsilon_r \epsilon_0 \nabla^2 \Phi = -\rho_{(free\ ions)} \quad (1.9)$$

where the charge distribution in the solution is expressed as

$$\rho_{(free\ ions)} = e \sum_i z_i c_i^*(\vec{r}), \quad (1.10)$$

where the \* on  $c_i^*$  indicates the measured concentration in molecules per cubic meter, while  $c_i^*(\vec{r})$  represents the local concentration of ions. Because the ions in the solution are free to respond to the electrical field, the solution's charge distribution  $\rho$  is not imposed externally. The electrostatic interaction favors an ordered and very localized ion arrangement, but entropic factors strive to generate a random uniform distribution of ions. In the case of an applied external potential, the compromise between energy and entropy results in a Boltzmann distribution,

$$c_i^*(\vec{r}) = c_{io}^* \exp\left(\frac{-z_i e \Phi}{kT}\right) \quad (1.11)$$

where  $z_i$  stands for the ion valency and  $c_{io}$  is the concentration of ion species  $i$  at a reference point where  $\Phi = 0$ , which usually means the solution as bulk. Substitution of 1.10 and 1.11 in 1.9 yields the Poisson-Boltzmann equation

$$\epsilon_r \epsilon_0 \nabla^2 \Phi = -e \sum_i z_i c_{io}^* \exp\left(\frac{-z_i e \Phi}{kT}\right). \quad (1.12)$$

When a charged planar surface which is extended in the X and Y directions is exposed on one side of an electrolyte solution, the variations in the Z-direction are alone important and in this case equation 1.12 reduces to an ordinary differential equation

$$\frac{d^2\Phi}{dZ^2} = -\frac{e}{\varepsilon_r \varepsilon_o} \sum_i z_i c_{io}^* \exp\left(\frac{-z_i e \Phi}{kT}\right) \quad (1.13)$$

Electroneutrality requires that the surface charges be fully neutralized by ions in the solution, and at sufficiently large distances from the surface

$$\left. \frac{d\Phi}{dZ} \right|_{Z \rightarrow \infty} = 0, \quad (1.14)$$

which follows from Gauss's law. Letting  $\Phi = 0$  for large Z is a natural choice under these circumstances because  $c_i^*$  simply represents the bulk electrolyte concentration. If the ions are at the surface ( $Z = 0$ ), then the surface will be like a capacitor which can be described by the following equation

$$\left. \frac{d\Phi}{dZ} \right|_{Z=0} = \frac{-\sigma}{\varepsilon_r \varepsilon_o}. \quad (1.15)$$

Equation 1.13 may be integrated (see reference 131-page 112-113 for details) between the limits Z and  $\infty$  yielding the following expression for  $\Phi(Z)$

$$\Phi(Z) = \frac{2kT}{ze} \ln\left(\frac{1 + \Gamma_o \exp(-\kappa Z)}{1 - \Gamma_o \exp(-\kappa Z)}\right) \quad (1.16)$$

the coefficient  $\Gamma_o$  in the above expression relates to the surface potential  $\Phi_o$  through

$$\Gamma_o = \frac{\exp(ze\Phi_o / 2kT) - 1}{\exp(ze\Phi_o / 2kT) + 1} \quad (1.17)$$

and  $\kappa$  is calculated from the equation

$$\frac{1}{\kappa} = \left( \frac{\varepsilon_r \varepsilon_o kT}{\sum_i (z_i e)^2 c_{io}^*} \right)^{1/2} \quad (1.18)$$

As  $\Phi_o \rightarrow 0$ ,  $\Gamma_o$  approaches zero, while as  $\Phi_o \rightarrow \infty$ ,  $\Gamma_o$  tends to unity.

The relation between the surface charge density and the surface potential is as follows

$$\sigma = (8kT c_i^* \varepsilon_o \varepsilon_r)^{1/2} \sinh\left(\frac{ze\Phi_o}{2kT}\right) \quad (1.19)$$

where  $\sinh(x) \equiv (\exp(x) - \exp(-x)) / 2$

The charged surface and the neutralizing diffuse layer of counterions are said to form an *electric double layer*. The thickness of the diffuse layer is of the order  $1/\kappa$ , the *Debye*

**screening length** which is given by the equation (1.18). Viewed this way, the arrangement of charges resembles that in a parallel plate capacitor.

Using equations (1.16), (1.17) and (1.19) the surface charge density is calculated and variation of electrical potential with the distance from the surface is shown in figure 1 for two different electrolyte concentrations. For a constant surface charge density, the initial slopes  $\alpha$  and  $\beta$  of using equation 1.11 are identical, but  $\Phi_0$  decreases upon adding an electrolyte, and ionic distance from the surface becomes less.

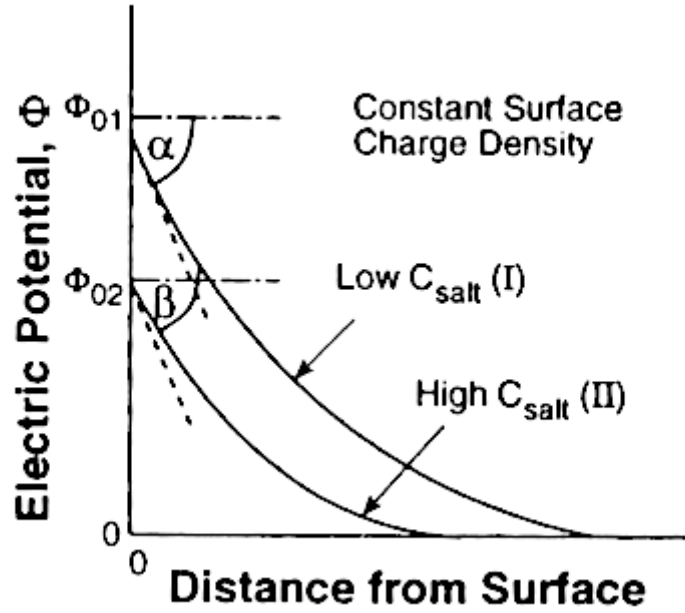


Figure 1.1: variation of electric potential with the distance from the surface at constant surface charge density

The total surface concentration of ions (when the ions are at the surface  $Z=0$ ) is defined as the sum of all surface concentrations  $c_i(0)$ , including both counter- and coions, and is given by

$$\sum_i c_i^*(0) = \frac{\sigma^2}{2kT\epsilon_r\epsilon_o} + \sum_i c_{io}^* = \frac{\sigma^2}{2kT\epsilon_r\epsilon_o} + \frac{\Pi_{osm}}{kT} \quad (1.20)$$

In an ideal solution, the  $\sum_i c_{io}^* = \frac{\Pi_{osm}}{kT}$ , which follows from the definition of osmotic pressure  $\Pi_{osm}$ . In the limit of higher charge densities, the term  $\frac{\sigma^2}{2kT\epsilon_r\epsilon_o}$  dominates, so the

surface potential also becomes high. As a result, a few coions reach the surface, and in the expression for  $\sum c_i^*(0)$ , the counterion terms dominate.

The fore mentioned theory can indeed be applied for the case of charged colloids, or charged vesicles. More specifically, multilamellar vesicle has a sequenced charged bilayers which are separated by interlamellar distances. If one adds an electrolyte to their vesicular solutions then the interoperations corresponding to figure 1.1 may be exploited.

Experimentally, one can control the charge density of the vesicles by choosing a suitable mixing ratio, or a charging degree (for example mixing cationic surfactants with anionic surfactant, or making a protonation for the head groups of the vesicles). The resulting potential will determine the distance between the counterions and the micellar surface, which is also known as the shielding effect of the counterions, and maintaining the distance for the coions as described in equation 1.20.

### 1.3 Hydrophobic Counterions/Cationic Surfactants and Catanionic System:

The effects of hydrophobic counterions on the rheological behavior of cationic surfactants have been studied by many authors. The relation between micelle length of cetyltrimethylammonium bromide CTAB and aqueous salicylic acid solution and viscoelasticity was studied by Shikata and coworkers [61-66]. It has been found that different size aggregates are obtained by altering the pH and using decyltrimethylammonium bromide, which alone could not induce viscoelasticity. Sodium p-toluenesulfonate (NapTS) and Sodium Salicylate (SS) hydrophobic counterions were added to CTAB, and the resulting viscoelasticity was investigated in details. It has also been found that the relaxation time depends on the ratio of counterions/surfactants and surfactant concentration. Small angle neutron scattering (SANS) studies on SS and different CTAB concentrations have shown that the resulting micelles are rigid rods and their exponential length distribution behaves similar to those of living polymers beyond the first viscosity maximum [67]. Hoffmann et al [68] observed that the effect of addition of SS to cetylpyridinium chloride CPC rises the viscosity of the system sharply until slightly above a 1:1 molar ratio of CPC/SS and then the viscosity drops off drastically. Upon adding SS further, the viscosity rises until the ratio reaches about 1:4 and then drops off again with continued addition of SS. This feature was observed for several concentration of CPC and there does not seem to be any satisfactory explanation of this phenomenon until this date.

Sodium 3 hydroxy 2 naphthoate 3,2 SHCN hydrophobic counterion was investigated by C. Manohar and co workers [69-76]. The 3,2 SHNC which is structurally comparable to SS is strongly adsorbed on the micellar surface with the carboxylic and hydroxyl group protruding out of the micelle. The presence of naphthalene ring in HNC<sup>-</sup> was expected to confer more hydrophobicity on the molecule as compared to SS. It was also proved from surface tension measurements that SHCN is mildly surface active and in view of the concentrations, it could be regarded as a hydrotope. H<sup>1</sup>NMR spectra of SHNC showed penetration of SHCN into CTAB micelles. NMR spectra showed that the protons at the 4, 5, 6, and 7 positions are present in a nonpolar environment inside the micelles of CTAB. SHNC is oriented to the micellar surface keeping the naphthalene moiety penetrated into the micelle.

This orientation is consistent with the surface active nature of SHNC ( compared to SS), however this CTAB-SHNC system differ in a major way from CTAB-SS system through the presence of a sequence of phases from small micelle aggregates, an isotropic gel phase (non-birefringent rodlike micelle, L<sub>1</sub>-Phase), anisotropic liquid crystal (birefringent Lamellar, L<sub>α</sub>-Phase) -precipitate-liquid crystal and gel again (birefringent multilamellar vesicles, L<sub>α</sub>-Phase). It was pointed out that the more surface activity of SHNC compared to SS has a significant role in these observations, and to regard the mixture of CTAB-SHNC as a mixture of two opposite charged surfactants, one with a chain length of 17 Å and the other with a much shorter chain length of about 4.8 Å. As a result of this, SHCN is classified as an ionic surfactant or a cosurfactant.

CTAB-SHNC system is comparable to opposite charged headgroup surfactants which form vesicles. With addition of SHCN to a CTAB micellar solution, the former adsorbs onto CTAB micelle converting the micelles into cylindrical (or a polymeric) micelles. The transformation is assisted by the decreasing in the area of the polar head group (electrostatic interaction reduced) of the new surfactant entity, thus increasing the packing parameter. At this stage the micelles are positively charged. Further addition reduces the coulomb repulsion as SHNC adsorbs onto a surface neutralizing the charge and the cylinders are able to come closer to form a nematic phase. When the system is approached the equimolar ratio, the surface charge becomes so small that the micelles coagulate producing a thick precipitate. On continued addition the system is driven to the gel state as before and this mechanism explains the symmetry of the transition. The symmetry of the transitions and the surface active nature of

## 1. Introduction and Aims of The Present Work

SHNC suggest comparisons with the spontaneous vesicular systems produced by mixing two surfactants of opposite charges. Ionic surfactants change its morphology when oppositely charged surfactants are mixed in aqueous solution. This unexpected finding is also a direct consequence of the strong nonideal interaction between oppositely charged head groups in surfactant aggregates. The direct example of these mixtures is the cationic and anionic surfactants mixed systems, or catanionic surfactants. catanionic surfactants are defined as salt of an amphiphilic anion with an amphiphilic cation [77]. The effective “neutralization” in the head group plane reduces the repulsion between head groups, and as a result, the effective surfactant packing parameter depends on composition. Special emphasis is placed on the influence of factors such as surfactant mixing ratio and symmetry/asymmetry effects of alkyl chain lengths on the aggregate structures. Mixing ratio of the anionic surfactant or the anionic hydrophobic counterion participate in determining the equilibrium microstructure of cationic surfactant. Catanionic surfactant mixtures are investigated with regard to phase behavior and microstructures by Zasadzinski and coworkers [78-81]. They focused on the effect of surfactants geometry on the resulted phase diagram. It has been found that surfactant geometry strongly affects the microstructure present in cationic and anionic mixtures [82]. It has been reported that the micellar and vesicle phases are stabilized in water-rich part of the phase diagram for catanionic surfactant mixtures containing one short chain surfactant and another long chain surfactant. Alkyl chain asymmetry also plays a dominant rule in the formation and stability of phases for mixed catanionic system. A crystalline precipitate dominates the phase behavior when the two surfactants are linear and symmetric in chain length. Micelles and vesicles are only observed at higher concentration. When the surfactants are branched and/or contain a bulky substituent (e.g. a benzene group) in the tail group, the precipitate phase stability is reduced relative to that of micellar and vesicular phases. As a result, wide regions of vesicles phase stability may be observed. The transition from micelle to vesicle occurs over a narrow region in composition and is abrupt.

### 1.4 Aims of The Present Work:

The aim of this work is to correlate the microstructure and solution properties for finding useful and desired application areas for the novel surfactant mixtures. It is important to understand how the solution composition and chemical structure of surfactants or counterions influence the resulting microstructure, phase behavior and rheological behavior. The present work mainly aims at characterizing the microstructures that results in the associate of novel mixed surfactant systems generated out of mixing cationic surfactants with hydrophobic counterions of different geometries. In the first part of this work, the position of the substituents connected to the hydrophobic counterion will be varied and attempt will be made to characterize the different phases that would result under different solution conditions. These conditions will be mainly achieved by varying the concentration the hydrophobic counterions, the chain length of cationic surfactants hydrocarbon tail and the concomitant change in the pH and conductivity of the systems. Some measurements will be made at different temperatures and at different time intervals. Then later on, the phase behavior would be monitored. The microstructure of different phases will be investigated by using different microscopic methods. Neutron scattering measurement will also be used to characterize the specific features in the phase systems. Rheological measurements will be taken up on these systems to understand the behavior in term of various rheological responses. Different models would be applied to calculate some of the properties for comparing them with the experimentally observed data. Finally, a correlation will be established between the phase behavior observed and the properties measured.

## 2. Experimental Theory

### 2.1 Birefringence [83-87]:

The light is an electromagnetic wave which move with a certain speed through certain medium. The speed of the light in the vacuum is different from that when the light pass through other mediums. The speed of the light in the vacuum  $c_o$  per its speed in certain medium  $c$  is called refractive indexes  $n$  :

$$n = \frac{c_o}{c} \quad (2.1)$$

The speed of the light in the vacuum is higher than its speed in other mediums, so  $n$  usually is higher than unity.

In the optically isotropic mediums the light speed in the whole directions  $(x, y, z)$  is the same, so the resulted refractive indexes are also similar  $(n_x = n_y = n_z)$ . On the another hand in the anisotropic mediums, the light reacts with different morphologies, and as a result its speed in one direction is different from other directions. At least two refractive indexes are not the same. The light direction are perpendicular or parallel to the optical axes. Therefore, two refractive indexes for each direction are calculated.

$$c_{\parallel} = \frac{c_o}{n_{\parallel}}, \quad c_{\perp} = \frac{c_o}{n_{\perp}} \quad (2.2)$$

The difference between the parallel and the perpendicular refractive indexes is called the birefringence  $\Delta n$  of the medium. It has the following form.

$$\Delta n = n_{\parallel} - n_{\perp} \quad (2.3)$$

for the colloidal systems and depending on the birefringence one can find the orientation of the colloidal particles. The following equation represent such type of relation:

$$\Delta n = \Delta n_s \cdot \Omega \quad (2.4)$$

where  $\Omega$  is the orientation function which is given by the following equation:

$$\Omega = \left[ \frac{3}{2} \cdot \cos^2(\Theta) - \frac{1}{2} \right] \quad (2.5)$$

where  $\Theta$  is the angle between the particle center and the orientation direction.  $\Delta n_s$  can be given for surfactant solutions using the equation:

$$\Delta n_s = \Delta n_e - \Delta n_f, \quad (2.6)$$

where  $\Delta n_e$  is the birefringence of the molecules when they are as monomer,  $\Delta n_f$  is the birefringence for the aggregates.

If a solution with lamellar aggregates is seen between two crossed polarizers, it shows birefringence. The non polarized light (light in the whole directions) can be filtered by the first polarizer and only one-direction light is passed. This polarized light can be classified as two vectors which are perpendicular with angle  $90^\circ$ . These two components interact with the anisotropic solution and two different refractive indexes can be resulted. Therefore, a type of phase shift  $\delta$  is happened. The degree of phase shifting depends on the thickness of the anisotropic medium  $l$ , the optical properties of the medium and the wave length of the incident light  $\lambda$  as it is described by the following equation:

$$\delta = \frac{2\pi}{\lambda} \cdot \Delta n \cdot l \quad (2.7)$$

The linear polarized light becomes elliptical after this shift, so it passes through the second polarizer, and the solution exhibits birefringence.

### 2.2 Conductivity [88-89]:

When an voltage is applied through a cell has two electrodes and an electrolyte solution between them, the electrolyte will exhibit a certain type of resistance  $\mathbf{R}$  (Ohm) against the applied current. The resistance of the solution is proportional to the cell length  $l$  (cm) (the distance between the electrodes) and has inverse proportionality with its cross-sectional area  $A$  (cm<sup>2</sup>) (the area of the electrodes in direct contact with the solution). To convert the proportionality into equality, a multiplication by a constant  $\rho$  has to be made. This can be mathematically described by the equation :

$$R = \rho \times \frac{l}{A} \quad (2.8)$$

The constant  $\rho$  is called the resistivity. The conductivity of a solution is the inverse of the resistivity,  $\rho = \frac{1}{\kappa}$ , so equation 2.8 will be converted into:

$$R = \frac{1}{\kappa} \times \frac{l}{A} \quad \text{or} \quad \kappa = \frac{l}{RA} \quad (2.9)$$

The direct inverse of  $\mathbf{R}$  is called the conductance  $\mathbf{G}$ , and its unit is (Siemens = S = 1/ohm), so the conductivity has the unit S/cm. The conductivity of a solution depends on the number

of ions present, and this leads us to introduce the concept of molar conductivity  $\Lambda_m$  which is defined as :

$$\Lambda_m = \frac{\kappa}{c} \quad (2.10)$$

C is the molar concentration of added electrolyte, and its unit is  $S \cdot cm^2 / mole$ . It was proven that the Conductivity of bulky ions such as  $R_4-N^+$  and  $RCO_2^-$  decreases with increasing solvent viscosity and ion size. This was not correct for small ions. Since the size and the viscosity of self assembly molecules can be changed by many factors, the results of conductivity are used in surfactant science for many purposes. Conductivity is used for determination the cmc of ionic surfactants, or in general, the results of conductivity can give some information about the micelle morphology and its phases.

### 2.3 Differential Interference Contrast Microscopy (DICM) [90]:

DICM is one kind of light microscopy which shows more details of the object due to its higher contrast compared to normal light microscopy. Figure 2.1 shows the steps of magnification using DICM. The light which comes from the source is firstly polarized by the polarizer, and then divided by a prism (called Wollaston prism) into two beams.

They are in perpendicular polarization plane, and they become closer at a certain point. The two light beams are made parallel by a condenser. When these beams interact with the object a larger phase shift between the beams is caused. This can be illustrated by different refractive indexes that beams can have when they interact with different topologies of the sample. By the objective and second Wollaston prism the two beams is reunited and interfered. Using an analyzer perpendicular to polarizer, the difference in the refractive indices gives the object details.

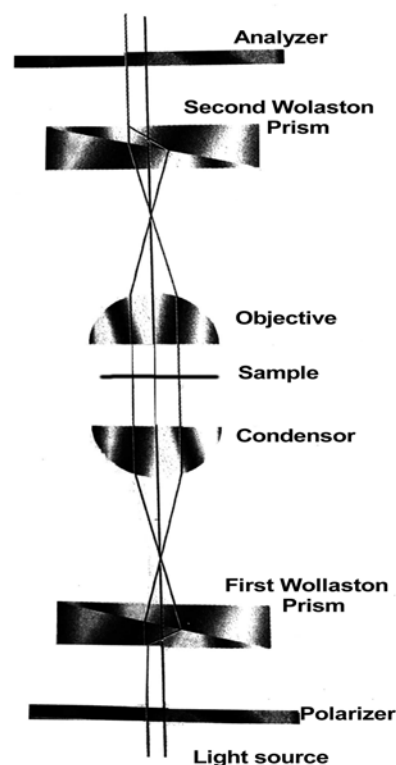


Figure 2.1: DICM Setup.

2.4 Freeze-Fracture Electron microscopy (FF-TEM) [91-97]:

FF- is a widely used technique for biological or other specimens with a high water content . By FF-technique, it is necessary to sputter the fractured plane with Pt/C (Pt: Platinum, C: Carbon) which is followed with carbon and then dissolve the frozen solution from the Pt/C and finally to look at the imprints with transmission electron microscopy (TEM).

FF-technique has five sequenced steps in it's process. They are shown in figure 1 and described as follows:

**(A) Freezing of the sample:** The liquid sample has the microstructure is laid onto copper carrier and covered by the second one (copper has a good thermal conductance). After that, the copper sandwich is impressed into liquid propane, which is cooled by liquid nitrogen. Extremely fast freezing rates of  $\geq 10^4$  K /s can minimize the size of ice crystals formed which results in unfavorable cryofixation. Good cryofixation is important for ultrastructural investigation with the electron microscope. After freezing the sample for few seconds in liquid propane, it is transferred into special sample holder, which is also cooled by liquid nitrogen. After that, the sample is transferred into the freeze fracture apparatus.

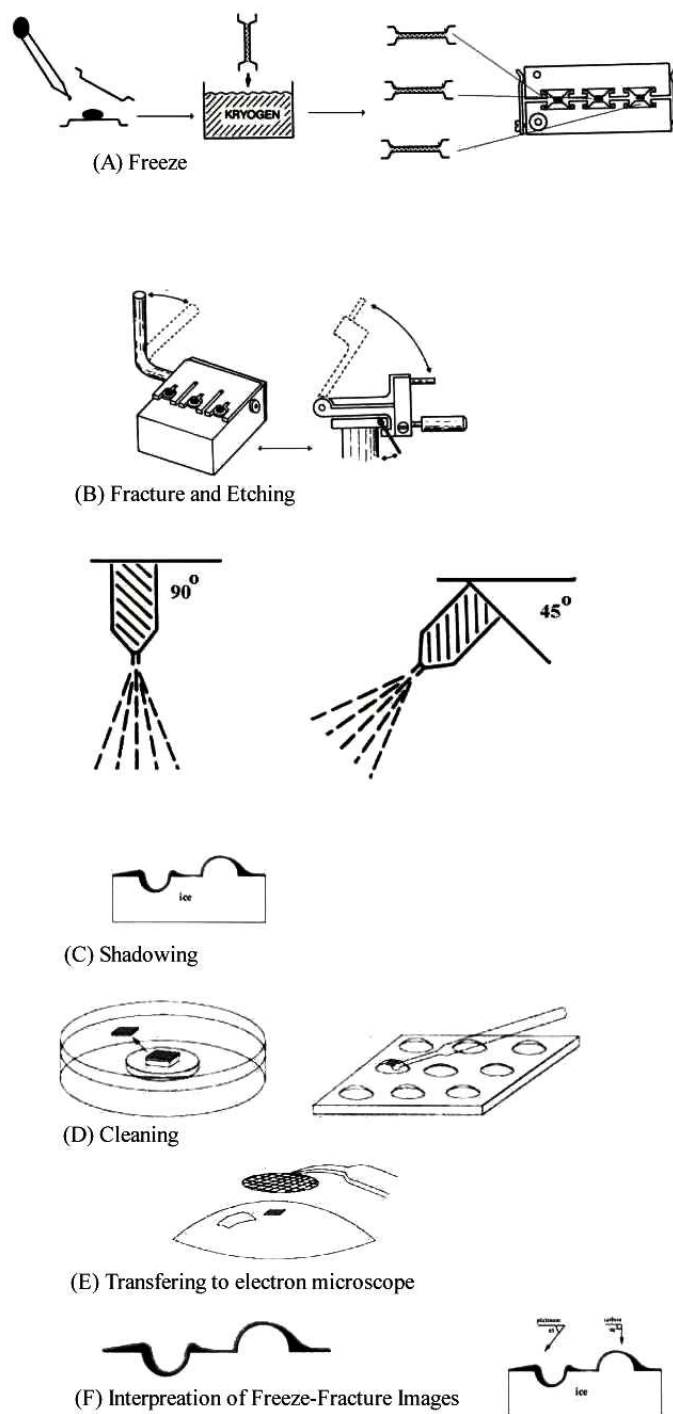


Figure 2.2 : Different steps of Freeze fracture technique (freezing, fracture and etching, shadowing, cleaning, transferring to electron microscope, and interpreting the results ).

(B) **Fracturing and Etching:** In the fracture and etching unit, which is under vacuum  $> 2 \times 10^{-6}$  mbar, the sample holder is fixed on the specimen table at temperature  $< -100$  °C. Liquid nitrogen is used to control the cooling process. A fracturing tool is operated from outside the chamber and viewed with a binocular microscope. As the sample holder is opened, the frozen solution between the copper sandwich is fractured into two parts. Each part has on its surface the microstructure information from the solution. To have more specific information of the fractured surface microstructure, it is possible to remove some ice of the fracture face by sublimation (Etching). In practice, etching is made by rising the temperature of specimen table to about  $-90$  °C, then waiting for few seconds and re-cooling again. The final process is called etching. It is not necessary to do it, and sometimes better results are obtained without etching.

(C) **Shadowing and Replication :** In this step, the fractured surface is coated by a thin layer of platinum, which covers the surface and makes a copy of its details. The thickness of the layer is controlled by the time of sputtering. Platinum produces fine particles upon sputtering, which can cover smoothly the fractured surface topology. Platinum is produced from a cathode, which is directed in  $45^\circ$  toward the specimen. This shadowing leads to a clearer copy of the surface. Following shadowing, a carbon backing is evaporated at a normal ( $90^\circ$ ) angle to the surface. This gives sufficient strength to the replica so that when it is removed from the surface it won't break.

(D) **Cleaning of the replicas:** The replicas are rolled up from the copper surface by impressing them in water or other organic solvents such as; acetone, ethanol, chloroform, etc. A problem often encountered in freeze-fracturing is that platinum-carbon replicas are broken into fragments during replica washing. This differs from one solution to another depending on the existing chemicals. After washing, the replica is placed on a narrow-mesh specimen grid, and left until it becomes dry.

(E) **Transferring to Electron Microscope (EM) :** The replica is picked up on a grid and examined with a transmission EM. TEM depends for its operation on the wave nature of the electron and the fact that electric and magnetic fields of suitable geometry are able to function like lenses to refract, deflect, and focus an electron beam. A thin specimen is irradiated with an electron beam of uniform current density. Electrons are emitted in the electron gun by thermionic emission from tungsten hairpin cathodes, C, and accelerated towards an aperture in the anode. The resulting electron beam which crosses the anode interacts with the specimen. The thick points of the replica retard the accelerated electrons more than the thin one. The phase of the electron waves behind the specimen is modified by the electromagnetic

lenses. At the end, the magnified electrons beam will react with a fluorescence screen, which shows dark and white region depending on the energy that electrons have. The whole process is done under vacuum to avoid electron scattering caused by air.

(F) Interpretation of Freeze-Fracture Images: Knowing the direction of shadowing enables one to conclude whether a given structure in a replica is elevated (outside) or depressed (inside) with respect to the general background. Thus if the buildup of metal shadowing material (dark on a positive print) on a given structure is similar to that of a known particle nearby, the structure must be similarly elevated. In figure 2.3 the effect of shadowing on the resulted pictures is shown. The dark region were in the direction of shadowing while the brighter region were in the opposite direction.

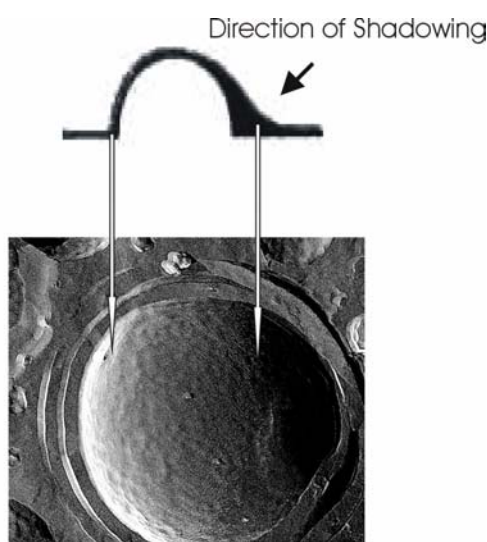


Figure 2.3: Effect of shadowing on the resulted picture.

By cryo-technique a very thin films of the micellar solution are quenched rapidly to the glassy state and the thin film is then directly viewed by TEM. The whole process is made under cooling with liquid nitrogen, so more attention has to be given to keep the sample in the frozen state without temperature fluctuation.

### 2.5 Small Angle Neutrons Scattering (SANS) [98-102]:

SANS is useful for colloid and polymer science since neutron radiation is produced to cover a range of wave length; 0.1-3 nm. Colloids are usually in the range of 1 nm to 1000 nm. Angle-dependent scattering of the colloidal system which contains structural can be obtained when the particle size and the wavelength of the radiation are similar. That is why SANS is useful

for colloidal systems. The interaction of neutrons with matter is weak and the absorption of neutrons by most materials is correspondingly small. This adds new advantages for SANS, being very penetrating and useful for studying the sensitive samples, such as biological materials. Neutrons are neutral and of much higher mass compared to electrons, so they are scattered by the nucleus itself. Because atomic nuclei are some  $10^4$ -  $10^6$  times smaller than typical neutron wavelengths, the nuclei effectively act as point of scatters. The result of this is that the nuclear scattering remains constant as the scattering angle increases, allowing scattering patterns to be collected over the full range from forward to backward angles. The scattering is spherically symmetric. Usually the neutrons are released by the fission of uranium-235.

In any SANS experiment; A beam of neutrons is directed at a sample, illuminating a small volume,  $V (= At_s)$ , where  $A$  is the cross-sectional area of the beam and  $t_s$  is the pathlength of the sample). The radiation can be absorbed, transmitted or scattered by the sample. A detector of dimension  $dx \times dy$  is placed at some distance,  $L_{sd}$ , and scattering angle,  $\theta$ , from the sample then records the flux of radiation scattered into a solid angle element,  $\Delta\Omega (= dxdy / L_{sd}^2)$ . This flux,  $I(\lambda, \theta)$ , may be expressed in the general terms in the following way :

$$I(\lambda, \theta) = I_0(\lambda) \Delta\Omega \eta(\lambda) T V \frac{d\sigma}{d\Omega}(Q) \quad (2.11)$$

where  $I_0$  is the incident flux,  $\eta$  is the detector response,  $T$  is the sample transmission and  $\frac{d\sigma}{d\Omega}(Q)$  is a function known as the differential cross-section. The first three terms of the equation 2.11 are clearly instrument-specific while the last three terms are sample-dependent. The last term contains all the information on the shape, size and interaction of scattering bodies, and its given by:

$$\frac{d\sigma}{d\Omega}(Q) = N_p V_p^2 (\Delta\delta)^2 P(Q) S(Q) + B_{inc} \quad (2.12)$$

where  $N_p$  is number concentration of scattering bodies,  $V_p$  is the volume of one scattering body,  $(\Delta\delta)^2$  is the square of the difference in neutron scattering length density,  $P(Q)$  is a function known as the form factor,  $S(Q)$  is interparticle structure factor,  $Q$  is the magnitude of the scattering vector and  $B_{inc}$  is the (isotropic) incoherent background signal.

$Q$  is given by :

$$|Q| = |k_f - k_i| = \frac{4\pi}{\lambda} \text{Sin}\left(\frac{\theta}{2}\right) \quad (2.13)$$

where  $k_i$  is the incident wave vector and  $k_f$  is the scattered wave vector. Substituting equation 2.13 into Bragg's law of Diffraction

$$\lambda = 2 d \text{Sin}\left(\frac{\theta}{2}\right) \quad (2.14)$$

yields a very useful expression :

$$d = \frac{2\pi}{Q} \quad (2.15)$$

where  $d$  is the distance.  $\delta$  can be given by the relation:

$$\delta = \sum_i b_i \frac{DN_A}{M_w} \quad (2.16)$$

where  $D$  is the bulk density of the scattering body and  $M_w$  is its molecular weight. The contrast is simply the difference between that part of the sample of interest,  $\delta_p$ , and the surrounding medium or matrix,  $\delta_m$ , all seured; i.e.,

$$(\Delta\delta)^2 = (\delta_p - \delta_m)^2 \quad (2.17)$$

For the form factor, selections of form factors for some microstructures are shown in the following equations:

sphere of radius  $R_p$  is given by the equation:

$$P(Q) = \left[ \frac{3 ( \text{Sin} (QR_p) - QR_p \text{Cos}(QR_p) )}{(Q R_p)^3} \right]^2 \quad (2.18)$$

while for Rods of negligible cross section and length  $L$  can be given by :

$$P(Q) = \frac{2 S_i(QL)}{QL} - \frac{\text{Sin}^2(QL/2)}{(QL/2)} \quad (2.19)$$

where  $S_i$  is the Sine integral function.

Form factor describes the size and the shape of individual particles, while the structure factor  $S(Q)$  describes the interparticle correlation.

### 2.6 Rheology [103-111]:

Surfactant solutions with small micellar aggregates always have a low viscosity. The theoretical basis for the viscosity  $\eta$  of globular particles is Einstein's law according to which the viscosity is linearly increasing with the volume fraction  $\phi$  of the particles.

$$\eta = \eta_s (1 + 2.5\phi) \quad (2.20)$$

where the  $\eta_s$  is the viscosity of the solvent. The constitutive or equation of state for our Newtonian fluid is :

$$\sigma = \eta \dot{\gamma} \quad (2.21)$$

where  $\sigma$  is the shear stress and  $\dot{\gamma}$  is the shear rate.

On the other hand many surfactant systems show high viscoelastic properties at low surfactant concentrations. They have both viscosity as liquids and elasticity as solids. Solutions that are that viscous have usually also elastic properties because the zero shear viscosity  $\eta^o$  is the result of a transient network, which is characterized by a shear modulus  $G^o$  and structural relaxation time

$$\eta^o = G^o \cdot \tau_s \quad (2.22)$$

If the network is deformed by a shear stress  $\sigma$  in a shorter time than it can reach equilibrium, it behaves like any solid material with a Hookean constant  $G^o$ , which is called the shear modulus and the following simple relation is obtained.

$$\sigma = G^o \cdot \gamma \quad (2.23)$$

where  $\gamma$  is the deformation. If the network is deformed slowly it behaves like a viscous fluid with a zero-shear viscosity  $\eta^o$  as it is described by equation 2.22.

An analogous mechanical model for viscoelastic solutions:

As described above that viscoelastic solutions have both the features of viscous fluids and elastic solids. To describe this complex rheological behavior, many models were proposed.. In this section, the viscoelasticity and its analogous mechanical model (Maxwell) is explained. Summation of equation 2.21 and 2.23 and after rearranging results in the following equation:

$$\dot{\gamma} = \frac{\dot{\sigma}}{G^o} + \frac{\sigma}{\eta} \quad (2.24)$$

### Oscillation Response:

In the case of oscillated stress the same equation as above (2.24) is valid, but we have to use the complex notation because the equation is valid in real number range.

$$\dot{\gamma}^* = \frac{\dot{\sigma}^*}{G^o} + \frac{\sigma^*}{\eta} \quad (2.25)$$

After solving this equation storage and loss modulus are obtained, at which storage modulus is :

$$G'(\omega) = G^o \frac{(\omega\tau_m)^2}{1 + (\omega\tau_m)^2} \quad (2.26)$$

It gives information about the elastic part of the sample ; and the loss modulus is :

$$G''(\omega) = G^o \frac{\omega\tau_m}{1 + (\omega\tau_m)^2} \quad (2.27)$$

It gives information about to the viscous part of the sample ; and the complex viscosity is given by :

$$|\eta^*| = \frac{\tau G^o}{\sqrt{1 + \omega^2 \cdot \tau^2}} \quad (2.28)$$

At high frequencies the loss modulus is closed to the normal modulus:

$$G^*(\omega \rightarrow \infty) = G'(\omega \rightarrow \infty) = G^o \quad (2.29)$$

while at very low frequencies the complex viscosity will is equal to dynamic viscosity:

$$\eta^*(\omega \rightarrow 0) = \eta^1(\omega \rightarrow 0) = \eta^o \quad (2.30)$$

### Stress relaxation:

In Maxwell fluids, the applied stress can relax with time according to the following equation :

$$\sigma(t) = \sigma(0) \exp\left(-\frac{t}{\tau}\right) \quad (2.31)$$

The relaxation time is related to the viscosity per the modulus.

$$\tau = \frac{\eta}{G^o} \quad (2.32)$$

$$G^o(t) = \frac{\sigma(t)}{\gamma} = \frac{\sigma(0)}{\gamma} \exp\left(-\frac{t}{\tau}\right) \quad (2.33)$$

then,

$$G^o(t) = G^o \exp\left(-\frac{t}{\tau}\right) \quad (2.34)$$

when the time is very short  $G^o$  will be equal to  $G^o$

$$G^o(t \rightarrow 0) = G^o \quad (2.35)$$

### Normal stress [109]

The force acting on a volume element of a fluid can be volumetric (gravity force, electric force ) or surface force. An important example of a surface force is the viscous force. The mathematical description of the surface force is done naturally with the help of tensor quantities in the following way:

- 1- Small surface element emerged in a bulk of fluid.
- 2- Surface element is described by its normal vector. Vector normal to the surface  $\vec{N}$  of three components in respect to a general coordinate system:  $\vec{N} = (n_x, n_y, n_z)$
- 3- On the small surface acts a force with three components respect to normal vector of surface  $\vec{N}$ . So the force will be in the following form:  $\vec{F} = (F_{nx}, F_{ny}, F_{nz})$ .
- 4- When surface components are combined with force components,  $3 \times 3 = 9$  component object are resulted and they are called stress tensors.

The above steps are explained in the following steps:

The component which is perpendicular to the surface is defined as normal vector. Normal vector has three components in Cartesian coordinates  $n_x, n_y, n_z$ .

If a force is applied on a small area of a body which is small enough for the stress components to be regarded as constant, this force will have also three components in Cartesian coordinates  $\sigma_x, \sigma_y, \sigma_z$  or  $F_{nx}, F_{ny}, F_{nz}$  as shown in figure 2.4.

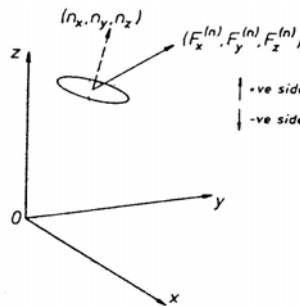


Figure 2.4. : The mutually perpendicular axes  $0x, 0y, 0z$  are used to define the position and orientation of the small area  $\Delta s$  and the force on it. (Reference 109, page: 7)

Now, if we get each component of the force components, everyone will have three orientations in respect to the normal vector components. The force components are used as

$$\vec{F} = (\sigma_{nx}, \sigma_{ny}, \sigma_{nz}) \text{ instead of } \vec{F} = (F_{nx}, F_{ny}, F_{nz}).$$

As a results of this 9 components are obtained for the orientation on the surface and its regard to the force components. Using tensor-algebra (see ref. 110 for an arbitrary list of introductions to tensors), the components can be presented in the following way:

$$\hat{\sigma} = \begin{pmatrix} \sigma_{xx} & \sigma_{xy} & \sigma_{xz} \\ \sigma_{yx} & \sigma_{yy} & \sigma_{yz} \\ \sigma_{zx} & \sigma_{zy} & \sigma_{zz} \end{pmatrix} \quad (2.36)$$

at which the first index refers to the orientation of plane surface and the second index refers to the direction of the stress. The viscosity which represent the system as a result of the whole stress distributions is given by the following equation :

$$\vec{v} = \hat{\sigma} \times \nabla, \quad \nabla = \left( \frac{d}{dx}, \frac{d}{dy}, \frac{d}{dz} \right) \quad (2.37)$$

From all of these 9 components, only 6 components are different, because there are 6 symmetrical components, so only 6 components are effective.

$$\hat{\sigma} = \begin{pmatrix} \sigma_{xx} & \sigma_{xy} & \sigma_{xz} \\ \sigma_{yx} & \sigma_{yy} & \sigma_{yz} \\ \sigma_{zx} & \sigma_{zy} & \sigma_{zz} \end{pmatrix}$$

For example,  $\sigma_{xx}, \sigma_{yy}, \sigma_{zz}$  are the effective components. If both the orientation of plane surface and direction of stress are similar, then they are called normal stress, so  $\sigma_{xx}, \sigma_{yy}, \sigma_{zz}$  are normal stress components. While the other three components have different stress direction from plane surface orientation (perpendicular to normal force), so they are called shear stress.

### Normal stress of Newtonian liquids.

If one imagines that there is a base moving in x-direction, as a result of applying constant shear rate on liquid that consists of many layers, then the layers which are close to the base will be moving faster than the layers which are distant.

$$Velocity \propto y, \quad Velocity = (\dot{\gamma})y \quad (2.38)$$

y is the distance from the base in the y-direction. Since the direction of the velocity is in the x-axis and the distance between the base and liquid layers in the y-axis, then

$$V_{(x)} = (\dot{\gamma})y, V_{(y)} = 0, V_{(z)} = 0 \quad (2.39)$$

Since this movement is applied on the sample, the resulted stress will be distributed in the same way that was explained before as 6 components. The normal force which is represented by the three components of  $\sigma_{xx}, \sigma_{yy}, \sigma_{zz}$  is equilibrated by the isotropic pressure in the sample (P); since the two forces are working in different directions, then  $\sigma_{xx} = -p, \sigma_{yy} = -p, \sigma_{zz} = -p$ . Shear stress components  $\sigma_{yz}, \sigma_{yx}, \sigma_{xz}$ , which represent the perpendicular stress to the normal force has only one effective component which is the movement direction  $\sigma_{yx}$ , and it is proportional to the applied shear rate by the relation

$\sigma_{yx} = \eta \dot{\gamma}$ , while the other components are equal to zero, because there is no applied stress in their directions  $\sigma_{yz} = 0, \sigma_{xz} = 0$ . Since the normal stress components are all equal to P (isotropic pressure); then their difference is equal to zero,  $\sigma_{xx} - \sigma_{yy} = 0$  and  $\sigma_{yy} - \sigma_{zz} = 0$ . Since the normal components are equal to zero, so the difference between them is also zero. As a result of that, the newtonian liquids exhibit no normal stress difference [109, page 8].

### Normal stress of Non-Newtonian liquids:

In the case of non-Newtonian liquids, for example a sample has rod like micelle phase structure, if a stress is applied on a sample in certain direction, this will be resulted in stretching of the rods, and they will relax in the opposite direction proportional to the applied shear rate.  $\sigma_{xx} - \sigma_{yy} = N_1(\dot{\gamma})$  and  $\sigma_{yy} - \sigma_{zz} = N_2(\dot{\gamma})$ , where  $N_1$  and  $N_2$  are the normal stress coefficients.  $N_1$  is called the first normal stress difference while  $N_2$  is called the second normal stress difference. The other shear stress components are given by the following

equations :  $\sigma_{yx} = \eta\dot{\gamma}(\dot{\gamma})$  and  $\sigma_{yz} = 0, \sigma_{xz} = 0$ . Usually the difference between normal stress components appears after critical shear rate  $\dot{\gamma}_c$ , so they are also represented as

$$\sigma_{xx} - \sigma_{yy} = N_1(\dot{\gamma} - \dot{\gamma}_c)$$

### Method of measuring $N_1$

Cone- and-plate flow is the most commonly used for determining the normal stress differences. The test liquid is contained between a rotating cone and a flat stationary plate. The normal stress differences can be calculated using the following equation:

$$F = \frac{\pi a^2}{2} N_1(\dot{\gamma}) \quad (2.40)$$

Where  $F$  is the total normal force and  $a$  is the radius of stationary plate. This force acts in the direction of the axis of rotation and pushes the cone and plate apart. It is essentially the same force that produces the Weissenberg rod-climbing effect [109, page: 67].

### 2.7 Differential Scanning Calorimetry :

Differential Scanning Calorimetry DSC is a thermal technique in which the temperature of a sample, compared with the temperature of thermally inert material, is recorded as a function of the furnace temperature as the sample is heated or cooled at a uniform rate. Temperature changes in the sample are due to endothermic or exothermic enthalpy transition such as that caused by chemical reactions or phase changes. In the most DSC design, two pans sit on a pair of identically positioned platforms connected to a furnace by a common heat flow path. In one pan, the tested sample is introduced, while the another one is the reference pan (it contains usually the solvent). When the furnace is turned on by the connected computer, the two pans are heated or cooled at the same time and at a certain specific rate. The computer assures that the two heating (cooling) rates for the sample and the reference remain the same. At the transition points, for example endothermic transition, more heat is given for the sample to keep the temperature of the sample pan increasing at the same rate as the reference pan. If the temperature increases is plotted on the x-axis and the difference in the heat flow between the sample and the reference on the y-axis, DSC plot is obtained. Heat flow is the result of dividing the amount of heat ( $q$ ) per time( $t$ ), while the heating rate is the temperature increase( $\Delta T$ ) per time. Dividing both quantities produce the heating capacity ( $C_p$ ). This can mathematically be represented as follows:

$$\frac{\text{heat}}{\text{time}} = \frac{q}{t} = \text{heat flow}, \quad \frac{\text{Temperature increase}}{\text{time}} = \frac{\Delta T}{t} = \text{heating rate}$$

$$\frac{\text{heat flow}}{\text{heating rate}} = \frac{\frac{q}{t}}{\frac{\Delta T}{t}} = \frac{q}{\Delta T} = C_p \quad (2.41)$$

### 2.8 Surface Tension Measurement [89,112]:

Surface tension is the force in dyne requires to break a film of length 1 cm (dyn/cm, or mN/m). Equivalently, it is stated as surface energy in ergs per square centimeter (erg/cm<sup>2</sup> or J/m<sup>2</sup>). Thermodynamically, surface tension is given by the equation:

$$\sigma = \left. \frac{\partial U}{\partial A} \right|_{V,S,n} \quad (2.42)$$

which means that the internal energy  $U$  for a body (condensed phase) at certain volume, enthalpy, and mole is depending on the area of the surface. Surface tension is measured using many methods; droop volume method, capillary method, and ring method. In this work, the surface tension was measured using the ring method at 25 °C. The ring is made from platinum-Iridium. It is burned before starting the measurements to distract the impurities. The ring is impressed in the measured solution and then pulled out slowly. After the pulling a thin film from the solution is formed. Briefly before pulling the thin film from the solution surface, a maximum force is needed  $F_{\max}$ . This maximum force  $F_{\max}$  is measured and recorded by the tensiometer. Using equation 2.43, surface tension can automatically be calculated as follows:

$$\sigma = \frac{K.F_{\max}}{2.U} \quad (2.43)$$

where K is correction factor, and U is the ring circumference.

### 2.9 Methods:

Freeze Fracture Transmission Electron Microscopy (FF-TEM), The microstructure of the samples was also examined by freeze-fracture electron microscopy (FF- TEM). For the FF-TEM, small amounts of the sample were placed on a 0.1 mm thick copper disk covered with a second copper disk. The sample was frozen by plunging this sandwich into liquid propane (cooled by liquid nitrogen). Fracturing and replication were carried out in a freeze fracture apparatus (Balzers BAF 400, Germany) at a temperature of -140 °C. Pt/C was

deposited at an angle of  $45^\circ$ , and the formed replicas were examined in a CEM 902 electron microscope (Zeiss, Germany).

**Cryogenic Temperature Transmission Electron Microscopy (Cryo-TEM)**, very thin films of the micellar solution is placed on a narrow-mesh specimen grid and quenched rapidly to the glassy state and the thin film is then directly viewed by TEM (LEO 912AB, 120 kv Instrument, Germany).

**Differential Interface Contrast Microscopy (DICM)**, some drops of the solution are placed on microscope glass and covered by another one and examined by the DICM which is from LEICA DMREX company (Germany).

**Polarizers**, The texture of the multilamellar vesicles phases was determined using a Standard Pol16 of Zeiss (Germany) equipped with a hot stage (Mettler FP 82).

**Small Angle Neutron Scattering (SANS)**, D11 small angle diffractometer instrument was used ( The measurements were made in the institute of Laue-Langevin (ILL) in Grenoble- France).

**Rheological Measurements**, a Haake stress-controlled RS600 (RheoStress RS600) was used. The rheometer is connected to a thermostat TC81 for thermal control. Both a cone plate (C60/1° Titanium with gap 0.051 mm) measuring system and a double gap system were used. The double gap (DG41 Titanium with gap 5.100 mm) is applicable for solutions of low viscosity, while cone plate is used for viscous solutions. For oscillation measurements a frequency from 10 to 0.001 Hz was applied at constant deformation of 0.01 for the whole measurements at  $25^\circ\text{C}$ . First normal stress difference was measured as a function of applied shear rates ( $0.1 - 1000 / \text{s}^{-1}$ ). Sweep measurements were carried out at constant stress ( 0.00 Pa - 70.00 Pa) at frequency of 1.000 Hz. Yield stress measurement at constant stress ( 0.00 Pa - 12.00 Pa.). For double gap measurements a shear rate of ( 0.10 1/s - 1000.00 1/s) was applied. The experimental conditions were kept the same for the whole solutions to have reasonable comparison.

Conductivity measurements, a WTW (Wissenschaftlich-Technische Werkstätten GmbH, Germany) conductivity instrument was used with electrode (TetraCon 325, Standard-Conductivity cell).

pH measurements, a WTW (Wissenschaftlich-Technische Werkstätten GmbH, Germany) pH-DIGI 520 meter was used.

Differential Scanning Calorimetry (DSC) measurements, a "Micro-DSC" of Setaram (France) was employed. The samples were sealed in aluminum pans. As reference a sealed pan with the corresponding amount of water was used. To check water evaporation the pans were weighed before and after the DSC measurements. The DSC thermograms were recorded in the temperature range from 1 to 70 °C, at heating rate 0.2 °C/min and cooling rate 0.2 °C/min.

**Surface Tension Measurements :** The measurements were carried out using LAUDA (TEIC) Tensiometer measures with ring method.

### 2.10 Chemicals:

Cetyltrimethylammonium Bromide CTAB was purchased from Fluka with purity > 99%. Tetradecyltrimethylammonium Bromide TDTAB, Dodecyltrimethylammonium Bromide DOTAB, Decyltrimethylammonium Bromide DTAB and Octyltrimethylammonium Bromide OTAB were from Aldrich with purity > 99%. CTAOH, TDTAOH, DOTAOH, DTAOH and OTAOH stock solutions were prepared from CTAB, TDTAB, DOTAB, DTAB and OTAB - solutions by ion-exchange at 25°C (for CTAB at 35°C). The Ion exchanger was from Merck (Strongly basic anion exchanger with ion exchanging capacity > 0.9 mmole/ml). The concentration of the resulted  $C_x$ TAOH ( $x = 8, 10, 12, 14$  or  $16$ ) was determined by pH-titration against 0.1mM HCl.  $x$ -hydroxy,  $y$ -naphthoic acid  $x,y$  HNC (3,2, 2,1 and 6,2 HNC) were from Fluka with purity >97%. All used without further purification. The solutions were prepared by adding an increasing amount of the acids to 100 mM of  $C_x$ TAOH. The solutions were homogenized by mixing and room temperature for at least one day. For 2,1 and 6,2 HNC mixed with CTAOH, solutions were allowed to equilibrate for at least one week at 25 °C, while for 3,2 HNC mixed with CTAOH, they were allowed to equilibrate for at least one week at 40 °C. NaCl was from Merck with purity > 99.5 %.

### 3. Results and Discussion

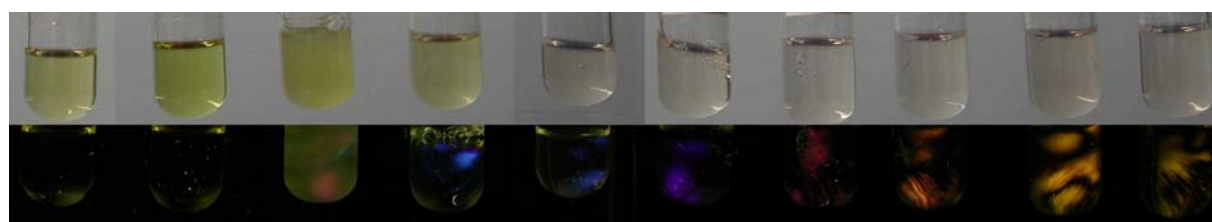
#### 3.1 The System 2,1HNC /CTAOH /water

Horbarschek et al [113] have studied the system 3-hydroxy-2-naphthoic acid/cetyltrimethylammonium hydroxide (3,2 HNC/CTAOH) and reported a single phase in the mixed system of 3,2 HNC/CTAOH up to a mole ratio  $r \sim 0.95$ . With further increase in the  $r$ -value (0.95 to 1.1), the authors noted a turbid phase region at 40 °C. Addition of excess 3,2 HNC was however found to be retained in an un-reacted form. Manohar et al. prepared CTAHNC by mixing equimolar solutions of NaHNC (made from 3,2 HNC) and CTAB, then extracted the resulting CTAHNC counterions with methyl isobutyl ketone as extracting solvent[76]. The authors noticed that the addition of ionic surfactants such as CTAB induces a transition from vesicles to rodlike micelles probably by the charging of the former. With an attempt to study the effect of relative position of hydroxyl and carboxyl groups on naphthoic moiety, the present study reports the mixed system of 2-hydroxy-1-naphthoic acid (2,1 HNC) /CTAOH with a wide variation in the mole ratio, i.e  $r = 0.0-1.5$ . It was observed that the CTAHNC obtained from the equi-mole compositions of 2,1 HNC and CTAOH is present as a single clear phase at room temperature in contrast to the two phase region formed from the mixing of 3,2 HNC and CTAOH in equi-mole composition [110]. It is further found that the excess addition of 2,1 HNC to 100 mM CTAOH, ( $r \sim 1.5$ ), the resulting complex still solubilized the excess 2,1 HNC and the solutions were found to change their color systematically when they were observed between two crossed polarizers.

##### 3.1.1 Phase Behavior

The solutions with different mixtures containing a fixed amount 100 mM CTAOH (prepared via ion exchange process from CTAB) and varying concentration of 2,1 HNC (0-150 mM) were prepared. The appearance of the phases when the solutions were placed between two crossed polarizers in all the solutions at 25 °C has been displayed in figure 3.1. The initial pH 12 for the CTAOH solution alone started decreasing with increasing addition of 2,1 HNC. This change in pH also caused simultaneous change in the color of the appearance. The solutions showed a yellow color in basic pH, while they are colorless in the acidic pH. Though the pH of the solutions prepared from equimolar composition is 7, the turbidity started setting in before this composition ( $r \sim 0.85-0.9$ ). The solutions prepared with a ratio of  $r \sim 0.8$  or less were found to be in a single micellar phase region and optically isotropic. The solutions with turbidity were partly birefringent and represent coexisting phases (2-phase-region). The coexisting phases do not separate completely because of the high viscosity of the

solution, however, they exhibit lower viscosity compared to the gel regions as shown in the rheological behavior (Figure 3.11). These turbidity in the samples was stable even for few months and did not settle down even after centrifugation. All the solutions with  $r \sim 0.5$  or less were low viscous. Beyond  $r \sim 0.55$  the viscosity starts to rise, and viscoelastic solutions resulted for the ratio  $r \sim 0.6$ . These isotropic viscoelastic solutions that made from rodlike micelles continue to form until the turbid region is reached. When the molar ratio of 2,1 HNC/CTAOH was more than 0.9, a transition was seen to occur from entangled rodlike micelles to vesicles as reflected in the observed birefringence. The solution with 92 mM 2,1 HNC is already in the vesicle phase region. It is birefringent and totally clear. The monitoring of the rheological behavior and color appearance (without polarizers and when they are directly seen) showed that the solutions displaced slight change in color with time up to six months, but without losing either their original phase structure or rheological behavior. This conclusion was further supported from another independent SANS (small angle neutron scattering) measurements where in the spectra remained the same for the solutions initially as well as after six months. In order to understand the reason for the color change in the solutions with time, the same samples were kept under argon atmosphere. It was found that the change in the color was still exists but with slower rate. These results indicate that the change in color (in high and low pH values) takes place due to both hydrolysis and also oxidation, etc .



**20      80      85      90      100      110      120      130      140      150**  
*c* (2,1 HNC)[mM]

*Figure 3.1: Phase behavior of the system CTAOH/2,1 HNC at 25 °C. Samples with 100 mM CTAOH and an increasing amount of 2,1 HNC without polarizers (top row) and between two crossed polarizers (bottom row). The numbers below the pictures indicate the concentration of 2,1 HNC.*

#### 3.1.2 Conductivity and pH Measurements:

The variation of conductivity of solutions prepared by mixing 100 mM CTAOH with increasing amounts of 2,1 HNC at  $T = 25^{\circ}\text{C}$  is shown in figure 3.2. For the proportion which are excess in CTAOH, the solution conductivity decreases almost linearly with increasing concentrations of 2,1 HNC before reaching a value corresponding to the turbid region. The conductivity values in the turbid region show slow decrease before leveling off at higher proportions which correspond to multilamellar phase region. The addition of 2,1 HNC to solutions of CTAOH leads to the neutralization of  $\text{OH}^-$  by the proton of the weak organic acid, i.e. 2,1 HNC and thus to the exchange of  $\text{OH}^-$  for  $\text{HNC}^-$  as counterion of  $\text{CTA}^+$ . The highly hydrated hydroxide is less effective at shielding the head group repulsion than the  $\text{HNC}^-$  counterion, so that the total free ions in the solution are reduced by adding more amount of 2,1 HNC, and consequently causes the conductivity decrease. This decrease can also be attributed to the low mobility of  $\text{HNC}^-$  ions in comparison to  $\text{OH}^-$  ions. After the neutralization, the conductivity remains unaltered even though when the concentration of 2,1 HNC is increased. This result proves that the excess 2,1 HNC has to be in the molecular form and gets solubilized in the hydrophobic surfactants tail regions between the head groups of the two surfactant molecules that consist the exterior part of the bilayers.

Figure 3.2 also shows the variation in the pH as a function of 2,1 HNC concentrations. The most interesting thing about the pH variations is that the solutions with almost equal mole ratio are characterized by neutral ( $\text{pH} = 7$ ) and the solution is clear in appearance with the single phase system. The turbid regions are still seen in the acidic pH range. The observed initial decrease in the pH up to the equimolar composition also directly indicate the acid-base reaction. What is more interesting and logical is the observed constant pH values beyond equimolar composition. As discussed previously the added excess 2,1 HNC has to be enclosed within the two oriented tails of the bilayers, and hence does not contribute to the pH of the solution; thus from simple measurements of conductivity and pH variation, one can draw important conclusion about the residence of water insoluble hydrophobic acid in the complex environment of vesicular solution.

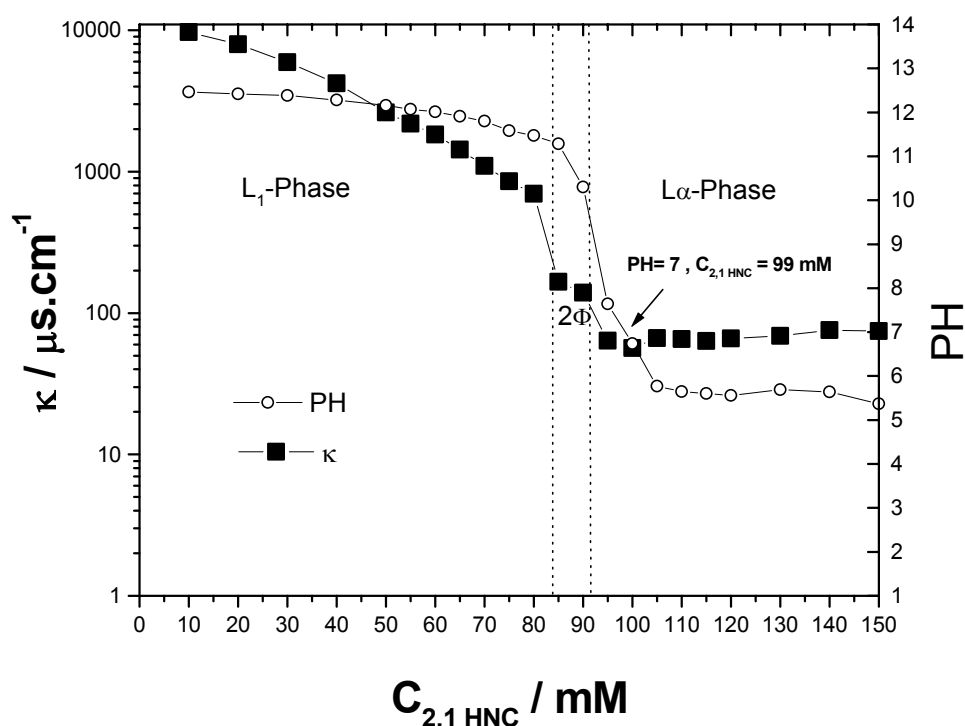


Figure 3.2: Conductivity and pH of 100 mM CTAOH and increasing amounts of 2,1 HNC.

### 3.1.3 Differential interference contrast microscopy

The liquid crystalline phase in the system 2,1 HNC/CTAOH/Water at 25 °C:

Differential interference contrast microscopy was used to characterize the liquid crystalline phases in the system 2,1 HNC/CTAOH at 25 °C. Figure 3.3 shows micrographs of the liquid crystalline phases for the solutions with concentrations of 110, 120, 130 and 140 mM 2,1 HNC mixed with 100 mM CTAOH. The photographs confirm directly the microstructure of the multilamellar vesicles. As the concentration of 2,1 HNC was increased, multilamellar vesicles were more pronounced. At 100 mM of 2,1 HNC, poor contrast was obtained. The multilamellar vesicles are polydisperse in the size distribution. The biggest one has diameters of about 60  $\mu\text{m}$  in the solution containing 140 mM 2,1 HNC. It can further be seen from the figure that out of all the solutions studied, few of them displayed big structured vesicles besides the smaller ones.

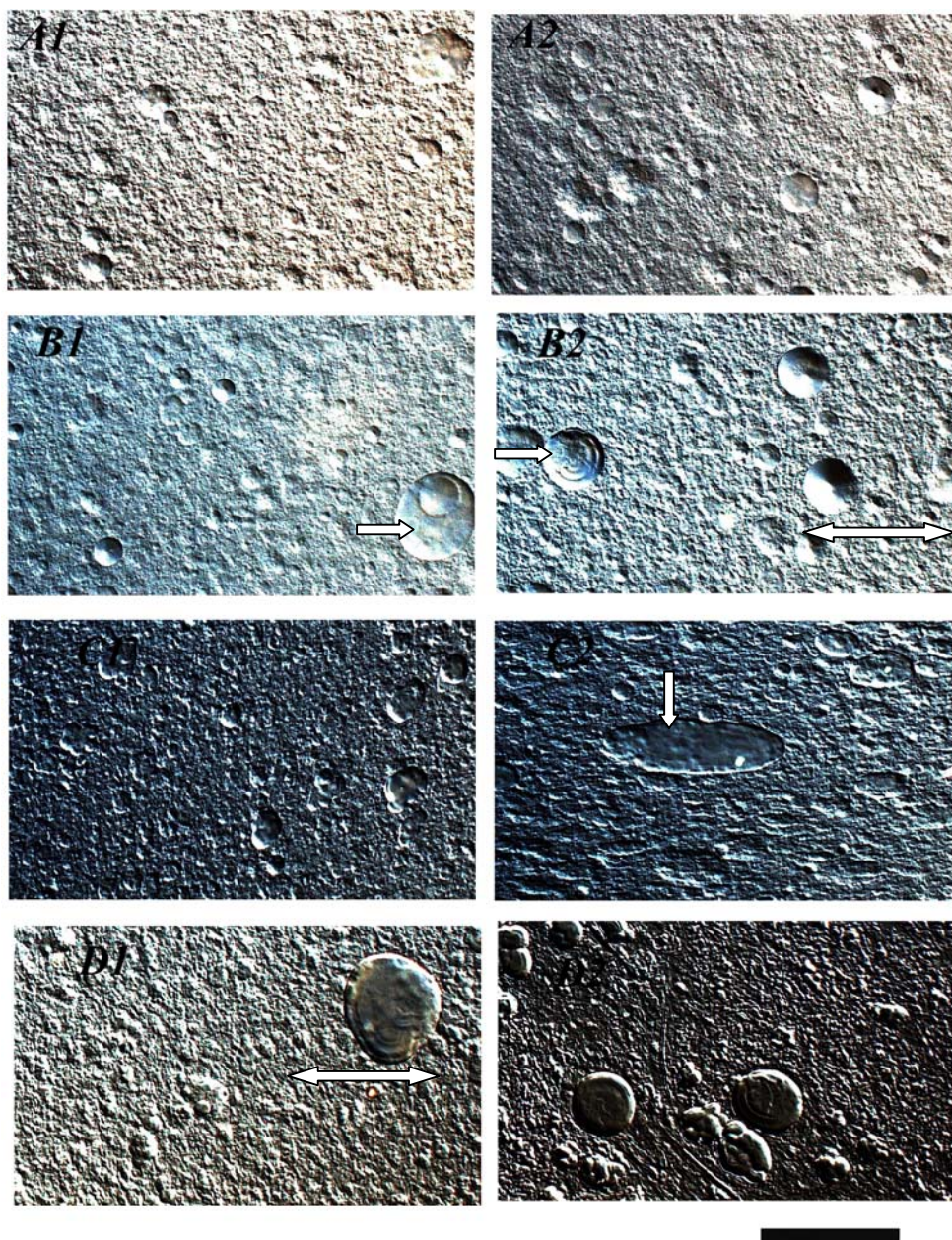


Figure 3.3: Differential interference contrast micrograph for solutions with 100 mM CTAOH and 110 (A1,2), 120 (B1,2), 130 (C1,2) and 140 (D1,2) mM 2,1 HNC at 25 °C. The solutions contain polydisperse multilamellar vesicles. These pictures were obtained from the film of about 20  $\mu\text{m}$  thickness as formed between a cover slip and the glass slide by placing drops of solution in between. The bar (at bottom to right) refers to 100  $\mu\text{m}$ .

The big onion type structures consist either of multitude of layer shells or form because of the deformed lamellar aggregates (as seen in the sample C2, B1, B2, D1 and D2). These vesicles are made from lamellar membranes. These results demonstrate that the technique of

differential interference contrast microscopy is a powerful one for elucidating the microstructure of multilamellar vesicle system.

#### 3.1.4 FF-TEM Micrographs:

It was shown previously (by DICM) that the solutions of 100 mM CTAOH and 2,1 HNC of concentrations higher than 92 mM contain multilamellar vesicles which are densely packed so that they cannot pass each other when a small shear stress is applied to the solution. Multilamellar vesicular structures are clearly visible in freeze-fracture or cryo-TEM micrographs. A typical micrograph obtained from a freeze-fracture replica of 100 mM CTAOH and 100 mM 2,1 HNC is shown in figure 3.4. The picture illustrates that the vesicles are polydisperse in nature. These multilamellar vesicles were uniformly distributed through the sample, indicative of good freezing. The vesicle's membranes are primarily spherical, although some of them are elliptically-shaped. It seems that vesicles exist in the system that consist of one to at least ten different bilayers. For this sample, the interlamellar spacing is in the range of 60 nm. These vesicles represent the same visualized by DIC microscopic technique. The A, B, C and D parts of figure 3.4 represent the pictures with different magnifications and also from different focusing locations for the same solution. The vesicles in general are about 100-1200 nm in diameter. In (Figure 3.4, A) the arrow indicates the membrane rupture caused during preparation conditions (probably in the fracture process). In Figure 3.4, B the four arrows represent a diameter of 932 nm, and it is the diameter for the biggest vesicle which covers the others in the onion shape, so the internal vesicles have to be with smaller diameter. Because the distance between the membranes is about 60 nm, then one can expect about at least ten bilayers in the onion structure. The elliptical shaped and bigger vesicles shown by an arrow in figure 3.4 C would have resulted due to the deformation caused during the specimen preparation. An interlamellar thickness of about 60 nm is ascertained from the indicated opposing arrows of figure 3.4 D.

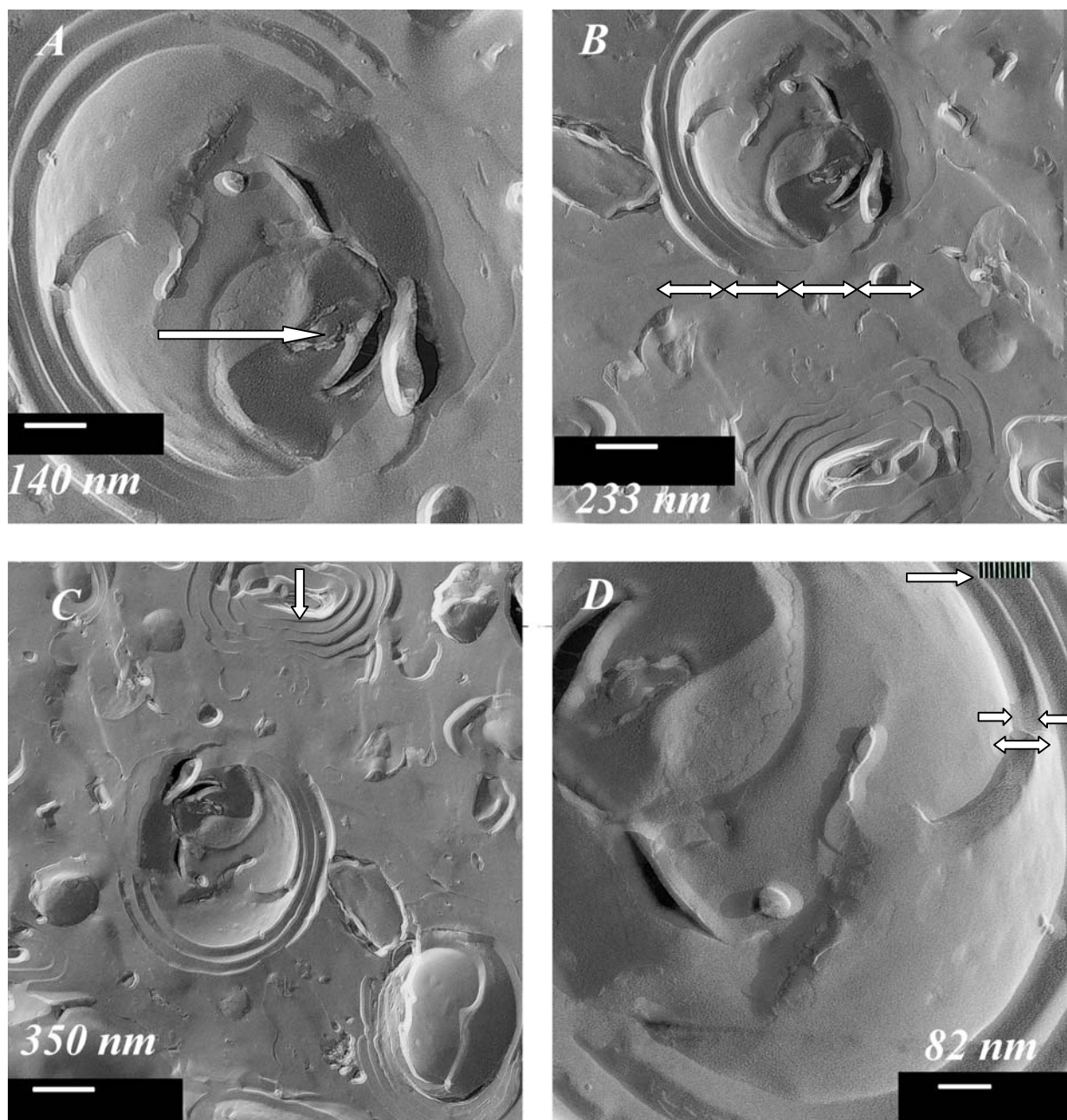
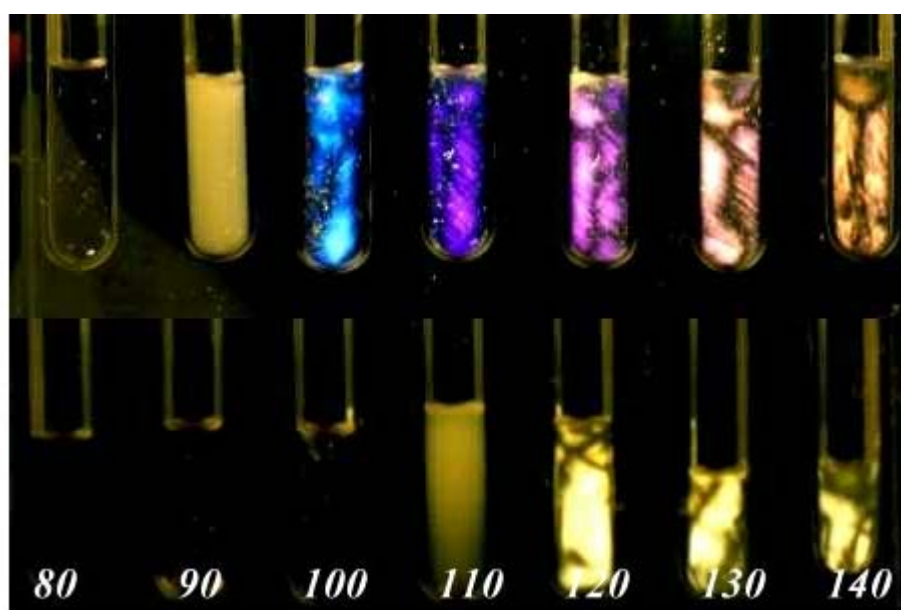


Figure 3.4: FF-TEM electron micrograph for solution with 100 mM CTAOH and 100 mM 2,1 HNC. Figure shows multilamellar vesicles about 100-1200 nm in diameter. A, B, C and D all for the same sample but with different magnifications. In (A) the arrow refers to membrane rupture because of preparation conditions, (B) These four arrows represent 932 nm diameter, and it is the diameter for the biggest vesicle which covers others in the onion (C) the arrow indicates deformed onion, (D) The two opposing arrows indicate the interlamellar spacing of about 60 nm, and each bilayer has about 4 nm thickness.

### Effect of Glycerol on Phase Behavior

The phase behavior in solutions containing 100 mM CTAOH and increasing amounts of 2,1 HNC was examined both in aqueous solutions with and without 20% wt/wt glycerol at room temperature. The addition of glycerol caused a shift of the phase boundaries but does not change the sequence of the phases. Similar results were reported in the literature [114-115]. In this work, the solution of 100 mM CTAOH and 110 mM 2,1 HNC shows slight birefringence after mixing with 20% wt/wt glycerol, and the phase structure consists also of multilamellar vesicles as confirmed by FF-TEM. Figure 3.5 represents the color appearance of the solution without and with glycerol between two crossed polarizers. It can be seen that the addition of glycerol causes a shift of the phase boundaries but does not change the sequence of the phases.



*Figure 3.5 : The addition of glycerol causes a shift of the phase boundaries but does not change the sequence of the phases. The first row shows the solutions between two crossed polarizers before adding glycerol, while the second row shows the same solutions after adding 20% wt/wt glycerol. The solutions are prepared by mixing an increasing amount of 2,1 HNC with 100 mM CTAOH. The numbers at the bottom of the picture indicate the concentration of 2,1 HNC (mM).*

#### The Effect of Glycerol on FF-TEM micrographs:

An electron micrograph of the vesicular phase for system containing 100 mM CTAOH and 110 mM 2,1 HNC with 20% wt/wt glycerol is shown in Figure 3.6. A perusal of the micrographs show the presence of densely packed multilamellar vesicles. The whole volume of the sample is more or less densely filled with bilayers. This is a good indication that the micrographs were taken from a sample in a single-phase region. The vesicles have different diameters and sizes, so, they are polydispersed. The vesicles were found to have similar size range that is 100 to 1000 nm with 60 nm interlamellar distance between the bilayers and the structures correspond to the same in water (figure 3.4). Since the interlamellar thickness is about 60 nm and keeping the requirement of minimum degree of curvature for a vesicle to form, it can be reasoned that the smallest structures (with a diameter of 100 nm) have to be unilamellar only. In the interior of the vesicles there is a solvent from the bulk which surrounds also the vesicle bilayers membrane. Some of the vesicles were covered by larger one, and because of fracture process these vesicle caps were disjoined.

Another electron micrograph of the vesicular phase for the system 100 mM CTAOH and 120 mM HNC mixed with 20% glycerol is shown in figure 3.7 The micrograph looks similar to other micrographs from the other systems, which form multilamellar vesicles [120-129]. As it appears from the figure 3.7, the shape of the vesicles is mostly spherical with some of them in elongated form. This diversity in the shape indicate that the membranes of the vesicles are flexible. The biggest vesicle has a diameter of 800 nm, even though there are several smaller ones. The interlamellar spacing between them is almost similar to those in figure 3.6 i.e. about 60 nm. The vesicles are polydisperse. Sometimes the membranes of the vesicles are found to be broken and these shells do not surround the whole vesicle. There are also some elongated vesicles as shown by the colored arrows on the same figure.

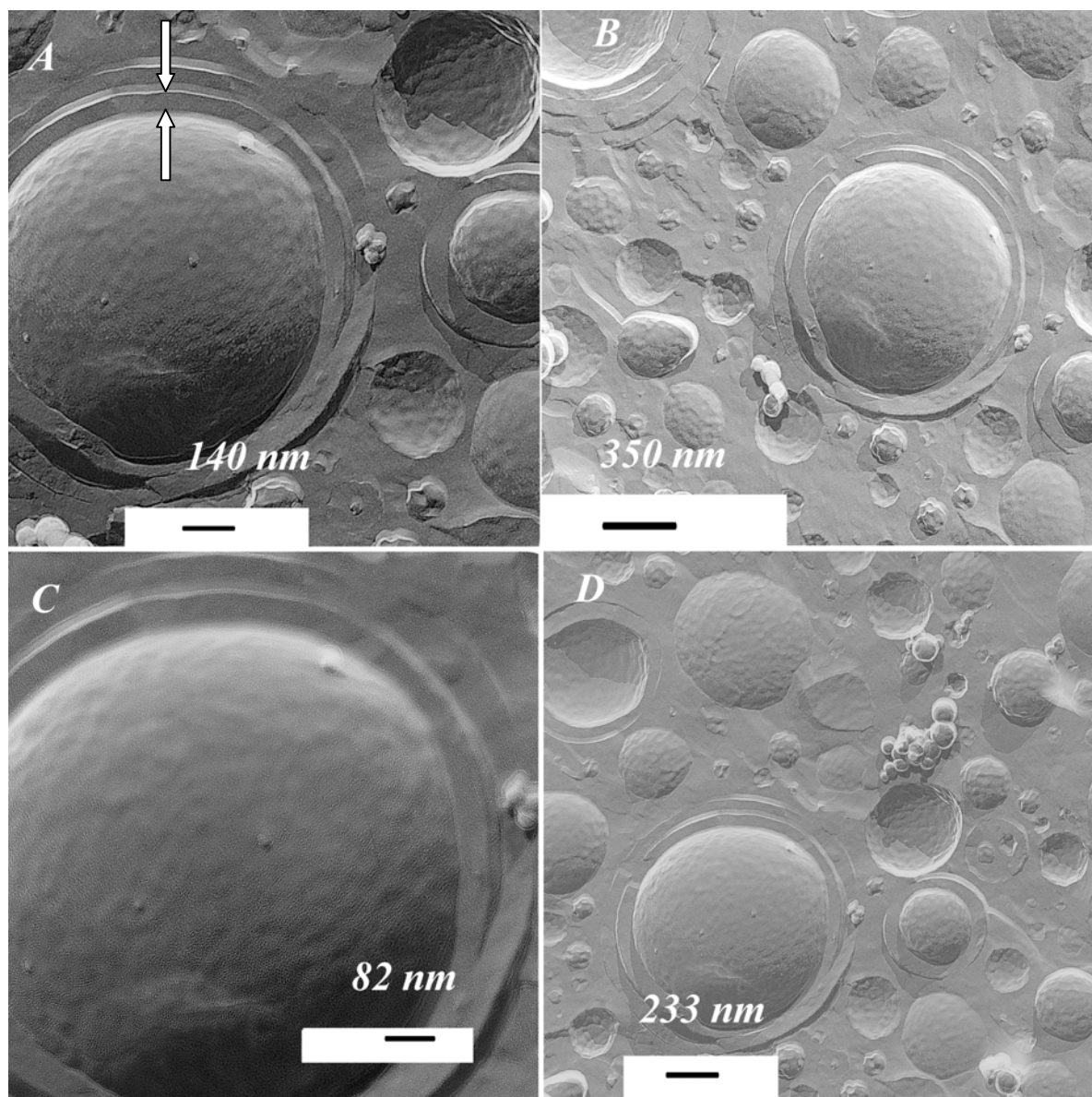


*Figure 3.6: FF-TEM electron micrograph for solution with 100 mM CTAOH and 110 mM 2,1 HNC mixed with 20% wt/wt glycerol showing multilamellar vesicles about 100-1200 nm in diameter. The interlamellar spacing is about 60 nm thickness. A, B, C and D all for the same solutions but with different magnifications.*

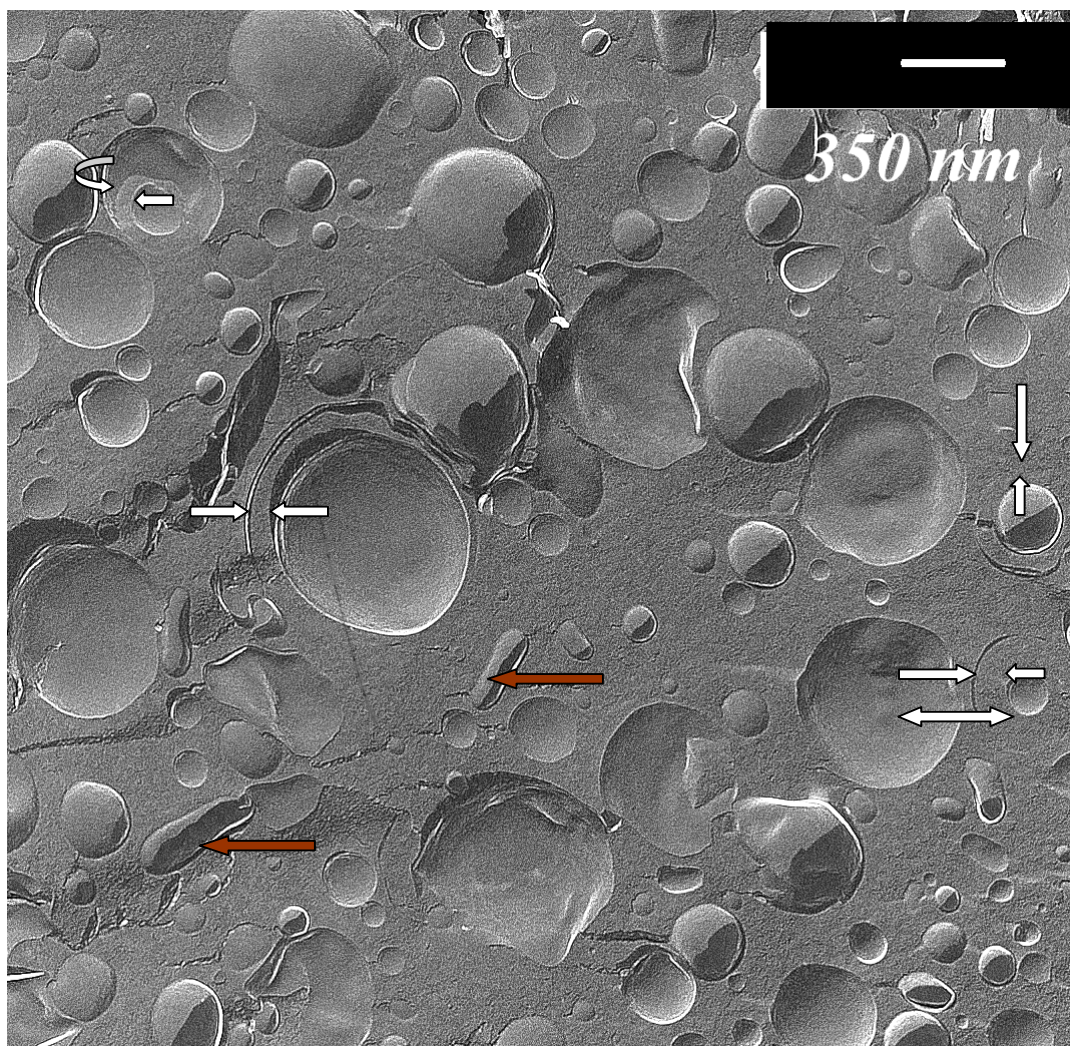


*Figure 3.7: FF-TEM electron micrograph for solution with 100 mM CTAOH and 120 mM 2,1 HNC mixed with 20% wt/wt glycerol. The picture shows multilamellar vesicles about 100-800 nm in diameter, and small vesicles. The interlamellar spacing is about 60 nm thickness. Some arrows indicate to the thickness of the interlamellar spacing between the bilayers, and some of them indicate the elongated vesicles.*

### 3.1.5 Cryo-TEM Micrographs:

The solution containing 100 mM CTAOH and 50 mM 2,1 HNC have micellar aggregates probably with a globular shape. When the concentration of 2,1 HNC is increased beyond 55 mM (as will be described later in the rheological behavior), there is a transition from globular shape to rodlike micelles. The solutions under this transition become highly viscoelastic. The feasibility of such a micellar growth is mainly attributable to a physical effect. This effect has origin in the increased geometric packing parameter of the aggregates of the mixed systems. In micelles of a single ionic surfactants the close approach of the headgroups is limited because of repulsive interactions. It was suggested that the hydrophobicity of the counterion plays an important role in deciding the structure of the supramolecular assemblies such as vesicles or micelles. An electron micrograph of the vesicular phase in the system 100 mM CTAOH and 55 mM HNC is shown in figure 3.8. The microstructure of this solution was revealed by the cryo-TEM micrographs. In this technique, very thin films of micellar solutions were quenched rapidly to the glassy state and the thin film is then directly viewed by TEM. This picture represents the state of associate in the solution. The electron micrograph shows that associates have structures with relatively bigger size than one expects for spherical simple micelles. Thus, the micrographs presented in the figure represent the transition structures from globules to rodlike micelles. The whole volume of the sample is totally filled with these aggregates. Such micelles are too small to be seen by TEM using FF- technique. In cryo-TEM, high magnifications are possible so that detailed microstructures can be characterized. Another feature that can be observed from the micrograph is that the aggregate grow into a continuous network. In Figure 3.8, A, B, C, D and E all for the same solution but with different magnifications or focused locations. In figure E, the aggregates are with linear dimension of about 10-20 nm. They are not spherical-shaped, but elongated. Some of them are with globular-shaped, but longer. They are not long enough like rodlike micelles, so it is highly possible that this is the transition structure of globular-rodlike micelle.

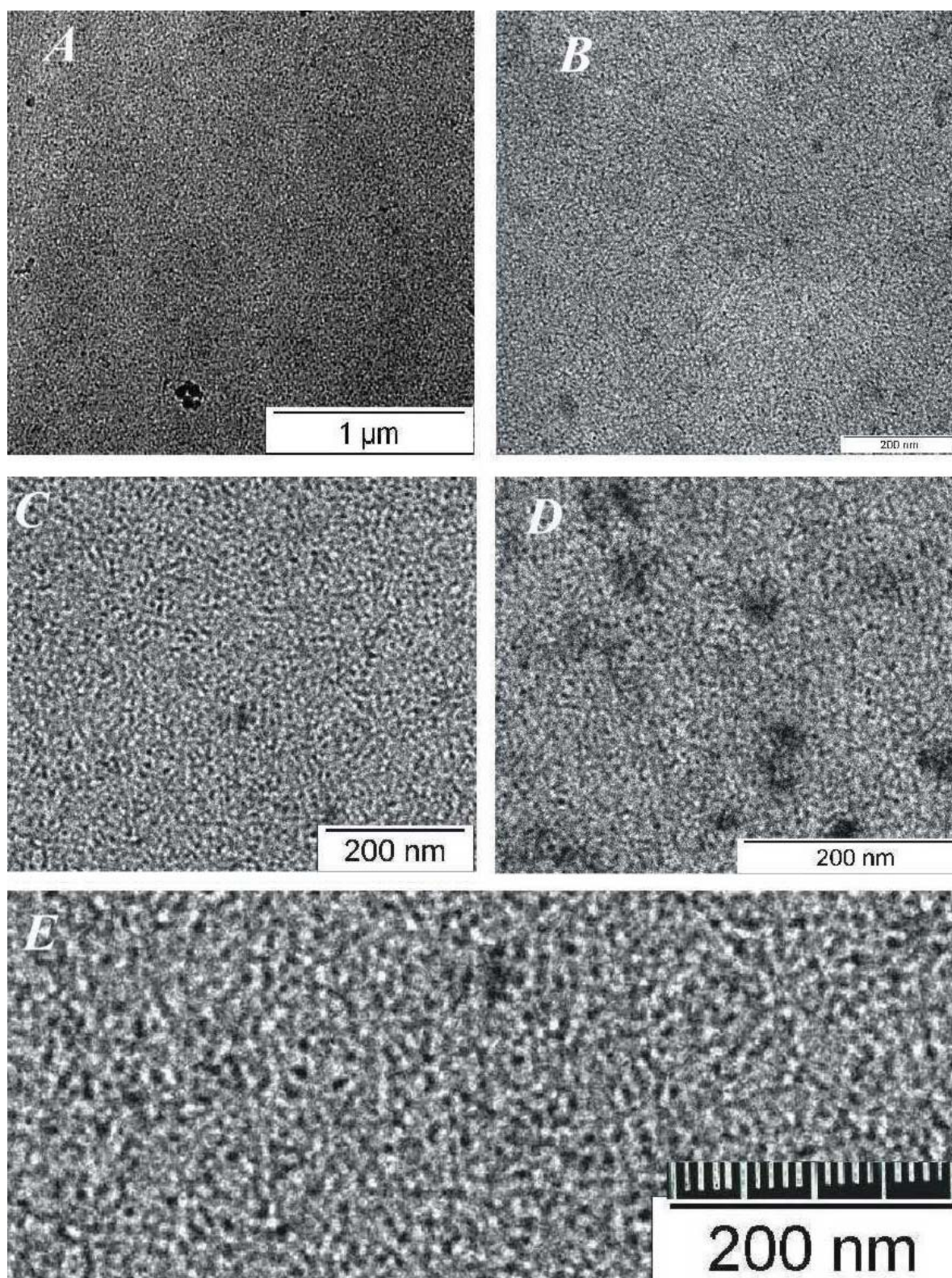


*Figure 3.8: Cryo-TEM micrographs of aggregates in solution consisting of 100 mM CTAOH and 55 mM 2,1 HNC at 25 °C. The aggregates look like a condense and continuous network. This structure represent the transition in shape from globular to rodlike for the micelles.*

Another electron micrograph of the vesicular phase in the system 100 mM CTAOH and 110 mM HNC is shown in figure 3.9. The solution was mixed with 10% wt/v ethanol to decrease the high viscosity of the solution. It has been proven that the vesicles of cationic systems are formed in a mixture of water/ethanol or in pure ethanol [116]. The electron micrographs shown in the figure establish the presence of deformed densely packed multilamellar vesicles. The whole volume of the solution is densely filled with bilayers. This is a good indication that the micrograph was taken from a sample in a single-phase region. The vesicles are polydisperse. Similar results were obtained from FF-TEM for this sample. Here, the diameter varied from 100 nm for smaller vesicles, which covers the core to 1000 nm and more for the outer vesicles. The interlamellar distance between the bilayers is ranged at least from 10 nm to higher side of 100 nm. In some pictures, it appears that the small vesicles are inside big ones, but this may not be a true picture because the technique photographs the cross section of the film and so one can expect the intermingling of associate from different layers. The number of the membranes can be accounted and it is in the range of seven membranes. No unilamellar vesicles are seen alone. In the interior of the vesicles and between the shells there is a solvent from the bulk. The vesicles in the interior are almost spherical-shaped in comparison to bigger ones, because of less flexibility of the membrane when the vesicles are smaller. Such shapes are the equilibrium conformations of vesicles because of the low bending rigidity of mixed bilayers, or they reflect deformation due to shear during sample preparations. The Cryo-TEM look clearer than FF-TEM, since the FF-technique shows only a replica of the surface. The thickness of the bilayer is about 4 nm (as shown in D). Another feature revealed from figure 3.9 B is that the multilamellar vesicles consist of several structures having the size ranging from 100 nm on the smaller side to 1000 nm on the bigger side. Some structures within these multilamellar vesicles have sizes in between the above range. The spacing between the bilayers within the core part of the multilamellar structure was found to have an average value of 100 nm. While, the same spacing for the bilayers on the peripheral side was found to be 10 nm. However, It can be seen from the figure that the difference in the spacing of bilayers for the different parts of multilamellar vesicles is not always observed as some of them have the spacing value same for the inside and outside bilayers (see the arrows in figure 3.9 C). It may be worth mentioning that the conditions used during the specimen preparation for cryo-TEM studies also have a greater effect on the geometrics of the structures. For example, a strong deformation in the vesicles can result when the solution is placed on a flat narrow-mesh specimen grid, so the vesicle are extended to be flat instead of the spherical-shaped as in the bulk of the solution. Another factor is the

evaporation of the water during the preparation conditions. If the film is thin, and the surface area of the film is comparably high, so evaporation of water leads to decrease in interlamellar spacing between the bilayers. With these artifacts being considered, the results from all the microscopic techniques, namely, differential contrast microscopy, FF-TEM and Cryo-TEM discussed above, proved the formation of multilamellar vesicles in the ternary system of CTAOH/2,1 HNC and water.

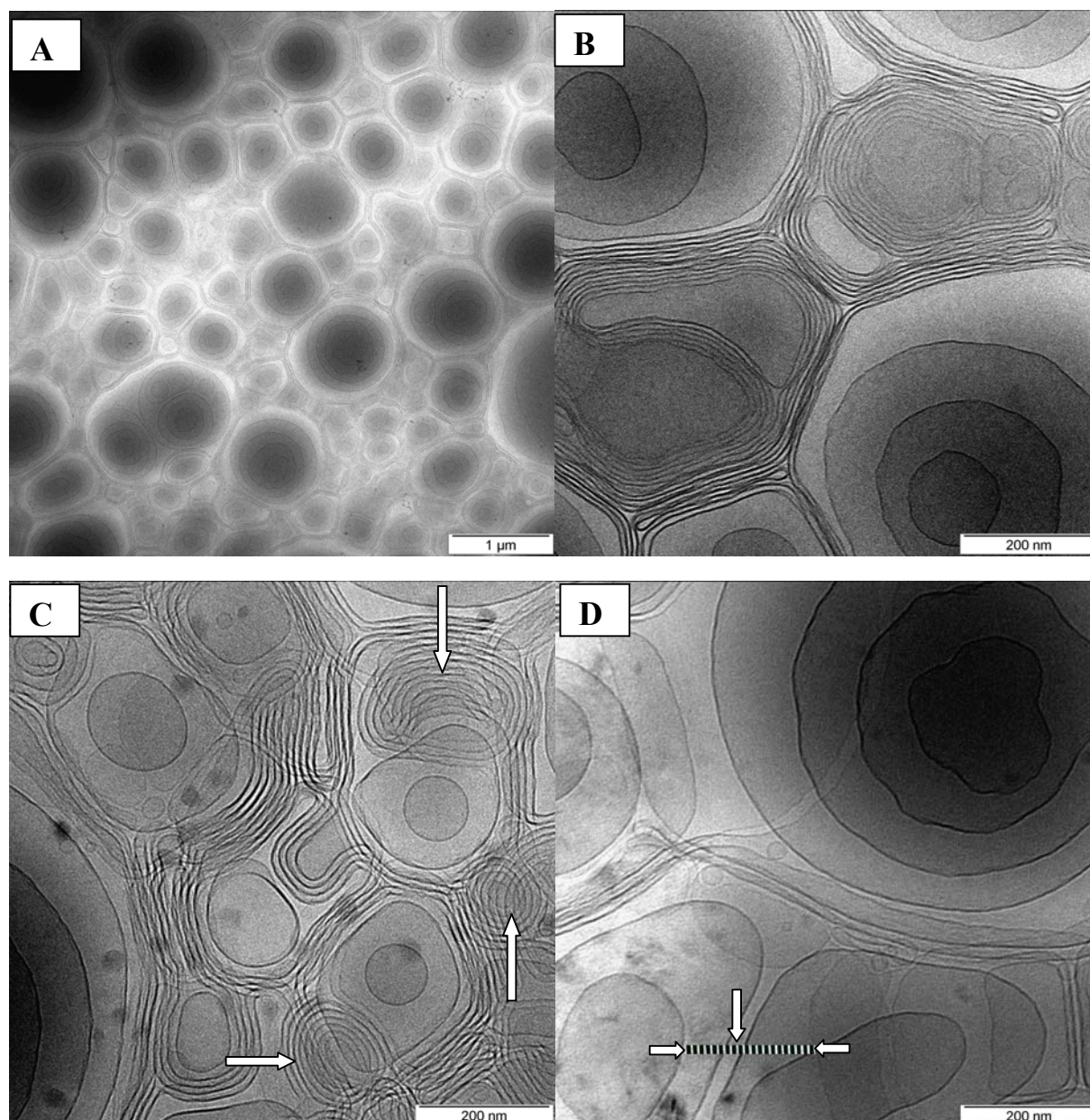
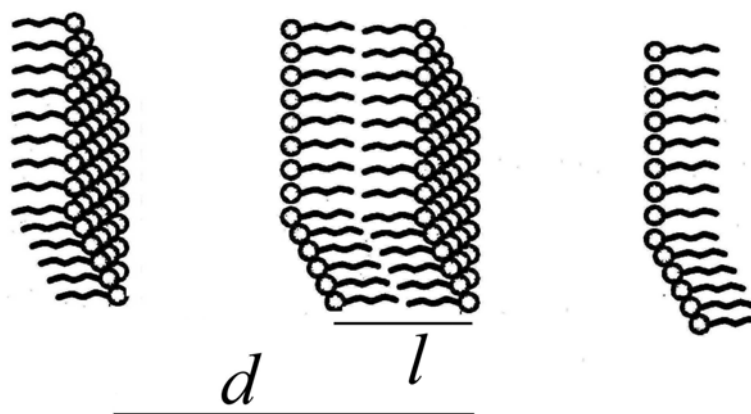


Figure 3.9 : Cryo-TEM for solution with 100 mM CTAOH and 110 mM 2,1 HNC mixed with 10 w/v ethanol at 25 °C. The electron micrograph shows deformed densely packed multilamellar vesicles. A, B, C and D are with different magnifications or with different locations in the same solution. The down arrow in D refers to thickness of the bilayer which is about 4 nm.

## 3.1.6 Small Angle Neutron Scattering (SANS):

SANS curves are shown in figure 3.10 for the solutions with 55, 60, 65, 100, 110 and 120 mM 2,1 HNC mixed with 100 mM CTAOH. The curves of the solutions with 55-65 mM 2,1 HNC show the typical scattering behavior of small aggregates, while the solution of 100, 110 and 120 mM 2,1 HNC show a correlation peak of multilamellar vesicles. Depending on the shape of SANS curve, both qualitative and quantitative information can be derived. From the shape of the curve it is possible to identify the structure of the aggregates, while scattering angle data are used as inputs for some mathematical models to calculate other parameters of the system. Table 3.1 shows some calculations depending from the SANS curves. Scattering vector of maximum intensity i.e.  $q_{\max}$  is used for calculating the bilayer thickness and the interlamellar distance,  $d$  from the relation  $d = 2\pi / q_{\max}$ . Accordingly, the  $d$  values of 62, 60 and 58 nm are calculated for the solutions of 100, 110 and 120 mM 2,1 HNC respectively. These results are in agreement with those obtained from FF-TEM. The thickness of the bilayer is calculated assuming  $\phi = \frac{l}{d}$ , where  $\phi$  is the volume fraction, and  $l$  is the bilayer thickness. These parameters are defined in the following figure:



As listed in the table 3.1, the values of  $l$  is about 30 Å which is in agreement with the chain length of C<sub>16</sub> chain. Here, the bilayer thickness is approximately twice of C<sub>16</sub> chain length. It is shown that as the concentration of 2,1 HNC increases,  $d$  decreases. Increasing the concentration of 2,1 HNC enforce the charged bilayers to become closer. The changing in the interlamellar distance could be also the reason for the systematic changes in the color of solutions when they are seen between two crossed polarizers and also reflected in the phase behavior. For smaller aggregates,  $\phi$  and  $d$  are used to calculate the radius  $R$  of the rodlike

micelles using the relation  $R = \sqrt{\frac{\phi}{\pi}}d$  with the assumption that the rods are arranged in a regular manner (hexagonal nematic order). It can be seen from table 3.1 that the rodlike micelles have a radius of about 16 Å and this could be easily expected for a C<sub>16</sub> hydrophobic chain.

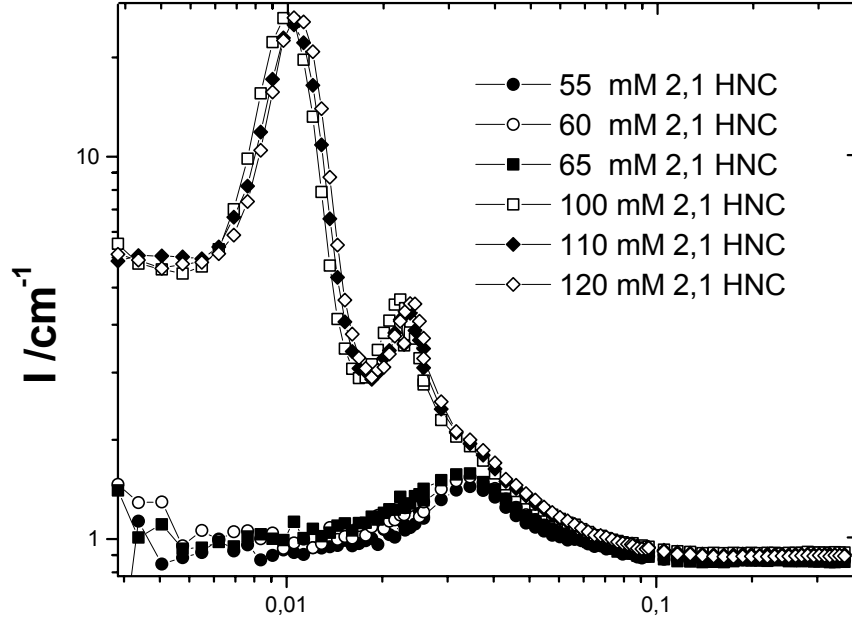


Figure 3.10: The SANS spectra at 25 °C  $q/\text{Å}^{-1}$  correlation peak of multilamellar vesicles for the solutions with 100, 110 and 120 mM 2,1 HNC mixed with 100 mM CTAOH. At concentrations of 55, 60 or 65 mM 2,1 HNC mixed with 100 mM CTAOH, the peak corresponds to smaller micellar aggregates.

Table 3.1:  $\phi$ ,  $q_{\max}$ ,  $d(\text{Å})$  and  $R(\text{Å})$  for the system of 55, 60, 65, 100, 110, and 120 mM 2,1 HNC mixed with 100 mM CTAOH at 25 °C.

Con.	$\phi_{2,1}$ HNC	$\phi_{\text{CTAO}}$ H	$\phi_{\text{CTAOH}}$ + 2,1 HNC	$q_{\max}$	$d(\text{nm})$	$l(\text{Å})$	$R(\text{Å})$
100	0,018	0,029	0,048	0,010	61,99	29,6	
110	0,020	0,029	0,050	0,011	59,73	29,6	
120	0,022	0,029	0,051	0,011	58,03	29,8	
55	0,010	0,029	0,040	0,030	20,65		16
60	0,011	0,029	0,040	0,030	20,65		16
65	0,012	0,029	0,041	0,030	20,65		17

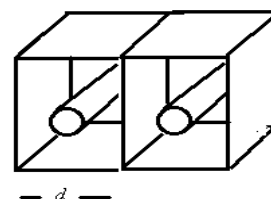
The correlation peak ratio C for the two peaks in L $\alpha$ -phase may be expressed as

$$C = \frac{q_2}{q_1} \text{ or } C = \frac{I_2}{I_1}$$

so accordingly the ratio of the first and second scattering vector at maximum of intensity, which is about  $C = \frac{0,0215}{0,0104}$ , so C is about 2, which is usually corresponded to the presence of lamellar microstructure in the system.

### ***Aggregation number of small rodlike micelles in the system***

For rod in the center of a volumetric cell with length  $d$  (see the figure), the volume of the rod is equal to the volume of the surfactants monomers  $V_m$  multiplied by the aggregation number  $N_{agg}$



$$V = \pi R^2 l = N_{agg} \cdot V_m \quad (1)$$

where  $R$  is the radius (is assumed to be 24 Å, the CTAOH is about 20 Å, and some contribution form the hydrophobic counterion about 4 Å) and  $l$  is the length.  $V_m$  is the volume of surfactant monomers which is given by

$$V_m = \frac{m_{surf}}{\rho} = \frac{M_{wt}}{N_A \cdot \rho} \quad (2)$$

where  $m_{surf}$  is the mass of the surfactant molecule,  $M_{wt}$  is the molecular weight of surfactant molecule and  $\rho$  is the density of the surfactant solution (about 1 g/cm<sup>3</sup>). Accordingly, the volume of surfactant is equal to the volume of CTAOH ( $M_{wt} = 300$  g/mole) and 2,1 HNC ( $M_{wt}=188,18$  g/mole) which is about  $8,1 \times 10^{-22}$  cm<sup>3</sup>. The volume of the cell containing the rods is given by the simple equation

$$V = d^3 \quad (3)$$

The micellar volume fraction for the system 60 mM 2,1HNC and 100 mM CTAOH,  $\phi$  is about 0,040 (as shown in table 3.1).  $d$  is calculated from SANS data using  $d = \frac{2\pi}{q_{max}}$ , so it

is about 206,5 Å (about  $2 \times 10^{-6}$  cm), so the volume of the cell is about  $8 \times 10^{-18}$  cm<sup>3</sup>. The length of the rods is given by  $l = \frac{d^3 \cdot \phi}{\pi R^2}$ . Accordingly the length of the rod is about 194 Å. By

substituting the length and the volume of surfactant molecules in equation 1, the aggregation number will be about **819**. The length of the rods is 8 times bigger than it's radius and the aggregation number is about 16 times higher than the aggregation at cmc. If one assumes lower radius value for the rods, they will be longer than the diameter of the cell  $d$ .

## 3.1.7 Rheological Behavior of the System 2,1 HNC/CTAOH:

The rheological behavior of the system with 100 mM CTAOH and increasing concentrations of 2,1 HNC is depicted in figure 3.11. The variations in the zero shear viscosity for low viscous solutions and complex viscosity for viscoelastic solutions (at a frequency  $\omega = 0.01$  Hz) are shown as a function of 2,1 HNC concentration. The solutions of 2,1 HNC are low viscous when it's concentration is up to 40 mM. At a 2,1 HNC-concentration of 50 mM the viscosity starts to increase and at 60 mM the solutions are strongly viscoelastic, indicating the formation of entangled rodlike micelles. The viscosity decreases again in the turbid region, which starts at 2,1 HNC-concentration of 75 mM. It reaches a minimum of 12 Pas in the two phase region. As the transition to multilamellar vesicle starts, the viscosity rises again and reaches a plateau value of about 600 Pas. This system exhibits unusual and interesting rheological behavior in which two different phase microstructures, namely  $L_1$ - and  $L_{\alpha}$ -phases have similar rheograms. Otherwise, the rheological profile of the solutions can be classified into four different regions (I, II, III and IV). Only the micellar microstructure differs among the regions.

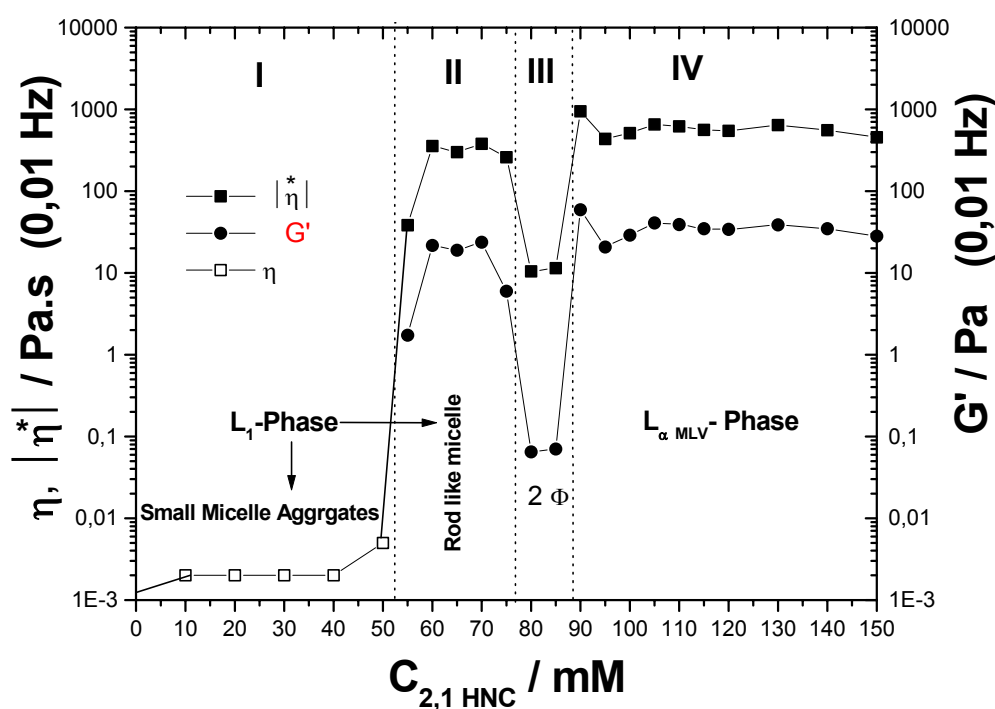


Figure 3.11: Viscosity ( $\eta$ ) obtained by double gap method (DGM), complex viscosity ( $\eta^*$ ) and storage modulus ( $G'$ ) (at 0,01 Hz) obtained from oscillation measurements for 100 mM CTAOH as a function of increasing amounts of 2,1 HNC in (mM) at 25 °C.

Rheological behavior of the low viscosity solutions (region I):

At low concentrations of 2,1 HNC (0-40 mM), the solutions behave as Newtonian fluids and exhibit low viscosity. Double gap method was used for measuring the viscosity of these solutions. Surfactant solutions with small micellar aggregates (globular shaped) always have a low viscosity. The theoretical basis for the viscosity  $\eta$  in this region is according to Einstein's law which says that the viscosity is linearly increasing with the volume fraction  $\phi$  of the particles  $\eta = \eta_s(1 + 2.5\phi)$  at which  $\eta_s$  is the viscosity of the solvent.

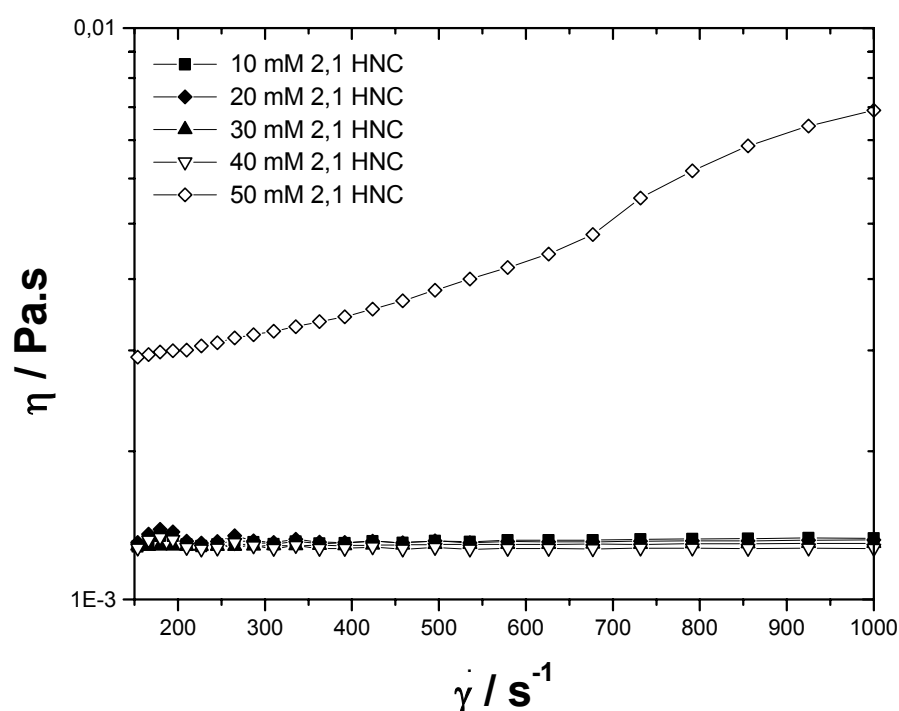


Figure 3.12: Variation of viscosity  $\eta$  versus shear rate  $\dot{\gamma}$  for solutions with 100 mM CTAOH mixed with different concentrations of 2,1 HNC at 25 °C.

At 50 mM 2,1 HNC the solution exhibits shear induced structure, at which the viscosity increases as the shear rate increases. This also called shear thickening. After that the solutions exhibit viscoelasticity. Such behavior is displayed in figure 3.12.

$L_1$ -Phase (Region II) shows rheological behavior similar to  $L_\alpha$ -Phase (region IV)

The variation of storage modulus  $G'$  at 0.01 Hz with 2,1 HNC is also shown in figure 3.11. As the concentration of 2,1 HNC exceeds 55 mM, both complex viscosity and storage modulus rise abruptly. The increasing of storage modulus is accompanied with the micellar growth. As soon as the repulsion between the headgroups of the cationic surfactant are shielded by addition of strongly bound hydrophobic 2,1 HNC counterion, the micelles start to change their structure as a result of decreasing of the charge density at the surface. At 2,1 HNC concentrations higher than 55 mM, the rodlike micelles start to form. Some solutions in the concentration range of 55 to 75 mM, exhibit a viscoelastic behavior, characteristic of entangled rodlike micelles or worm like micelle (Maxwell behavior), while others lack the characteristic features typical of the rodlike micelles. Some of solutions exhibit long relaxation time ( $>1000$  sec), so the solutions show storage modulus parallel to loss modulus in the frequency range 0,001 to 10 Hz which is usually typical for a system with densely packed multilamellar vesicles. This similarity between region II and IV creates some difficulties in distinguishing the phases on the basis of rheograms.

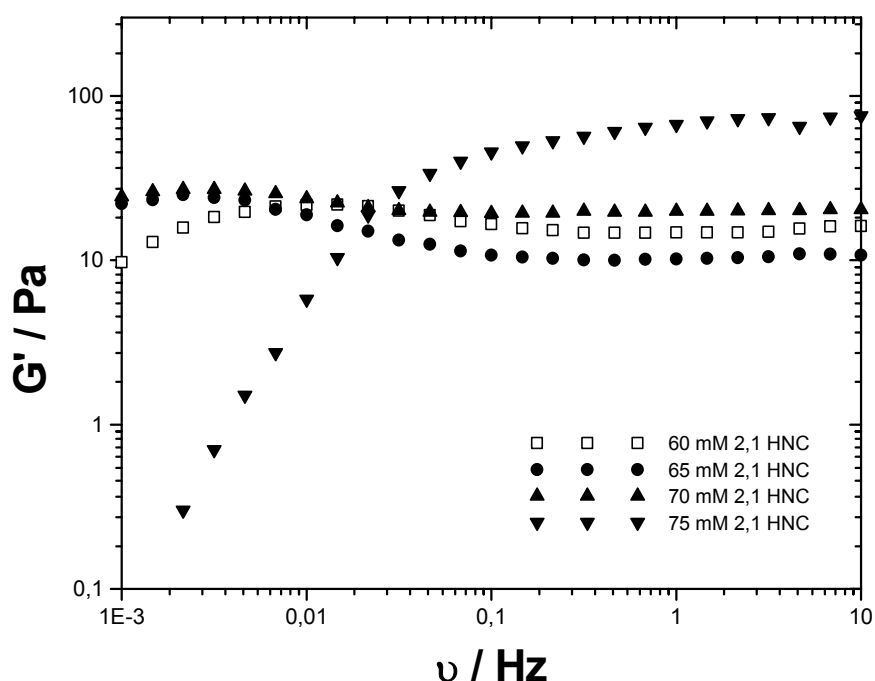


Figure 3.13: Variation of the storage modulus  $G'$  versus frequency  $\nu$  for solutions with 100 mM CTAOH mixed with different concentrations of 2,1 HNC at 25 °C.

Figure 3.13 shows the storage modulus  $G'$  versus frequency for solutions of 60, 65, 70 and 75 mM of 2,1 HNC mixed with 100 mM CTAOH. Solution of 60 mM 2,1 HNC shows relaxation at 0.001 Hz, while 65 and 70 mM 2,1 HNC have relaxation times higher than 1000 seconds (they can't be determined from the rheograms). At 75 mM 2,1 HNC, the system has a remarkable feature and behaves like a simple Maxwell fluid, which means that its rheological properties can be described over a large frequency or shear rate range with single relaxation time. Figure 3.14 shows the complex viscosity versus frequency for the above solutions. Here, the complex viscosity decreases over the whole frequency range from 0.001 Hz to 10 Hz with a slope of about  $-1$  for the solutions of 65 and 70 mM 6,2 HNC, while 60 mM show small relaxation at low angular frequencies. Even these solutions consist of rodlike micelles, but some of them show similar rheograms as for the systems consisting of densely packed multilamellar vesicles.

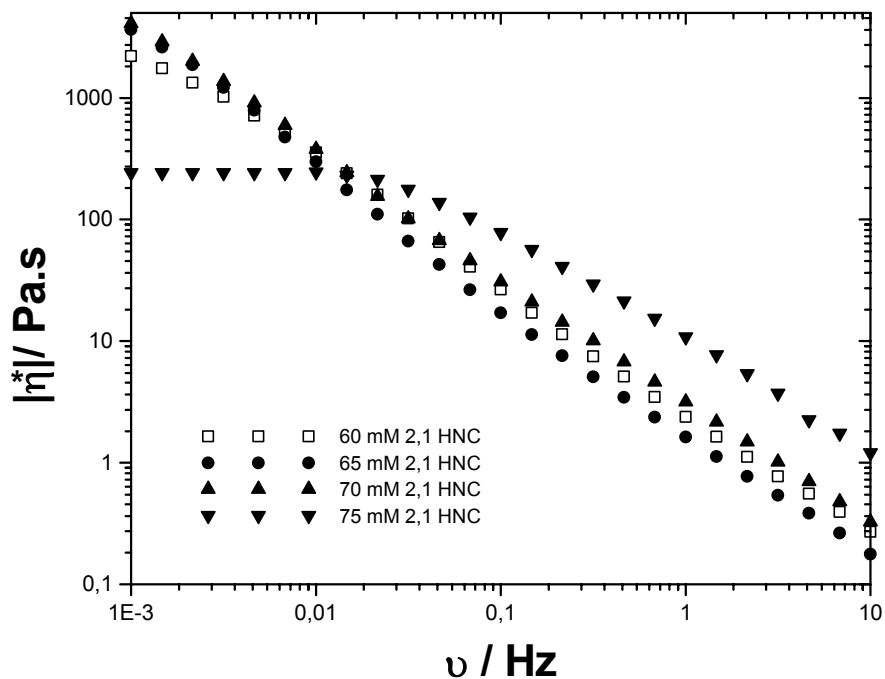


Figure 3.14: Variation of the complex viscosity ( $\eta^*$ ) versus frequency ( $\nu$ ) for solutions with 100 mM CTAOH mixed with different concentrations of 2,1 HNC at 25 °C.

The  $L_1$  phase does not have a true yield stress value but has a finite long structural relaxation time. Small bubbles which are dispersed in the phase, rise within one week or two weeks, even though they seem stationary on a small time scale. If one determines the yield stress value by plotting the shear rate versus the applied stress, these solutions consisting of entangled rodlike micelles show apparent yield stress values. These values of yield stress are the result of long relaxation time due to the retardation of the movement of the rodlike micelles. Long rodlike micelles may build up a temporary quasi-network made from the entanglement of these rods, and as a result the yield stress values are apparent. The value of the yield stress which is an important indicator to distinguish these two different phases is also indicating a new type of similarity. Figure 3.15 A shows that the values of yield stress for 60, 65 and 70 mM 2,1 HNC solutions to be 5.5, 11.5 and 6.7 Pa respectively.

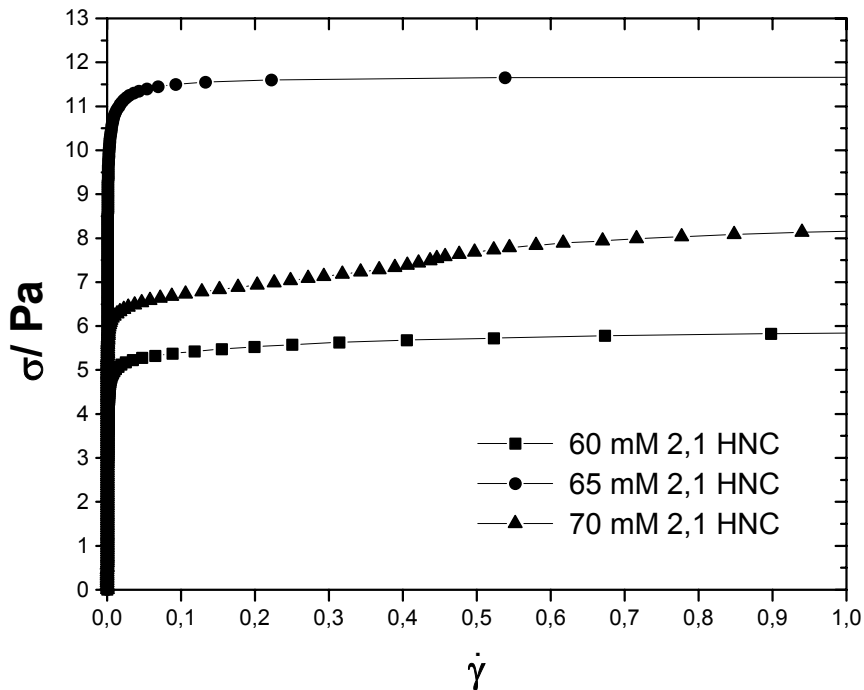


Figure 3.15 A: Applied shear stress ( $\sigma$ ) versus shear rate ( $\dot{\gamma}$ ) for solutions with 100 mM CTAOH mixed with different concentrations of 2,1 HNC at 25 °C.

To check if the solutions have true values of yield stress, the deformation is plotted versus applied stress for two different intervals of time  $\Delta t$ . Figure 3.15 B shows that the solution of 65 mM 2,1 HNC and 100 mM CTAOH dose not have a true yield stress value. The shear rate deformation curves deviate even at small deformation at two interval of time, indicating the absence of true yield stress. This is in agreement with the visual observations for dispersed

bubbles in the phase, at which for the first time small bubbles rise within one week or two weeks, even though they seem stationary on a small time scale. In multilamellar vesicles the dispersed bubbles don't rise even after very long time.

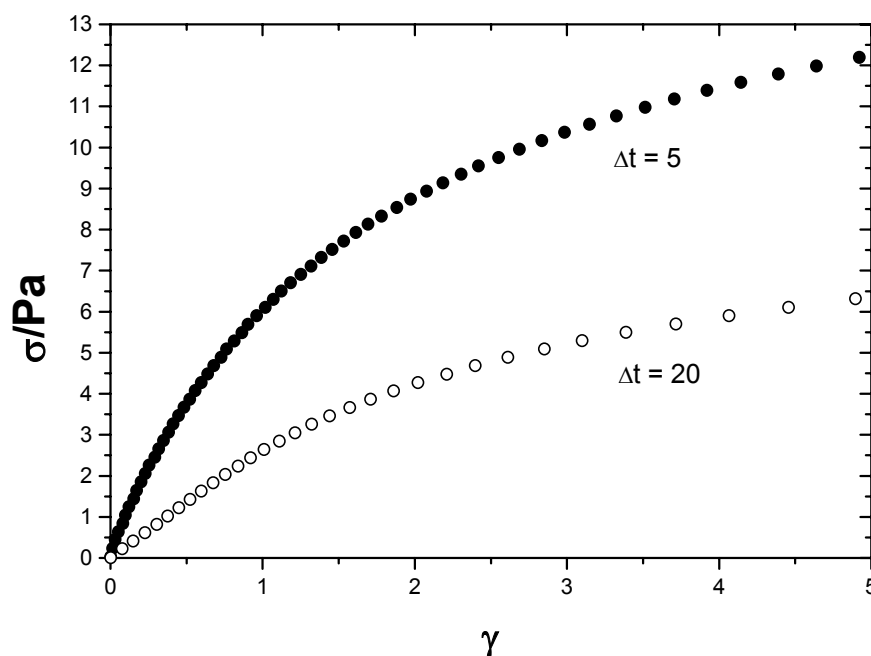


Figure 3.15 B: Applied shear stress ( $\sigma$ ) versus deformation ( $\gamma$ ) for solutions with 100 mM CTAOH and 65 mM 2,1 HNC at 25 °C.

#### Rheological behavior $L_{\alpha}$ -Phase (region IV):

The rheograms of the solutions in the concentration range between 90-150 mM 2,1 HNC show the characteristic features of a system of densely packed multilamellar vesicles. As in Figure 3.16 A, the complex viscosity decreases over the whole frequency range from 0.001 Hz to 10 Hz with a slope of -1. Storage modulus as well as loss modulus are almost independent of frequency. The storage modulus has a value of 30 Pa and thus is about a decade higher than the loss modulus. The value of the yield stress was determined by measuring the deformation of the vesicular solution in dependence of the applied stress (Figure 3.16 B). The yield value is then related to the energy required to deform the vesicles sufficiently so they can pass. The yield stress value was determined to be 1 Pa. The yield stress of this solution is high enough to prevent bubbles, which are trapped in the system from rising.

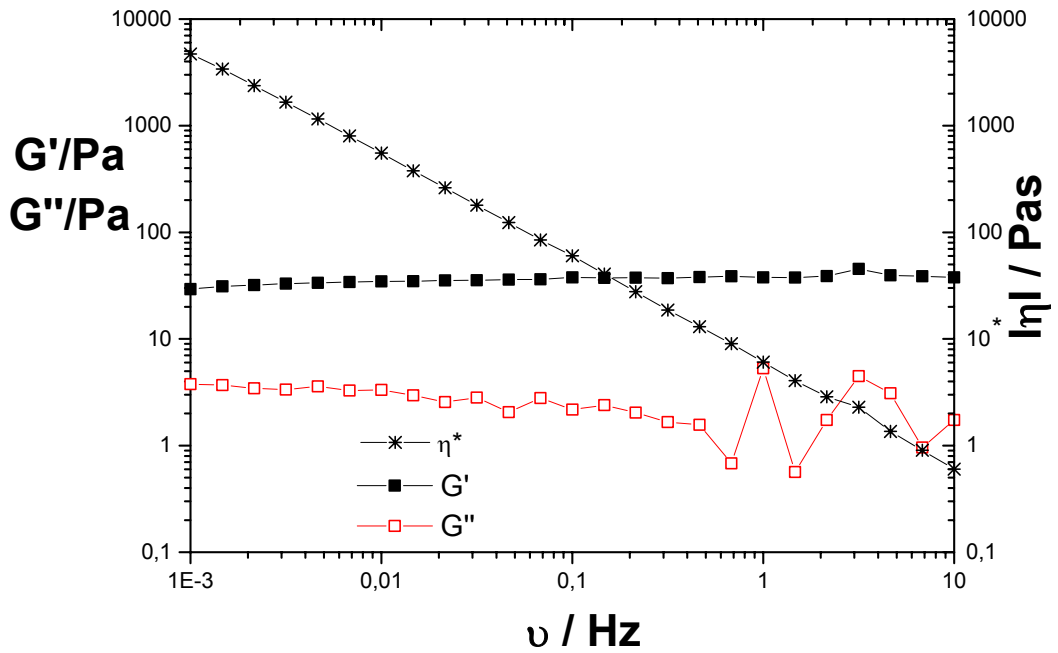


Figure 3.16 A: Variation of the complex viscosity  $\eta^*$ , storage modulus  $G'$  and loss modulus  $G''$  versus frequency for solutions with 100 mM CTAOH and 140 mM 2,1 HNC at 25 °C.

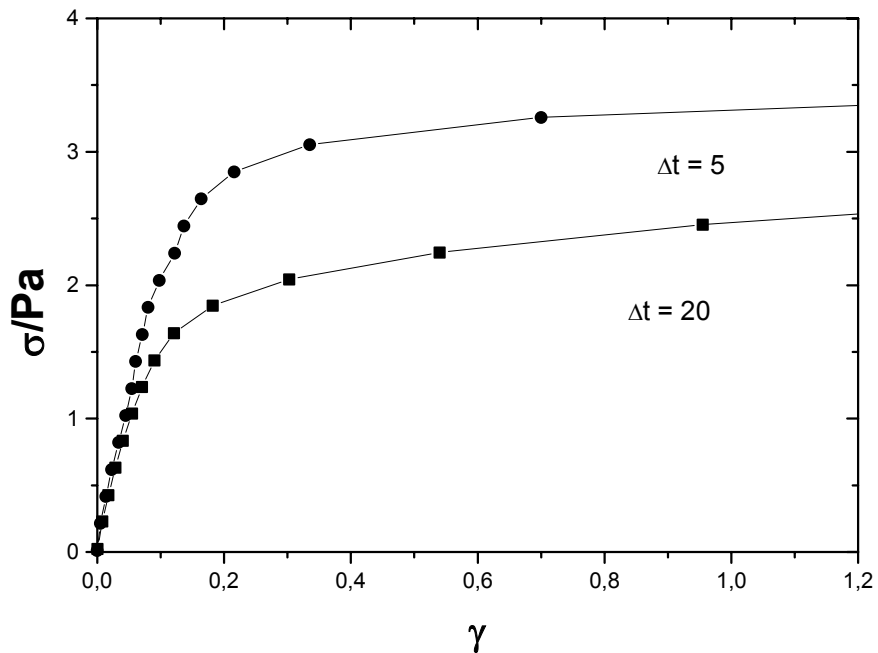


Figure 3.16 B: Applied shear stress ( $\sigma$ ) versus deformation ( $\gamma$ ) for solutions with 100 mM CTAOH and 140 mM 2,1 HNC at 25 °C.

The yield stress values increase slightly with the hydrophobic counterion concentration. Figure 3.17 A shows this relation. The yield stress values were determined from shear rate-shear stress curve (They are the apparent values for rodlike micelles). In the turbid region, no measurements were carried out. After neutralization, the excess 2,1 HNC is solubilized in the bilayers (between the tails) as has been previously proved by conductivity measurements. This may drives the vesicle to behave a little more rigidly, and as a result, the amount of energy required to break the vesicles-network is increased.

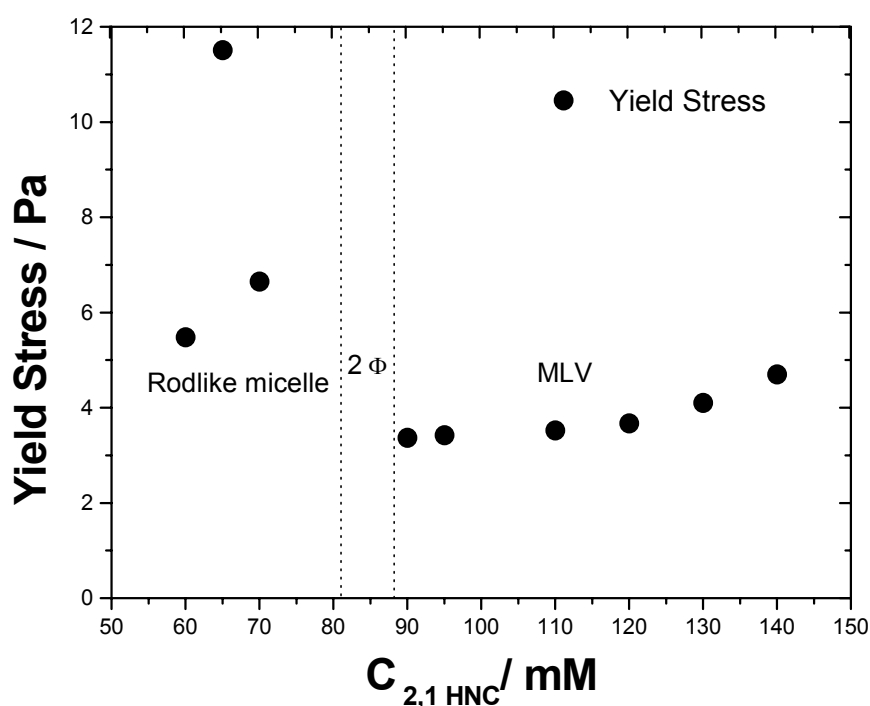


Figure 3.17 A: Yield stress versus 2,1 HNC concentrations (mM) in the mixed system of 100 mM CTAOH and different concentrations of 2,1 HNC at 25 °C.

The effect of 2,1 HNC concentration on the storage modulus in the vesicular region is shown in figure 3.17 B. Almost insignificant changing in storage modulus is observed upon changing the concentration of 2,1 HNC. The excess 2,1 HNC dose not contribute in shielding the charge density of CTAOH. The former is in the molecular form after neutrality. This also explain the only small changes in the yield stress values, at which the yield value is expected to be 10% of the shear modulus for the vesicle solutions.

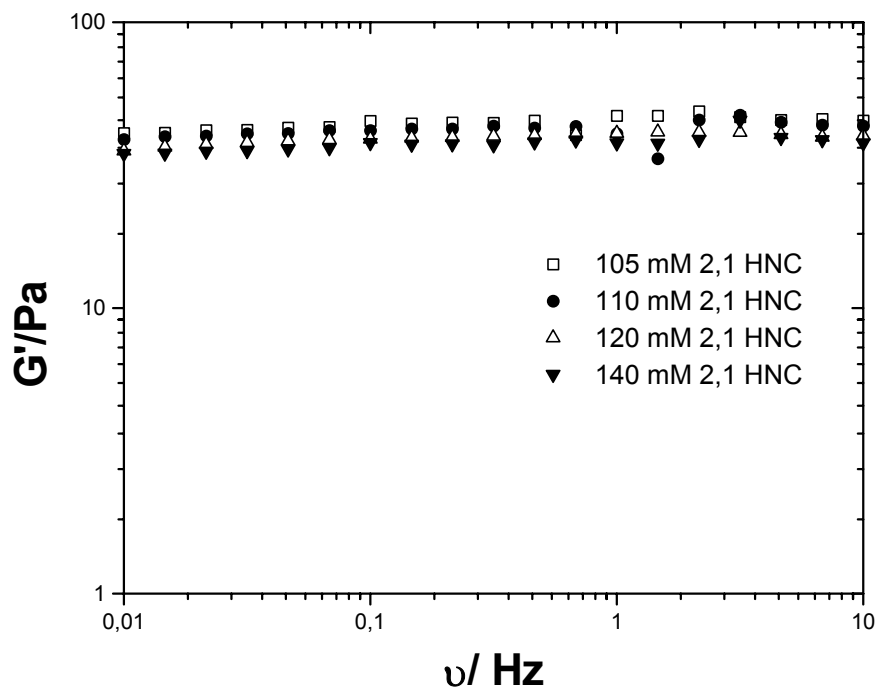


Figure 3.17 B: Storage modulus  $G'$  versus frequency for solutions with 100 mM CTAOH and different concentrations of 2,1 HNC (mM) at 25 °C.

Distinguishing between Regions II& IV by Rheology:

A: Sweep Measurements:

Figure 3.18 shows sweep measurements for solutions with 100 mM CTAOH and different concentrations of 2,1 HNC at 25 °C. In this type of measurements, the value of storage modulus is measured as a function of deformation. The storage modulus is constant at small deformations then starts to decrease at a certain value of deformation, which is the lowest value needed for deforming the network in viscoelastic solutions. They move after small deformations in the network ( $0.1 < \gamma < 0.4$ ) when the stress is applied. Rodlike micelles are more elastic. They can change their length and entanglement when the stress is applied, because of this they don't deform easily as vesicles and they need higher deformation ( $\gamma > 1$ ).

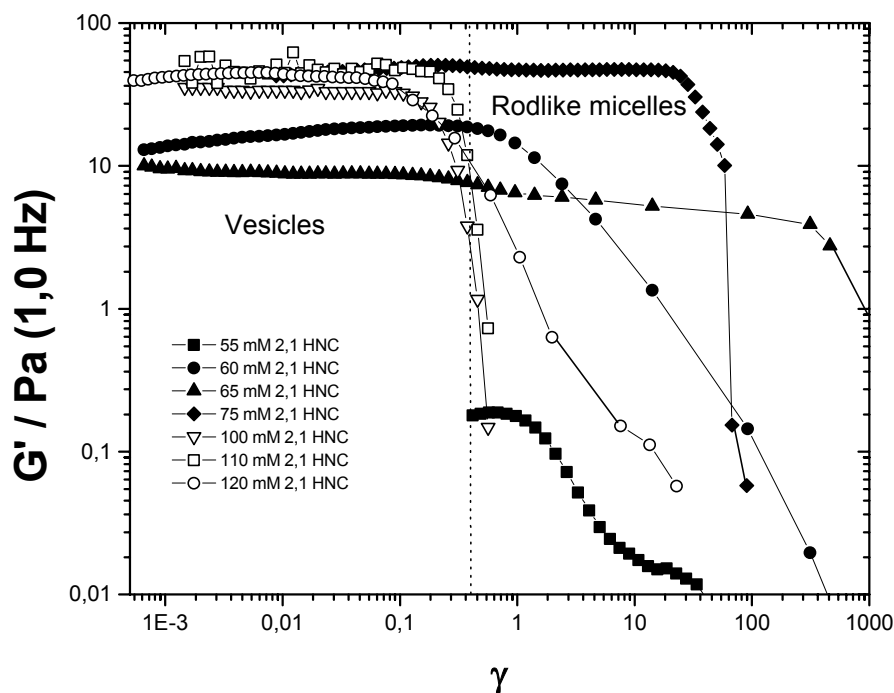
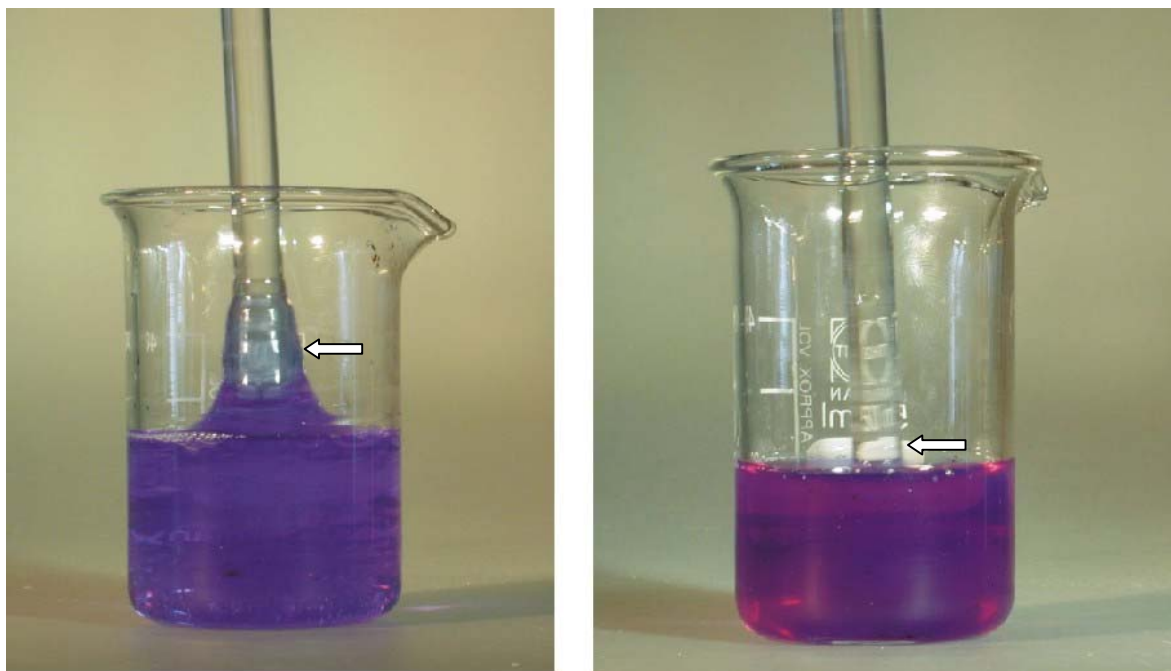


Figure 3.18: Storage modulus ( $G'$ ) versus deformation ( $\gamma$ ) for solutions with 100 mM CTAOH and different concentrations (mM) of 2,1 HNC at 25 °C.

#### B: First normal stress difference:

Weissenberg effect is due to the stress concentrated around a rod rotating quickly in a viscoelastic fluid. It appears that the material is climbing up along the rotating rod. This phenomena is contrary to what is usually observed for other Newtonian fluids, where the material tends to move away from the rod. This describes the rising up of the fluid containing polymer chains (dead polymer) and this is corresponding to rodlike micelle (living polymer) in the viscoelastic surfactant systems. In viscoelastic surfactant solutions at rest, entropic force determines the random distribution of the rod shaped aggregates. During flow, a dynamic orientation process occurs which is induced by hydrodynamic force. This phenomenon is associated with the formation of anisotropic restoring forces. Here, the restoring forces in the direction of flow are greater than that in the direction of the velocity gradient. As a result, a positive normal difference is seen and the fluid climbs up to the rotating rod [104]. In this work the results of normal stress of both  $L_1$  and  $L_\alpha$ -Phase are presented. Depending on these results, a new rheological measurement which distinguish  $L_1$  and  $L_\alpha$ -phase is presented.



*Figure 3.19: Weissenberg effect (left picture) in the solution of 100 mM CTAOH and 75 mM 2,1 HNC, at which the solution tries to climb on a rotating rod, while no such phenomenon is seen for the sample of 100 mM CTAOH and 130 mM 2,1 HNC, which has multilamellar vesicles phase structure.*

It is found that  $L_1$ -Phase (rodlike micelles) shows a positive value of first normal stress difference after reaching certain shear rate while  $L_{\alpha MLV}$ -phase shows negative value of first normal stress difference for the whole systems that have been studied in this work. Before carrying out any type of measurements, this phenomenon can be visually seen. Figure 3.19 shows the presence of Weissenberg effect in the solution of 100 mM CTAOH and 75 mM 2,1 HNC, at which the solution contains rodlike micelles climbs on a rotating rod, while no such phenomenon is seen for the solution of 100 mM CTAOH and 130 mM 2,1 HNC, which has multilamellar vesicles microstructure. Figure 3.20 shows the results of first normal stress difference  $N_1$  in dependence with shear rate  $\dot{\gamma}$ . The solutions which consist of rodlike micelles show positive slope of  $dN_1/d\dot{\gamma}$ . After reaching certain shear rate, these solution

start to exhibit positive values of  $N1$ . Multilamellar vesicles show almost zero  $dN1/d\dot{\gamma}$  over the whole applied shear rate.

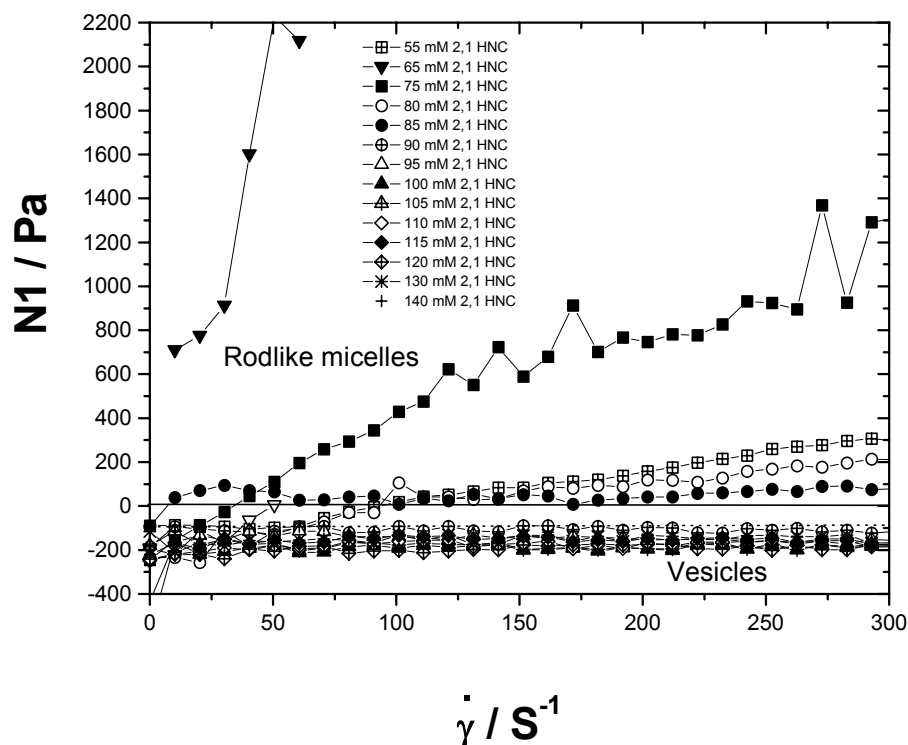


Figure 3.20: First normal stress difference  $N1$  versus applied shear rate  $\dot{\gamma}$  of 100 mM CTAOH and various concentrations (mM) of 2,1 HNC at 25 °C.

In figure 3.20, the value of  $dN1/d\dot{\gamma}$  is small for the solution of 100 mM CTAOH mixed with 55 mM 2,1 HNC, then starts to increase at 65 mM of 2,1 HNC followed by a decrease as the concentration of 2,1 HNC increases. The same behavior was observed to be apparent in yield stress measurements (shear rate against shear stress). The first normal stress difference at higher shear rates ( $>10 \text{ s}^{-1}$ ) in the solutions of 60 and 65 mM 2,1 HNC, which were highly viscoelastic with long relaxation time were difficult to be measured experimentally, while the same measurements were easier for solutions with rodlike micelle and shorter relaxation time. That is why only some measuring points are shown from the solution of 65 mM 2,1 HNC and 100 mM CTAOH, and no results for the solution of 60 mM 2,1 HNC and 100 mM CTAOH. It seems that the increase in the concentration of 2,1 HNC is accompanied by decrease in the relaxation time and an increasing in the entanglements of the rodlike micelles in the first stage. Then, the rodlike micelles start changing their structure as the concentration

of the hydrophobic counterion increases, especially before reaching the two phase region, so the  $dN1/d\dot{\gamma}$  starts to decrease again.

The dependence of  $dN1/d\dot{\gamma}$  on temperature is represented in figure 3.21 (A). Lodge[109] measured the first normal stress difference for 10% w/v polyisobutylene solution at different temperatures (20-50 °C), and he found almost a temperature independent  $dN1/d\dot{\gamma}$  in this range. Polymer solutions (dead polymers) differ from rodlike micelles from the view point that rodlike micelles can break and recombine on a time scale that is dependent on the system and on the physicochemical conditions. Hence they are called "living polymers".

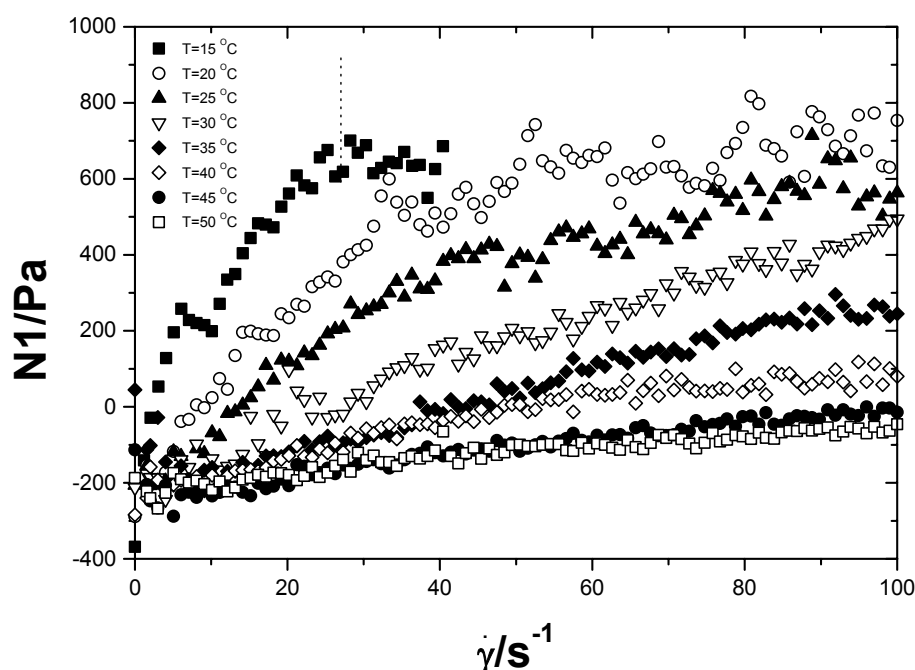
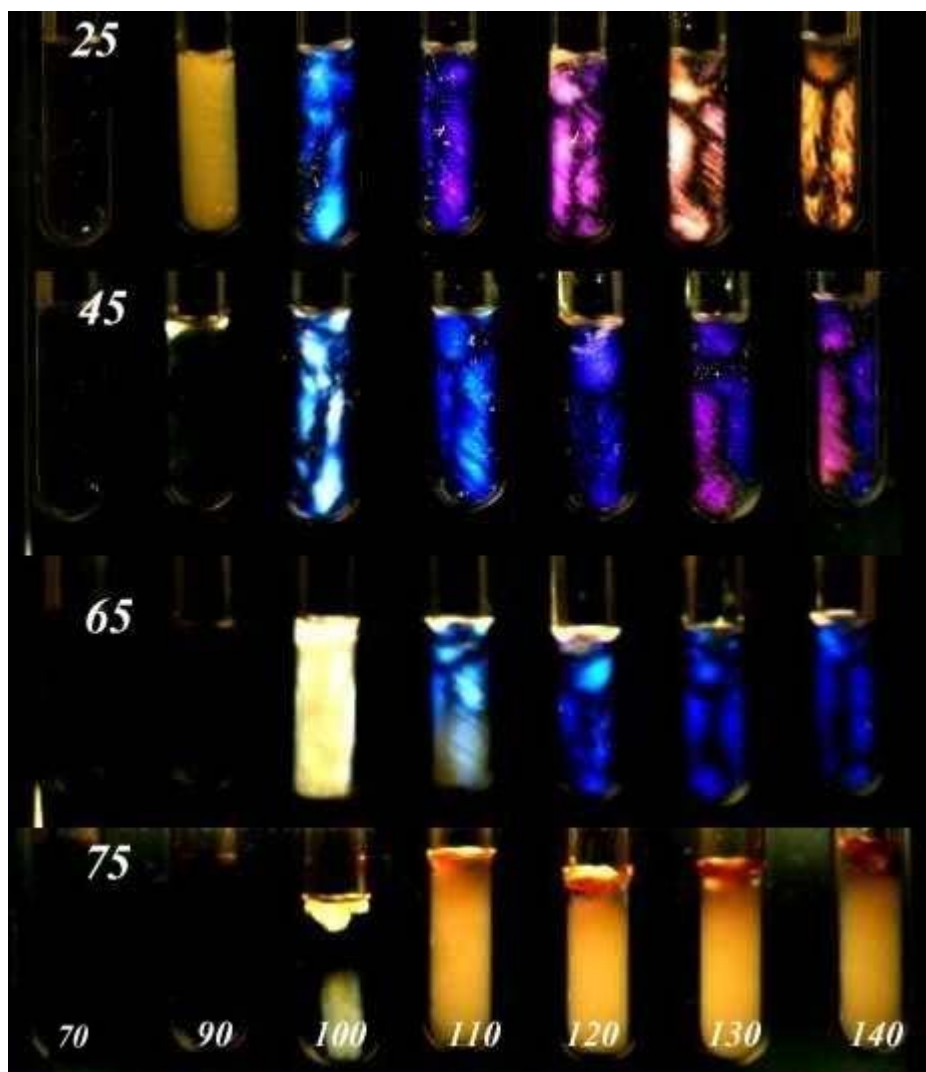


Figure 3.21(A): First normal stress difference  $N1$  versus shear rate  $\dot{\gamma}$  for solution with 100 mM CTAOH and 75 mM 2,1 HNC at different temperatures. As the temperature increases  $dN1/d\dot{\gamma}$  decreases.

Effect of temperature on the phase behavior is shown in Figure 3.21(B). After 50 °C, the solution shows phase separation. For  $N1$  measurements, at every temperature, a new solution was measured to avoid what is called by network-memory [103]. The shear can change the micelle structure, especially for high viscous solutions, and the network needs time to reach equilibrium, so measuring the same solution at different measurements can lead to unfavorable results. Aqueous solutions consisting of 75 mM 2,1 HNC and 100 mM CTAOH

shows short relaxation time, so it is easy to measure them. The solutions with long relaxation times tend to get slipped away from the cones. Solutions of 60 mM 2,1 HNC, and 65 mM 2,1 HNC mixed with 100 mM CTAOH exhibit this problem because of high viscoelasticity (or because of higher relaxation times).



*Figure 3.21 (B): Effect of temperature on the phase behavior for solutions with 100 mM CTAOH and an increasing amount of 2,1 HNC. The solutions are between two crossed polarizers. The numbers below the picture refer to the concentration of 2,1 HNC (mM), while the numbers to the left said of the pictures refer to the temperatures ( $^{\circ}\text{C}$ )*

#### C: Effect of electrolyte :

Figures 3.22 (A & B) show the storage modulus versus the frequency for both multilamellar vesicles in solutions containing 130 mM 2,1 HNC and 100 mM CTAOH and rodlike micelles in solutions consisting of 65 mM 2,1 HNC and 100 mM CTAOH at different concentrations of added NaCl. Upon addition of electrolyte, the storage modulus decreases dramatically with the concentration for multilamellar vesicles, while it changes only little when rodlike micelles are present. The result for ionic multilamellar vesicles indicate that the shear modulus is mainly determined by the electrostatic repulsion between the bilayers. As the concentration of electrolyte increases, the charge density of the bilayer surfaces is shielded and reduces the bilayer repulsion, and as a result decreases the storage modulus. Rodlike micelles are present in the solutions with excess of cationic surfactant. The concentration regime over which rodlike micelles are present can be divided into three different concentration regions. In the first region, the rodlike micelles don't overlap. While the second region represents a semidilute range in which the rods overlap and as a consequence the rods get entangled to form threadlike micelles which behave like transient temporary networks [126]. In figure 3.11 (region II) it was shown that the viscosity and storage modulus were independent of counterion concentration (corresponding to 60 to 75 mM 2,1 HNC). Since the hydrophobic counterion 2,1 HNC is much stronger in binding to the cationic micelle surface compared to NaCl, no effect is expected on the value of storage modulus upon addition of NaCl. Thus, the fact that the added NaCl did not affect the storage modulus is not unreasonable. In multilamellar vesicles region in figure 3.11, adding more 2,1 HNC has no influence on the charge density since 2,1 HNC is in the molecular form.

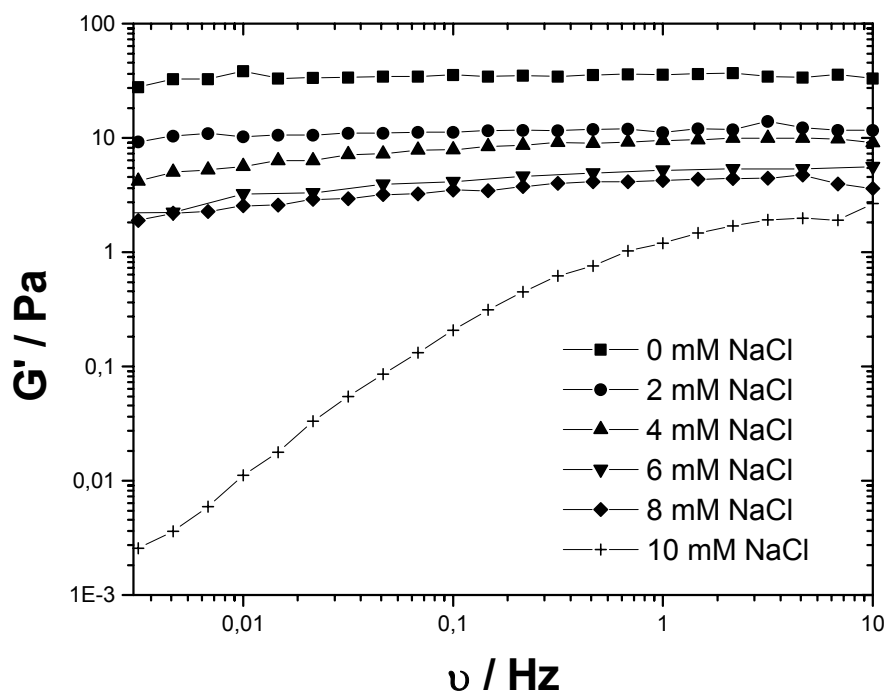


Figure 3.22, A: Variation of the storage modulus versus frequency for solutions of 100 mM CTAOH mixed with 130 mM 2,1 HNC and different concentrations of NaCl at 25 °C.

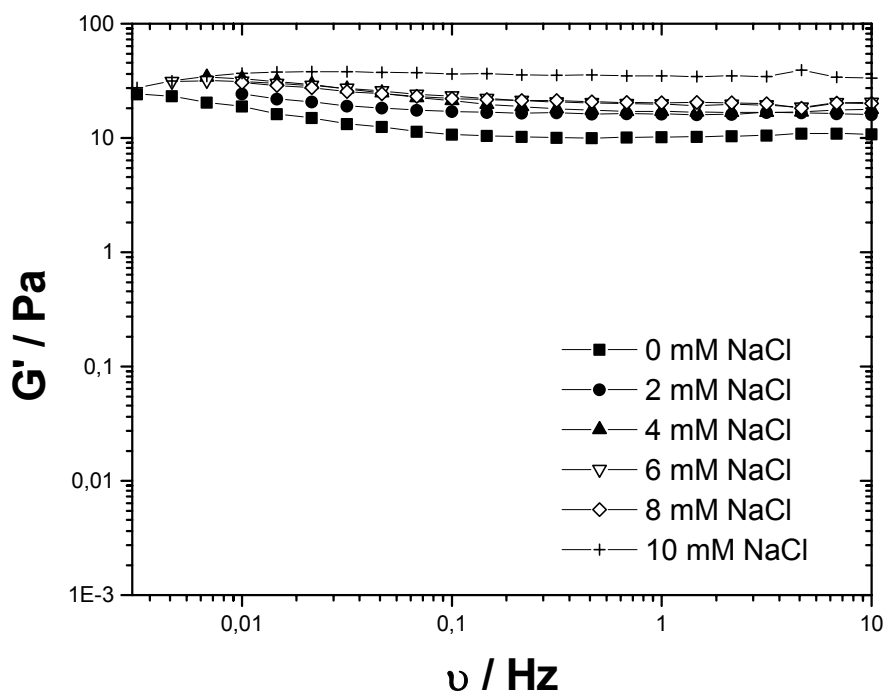
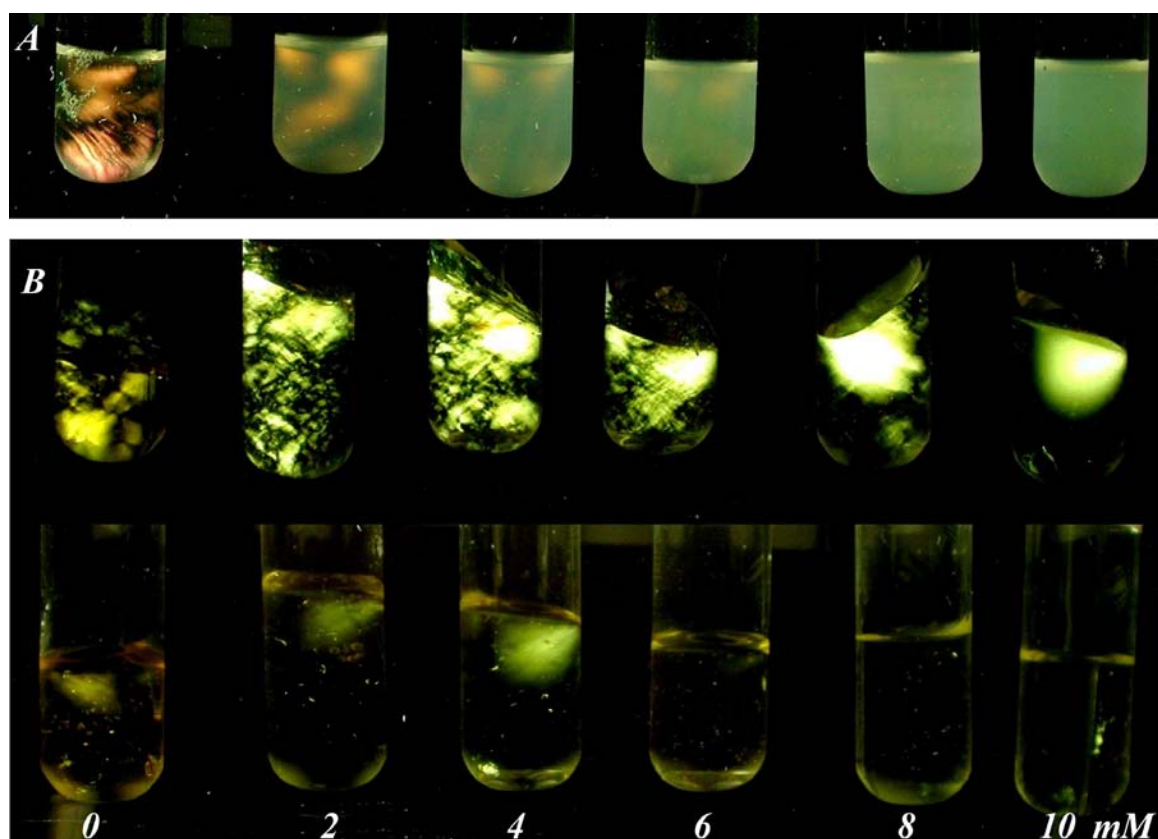


Figure 3.22, B: Variation of the storage modulus versus frequency for solutions of 100 mM CTAOH mixed with 65 mM 2,1 HNC and different concentrations of NaCl at 25 °C.

The birefringence pictures from the solutions containing added electrolyte and consisting of multilamellar vesicles or rodlike micelles are displayed in figure 3.23. Multilamellar vesicles start to lose their birefringence as the concentration of the salt increases. These solutions become also turbid (but they don't show two phase region) when the concentration of NaCl increases. Since the electrolyte can shield the surface charge and reduce the repulsion between the bilayers. For the rodlike micelle solutions, the salt shortens the relaxation time. This result is proved in figure 3.23, B. Rodlike micelles show flow birefringence upon tilting or shearing. In the second row (B), the solutions were exposed to shear for 5 min by centrifugation with 875 rpm, while the third row shows the same solutions after 120 minutes. As the concentration of electrolyte increases, the flow birefringence relaxes faster.



*Figure 3.23: Phase behavior for solutions of 100 mM CTAOH mixed with 130 mM 2,1 HNC (A: top row) or 65 mM 2,1 HNC (B: second and third row) and different concentrations of NaCl at 25 °C. In the second row (B), the solutions were shaken for 5 min with centrifuge of 875 rpm, while the third row (B) shows the same solutions after 120 minutes of relaxation. The numbers at bottom of the picture indicate NaCl concentration in (mM).*

The addition of salt to the systems show a definite first normal stress difference, while the same was not measurable for the same systems in water. That means the added NaCl has a role to play in which when added excess, it shields the charges of the micellar surface. this shielding of charges decreases the relaxation time and hence it possible to measure first normal stress difference N1 in solutions with rodlike micelles. Figure 3.24 shows the first normal stress difference for the solutions with rodlike micelles. The solutions with multilamellar vesicles do not show normal stress difference values (figure 3.25). Hence it can be concluded the positive response to first normal stress difference has a direct relation with the microstructures in the systems.

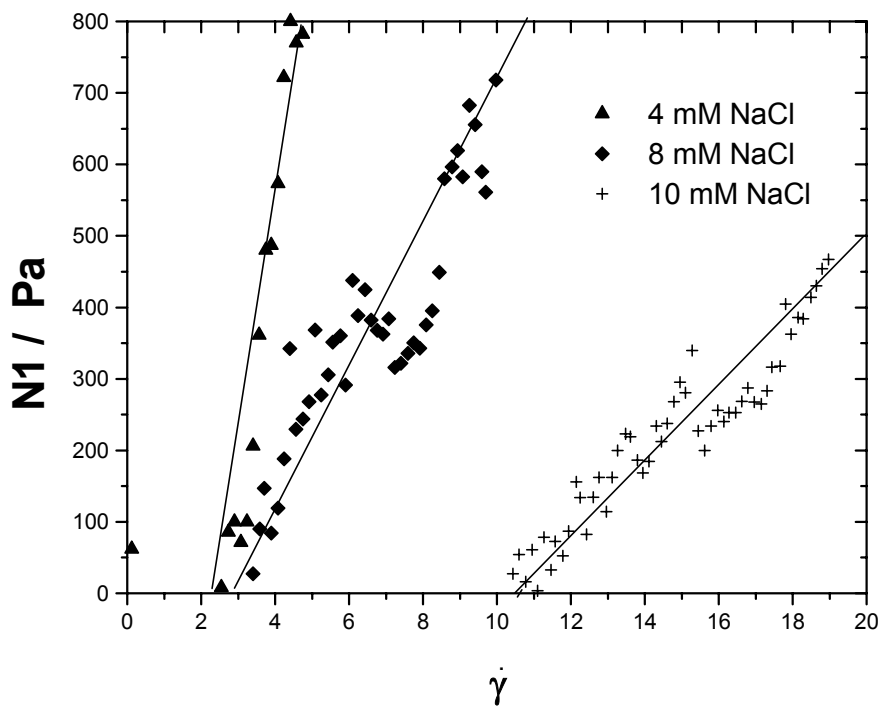


Figure 3.24 : First normal stress difference versus shear rate for solutions with 100 mM CTAOH / 65 mM 2,1 HNC and different concentrations of electrolyte at 25 °C.

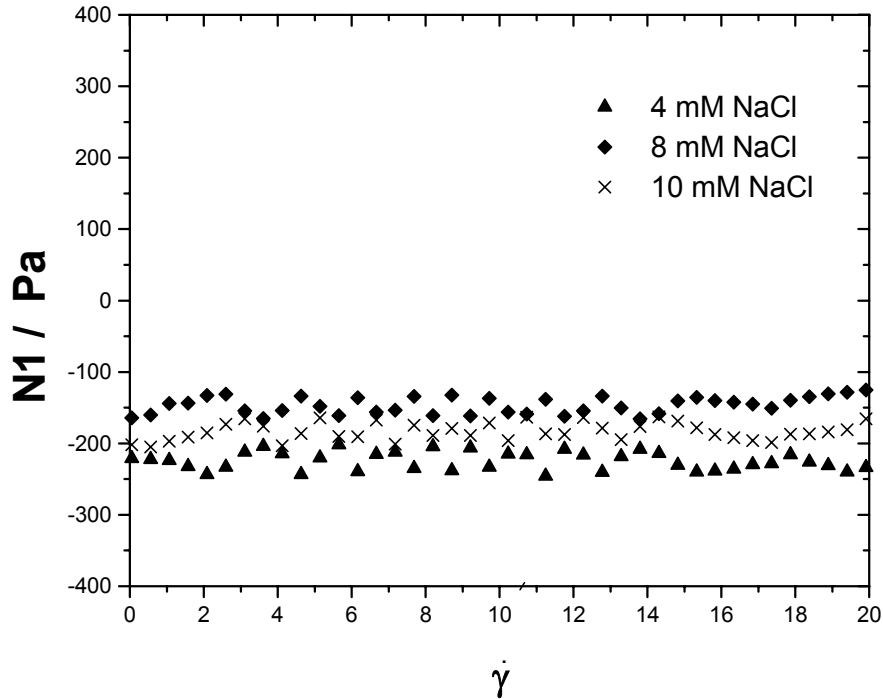


Figure 3.25 : First normal stress difference versus shear rate for solutions with 100 mM CTAOH /130 mM 2,1 HNC and different concentrations of added electrolyte at 25 °C.

$dN1/d\dot{\gamma}$  is reduced with the increase in electrolyte concentration for the solutions of rodlike micelles. This shows the dependence of  $dN1/d\dot{\gamma}$  on the relaxation time and not on the storage modulus, which is almost the same for these solutions. Multilamellar vesicles show  $dN1/d\dot{\gamma}$  almost equal to zero. The finding is expected, since  $N1$  is resulted from rodlike micelle stretching and relaxation. As the elasticity of multilamellar solution is reduced by adding electrolyte, a corresponding decrease in the yield stress is obtained as shown in figure 3.26. In the same figure the values of the apparent yield stress (quasi value) for rodlike micelle are shown. The apparent yield stress values of rodlike micelles are almost constant and independent of the added electrolyte concentration. Since the elasticity of these solution is the same (the same storage modulus), similar apparent -yield stress values are expected.

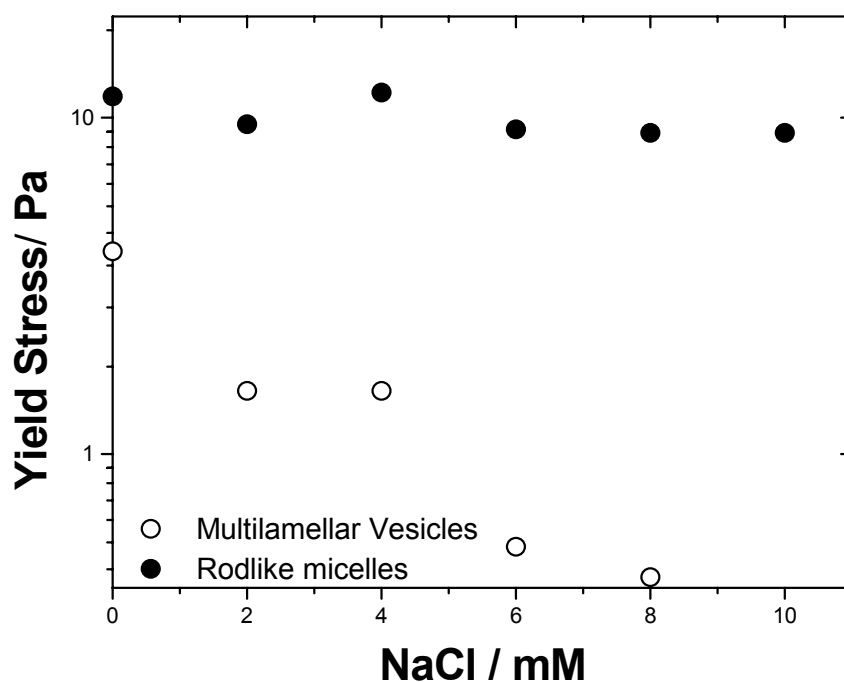


Figure 3.26 : Yield stress values for the solutions with 100 mM CTAOH / 65 mM 2,1 HNC (rodlike micelles) or solutions with 100 mM CTAOH / 130 mM 2,1 HNC (multilamellar vesicles) versus NaCl concentrations at 25 °C.

#### (D) Relaxation curves:

Figure 3.27 shows the shear stress as a function of time when a certain shear rate is suddenly applied at  $t = 0$  for a solution with 100 mM CTAOH and 65 mM 2,1 HNC (Rodlike micelle) or with 100 mM CTAOH and 130 mM 2,1 HNC (multilamellar vesicles). For both solutions the applied shear rates  $\dot{\gamma}$  are  $1 \text{ s}^{-1}$ . If the shear is stopped, the shear stress relaxes. For the rodlike micelles, the shear stress peaks to a maximum before levelling off to its stationary state. While the multilamellar vesicles relax to a value corresponding to yield stress. When small shearing is applied on vesicles, they are deformed without any damage in the packing and hence they return their original microstructure some time under no shear. For the rodlike micelles, however, a change occurs in their initial network structures before reaching the original stress after the relaxation. Since the shear stress goes to zero after some time, the yield stress observed is not a real one. This behavior is important because rodlike micelles can

be easily disturbed and reformed and thus the shear stress relaxation curves can be used to distinguish both the above morphologies.

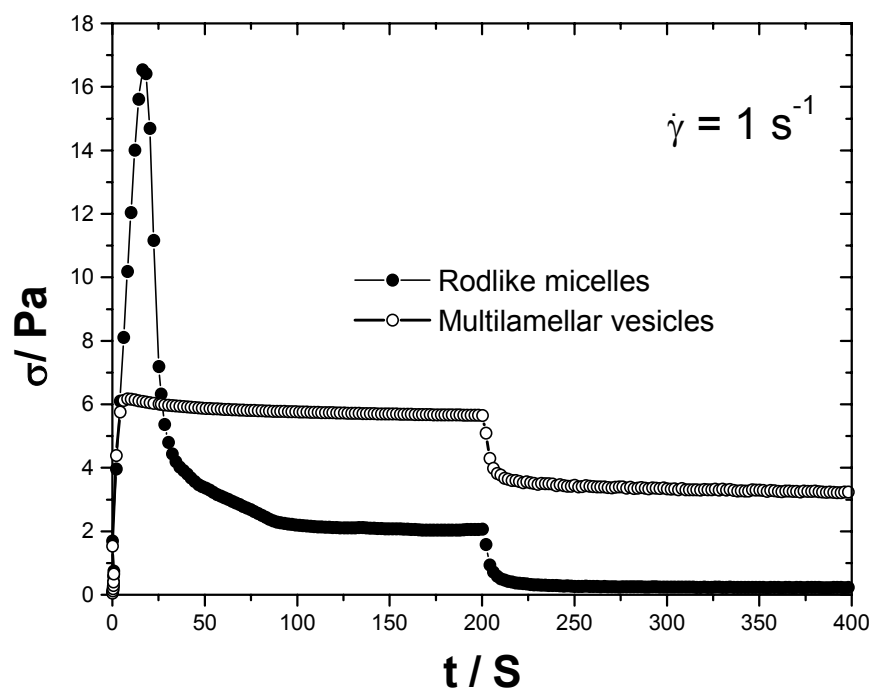


Figure 3.27: Shear stress relaxation for the solution with 100 mM CTAOH and 65 mM 2,1 HNC (rodlike micelles) or solution with 100 mM CTAOH and 130 mM 2,1 HNC (multilamellar vesicles) at 25 °C.

### 3.2. The System 6,2 HNC /CTAOH /water

In order to understand and study the effect of relative positions of the carboxyl and hydroxyl group on the one of the components i.e. HNC on the over all association behavior in it's ternary system with CTAOH and water, similar measurements as reported in the previous section are presented as below.

#### 3. 2.1 Phase Behavior

At first , the different phases that result when 6-hydroxy-2-naphthoic acid (6,2 HNC) reacts with a solution of 100 mM cetyltrimethylammonium hydroxide CTAOH are discussed. Figure 3.28 shows the phase behavior of the system 6,2 HNC/CTAOH at 25 °C. The system also showed color changes with pH of the solutions. In basic pH region yellow color is observed while more bright yellow solutions are observed at acidic pH. At equimolar concentration of CTAOH and 6,2 HNC, the neutralization is reached and the un-reacted 6,2 HNC starts to appear. The samples with a 6,2 HNC/CTAOH ratio,  $r \sim 0.95$  or less are in a single micellar phase region which is optically isotropic. The whole solutions are isotropic when they are seen between two crossed polarizers. The two phases after  $r \sim 0.95$  can separate completely because of the moderate viscosity of the solution. At 6,2 HNC/CTAOH molar ratio more than 0.8 there is a transition of small micellar aggregates (globular) to rodlike micelles that causes an increase in the viscosity of the solutions. All solutions with  $r \sim 0.8$  or less have a low viscosity. At  $r \sim 0.7$  the viscosity starts to rise, and viscoelastic solutions are resulted in  $r \sim 0.8$ . These isotropic viscoelastic solutions, which are made of rodlike micellar phases continue to form until the 2-phase-region is reached. Such results are different from that were obtained for the systems of 3,2 HNC / CTAOH and the system 2,1 HNC / CTAOH.



**20 80 85 90 100 110 120 130 140 150**  
*c (6,2 HNC)[mM]*

*Figure 3.28 : Phase behavior of the system CTAOH/6,2 HNC at 25 °C. Solutions are with 100 mM CTAOH and an increasing amount of 6,2 HNC without polarizers (top row) and between two crossed polarizers (bottom row). The brightness of some solutions with 100 mM 2,1 HNC or higher is because of some fine precipitate particles, which cover the test tubes from inside and not because of liquid crystal structure. The numbers below the pictures indicate the concentration of 6,2 HNC.*

## 3.2.2 SANS:

SANS curves for the systems with different concentrations (80, 90 and 100 mM) of 6,2 HNC and 100 mM CTAOH are shown in figure 3.29. The curves show the typical scattering behavior of small micelles. Table 3.2 shows the parameters as calculated from the SANS curves. Solution of 100 mM 6,2 HNC and 100 mM CTAOH shows some shift from the baseline. The radii of the rodlike micelles are constituent with the length of the  $C_{16}$  chain.

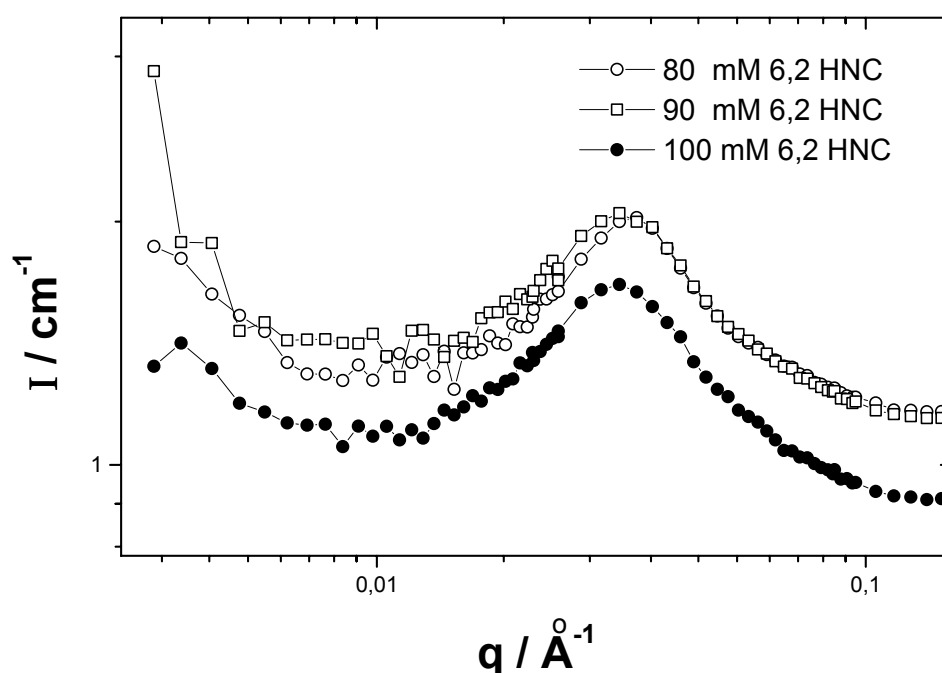


Figure 3.29 : The SANS spectra at 25 °C show a correlation peak of small micelle aggregates for solutions with 55, 60 or 65 mM 6,2 HNC and 100 mM CTAOH.

Table 3.2: Volume fraction  $\phi$ , scattering vector at maximum intensity  $q_{\max}$ ,  $d(\text{Å})$  calculated from the relation ( $d=2\pi/q_{\max}$ ) and rod radius  $R(\text{Å})$  for the system of 80, 90 and 100 mM 6,2 HNC mixed with 100 mM CTAOH at 25 °C.

Con. (mM)	$\phi_{2,1 \text{ HNC}}$	$\phi_{\text{CTAOH}}$	$\phi_{\text{CTAOH}+2,1 \text{ HNC}}$	$q_{\max}$	$d(\text{nm})$	$R(\text{Å})$
80	0,015	0,029	0,044	0,031	20,03	13,76
90	0,017	0,029	0,046	0,031	20,03	14,58
100	0,018	0,029	0,048	0,031	20,03	15,36

3.2.3 Rheological behavior:

The rheological behaviour of the solutions with 100 mM CTAOH and an increasing amount of 6,2 HNC is illustrated in figure 3.30 using the variations in the zero shear and complex viscosities at 0.01 Hz. Since all the solutions with a concentration ratio 6,2 HNC/CTAOH  $r \sim 0.8$  or higher behave as Maxwell fluids for which the complex viscosity is comparable to zero shear viscosity because of the short relaxation time constant and the frequency independent complex viscosity. The solutions with a 6,2 HNC content up to 65 mM are low viscous. At a HNC concentration of 70 mM the viscosity rises and the solutions become viscoelastic indicating the formation of rodlike micelles. Beginning from a 6,2 HNC concentration of about 90 mM the viscosity reaches the maximum of about 0,6 Pas. After neutralization at  $r \sim 0.95$ , solutions are in two phases, namely, the un-reacted 6,2 HNC in the lower phase and viscoelastic isotropic rodlike micelles in the upper phase.

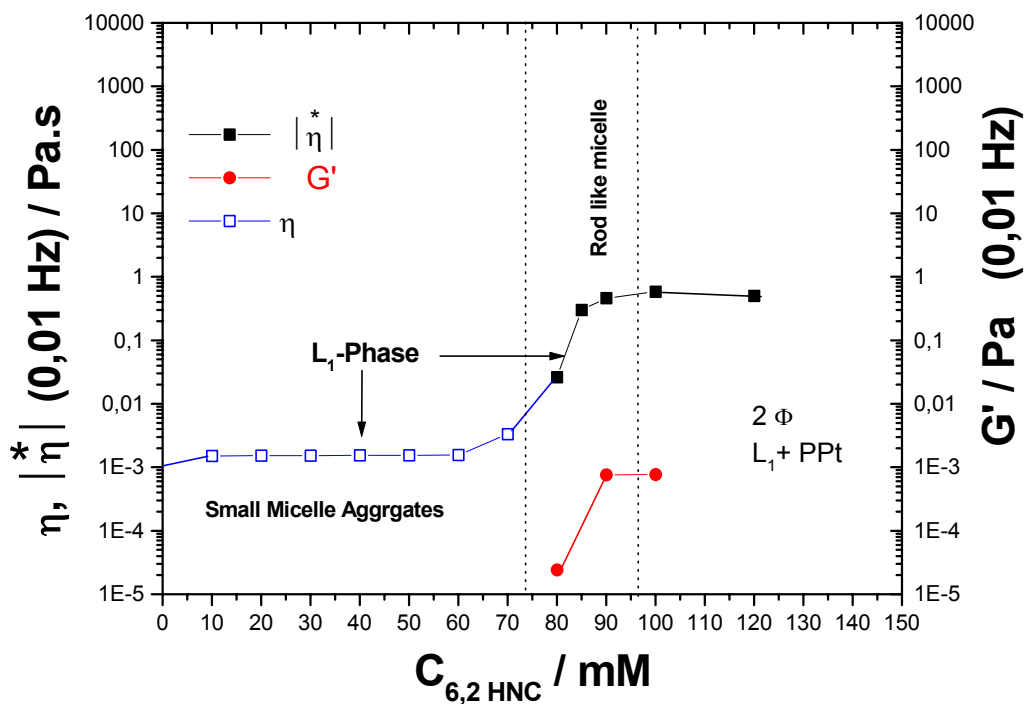


Figure 3.30: Viscosity ( $\eta$ ) obtained by double gap method (DGM), complex viscosity ( $\eta^*$ ) and storage modulus ( $G'$ ) (at 0,01 Hz) obtained from oscillation measurements for 100 mM CTAOH as a function of increasing amounts of 6,2 HNC (mM) at 25 °C.

The solutions with a 6,2 HNC content of 85 up to more than 100 mM behave as Maxwell fluids with single and short relaxation time, the storage and loss modulus are frequency

dependent, and the viscosity is frequency independent after relaxation. Figure 3.31 shows the rheogram of 90 mM 6,2 HNC mixed with 100 mM CTAOH. The relaxation time constant ( $\tau$ ) is calculated from the relation  $\tau = 1/2\pi\nu$ . It is about 0.016 second. This represents the time the solution needs to relax an applied stress. The other rodlike micellar solutions show also short relaxation times.

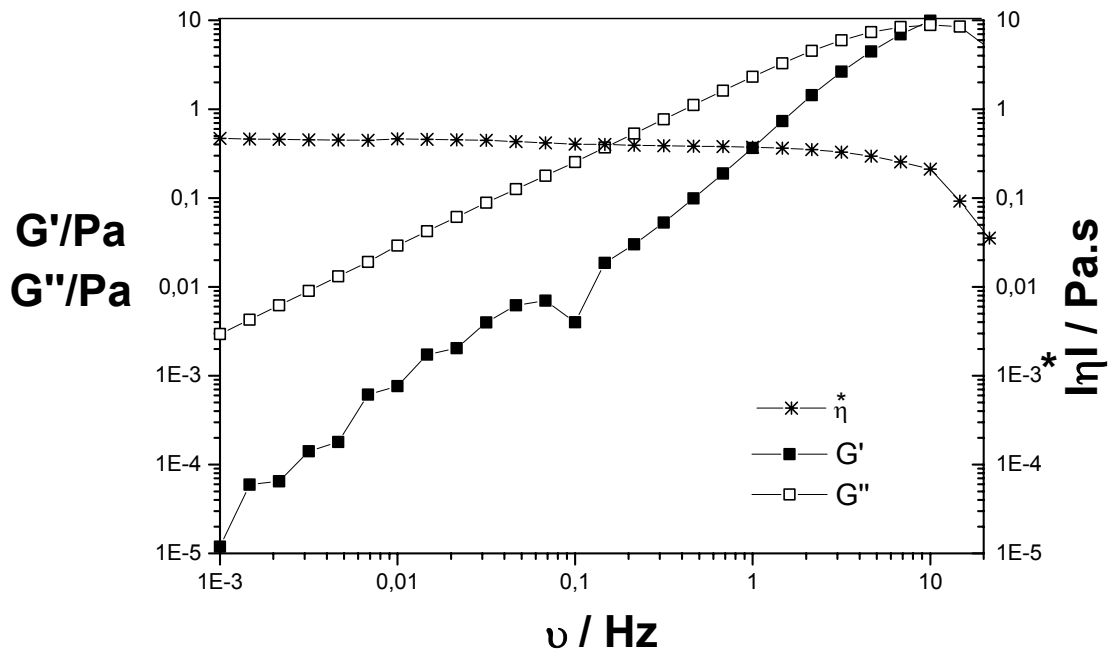


Figure 3.31: Variation of the complex viscosity  $\eta^*$ , storage modulus  $G'$  and loss modulus  $G''$  versus frequency  $\nu$  for solutions with 100 mM CTAOH and 90 mM 6,2 HNC at 25 °C.

The presence of rodlike micelles in the solutions is checked also by sweep measurements, at which rodlike micelles exhibit deformation higher than 1 (100%). Figure 3.32 show the storage modulus as a function of deformation. This measurement was carried out at 1 Hz frequency. All examined solutions with different storage modulus values deform almost similarly. Also the solutions show positive first normal stress difference after certain shear rate, which was corresponding to the solutions of rodlike micelles in the system of 2,1 HNC/CTAOH. Figure 3.33 shows  $N1$  as a function of applied shear rate for the solutions with 90 and 100 mM 6,2 HNC content. Both solutions show positive  $dN1/d\dot{\gamma}$  and the solutions start to show positive  $N1$  after certain shear rate  $\dot{\gamma}$ , however,  $dN1/d\dot{\gamma}$  for 100 mM 6,2 HNC is larger than that for 90 mM 6,2 HNC. The concentration of rodlike micelles which may be higher in the second solution is the reason for this difference.

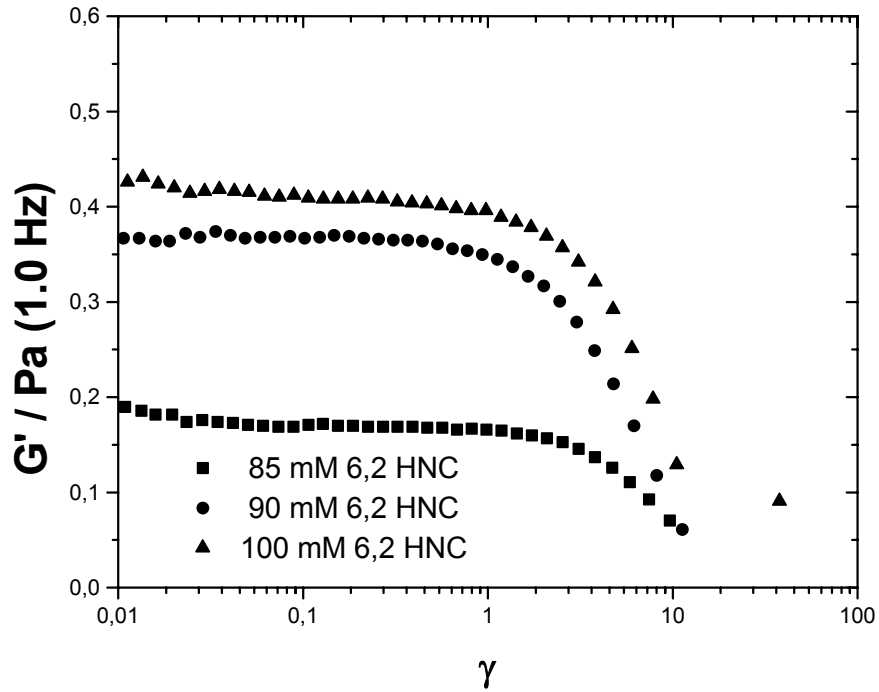


Figure 3.32: Storage modulus  $G'$  versus deformation  $\gamma$  for the solutions with 85, 90 or 100 6,2 HNC mixed with 100 mM CTAOH at 25 °C.

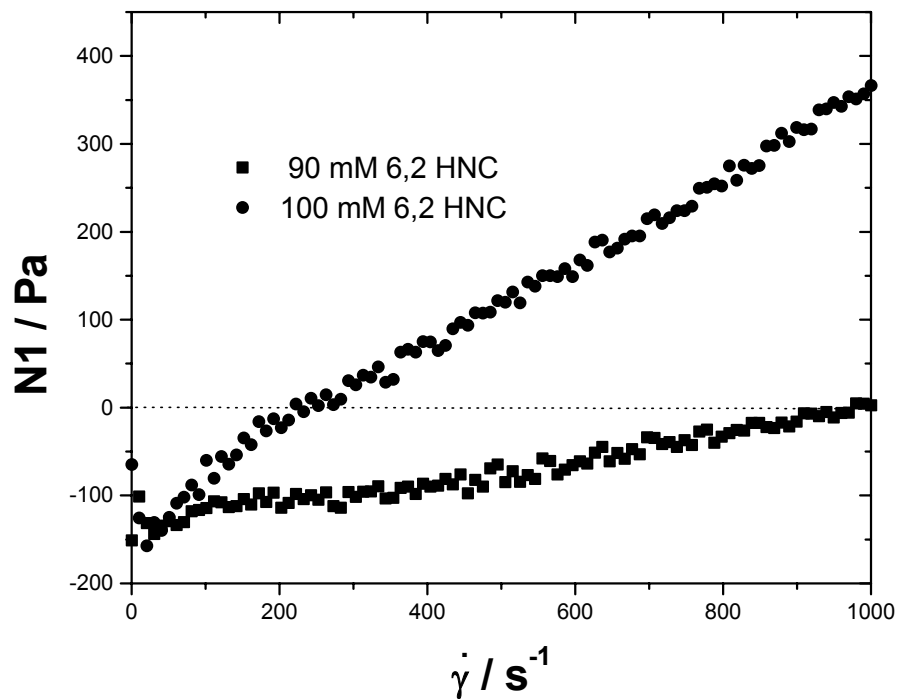


Figure 3.33: First normal stress difference  $N1$  versus shear rate  $\dot{\gamma}$  for the solutions with 90 or 100 mM 6,2 HNC mixed with 100 mM CTAOH at 25 °C.

### 3.2.4 The Influence of The Substituents on Phase Behavior:

It is important to ascertain the effect of the position of the carboxyl group, which acts as the hydrophobic counter ion, relative to the hydroxyl group.

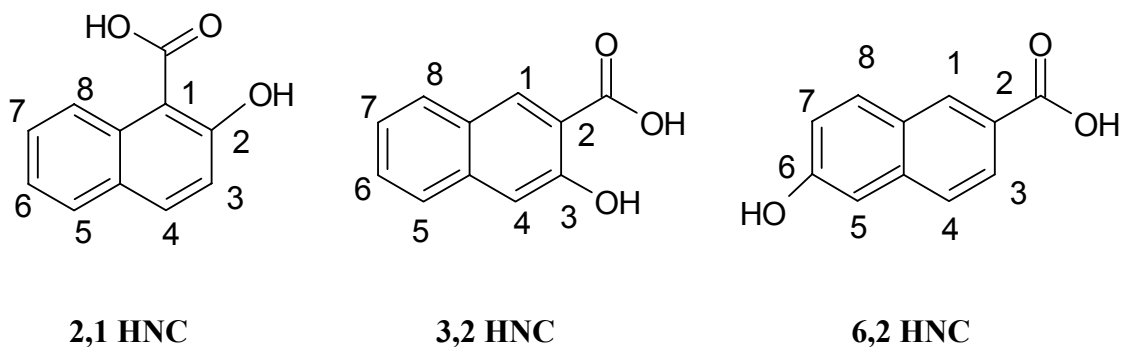


Figure 3.34: Chemical structures of different isomers of HNC.

#### (A) Phase Behavior

For the CTAOH/3,2HNC system at 40 °C one finds a low viscous solution, a viscoelastic gel, and a viscoelastic liquid crystalline  $L_{\alpha}$ -phase consisting of densely packed multilamellar vesicles having a yield stress value with the increasing concentration of 3,2 HNC [110]. The system 2,1 HNC/CTAOH at 25 °C shows similar behavior to that of 2,3HNC/CTAOH. At equal molar ratio, the system forms a viscoelastic liquid crystalline phase with densely packed multilamellar vesicles with a yield stress value. For the 6,2 HNC/CTAOH system, one finds a low viscous solution, rodlike micelles, and a two phases region after the neutralization with increasing concentration of 6,2 HN. The 6,2HNC/CTAOH system doesn't form a  $L_{\alpha}$ -phase at and above equimolar ratio. The results together show that the position of hydroxyl group on the naphthoic plays a big role for the various phases. For 6,2 HNC, the hydroxyl group is in position number 6 on the aromatic rings (see the chemical structure in figure 3.34), which means that the hydroxyl group is distant from the carboxyl group and hence the cationic charges are free because of the absence any dipole interaction with the far a way OH group. Physical interaction between the hydroxyl groups and the hydrocarbon tails is also not favorable. Both of these reasons prevent the geometrical packing of the heads from reaching a packing parameter value  $\cong 1$ , so no multilamellar vesicles are formed. Substitution of HNC

plays a main role in controlling the microstructure and other physical properties such as viscosity, Krafft point, ..as etc

#### (B) Rheological Behavior:

Depending on the resulted microstructure, the rheological behavior is varied. In the systems of 2,1 HNC/CTAOH, at equimolar ratio the rheological behavior of multilamellar vesicles is obtained, while the rheological behavior of rodlike micelle is proved for the systems with 6,2 HNC /CTAOH. Both 2,1 and 3,2 HNC form multilamellar vesicles upon mixing equally with CTAOH. So they have storage modulus ( $G'$ ) independent of frequency ( $\omega$ ), viscosity dependant of frequency, yield stress value and have negative first normal stress difference ( $N1$ ), or zero  $dN1/d\dot{\gamma}$ . 6,2 HNC forms rodlike micelles upon mixing equally with CTAOH, so they behave as a Maxwell fluids, storage modulus is frequency dependant after relaxation, viscosity is frequency independent after relaxation, no yield stress value, and have a positive first normal stress difference  $N1$  after exceeding certain shear rate ( $\dot{\gamma}$ ).

#### (C) Krafft Point:

The position of hydroxy substitution has strong effect on Krafft point: to illustrate, hydroxy substitution close to a hydrophilic head group increase the Krafft point, while hydroxy substitution distant to the hydrophilic group strongly decrease this temperature. This is seen from the dependence of the Krafft point of CTAHNC on hydroxy position. Laughlin [117] varied the position of hydroxy group in sodium x- hydroxypalmitates, and it is found that the hydroxy group far from head group resulted in high miscibility ( lower Krafft point), and as the substituent is closer to the head group, the miscibility decreases. Decreasing the distance between the hydroxy substituent and the hydrophilic group resulted into an increased hydrophilicity for the molecule. In the comparison of various x,y HNC mixed in an equimolar ratio with CTAOH, it is assumed that the resulted combination behaves as a single surfactant. Since CTAOH is the same for the whole combinations, then the structure of the hydrophobic counterion is the only varied parameter. When the hydroxy group close to head group as in 3,2 and 2,1 HNC; solutions exhibit Krafft points at about 28.2 and 22.5 °C

respectively, while there is no positive Krafft point for CTAHNC prepared from equimols of CTAOH and 6,2 HNC. The Differential scanning calorimetry DSC traces for the systems of different HNC isomers mixed equally with CTAOH are shown in figure 3.35

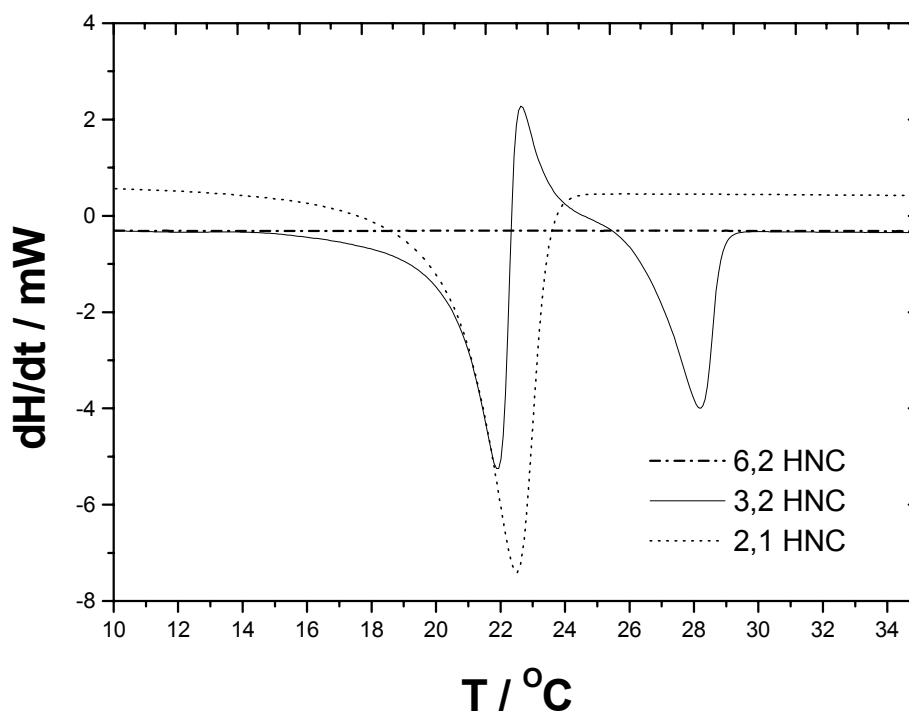


Figure 3.35: DSC traces for solutions of 100 mM CTAOH and 100 mM of different isomers of  $x,y$  HNC.

One single phase transition from crystal phase into the liquid crystal phase is seen for CTAHNC (from 2,1 HNC), while CTAHNC (from 3,2 HNC) shows a complex DSC behavior. The transition from crystalline state ( $L_\beta$ ) into the liquid crystalline state of multilamellar vesicles ( $L_\alpha$ ) is shown in the DSC curve (figure 3.35) as two endothermic peaks with an exothermic peak in between. The existence of two distinct endothermic peaks is resulted from the existence of CTAHNC in two polymorphic crystalline forms. It was suggested that these crystalline forms may differ in the degree of hydration. The first endothermic peak represents the transition from the first, probably more hydrated crystal morphology into  $L_\alpha$ , while the second endothermic peak represents the transition from the second crystal morphology, probably less hydrated crystalline state into  $L_\alpha$ . The exothermic peak between the two endothermic peaks which is shown in DSC-curve may be due to the reason that the  $L_\alpha$  phase is not stable with respect to the higher melting  $L_\beta$  phase. This leads to a crystallization of  $L_\alpha$ .

phase to form  $L_\beta$  phase. As reversal of the melting of the alkyl chain  $L_\alpha \rightarrow L_\beta$  this is an exothermic process [83].

#### (D) Synergism:

The surface versus concentration profile for CTAOH alone and CTAHNC systems resulting from 2,1 and 6,2 HNC and CTAOH are displayed in figure 3.36. It can be seen that the cmc systematically shifted to lower concentrations for the systems with both isomers, but CTAHNC (2,1 HNC) has lower cmc than the other. Not only this, the surface tension value at cmc has also been lowered almost by ten units for the CTAHNC (2,1 HNC) system. The systematic lowering of cmc and surface tension value of about 32 mN/m for this system at the cmc indicates that a good synergism exists and the system has catanionic nature (or nonionic nature). This conclusions are in agreement with the result of the phase behavior in which the CTAHNC (2,1 HNC) system forms multilamellar vesicles because of closed and better interaction and while interestingly the system CTAHNC (6,2 HNC) dose not display such synergism and also form multilamellar vesicles.

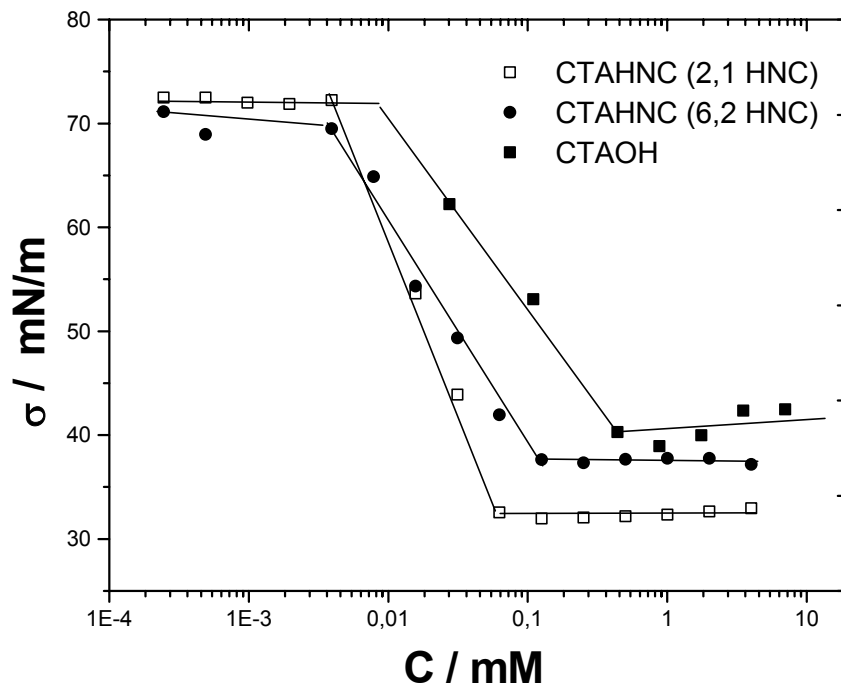


Figure 3.36 : Surface tension of 100 mM CTAOH, 100 mM CTAHNC (prepared from CTAOH and 6,2 HNC) and 100 mM CTAHNC (prepared from CTAOH and 2,1 HNC). The minimum in the surface tension at cmc of CTAOH may be a result of contamination with some organic were connected to the ion exchanger resin.

#### 3.3 The Systems $C_{14}$ TAOH, $C_{12}$ TAOH, $C_{10}$ TAOH, $C_8$ TAOH /2,1HNC /water

Having established and characterized, the different phases in 2,1 HNC/ $C_{16}$ TAOH/water in the previous sections, studies have also been made for the similar properties but on the systems consisting of initial cationic surfactants of varying hydrophobic chain length, so that the final system has counterions having different hydrophobic tails. In all of these phases the cationic surfactants alkyltrimethylammonium hydroxides  $C_x$ TAOH ( $x=8,10,12,14$ ) were prepared via ion exchange procedure from its counterpart cationic surfactant alkyl trimethylammonium bromide  $C_x$ TAB. In the next sections, the phase behavior, conductivity and pH measurements, differential interface contrast microscopy, FF-TEM, SANS, and the rheological behavior of these different systems are presented.

##### 3.3.1 Phase Behavior:

The different phases that result when 2,1 HNC reacts with a solution of 100 mM hydroxide  $C_x$ TAOH are shown in figure 3.37 at 25 °C. The phase behaviors of the systems are discussed below

***The System  $C_{14}$ TAOH/2,1 HNC/Water:*** The observation of the solutions between crossed polarizers (figure 3.37, first system) revealed that the present system also has similar features to that of 2,1 HNC/ $C_{16}$ TAOH ; i) solutions with  $C_{16}$ TAOH/2,1 HNC ratio  $r \sim 0.5$  or less are low in viscosity which started rising at  $r \sim 0.55$  before yielding viscoelastic solutions at  $r \sim 0.6$ , ii) when the molar ratio is more than  $r \sim 0.85$ , the rodlike micellar phases (which existed at  $r \sim 0.65-0.75$ ) change to multilamellar vesicles, iii) a turbid region was found before the equimolar compositions and the coexisting phases don't completely get separated even when they are allowed to stand for few months and also even after centrifugation, iv) the added excess 2,1 HNC (150 mM) got solubilized in the 100 mM  $C_{14}$ TAOH taken initially.

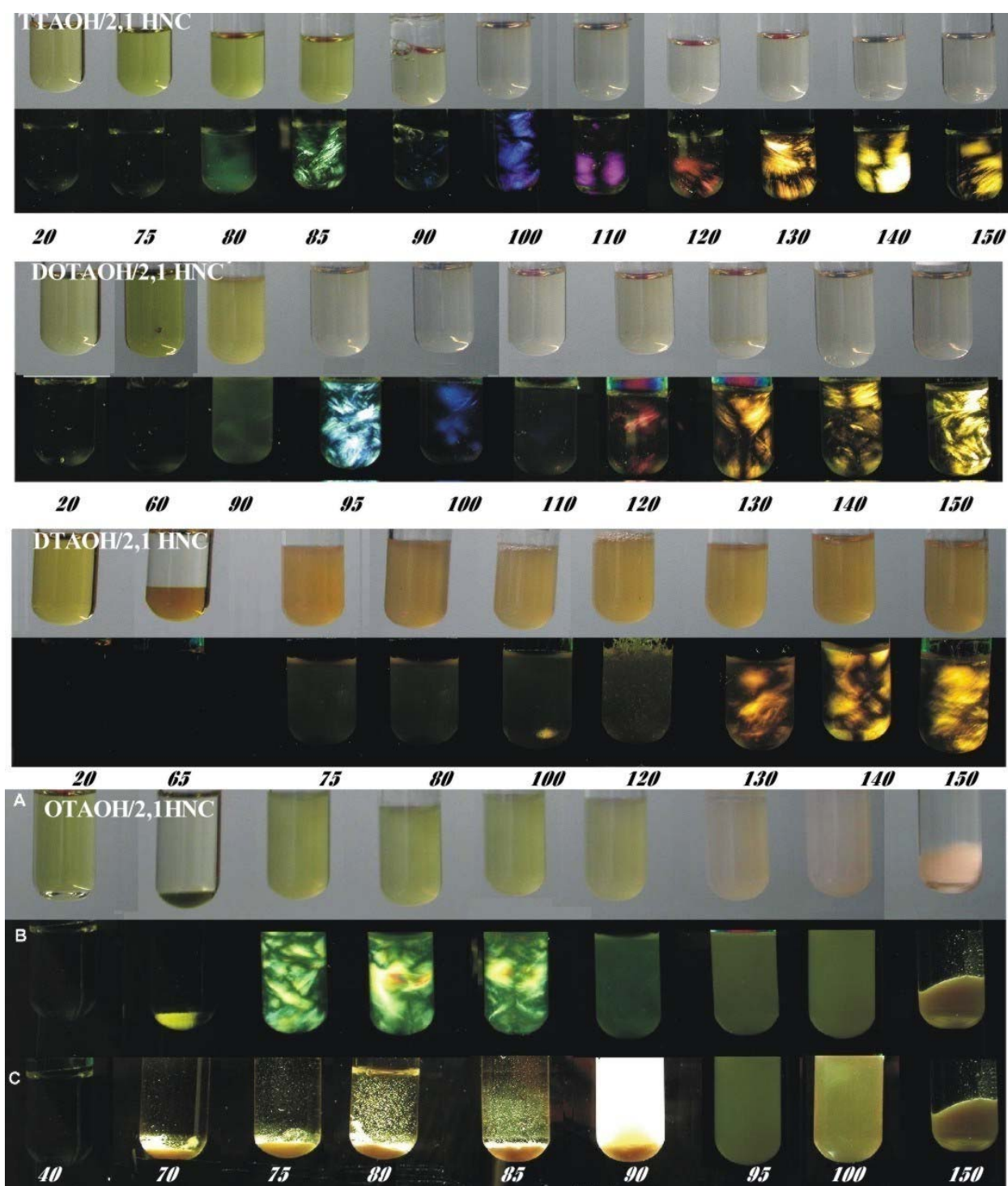
***The System  $C_{12}$ TAOH/2,1 HNC/Water:*** The phase behavior for this new system was also established and the appearance of the solutions for different molar ratio of  $C_{12}$ TAOH/2,1 HNC as observed between two crossed polarizers is displayed in figure 3.37 (second system). This system also shares the features which were described previously for the other two systems at 25 °C. At equimolar ratio of  $C_{14}$ TAOH and 2,1 HNC, the neutralization occurs with the pH of almost 7 for the system. However the turbidity in the system set in before the equimolar compositions and between 2,1 HNC/ $C_{14}$ TAOH ratio  $r \sim 0.80-0.90$ . The viscosity of

the isotropic solutions of this system is lower than the previous two systems. The turbid region is shifted to the equimolar ratio as the viscosity of the solutions decreases.

**The System  $C_{10}TAOH/2,1HNC/Water$  :** This system (third system in figure 3.37) shows different phase behavior compared to the other systems that have been studied. At 2,1 HNC contents less than 60 mM the samples are isotropic when they are seen between two crossed polarizers and all in single phase. The solutions with a 2,1 HNC/  $C_{10}TAOH$  ratio  $r \sim 0.6$  or less are low viscous. Further addition leads to a two phase region with two isotropic phases ( $r \sim 0.65$  to  $r \sim 0.75$ ). The upper phase is colorless and low viscous, while the lower phase has a brown color and a higher viscosity. When the 2,1 HNC content is about 80 mM, the two phase region disappears and single turbid phase which is slightly birefringent appears. By adding further content of 2,1 HNC, a birefringent phase can be seen between two crossed polarizers. The systems with  $r$ -values of  $\sim 0.95$  to 1.5 were of two phase in appearance and for the first time, a white precipitate was formed (2,1 HNC has white color), however, after two weeks of the preparation, the equilibrium was reached and the solutions had an appearance as shown in figure 3.37. The solutions were observed regularly between the crossed polarizers to check if there is a change in the phase behavior. It could be that the solubilization of unreacted hydrophobic counterion needs longer time. Similar results were observed in solubilization experiments of hydrocarbon in CTAHNC (prepared from CTAB and SHNC (3,2 HNC)), at which for the first time the hydrocarbon (Decane) and the surfactant were in a two phase region, then after some days of shearing, one single phase was formed. In addition to that, the concentration of the surfactants in the micellar form is less than those in previous systems ( $C_{16}TAOH$ ,  $C_{14}TAOH$  and  $C_{12}TAOH$  mixed with an increasing amount with 2,1 HNC), since the cmc of  $C_{10}TAOH$  is the highest one ( $\approx 50$  mM), which implies less concentration of surfactant in the micellar form, which is important for solubilization. This was not the case for the systems of  $C_{16}TAOH$ ,  $C_{14}TAOH$  and  $C_{12}TAOH$  mixed with an increasing amount with 2,1 HNC, at which all of them formed directly after mixing a stable phases. After almost six months of observations, it was found that these phases are still stable. In the acidic pH, the samples are of yellow-brown color, while milky-brown color is seen in the basic pH. As a result of that it is concluded that this system shows many microstructures and behaves differently from the previous systems. In this system the high viscosity due to the formation of rodlike micelles is not observed. Vesicles and multilamellar vesicles are formed after the neutralization. This finding suggests a transition from small micellar aggregates (globular) into vesicle (which can be seen between two crossed polarizers) through a two

phase region without coming across the rodlike micelles. One reason for lack of rodlike micelles formation for the systems having cationic surfactants carbon chain length equal or less than  $C_{10}$  can be the fact that the organic salt molecules with rigid aromatic ring would not allow the hydrophobic chains to come close to each other, so that their proper orientation needed for the growth of a rod is not realized. Because of this the value of packing parameter for these systems is always higher than the desired for rodlike micelles formation (is more closed to one). That is why the increase in the concentration of 2,1 HNC for these systems yields multilamellar vesicles.

***The system  $C_8TAOH$  /2,1HNC/Water*** : In this system the length of the cationic surfactant chain is only half of the length of the  $C_{16}TAOH$ . In figure 3.37 (forth system, A, B and C), the solutions were photographed two times, shortly after preparation and after one month of preparation. After preparation, one finds upon increasing the content of 2,1 HNC, single isotropic phase, two phase regions, strong birefringent phase region, slightly birefringent turbid phase region, and then two phase region again. After one month one finds, single isotropic phase, two phase region, two phase region resulting from the sedimentation of the birefringent aggregates, one turbid region, and two phases region. The solutions were regularly observed for almost half year, and it is found that the turbid region is also two phase region. The solutions in basic pH are with yellow color while milky -brown solutions are observed in the acidic pH. At 2,1 HNC/ $C_8TAOH$  ratio  $r \sim 0.4$  or less, the solutions are low viscous and consist of single isotropic phase. From  $r \sim 0.4$  up to  $r \sim 0.9$ , the samples are in two phase region. The upper region is an isotropic and colorless, while the lower is an isotropic phase or precipitated aggregates that were birefringent phases when the solutions were freshly prepared. The solutions at  $r \sim 0.95$  up to  $r \sim 1.0$  seem to be in one single turbid phase. The solution  $r \sim 0.95$  resisted the sedimentation for longer time (more than 4 months). They are slight birefringent. At  $r > 1.1$ , the solutions are in two phases. As a result of that one can concluded that this system has new phase behavior. Similar to other systems, vesicle formation is seen.



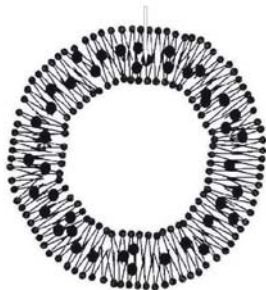
$c(2,1 \text{ HNC})[\text{mM}]$

Figure 3.37: Phase behavior in the systems  $C_{14}\text{TAOH}$ ,  $C_{12}\text{TAOH}$ ,  $C_{10}\text{TAOH}$  and  $C_8\text{TAOH}$  mixed with different concentrations (mM) of 2,1 HNC at 25 °C. For each system, solutions with 100 mM cationic surfactant and an increasing amount of 2,1 HNC without polarizers (top row) and between two crossed polarizers (bottom row). The numbers below the pictures indicate the concentration of 2,1 HNC. For the system  $C_8\text{TAOH}/2,1 \text{ HNC}$ , A (the solutions without polarizers) and B, C [between two crossed polarizers for freshly solutions(B) and after one month of preparation (C)]

### 3.3.2 Conductivity and pH Measurements:

The conductivity and pH of system of 100 mM  $C_x$ TAOH ( $x=8,10,12,14$ ) with increasing amounts of 2,1 HNC at  $T = 25^\circ\text{C}$  are shown in figures 3.38 and 3.39. The conductivity curve as a function of 2,1 HNC concentration is similar to that were obtained for the systems  $C_{16}$ TAOH mixed with an increasing amount of 2,1 HNC. For systems with two phase region  $C_8$ TAOH and  $C_{10}$ TAOH mixed with 2,1 HNC, the solutions were kept under stirring during the measurement. The conductivity decreases perceptibly from the beginning before reaching the turbid region, then as the new phase starts to form, the conductivity decrease again but with change in slope until reaching the equimolar ratio. After neutralization ( $\text{pH}=7$ ) further addition of 2,1 HNC changes the conductivity only slightly. This indicates that 2,1 HNC is present in the molecular form (water insoluble). Solubilization of non polar hydrocarbon in the vesicle phase was reported by Hoffmann, et [133]. It was concluded that the hydrocarbon molecules are not incorporated into the interior of the bilayers, but they are located in the palisade layer and oriented parallel to the surfactant chains. Similarly, but, for bulky non polar molecules, Jung et al.[38] reported the solubilization of styrene monomers in dioctadecyldimethylammonium bromide (DODAB) between the chains of cationic surfactants within the bilayers as shown in the below given figure

Water insoluble Particles



As a result of that one can conclude that the excess un-reacted 2,1 HNC is also solubilized in palisade layer of the surfactants. As the chain length increases, the conductivities minimum decrease due to the higher hydrophobicity in the system.

From the pH curve, it is concluded that total neutralization happens when the two substances are equally mixed as it is theoretically assumed and the pH curve is almost similar to conductivity curve. In the pH- curve, pH 7 has a correspondence to 100 Mm 2,1 HNC and 100 mM cationic surfactants.

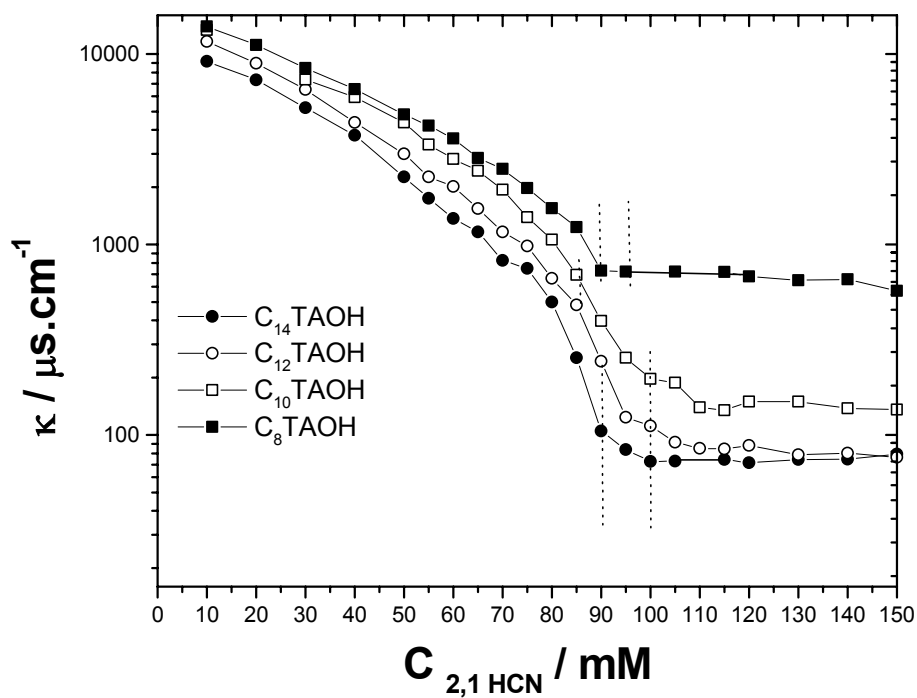


Figure 3.38: Conductivity of 100 mM  $C_x$ TAOH and increasing amounts of 2,1 HNC.

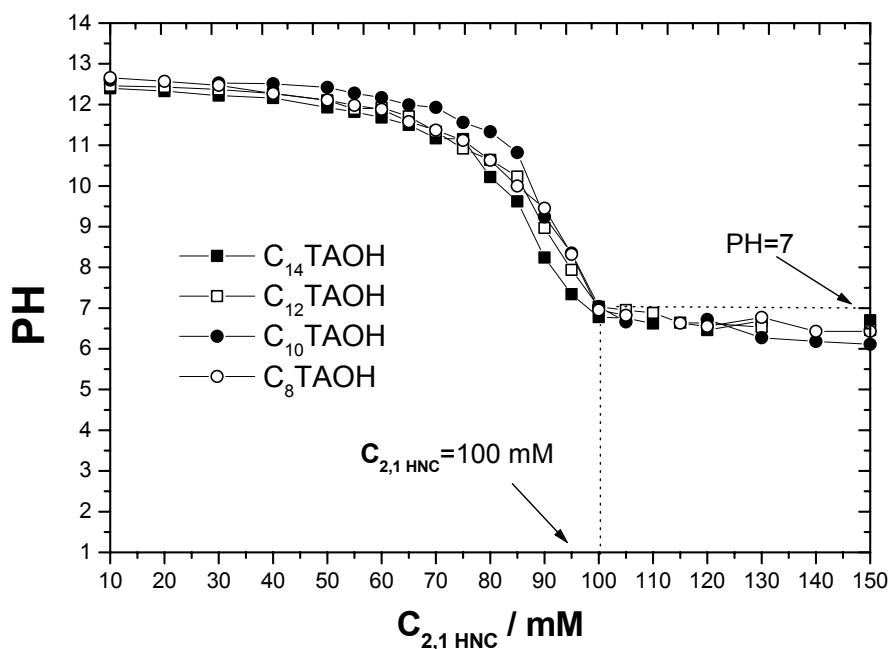


Figure 3.39: PH of 100 mM  $C_x$ TAOH and increasing amounts of 2,1 HNC.

### 3.3.3 Differential interference contrast microscopy

Differential interference contrast microscopy was used to characterize the liquid crystalline phases in the systems  $C_{12}TAOH/2,1$  HNC and  $C_{10}TAOH/2,1$  HNC at 25 °C. The features of these systems are discussed below.

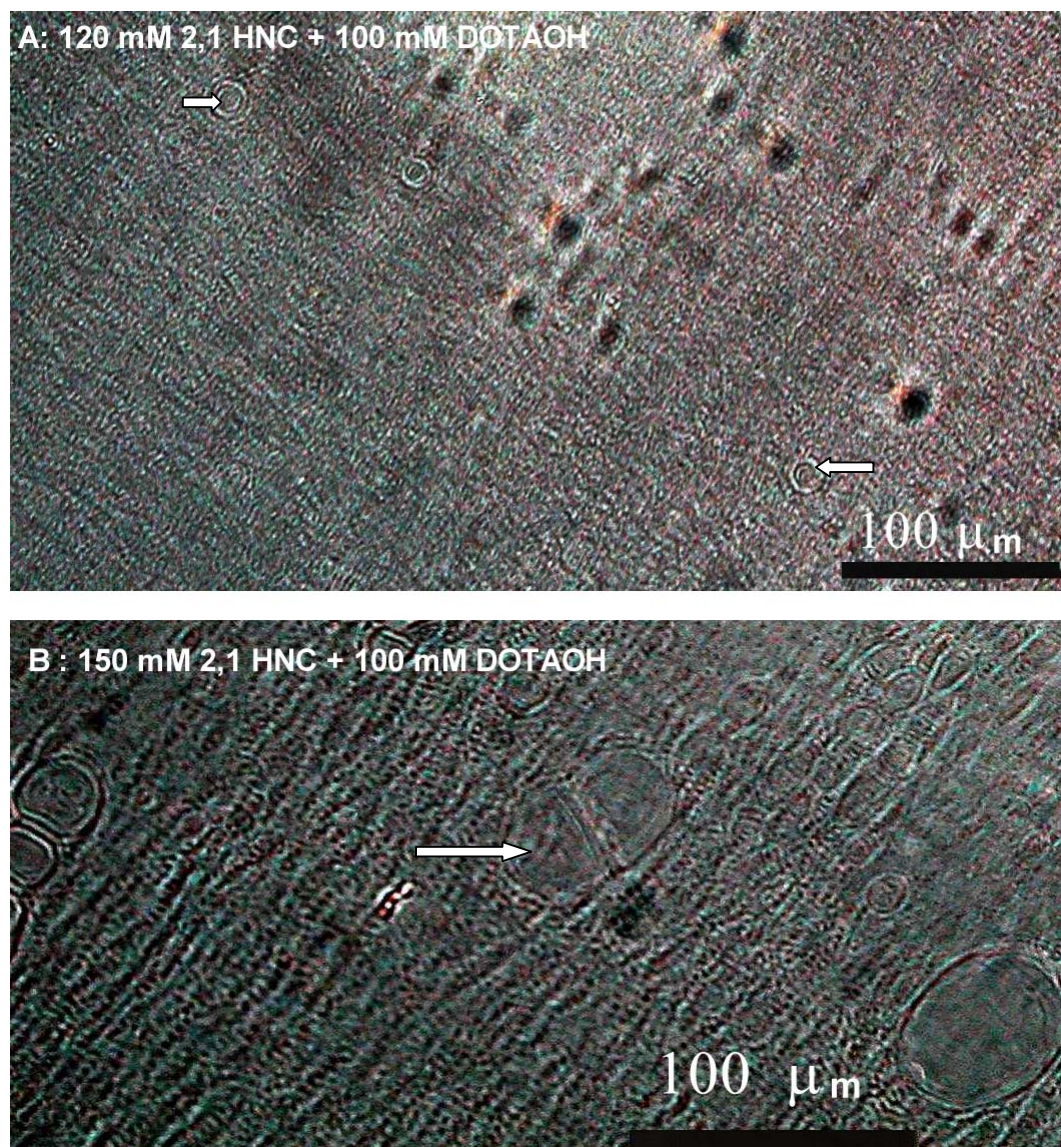
#### *The system $C_{12}TAOH/2,1$ HNC :*

Figure 3.40 shows micrographs of the liquid crystalline phase for the solutions consisting of 120 and 150 mM 2,1 HNC mixed with 100 mM  $C_{12}TAOH$ . The photographs show the structure of multilamellar vesicles. The multilamellar vesicles are polydispers, the biggest ones have diameters of about 60  $\mu\text{m}$  in the solution that has 150 mM 2,1 HNC. Some vesicles are deformed as seen in the sample of 150 mM 2,1 HNC. These vesicles are made from lamellar membranes. They have elliptically-shaped structure as indicated by the arrows on the picture. The specimen in the form of a film of 20  $\mu\text{m}$  thickness was prepared by placing droops of solution on a glass slide and covering it with a cover slip.

#### *The system $C_{10}TAOH/2,1$ HNC :*

Figure 3.41 shows micrographs of the liquid crystalline phase for the solutions consisting of 120 or 130 mM 2,1 HNC mixed with 100 mM  $C_{10}TAOH$ . The pictures show the vesicles structure. It was not possible to get higher quality pictures using this technique. The bar in the pictures refers to 100  $\mu\text{m}$ . few vesicles are with diameter of about 30  $\mu\text{m}$  (in picture B). Since there are vesicles with variation in the size, these solutions are classified to be polydisperse. It is difficult to decide whether these vesicles are multilamellar or not on the bases of their micrographs. Increasing the concentration of 2,1 HNC makes no significant difference on shape and the size of the vesicles in these pictures. The most clear picture is the one which contains 130 mM 2,1 HNC and 100 mM  $C_{10}TAOH$  and in this picture one can see vesicles which are deformed and elliptically-shaped. This can be explained in the same way the previous systems were explained, at which these irregular structures could be the result of the membrane flexibility or it is just the effect of laying the solution on the flat surface (glass table), and then cover it with another glass (deformation of vesicles). This causes a type of pressing force, which acts on these vesicles, and consequently they deform. As before, these vesicles are made from lamellar membranes.

As a result of this, differential interference contrast microscopy proves the formation of vesicle phase in the systems of  $C_{12}$ TAOH/2,1 HNC and  $C_{10}$ TAOH/2,1 HNC at 25 °C.



*Figure 3.40: Differential interference contrast micrographs for solutions with 100 mM  $C_{12}$ TAOH and 120 (A) or 150 (B) mM 2,1 HNC at 25 °C. The solution contains polydisperse vesicles. The bar (at bottom to right) refers to 100  $\mu$ m.*

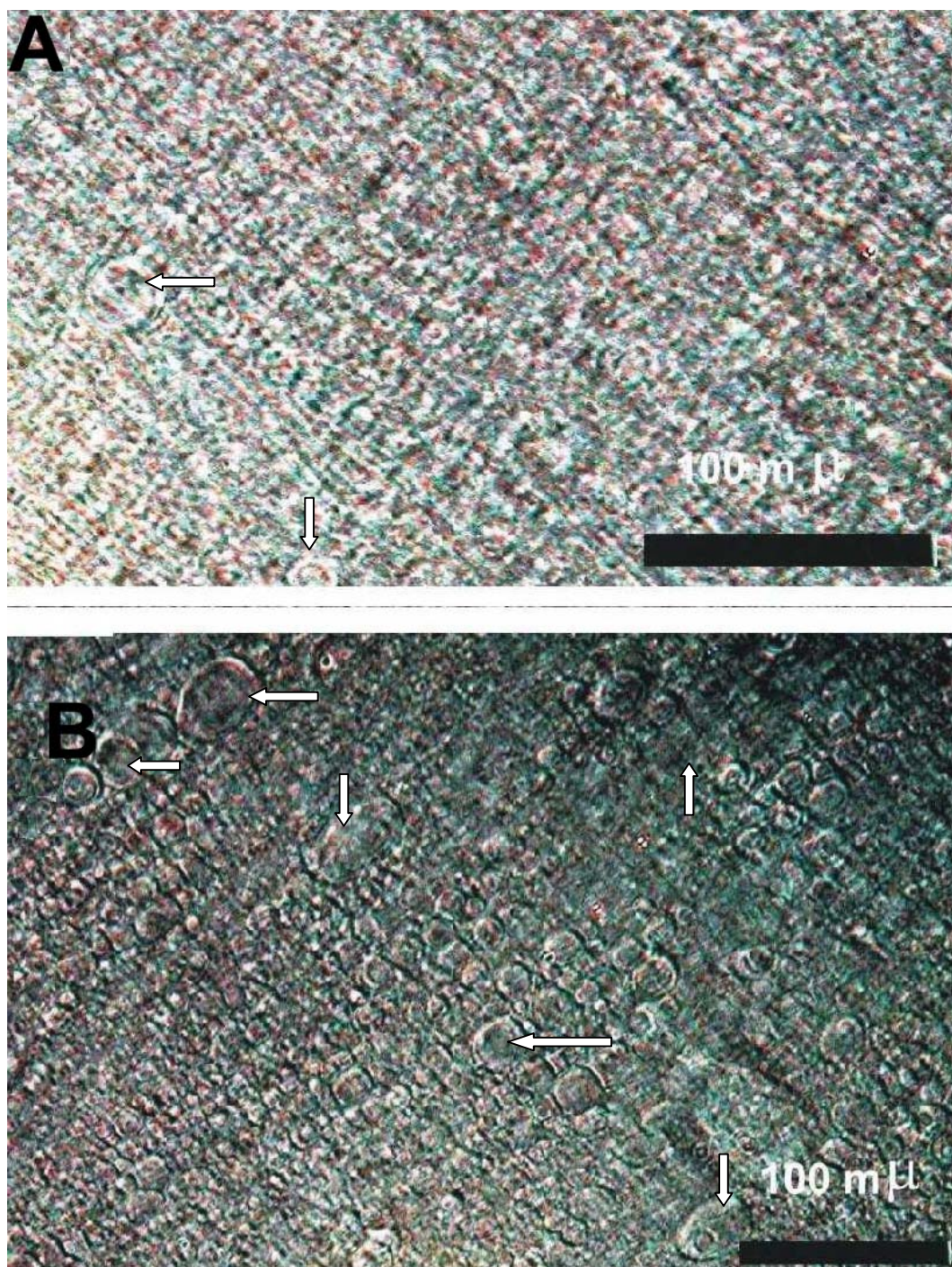


Figure 3.41: Differential interference contrast micrographs for solutions with 100 mM  $C_{10}TAOH$  and (A) 120 or (B) 130 mM 2,1 HNC at 25 °C. Both of these solutions show vesicles. The bar (at bottom to right) refers to 100  $\mu$ m.

## 3.3.4 Freeze- Fracture Electron Microscopy ( FF-TEM )

The results of FF-TEM for the different systems of  $C_x$ TAOH ( $x=14,12,10,8$ ) and 2,1 HNC are discussed below:

The system  $C_{14}$ TAOH/2,1 HNC

The FF-TEM micrograph for the system with 100 milli moles of each of 2,1 HNC and  $C_{14}$ TAOH is displayed in figure 3.42. The picture clearly reveals the presence of multilamellar vesicles with different shells. The larger vesicles consist of at least ten shells. The size of vesicles ranged from 100 to 2200 nm and hence the phase is polydispersed. As far as the shape of the vesicles is concerned, some of them are spherical in shape and while some others are elliptical.

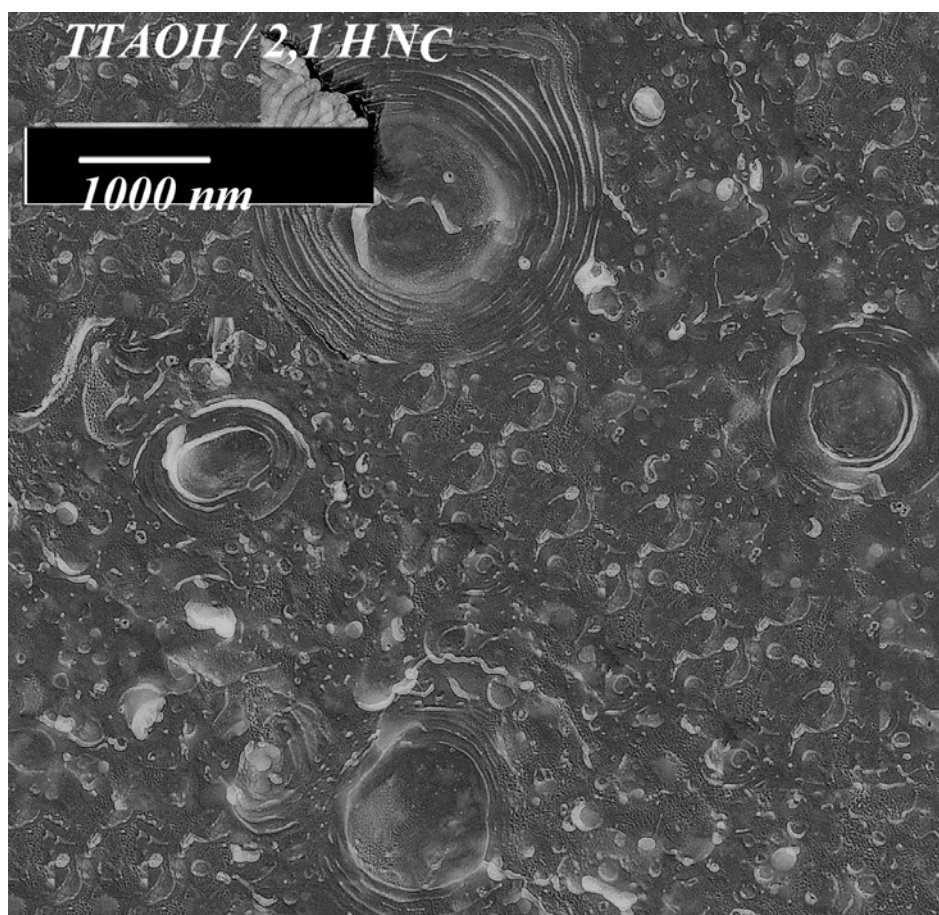


*Figure 3.42: FF-TEM electron micrograph for solution with 100 mM TTAOH and 100 mM 2,1 HNC showing multilammelar vesicles about 100-2200 nm in diameter. The arrow refers to elliptically-shaped vesicles.*

***The system  $C_{12}TAOH/2,1 HNC$*** 

The multilamellar vesicles are made visible with the freeze-fracture technique for the system of 100 mM 2,1 HNC and 100 mM  $C_{12}TAOH$ . A typical micrograph is shown in figure. 3.43, which illustrates that the vesicles have a large polydispersity as seen for the previous systems of  $C_{16}TAOH$ ,  $C_{14}TAOH$  mixed to equal molar ratio with 2,1 HNC. The vesicle's membranes are primarily spherical, although some of them are elliptically-shaped. It seems that the vesicles exist in the system that consist of one to at least ten bilayers. From the picture, the distance between the two sequenced shells is in the range of 60 nm. In figure 3.43, A, B, C and D all for the same system but with different magnifications. The vesicles have diameters ranging from 100 to about 1000 nm. In figure 3.43, A the arrow indicates to elliptically-shaped, or elongated vesicle. Such shapes may be the equilibrium conformations of vesicles because the mixed bilayers are somewhat flexible.

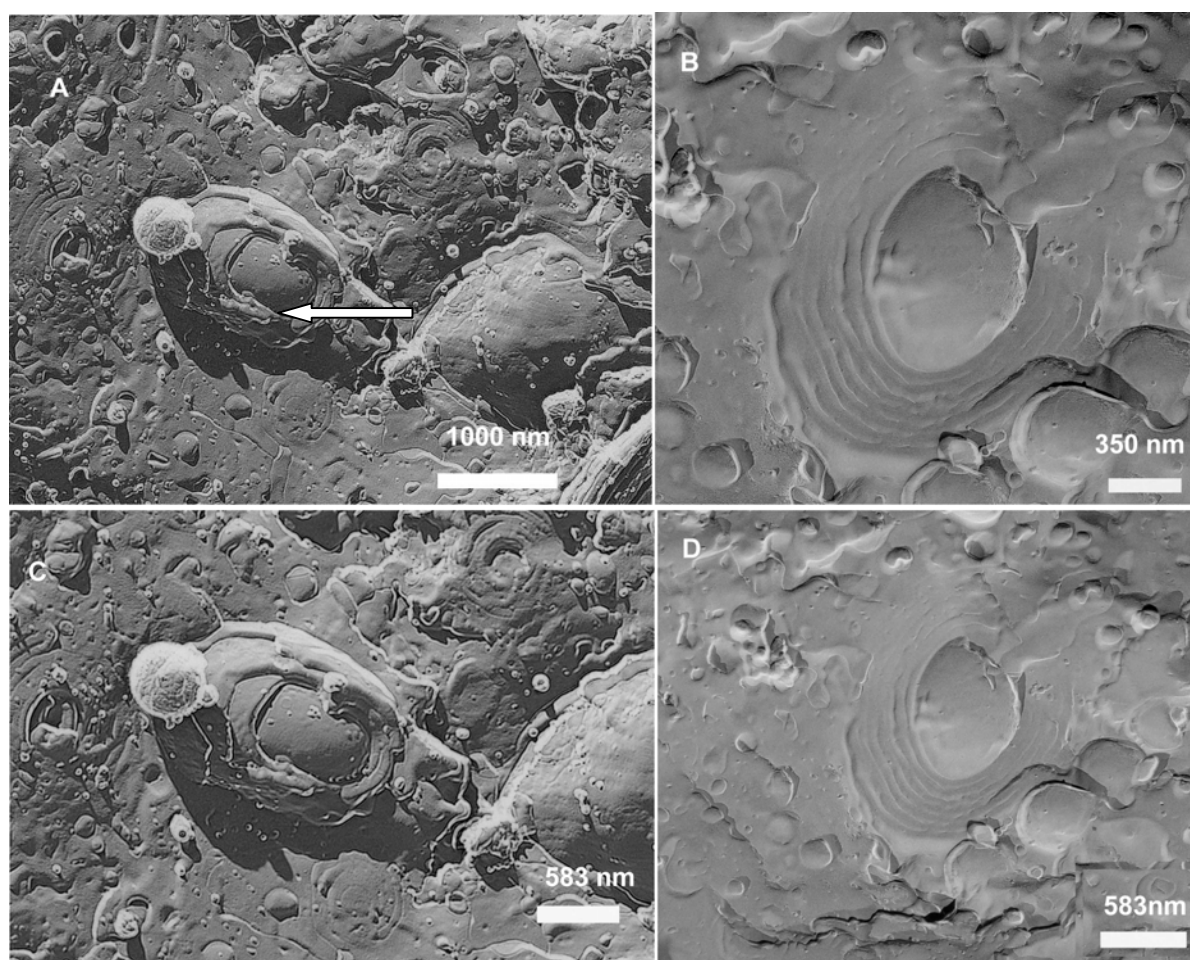


*Figure 3.43: FF-TEM electron micrograph for solution with 100 mM DOTAOH and 100 mM 2,1 HNC showing multilamellar vesicles of about 100 to 1000 nm in diameter. The interlamellar spacing is about 60 nm. A, B, C and D all for the same sample but with different magnifications. In (A) the arrow refers to elliptically-shaped vesicle.*

#### ***The system C<sub>10</sub>TAOH/2,1 HNC***

Multilamellar vesicles and the transition structure, which are seen in the phase behavior are made visible with freeze-fracture technique. FF-TEM micrographs of the solution of 80 mM, 100 mM and 150 mM 2,1 HNC mixed with 100 mM C<sub>10</sub>TAOH are shown in the figures 3.44, 3.45 and 3.46. The solutions of these samples seen between two crossed polarizers were found to be slight birefringent, more birefringent, and strongest birefringent respectively. This has its effect on the resulted structure as seen in the FF-TEM micrographs. The microstructure properties of each system is separately discussed.

#### ***The system of 100 mM C<sub>10</sub>TAOH and 80 mM 2,1 HNC :***

Figure 3.44 shows the microstructure from this system. The observed structures indicate the presence of morphologies similar to unilamellar vesicles. The vesicles are interlaced in a way so that they appear to be continuous (or like spongy-phase). Some of the structures are spherical, while the others are elongated and curved. These structures exhibit a diameter which ranges from 100 nm to 200 nm. The arrow in the figure indicates a vesicle which is surrounded by another one. This could be the nucleus for a big multilamellar vesicle upon increasing the concentration of 2,1 HNC in the solution.

#### ***The system of 100 mM C<sub>10</sub>TAOH and 100 mM 2,1 HNC :***

Figure 3.45 shows the presence of multilamellar vesicles in the solution of 100 mM 2,1 HNC and 100 mM C<sub>10</sub>TAOH. Figure 3.45 illustrates that the vesicles are polydisperse. The vesicle's membranes are spherical. It seems that vesicles exist in the system that consist of one to at least ten bilayers. The multilamellar vesicles have a diameter ranging from 100 to about 4000 nm. The deformed vesicles are indicated by the colored arrows. The deformation could have taken place during the fracturing process. The interlamellar spacing for the biggest vesicle has a thickness of about 60 nm. There is also membrane ruptures and some artifacts in the picture.

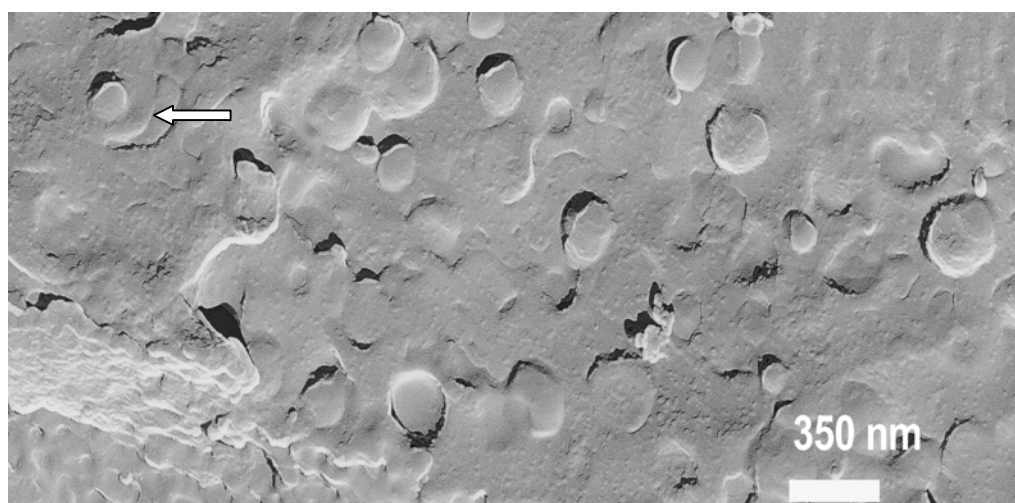


Figure 3.44: FF-TEM electron micrograph for solution with 100 mM  $C_{10}$ TAOH and 80 mM 2,1 HNC showing the transition microstructure structure into multilamellar vesicles. The structures have a diameter ranging from 100 to 200 nm. The arrow refers to structure which seems to have two bilayers.

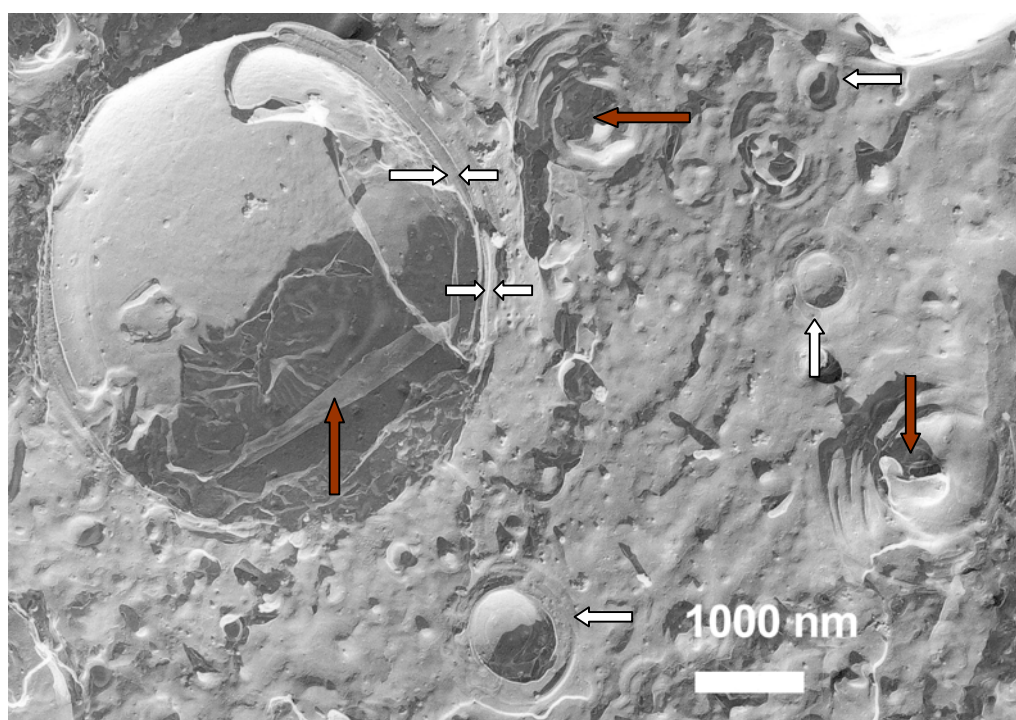


Figure 3.45: FF-TEM electron micrograph for solution with 100 mM  $C_{10}$ TAOH and 100 mM 2,1 HNC showing multilamellar vesicles with a diameter ranging from 100 to 4000 nm. The vesicle interlamellar spacing is about 60 nm. The arrows indicate some ruptured membranes.

***The system of 100 mM C<sub>10</sub>TAOH and 150 mM 2,1 HNC :***

Multilamellar vesicles are made visible with freeze-fracture for the solution with 150 mM 2,1 HNC and 100 mM C<sub>10</sub>TAOH. A typical micrograph is shown in figure 3.46, which illustrates that the vesicles have a large polydispersity. Such multilamellar vesicles were not seen with the concentration value of 80 mM 2,1 HNC and hence, the structures noted in figure 3.44 are the transition structures. Otherwise, the vesicles are primarily spherical, although some of them are elliptically-shaped. It seems that vesicles exist in the system that consist of one to at least nine bilayers. From the picture, the interlamellar spacing is in the range of 40 nm. In figure 3.46, the micrographs A, B, C, D, E and F are all for the same solution but with different magnifications, or the same magnification and different locations. The vesicles have a diameter ranging from 100 to about 4000 nm. Among the previous systems, it is the first time that such big vesicles are seen. The same phenomenon is seen in the picture of 100 mM 2,1 HNC and 100 mM C<sub>10</sub>TAOH. The previous systems exhibit a multilamellar vesicle with a average diameter of about 1000 nm. It seems that shortening the chain lengths leads to larger vesicles. This could be explained that the interaction between the chains decreases as they become shorter, and that is why cmc has usually inverse proportionality to chain length. As a result of that more flexible membranes with lower binding rigidity constant  $k_c$  are obtained, which may prefer larger vesicles size as a thermodynamic stable microstructure

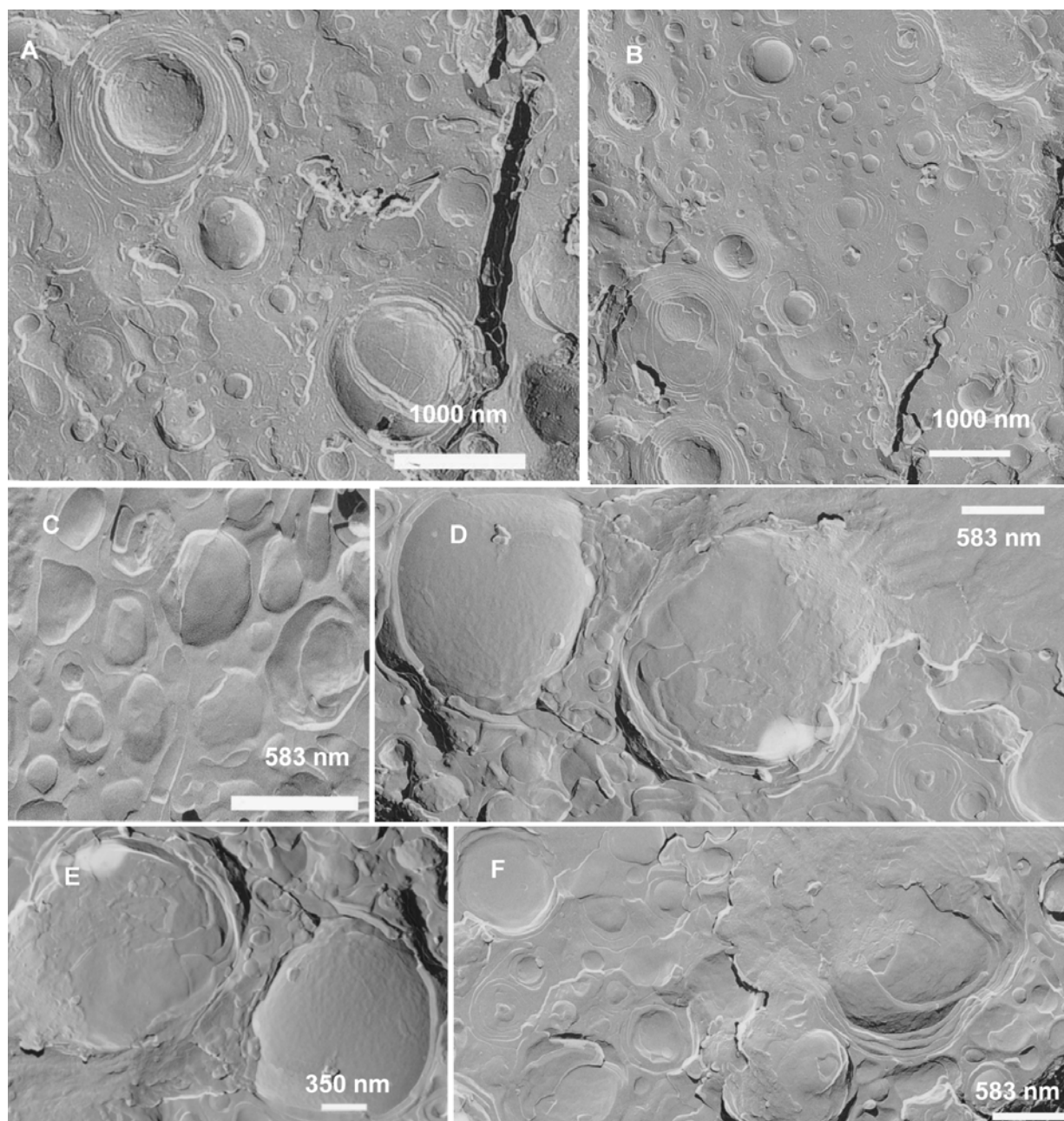
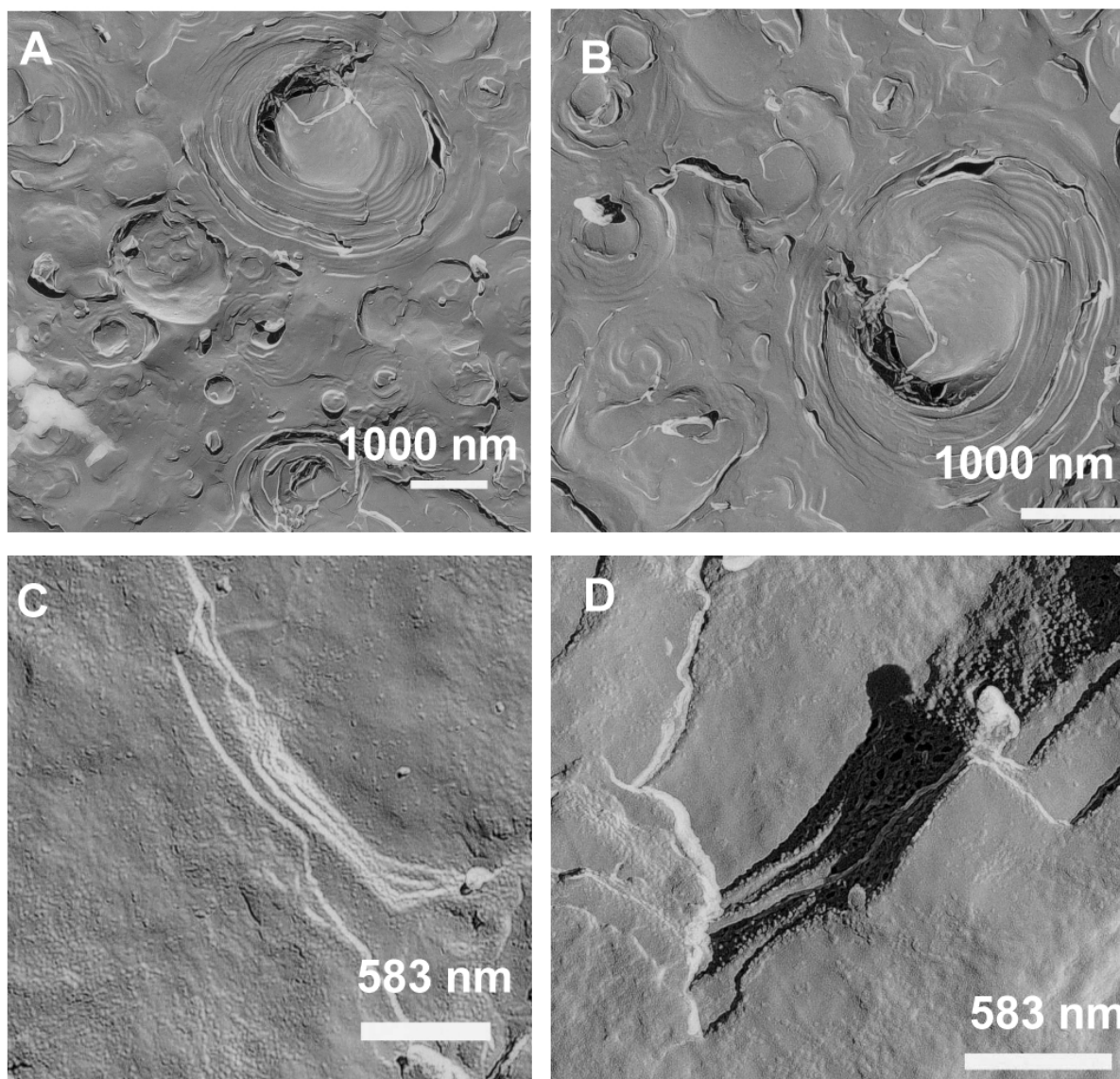


Figure 3.46: FF-TEM electron micrograph for solution with 100 mM  $C_{10}$ TAOH and 150 mM 2,1 HNC showing multilamellar vesicles with diameter ranging from 100 to about 4000 nm. A, B, C, D, E and F all for the same solution but with different magnifications, or different locations for the same magnification .

#### *The system C<sub>8</sub>TAOH/2,1 HNC*

The system with 100 mM 2,1 HNC and 100 mM C<sub>8</sub>TAOH shows the presence of multilamellar vesicles, which are made visible with the freeze-fracture technique. A typical micrograph is shown in figure 3.47, which illustrates that the vesicles have a large polydispersity as seen for the previous systems of C<sub>16</sub>TAOH, C<sub>14</sub>TAOH, C<sub>12</sub>TAOH mixed to equal molar ratio with 2,1 HNC. There are also some lamellar sheets in the solution. The vesicle membranes are primarily spherical, although some of them are deformed. It seems that the vesicles exist in the system that consist of one to at least eight bilayers. In figure 3.47, A, B, C and D all for the same sample but with different magnifications, or the same magnification and different locations. The vesicles have a diameter ranging from 100 to about 3500 nm. This system also shows large vesicles as the system 2,1 HNC/C<sub>10</sub>TAOH. It seems that the shortening of the chain leads to larger vesicles. This could be explained by the idea that the hydrophobic interaction between the chains decreases as they become shorter because of lower van der Waals forces, so they prefer to have a flat surface (lamella) or big multilamellar vesicles.



*Figure 3.47: FF-TEM electron micrograph for solution with 100 mM  $C_8TAOH$  and 100 mM 2,1 HNC showing flat lamella and multilamellar vesicles about 100 to 3500 nm in diameter. A, B, C, D, E and F all for the same solution but with different magnifications, or different locations for the same magnification .*

## 3.3.5 SANS:

SANS spectra are resulted from two factors. The first called structural factor which describes the interparticle correlations while the second one called form factor which describes the size and the shape of individual particles. SANS curves are shown in Figure 3.48 A, B, C, and D for the solution with 100 mM 2,1 HNC mixed with 100 mM  $C_x$ TAOH ( $x=8,10,12,14$ ). The result of each system is discussed below.

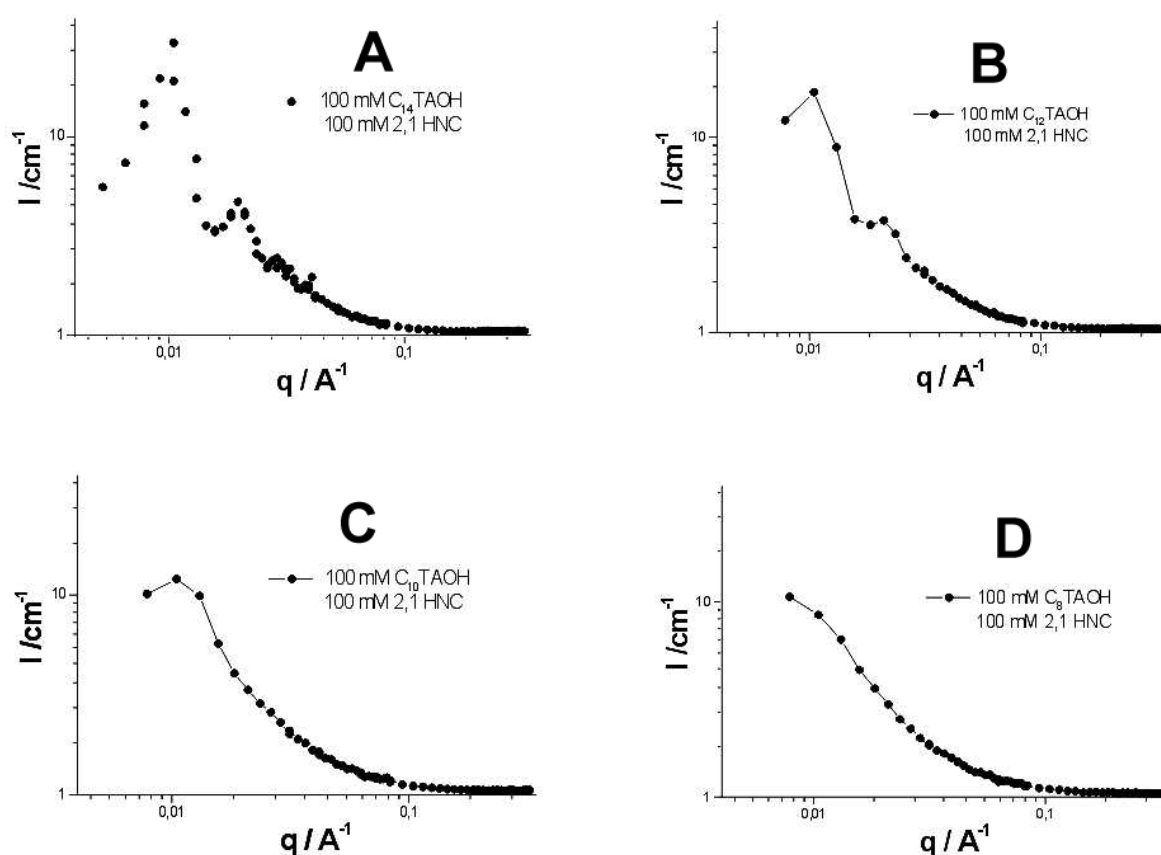


Figure 3.48 : The SANS spectra at 25 °C for the solutions with 100 mM 2,1 HNC and 100 mM  $C_x$ TAOH [ $x=14$ (A), 12(B), 10(C) and 8(D)].

**The system  $C_{14}$ TAOH/2,1 HNC :**

The curve of the solution shows a correlation peak of multilamellar vesicles as shown in figure 3.48 A. The  $q$ -value at maximum scattering angle ( $q_{\max}$ ) is  $0.0103 \text{ \AA}^{-1}$ . This value can be used for calculating the interlamellar distance ( $d$ ) by solving:  $d = 2\pi/q_{\max}$ . Accordingly, the  $d$  value is about of 61 nm which is almost similar for the system of 2,1

HNC/ C<sub>16</sub>TAOH. The thickness of the bilayer is calculated assuming  $\phi = \frac{l}{d}$ , where  $\phi$  is the volume fraction, which is about 0.0464 for C<sub>14</sub>AOH + 2,1 HNC, and  $l$  is the bilayer thickness. So  $l$  is about 28 Å which is in agreement with the chain length of C<sub>14</sub>. The bilayer thickness is approximately twice of C<sub>14</sub> chain. The correlation peak ratio  $C$  for the two peaks in L $\alpha$ -phase  $C = q_2/q_1$  is about 2. The system shows also a second small peak at higher  $q$ -values. This peak originates from structures with a different orientational order in the system. The maximum scattering intensity of these oriented aggregates is detected at higher angles.

***The system C<sub>12</sub>TAOH/2,1 HNC :***

SANS curves are shown in figure 3.48 B shows a correlation peak of multilamellar vesicles. This result is in agreement with that obtained by FF-TEM. Scattering vector at maximum intensity ( $q_{\max}$ ) is 0.01038 Å<sup>-1</sup>. Accordingly, the interlamellar distance ( $d$ ) is about 60.5 nm which is almost similar to that obtained from FF-TEM. The volume fraction of the surfactants ( $\phi$  of C<sub>12</sub>TAOH + 2,1 HNC) is about 0.045, so the thickness of the bilayer is about 27 Å which is almost in agreement with the chain length of C<sub>12</sub>, and by assuming that the bilayer thickness is as approximately as twice of C<sub>12</sub> chain length. The correlation peak ratio  $C$  for the two peaks in L $\alpha$ -phase is about 2.

***The system C<sub>10</sub>TAOH/2,1 HNC :***

SANS curves are shown in figure 3.48 C for the solution with 100 mM 2,1 HNC mixed with 100 mM C<sub>10</sub>TAOH. The scattering vector at maximum intensity ( $q_{\max}$ ) is 0.0104 Å<sup>-1</sup>. Accordingly, the interlamellar distance ( $d$ ) is about 60 nm. This result is similar to that one obtained from FF-TEM. The volume fraction of the surfactants ( $\phi$  of C<sub>10</sub>TAOH + 2,1 HNC) is about 0.0438, so the thickness of the bilayer is about 26,3 Å which is almost in agreement with the chain length of C<sub>10</sub> assuming that the bilayer thickness is approximately twice of C<sub>10</sub> chain length. The shape of the SANS curve presented in the figure 3.48 is quite different from the earlier curves. In the present case, the second small peak observed at little higher  $q$  is absent. It could be concluded that the interparticle arrangements become lower. FF-TEM shows a difference in the orientation of the multilamellar vesicles in the system of 100 mM 2,1

HNC mixed 100 mM C<sub>10</sub>TAOH and the solution of 150 mM 2,1 HNC and 100 mM C<sub>10</sub>TAOH.

#### *The system C<sub>8</sub>TAOH/2,1 HNC*

SANS curves are shown in figure 3.48 D for the solution with 100 mM 2,1 HNC and 100 mM C<sub>8</sub>TAOH. The shape of the SANS curve is different from that obtained for other systems (C<sub>16</sub>TAOH, C<sub>14</sub>TAOH, C<sub>12</sub>TAOH when they are mixed to equal ratio with 100 mM 2,1 HNC). for this system, the intensity in the lower q-region increases monotonously with decrease in q-values. No peaks were observed. As already indicated, this system does not show rodlike micelles formation and the multilamellar vesicles formed are not well defined and hence have not only a different orientational order but also poor packing.

### 3.3.6 The Rheological behavior of the systems $C_xTAOH(x=14,12,10,8)/2,1 HNC$

The rheological behavior for the systems consisting of 100 mM  $C_xTAOH$  ( $x=14,12,10,8$ ) with increasing amounts of 2,1 HNC is depicted in figures 3.49 A, B, C and D. The figures present the variation of zero shear viscosity (for low viscous solutions) and complex viscosity at a frequency  $\omega = 0.01$  Hz (for viscoelastic solutions). In all the systems, the solutions were low viscous up to 40 mM 2,1 HNC content.

For the systems  $C_{14}TAOH/2,1 HNC$  and  $C_{12}TAOH/2,1 HNC$ , at a 2,1 HNC-concentration of 55 mM, the viscosity starts to increase and at 60 mM it rises strongly and the solutions become highly viscoelastic, indicating the formation of entangled rodlike micelles. The viscosities at the maximum are about 378 and 1 Pa.s for the two systems respectively. The viscosity decreases again in the turbid region, which starts at 2,1 HNC-concentration of 75 mM. It reaches a minimum of 2 Pa.s for  $C_{14}TAOH/2,1 HNC$ , while  $C_{12}TAOH/2,1 HNC$  has viscosity minimum about 0.03 Pa.s in the turbid region. As the transition to multilamellar vesicle starts, the complex viscosities at 0.01 Hz rise again and reach a plateau of about 600 and 200 Pa.s for the two systems respectively. The entire profiles can be divided into four regions; the low viscous region (I), the isotropic viscoelastic region (II), the turbid region (III) and the viscoelastic liquid crystalline region (IV). The rheological behavior of the systems  $C_{10}TAOH/2,1HNC$  shows that the viscosity starts to rise beyond 50 Mm 2,1 HNC until it reaches the two phase region which is followed by a turbid one. After the turbid region, it rises strongly, as the vesicles start to form. Further addition of 2,1 HNC leads to an increase of the viscosity until the multilammellar vesicle region is reached where the viscosity reaches a plateau. This happens when the content of 2,1 HNC is about 120 mM, and the complex viscosity reaches a maximum of 40 Pa.s. Thus, the main regimes of this system can be divided into three regions. They are, the low viscous region (I), the two phase region (II), and region (III), which has the vesicles and the multilamellar vesicles. For the system,  $C_8TAOH/2,1 HNC$ , at a 2,1 HNC-concentration of higher than 40 mM, the solutions are in two phases, so no viscosity measurements were carried out. The viscosity increases again in the turbid region (two phase region but they look like one phase for long time after preparation) then the two phase region appears again. In the following paragraphs, more details about the rheological properties of these regions are discussed.

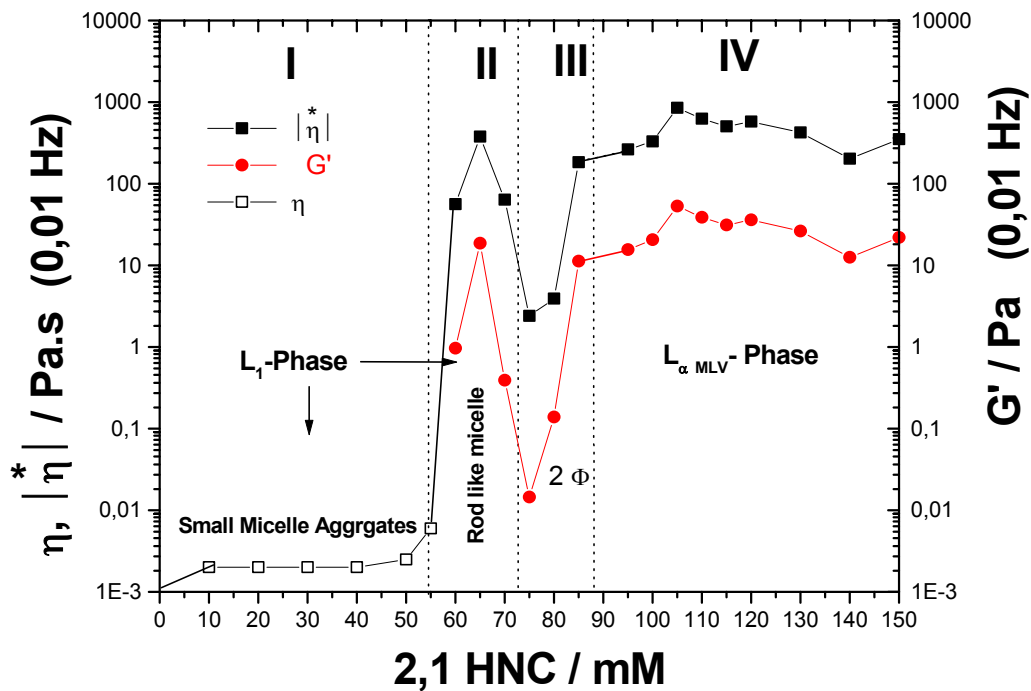


Figure 3.49A: Viscosity ( $\eta$ ) obtained by double gap method (DGM), complex viscosity ( $\eta^*$ ) and storage modulus ( $G'$ ) (at 0,01 Hz) obtained from oscillation measurements for 100 mM  $C_{14}TAOH$  as a function of increasing amounts of 2,1 HNC in mM at 25 °C.

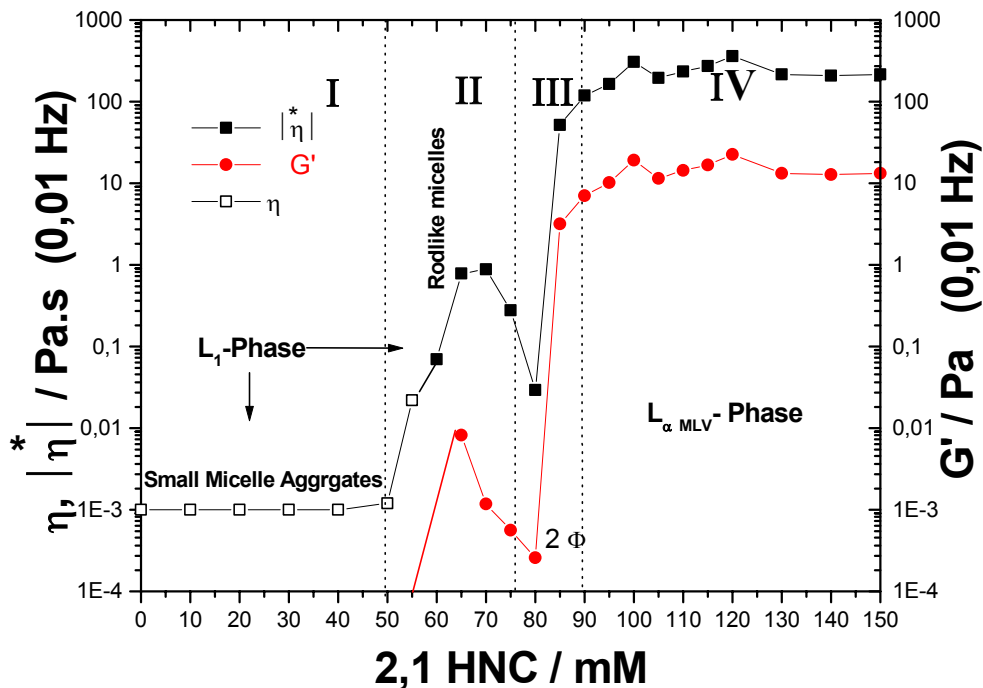


Figure 3.49B: The same as figure 3.49 A, but for the system  $C_{12}TAOH/2,1 HNC$ .

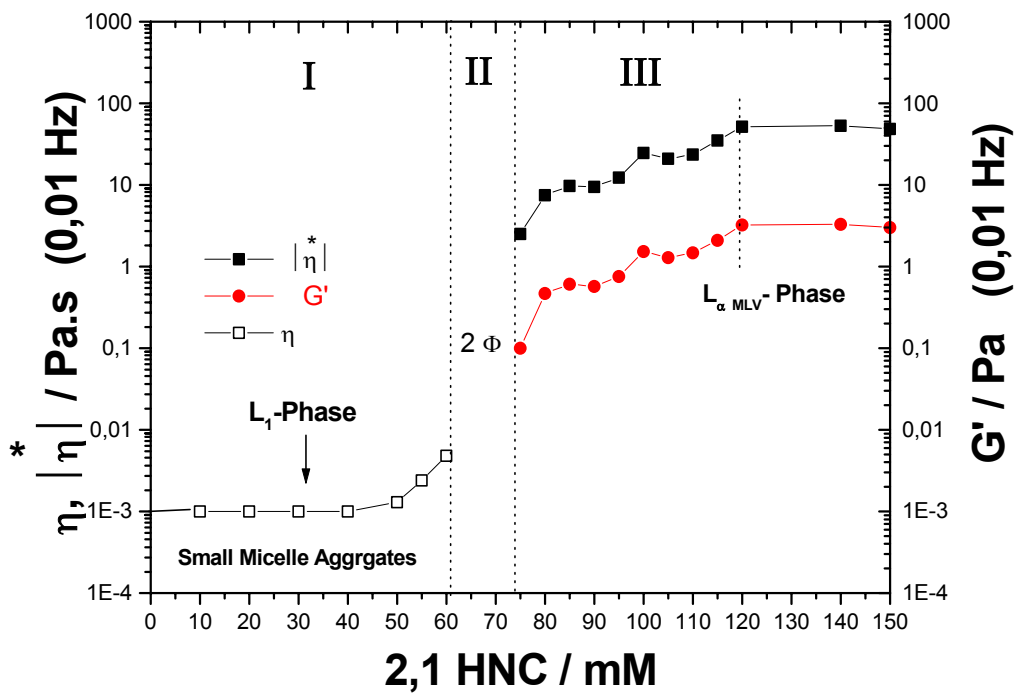


Figure 3.49C: The same as figure 3.49 A, but for the system  $C_{10}TAOH/2,1 HNC$ .

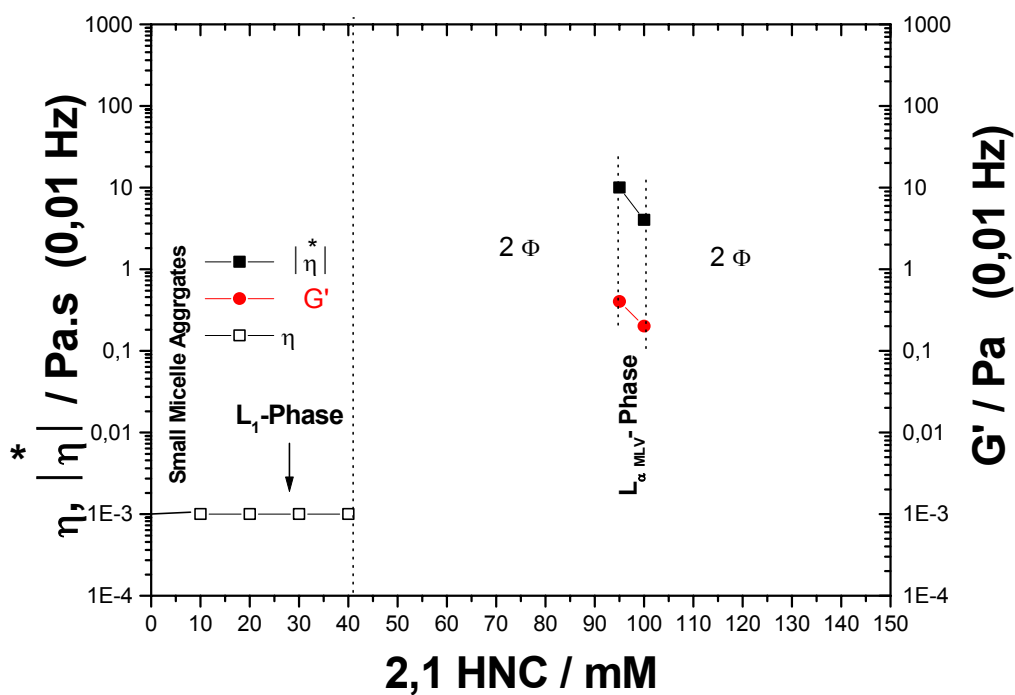


Figure 3.49D: The same as figure 3.49 A, but for the system  $C_8TAOH/2,1 HNC$ .

**Region I for the systems  $C_xTAOH(x=14,12,10,8)/2,1 HNC$ :**

As it is shown in the figures 3.49 A, B, C, solutions with a HNC-content less than 50 mM behave like Newtonian liquids. They have viscosity almost similar to the solvent ( $\sim 1$  mPa.s). The reason for such low viscosity is the presence of micelles with small sizes with either spherical or globular shapes. In this region the concentration of 2,1 HNC is not enough to shield the charge density on the micelle surface. At 55 mM 2,1 HNC the viscosity starts to rise. This is an indication of transition to another micellar structure. For the system  $C_8TAOH/2,1 HNC$ , this region ends when the concentration of 2,1 HNC is about 40 mM.

**Region II (Rod like micelles and two phase regions)**

**Rodlike micelles in the system  $C_{14}TAOH/2,1 HNC$ :** The solutions in this region exhibit high viscosity due to the presence of entangled rodlike micelles. The solutions show typical Maxwell behavior with one relaxation time compared to the system of 2,1 HNC/  $C_{16}TAOH$ . The relaxation time becomes longer when the concentration of 2,1 HNC is changed from 60 to 65 mM. At higher 2,1 HNC concentrations, the relaxation time becomes shorter and is shifted to higher frequency. Figure 3.50 shows this behavior at which the storage modulus starts to decrease at frequency about 0.1 Hz when the 2,1 HNC concentration is 60 mM, then 0.01 and 0.2 Hz for the concentrations 65, 70 respectively.

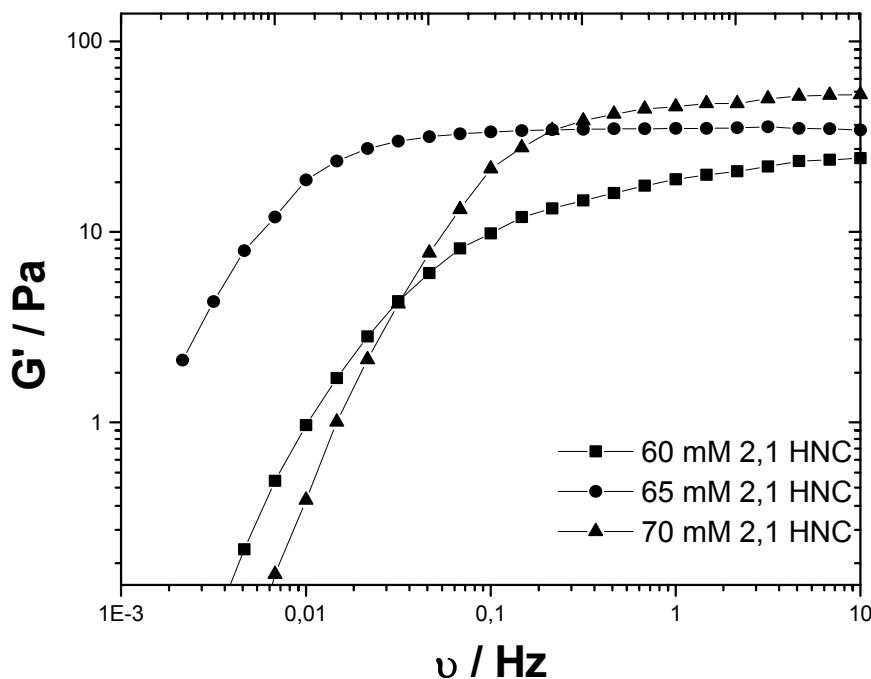


Figure 3.50: Storage modulus  $G'$  versus frequency  $\omega$  for 100 mM  $C_{14}TAOH$  mixed with 60, 65, and 70 mM 2,1 HNC at 25 °C.

This behavior of relaxation time can be explained in terms of Cate's theory [118-119]. Accordingly, the increase of both viscosity and relaxation time is explained by an increase of the micellar length owing to the more hydrophobicity of HNC<sup>-</sup>, which reduces the scission energy of the micelle due to the decrease of the electrostatic contribution. Second decrease of relaxation time is attributed to the formation of intermicellar connections, which is favored when the rodlike micelles are strongly shielded. The presence of intermicellar linkages accelerate the repetition process (discussed in details in the last chapter) and decreases the average micellar lengths thereby reducing viscosity and relaxation time. Figure 3.51 shows the rheogram for a solution with 70 mM 2,1 HNC content. In this Maxwell behavior one finds that both storage and loss modulus are frequency dependant and the viscosity becomes independent of the frequency when the storage and loss modulus cross each other.

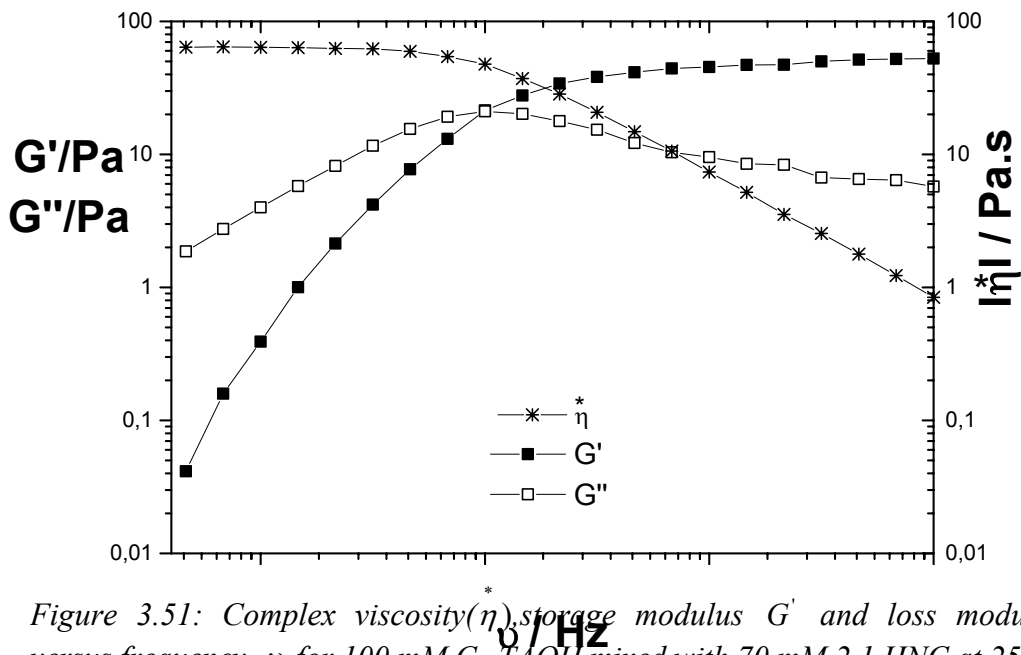


Figure 3.51: Complex viscosity ( $\eta^*$ ), storage modulus  $G'$  and loss modulus  $G''$  versus frequency  $\omega$  for 100 mM  $C_{14}TAOH$  mixed with 70 mM 2,1 HNC at 25 °C.

**Rodlike micelles in the system  $C_{12}TAOH/2,1$  HNC:** The complex viscosity (0.01 Hz) reaches a maximum which is three orders of magnitude higher than the viscosity of the solvent when the content of 2,1 HNC is about 65 mM. This differs from the result which has been obtained for the system of 2,1 HNC/ $C_{16}TAOH$ , at which the viscosity was six orders of magnitude higher than the viscosity of solvent. As a result, the chain length is an important factor in the resulted complex viscosity. Hoffmann and coworkers made a comparison for the magnitude of complex viscosity for a homologous solution series of alkylpyridiniumsalicyltates in the presence of NaCl and found similar behavior. As the chain length increases, the resulted complex viscosity increases [127]. Since the viscosity depends on the normal modulus and relaxation time, this changing of the viscosity was explained to be a result of changing in relaxation times of these solutions and not normal modulus. In that system there was also slight changing in the shear modulus which is explained by the fact that as the chain length decreases, the cmc increases, so the amount of surfactant which is in the micellar form decreases and this affects directly the value of shear modulus. In this system there is also a shift in the relaxation time to higher frequencies for the whole solutions in the rodlike micelles region. This is shown in figure 3.52 for the curves of loss modulus as a function of

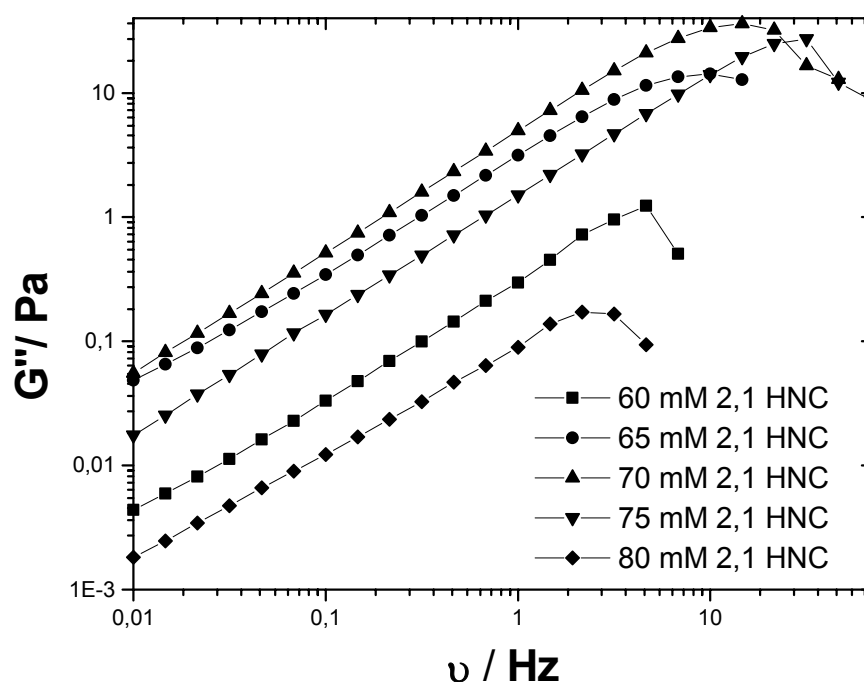


Figure 3.52 Variation of the loss modulus  $G''$  versus frequency for solutions with 100 mM  $C_{12}TAOH$  mixed with different concentrations of 2,1 HNC at 25 °C.

the frequency, at which the curves of loss modulus start to decrease from the higher end. The frequency at which this decrease occurs is used to calculate the relaxation time constant through the simple equation  $\tau = 1/2\pi\nu$ . In the system of 2,1 HNC/C<sub>16</sub>TAOH, the long relaxation times were the reason of higher viscosity and more elasticity, at which the storage modulus was higher than the loss modulus in the whole range of the studied frequencies. In the system of C<sub>12</sub>TAOH / 2,1 HNC the storage modulus is less than loss modulus in the frequency range from 0.001 to 10 Hz, which means that the solutions are more viscous than elastic. To calculate shear modulus from storage and loss modulus, the Cole-Cole relation can be used. This equation can be used when the solution behaves like Maxwell fluid. Accordingly, the shear modulus is easily evaluated by plotting the loss modulus versus the storage modulus [131-132]. After fitting procedure and using shear modulus  $G^o$  as adjustable parameter, the following equation was used:

$$(G' - G^o / 2)^2 + G''^2 = (G^o)^2 / 4. \quad (3.1)$$

Figure 3.53 shows a Cole-Cole plot for two solutions containing 65 mM 2,1 HNC mixed with 100 mM C<sub>12</sub>TAOH or C<sub>14</sub>TAOH. They show shear moduli of 31 and 28,5 Pa respectively.

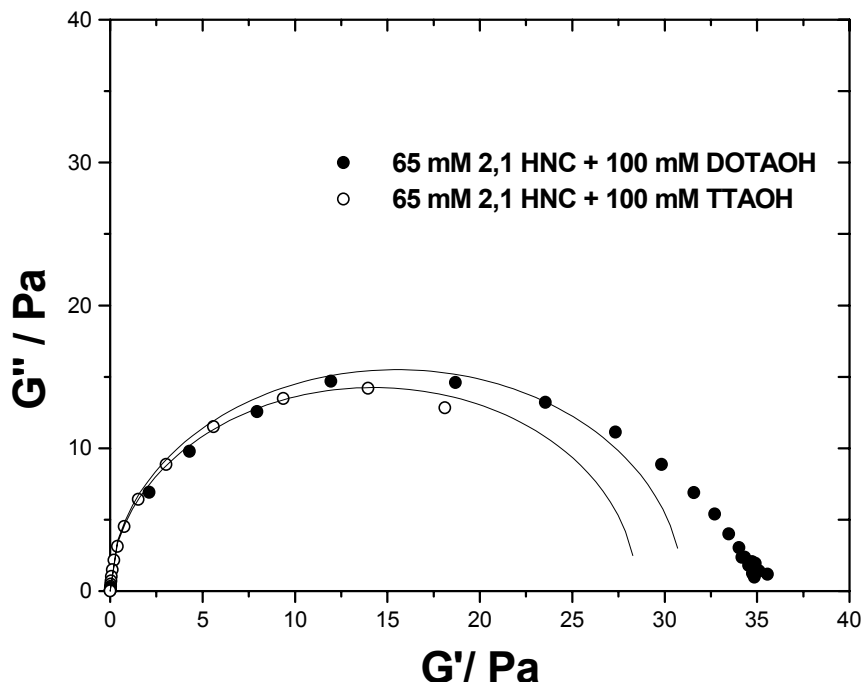


Figure 3.53: Cole-Cole Plots for solutions with 65 mM 2,1 HNC and 100 mM C<sub>12</sub>TAOH or 100 mM C<sub>14</sub>TAOH at 25 °C.

The relaxation times for these solutions are 0.015 and 19.26 seconds and the frequencies of corresponding relaxation are 10.40 and 0.0082 Hz. The micellar solutions of 65 mM 2,1 HNC

and 100 mM  $C_{16}$ TAOH which have rodlike structures can't be fitted by Cole-Cole relation because their rheograms showed no relaxation (storage modulus is about 30 Pa). Therefore, the change in the viscosity is a result of a kinetic process and not because of phase structure changing.

***Two phase region (region II) in the systems  $C_{10}$ TAOH/2,1 HNC:*** This region consists of two phases, which are in the liquid state. They are separated into two phases according to their density difference. The upper phase has a viscosity similar to water, while the lower phase looks more viscous. No rheological measurement were carried out for these two regions since its is easy to predict that the upper phase is Newtonian and the lower phase has a viscosity, which is not high enough to get a good rheogram when the frequency oscillation measurements are carried out.

***The systems  $C_8$ TAOH/2,1 HNC:*** This region consists of two phases. the first is in the liquid state, while the second is precipitate. The upper phase has a viscosity similar to water. No rheological measurement were carried out for these two regions.

#### ***Region III (Turbid region)***

##### ***Turbid region in the systems $C_{14}$ TAOH/2,1 HNC and $C_{12}$ TAOH/2,1 HNC***

The rheological behavior for this region is shown in figure 3.54. Since this region consists of two coexisting phases, it is more difficult to illustrate the resulting rheogram. However, the loss modulus is higher than the storage modulus and the complex viscosity monotonously decrease with increase in the frequency. In this region the transition from rodlike micelles to vesicles takes place. The surface charge of  $C_{14}$ TAOH or  $C_{12}$ TAOH becomes so small that the micellar network forms a turbid region. This is accompanied by a sharp decrease in the complex viscosity and storage modulus (figure 3.49 A, B).

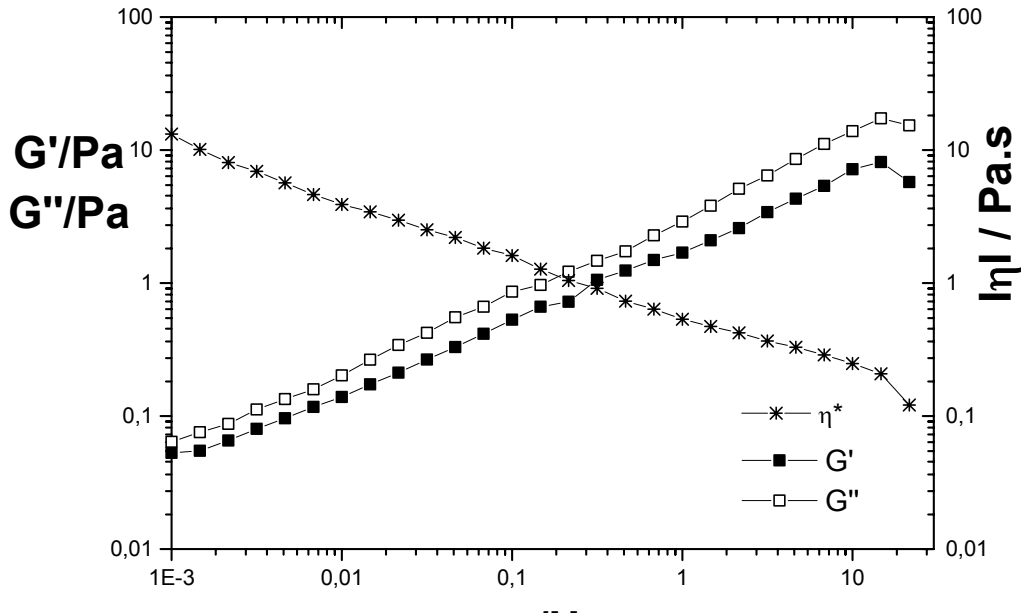


Figure 3.54: Complex viscosity ( $\eta^*$ ), storage modulus  $G'$  and loss modulus  $G''$  versus frequency  $\omega$  for 100 mM  $C_{14}TAOH$  mixed with 80 mM 2,1 HNC at 25 °C.

#### Region IV (Multilamellar vesicles)

**Multilamellar vesicles region in the system  $C_{14}TAOH/2,1 HNC$  :** As has been proven from the results of FF-TEM and SANS, the solutions in this region have multilamellar vesicle phase. The vesicles are sitting in a cage from which they cannot escape by a simple diffusion process without deformation of its shells. As a result of this, the systems have viscoelastic properties. In figure 3.55 the viscoelastic properties of multilamellar vesicle phase show that the storage modulus is larger than the loss modulus and both are independent of frequency in the whole range. The complex viscosity rises as the frequency decreases with a slope equal to  $-1$ . This system behaves like a soft solid with a yield stress value of about 2.1 Pa as it is shown in figure 3.56. The storage modulus for 2,1 HNC/ $C_{14}TAOH$ /water system is smaller than the corresponding value for the system 2,1 HNC/ $C_{16}TAOH$ /water, so this shows that the

storage modulus not only depends on the net electrostatic repulsion between the organizing vesicles but also on the bilayer thickness. Similar results for the rheological behavior of vesicles are reported in the literature [120-129].

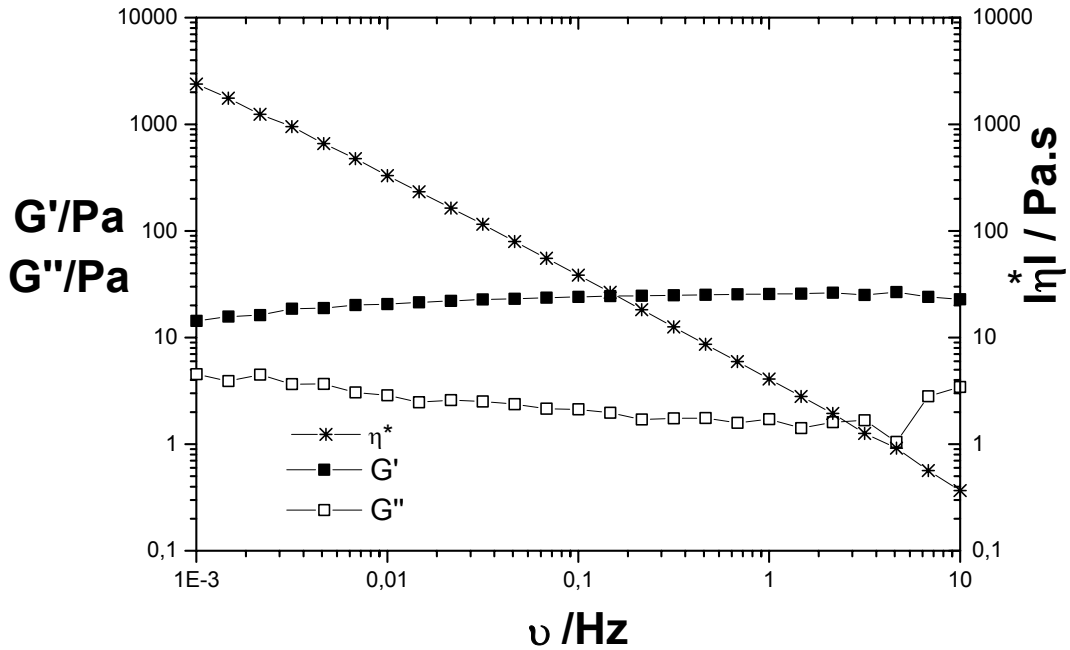


Figure 3.55: Complex viscosity ( $\eta^*$ ), storage modulus  $G'$  and loss modulus  $G''$  versus frequency  $\nu$  for 100 mM  $C_{14}TAOH$  mixed with 100 mM 2,1 HNC at 25 °C.

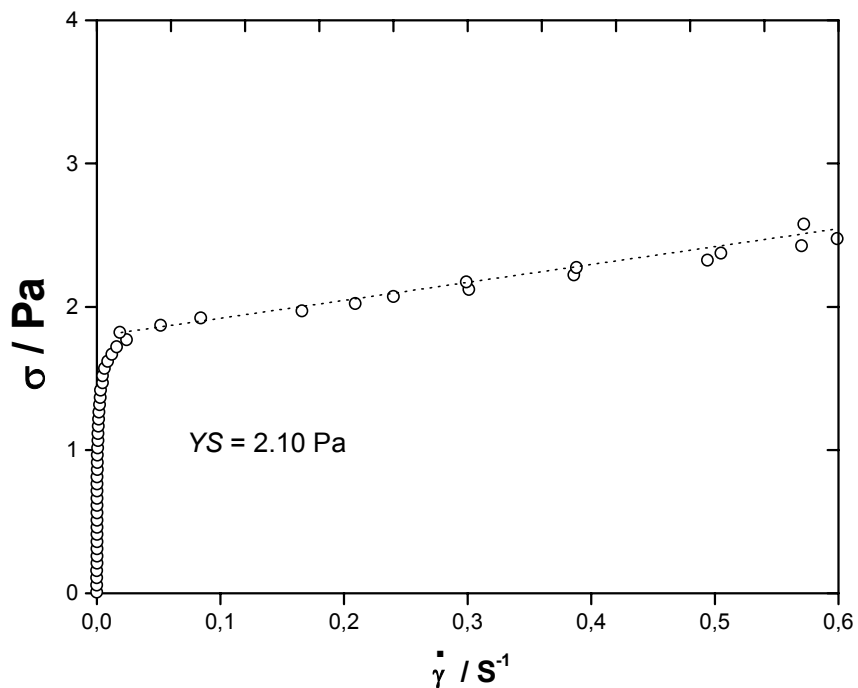


Figure 3.56: Applied shear stress ( $\sigma$ ) versus shear rate ( $\dot{\gamma}$ ) for solutions with 100 mM  $C_{14}TAOH$  and 100 mM 2,1 HNC at 25 °C.

There is no difficulty in distinguishing the regions II and IV from the rheograms unlike the case with 2,1 HNC/C<sub>16</sub>TAOH/water. The rheological behavior in these two regions is different. The solutions in these regions have different deformation values which are shown in figure 3.57. As in the system of 2,1 HNC/ C<sub>16</sub>TAOH, the deformation value of rodlike micelles is higher than that for vesicles.

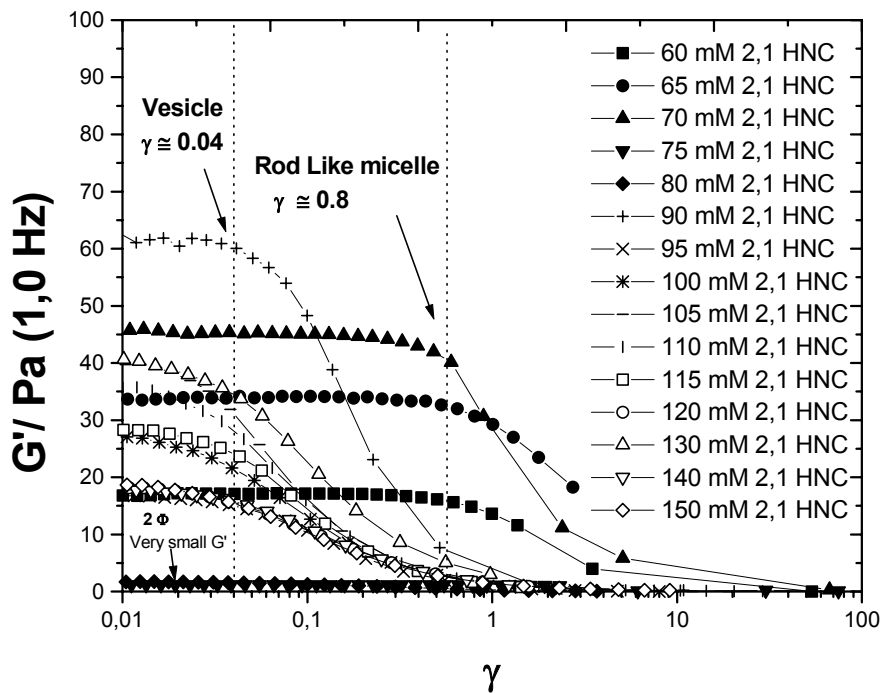


Figure 3.57: Deformation ( $\gamma$ ) versus storage modulus ( $G'$ ) for solutions with 100 mM C<sub>14</sub>TAOH and different concentrations (mM) of 2,1 HNC at 25 °C.

Since the rodlike solutions have shorter relaxation time there was no difficulty in measuring their first normal stress difference  $N_1$ . After reaching certain shear rate, these solutions start to exhibit positive values of  $N_1$ . Multilamellar vesicles show almost zero  $dN_1/d\dot{\gamma}$  and they continue behaving similarly even at high  $\dot{\gamma}$ . The results of  $N_1$  measurements are shown in figure 3.58.

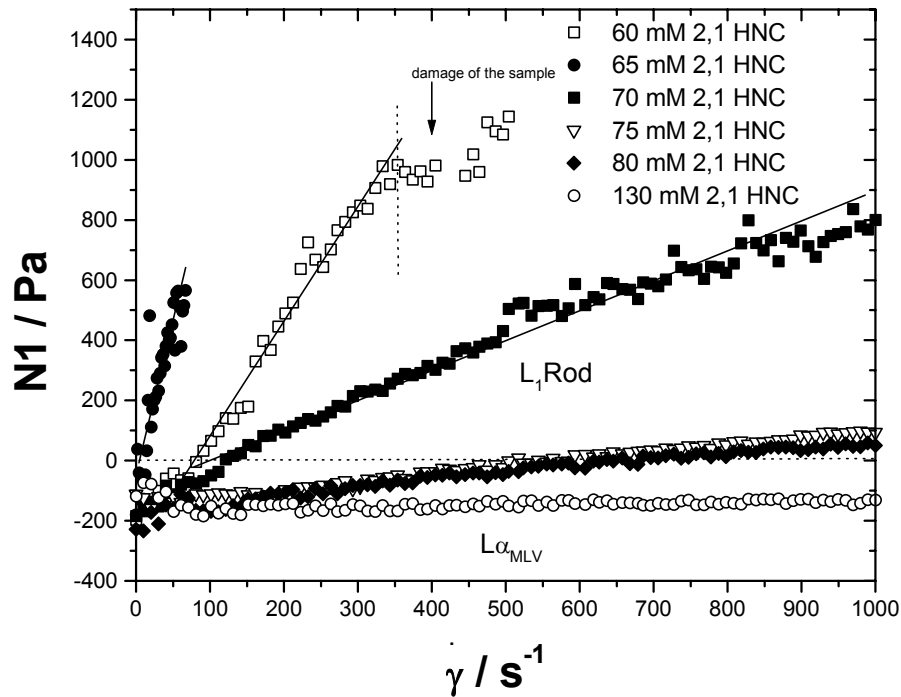


Figure 3.58 : First normal stress difference  $N_1$  versus applied shear rate  $\dot{\gamma}$  for solutions with 100 mM  $C_{14}TAOH$  and various concentration (mM) of 2,1 HNC at 25 °C.

The magnitude of  $dN_1/d\dot{\gamma}$  is increased when the concentration of 2,1 HNC changed from 60, to 65 mM then decreased again for the solutions of 70 and 75 mM. This increase is accompanied by a similar change in storage modulus values for these solutions. Figure 3.59 the relation between  $G'$  and  $dN_1/d\dot{\gamma}$ . From these results it can be said that there is a strong correlation between the value of  $dN_1/d\dot{\gamma}$  and storage modulus. Both increase with each other.

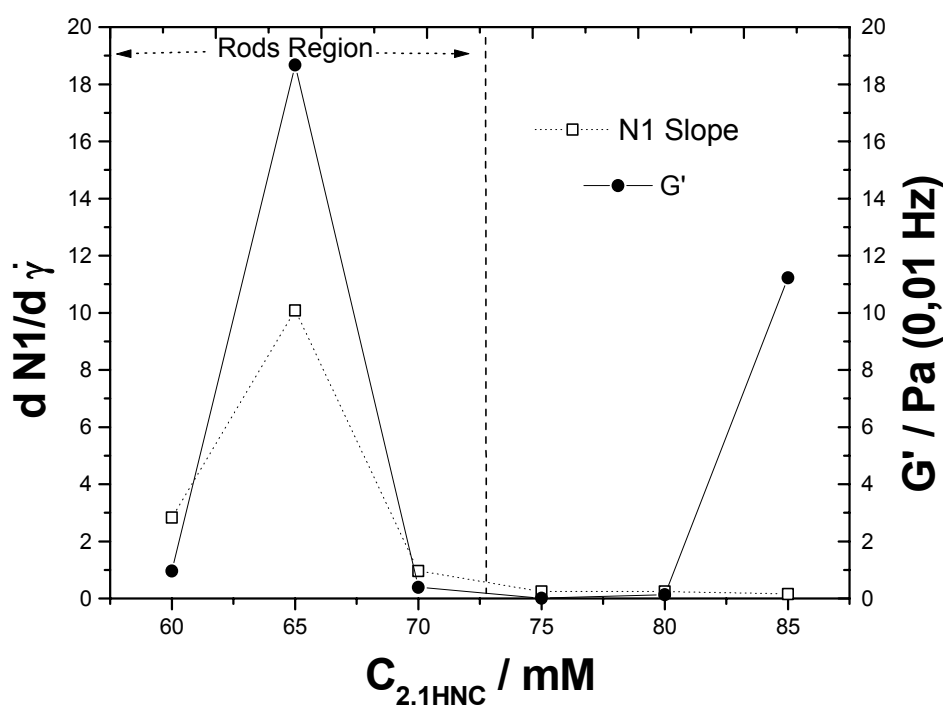


Figure 3.59:  $dN1/d\dot{\gamma}$  slope and storage modulus  $G'$  for the system with various concentrations of 2,1 HNC and 100 mM  $C_{14}TAOH$  at 25 °C.

**Multilamellar vesicles region in the system  $C_{12}TAOH/2,1 HNC$  :** In this region the complex viscosity at 0.01 Hz reaches a plateau of 200 Pas. In fact the viscosities of these solutions are not comparable to those obtained for rodlike micelles since the rodlike micelles are frequency independent at 0.01 Hz, and their viscosities are similar to zero shear viscosity, however, the viscosity of these solutions in this region seems to be three order of magnitude higher than that for rodlike micelles. The rheogram of these solution is the typical for multilamellar vesicles. Both the loss and storage moduli are frequency independent in the whole frequency range. Storage modulus is about one order of magnitude higher than loss modulus. The system behaves like a soft solid and has a yield stress value. The yield stress value is determined from the plot of the shear rate as a function of applied stress. The rheogram of 100 mM  $C_{12}TAOH$  and 100 mM 2,1 HNC is shown in figure 3.60, while the yield stress value for the same solution is shown in figure 3.61. This solution exhibits a yield stress value of about 0.82 Pa. The FF-TEM revealed that the system consists of multilamellar vesicles which are sitting in a cage from which they can not escape by a simple diffusion process without deformation of their shells, these solutions must have viscoelastic properties [130] This is exactly observed in the way the storage modulus, the loss modulus and the complex viscosity related to each other as a function of frequency.

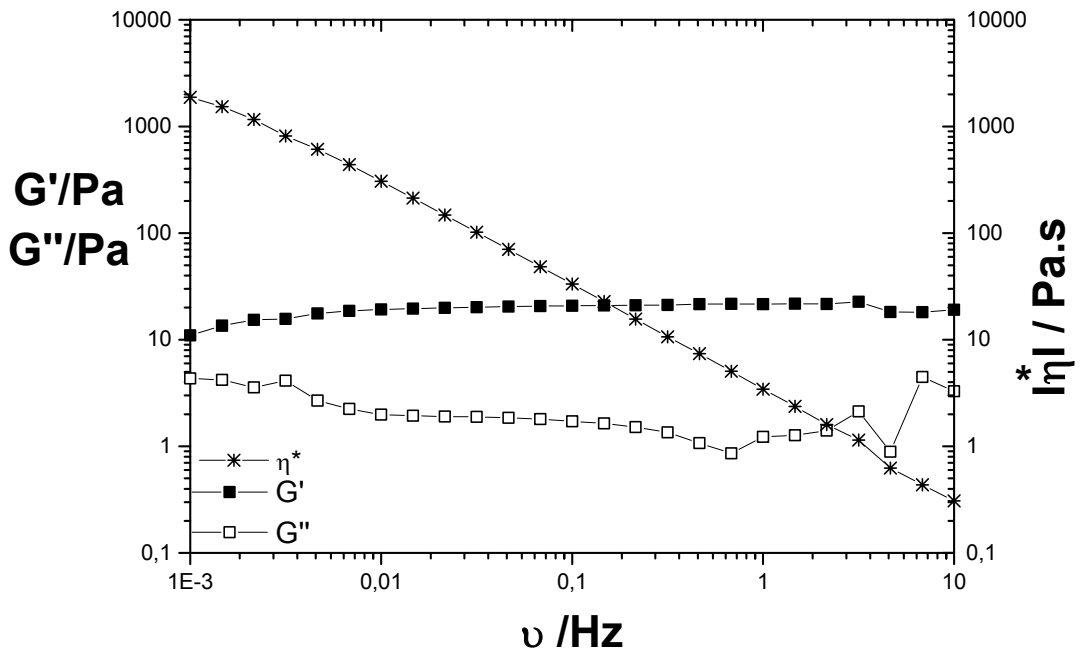


Figure 3.60: Complex viscosity( $\eta^*$ ), storage modulus  $G'$  and loss modulus  $G''$  versus frequency  $\nu$  for system with 100 mM  $C_{12}TAOH$  and 100 mM 2,1 HNC at 25 °C.

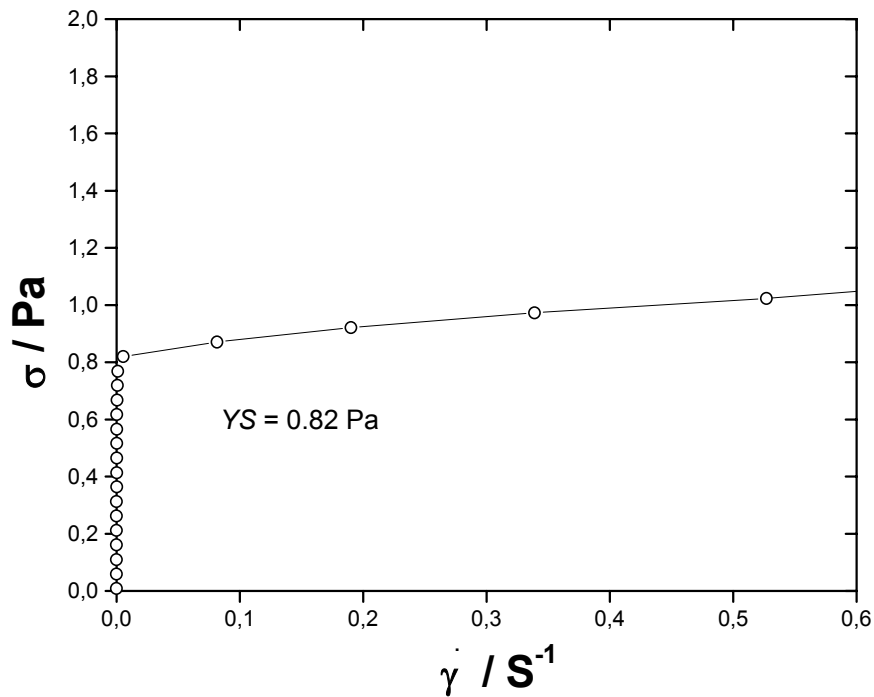


Figure 3.61 : Applied shear stress ( $\sigma$ ) versus shear rate( $\dot{\gamma}$ ) for system with 100 mM  $C_{12}TAOH$  and 100 mM 2,1 HNC at 25 °C.

The solutions in the region of rodlike micelles and multilamellar vesicles have different deformation behavior which is illustrated in figure 3.62. As noted in the system of 2,1 HNC / C<sub>16</sub>TAOH and 2,1 HNC / C<sub>14</sub>TAOH, the deformation value of rodlike micelle is higher than that for vesicles. Also the first normal stress difference measurements agree with the difference in the microstructures between these two phases. As was observed for the system 2,1 HNC / C<sub>14</sub>TAOH, solutions consisting of rodlike micelles show positive slope  $dN_1/d\dot{\gamma}$  for first normal stress difference as a function of applied shear rate. After reaching a certain shear rate, these solutions start to exhibit positive values of  $N_1$ . On the other hand, multilamellar vesicles show almost zero  $dN_1/d\dot{\gamma}$  and they continue behaving similarly even at high  $\dot{\gamma}$ . The results of  $N_1$  measurements are shown in figure 3.63.

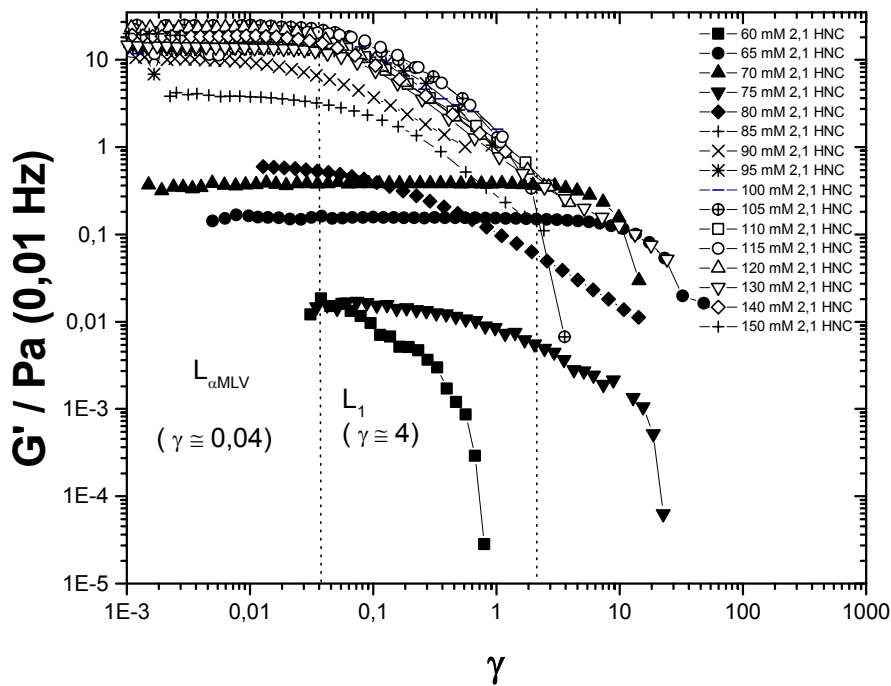


Figure 3.62: Deformation ( $\dot{\gamma}$ ) versus storage modulus ( $G'$ ) for solutions with 100 mM C<sub>12</sub>TAOH and different concentrations (mM) of 2,1 HNC at 25 °C.

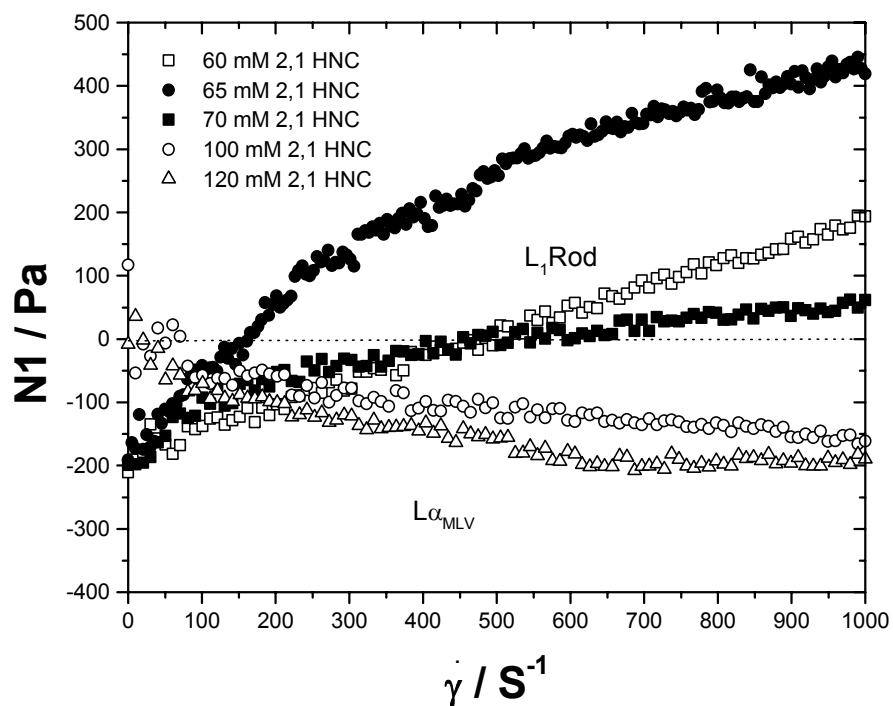


Figure 3.63: First normal stress difference ( $N_1$ ) versus applied shear rate ( $\dot{\gamma}$ ) of 100 mM  $C_{12}TAOH$  and various concentrations (mM) of 2,1 HNC at 25 °C.

**Multilamellar vesicles region in the system  $C_{10}TAOH/2,1HNC$  (Region III):**

All solutions with 2,1 HNC contents of higher than 80 mM show the typical rheogram of multilamellar vesicles. Both loss and storage modulus are frequency independent. The storage modulus is higher about one order of magnitude than loss modulus. The features of this rheogram are the same as other systems which have been studied in this work. The viscosity increase as the frequency decreases in the frequency range. In figures 3.64, 3.65, 3.66, 3.67 and 3.68, the rheograms and the yield stress values (true yield stress for 100 mM 2,1 HNC/100 mM  $C_{10}TAOH$ ) are shown for a solution with 100 or 150 mM 2,1 HNC and 100 mM  $C_{10}TAOH$ . For the systems the yield values are about 0.37 and 0.8 Pa respectively. In figure 3.69, yield stress values with increasing amounts of 2,1 HNC show an S-type curve in which the initial and final values vary very little with the concentration, while a linear proportional relation was observed for in between values.

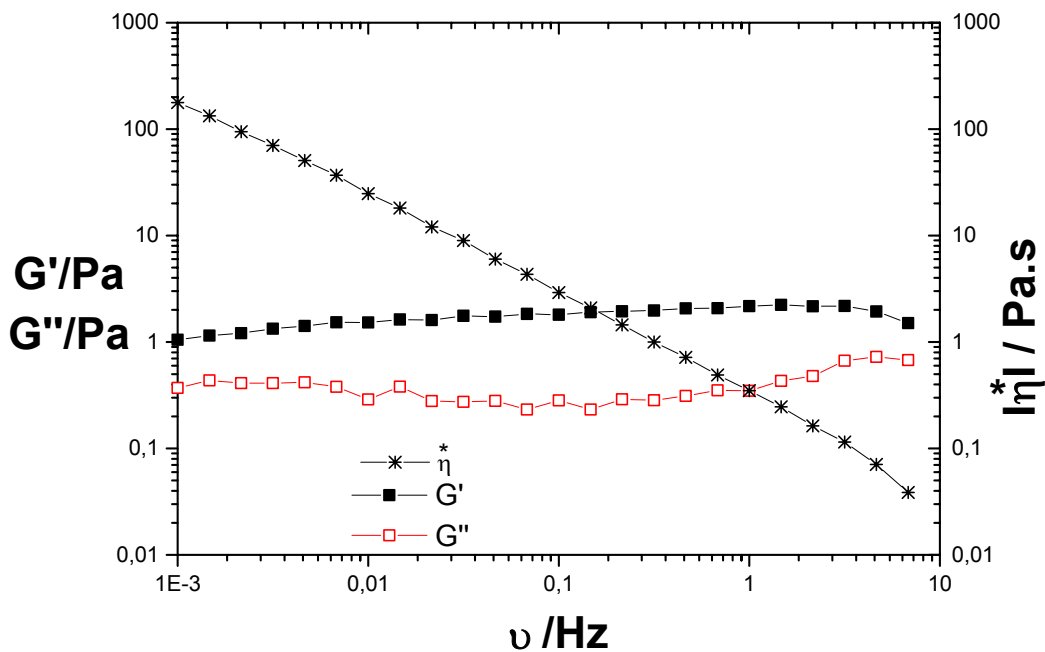


Figure 3.64 : Complex viscosity( $\eta^*$ ), storage modulus  $G'$  and loss modulus  $G''$  versus frequency  $\omega$  for system with 100 mM  $C_{10}TAOH$  and 100 mM 2,1 HNC at 25 °C.

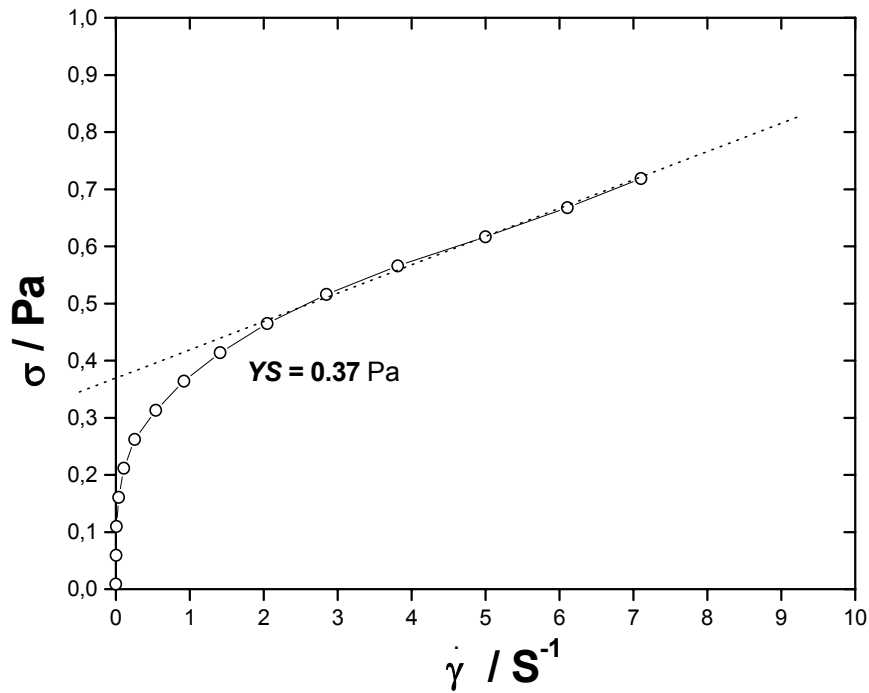


Figure 3.65 : Applied shear stress ( $\sigma$ ) versus shear rate ( $\dot{\gamma}$ ) for system with 100 mM  $C_{10}TAOH$  and 100 mM 2,1 HNC at 25 °C.

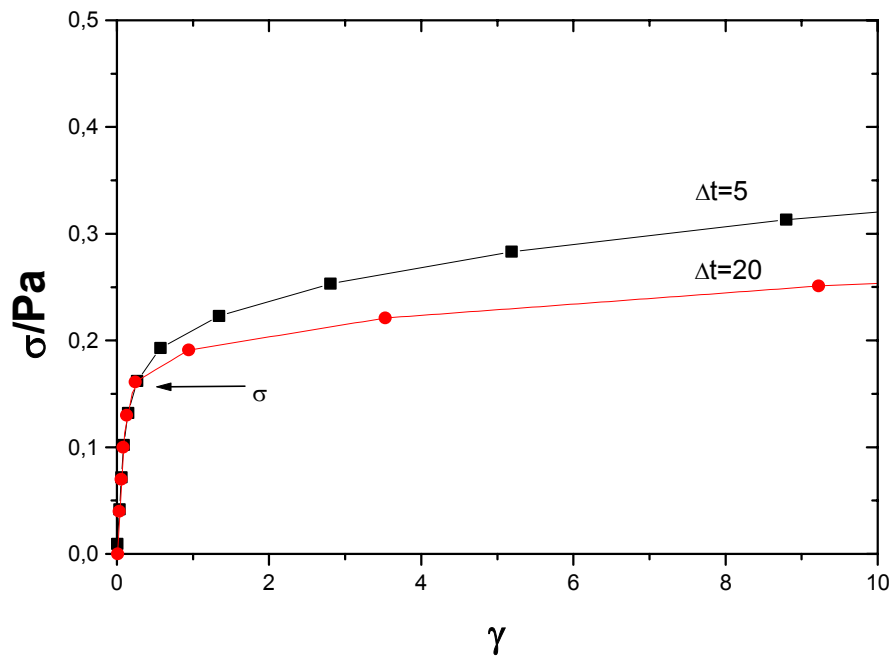


Figure 3.66 : Deformation ( $\gamma$ ) versus shear stress ( $\sigma$ ) for system with 100 mM  $C_{10}TAOH$  and 100 mM 2,1 HNC at two intervals of time (500 and 2000 seconds) at 25 °C.

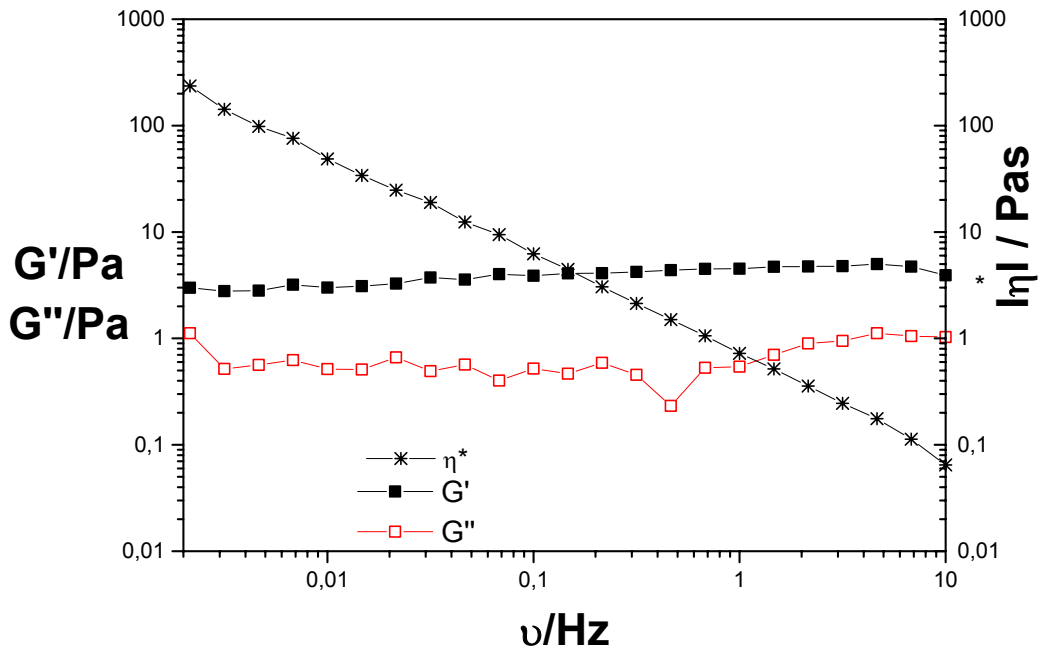


Figure 3.67 : Complex viscosity( $\eta^*$ ), storage modulus  $G'$  and loss modulus  $G''$  versus frequency  $\nu$  for system with 100 mM  $C_{10}TAOH$  and 150 mM 2,1 HNC at 25 °C.

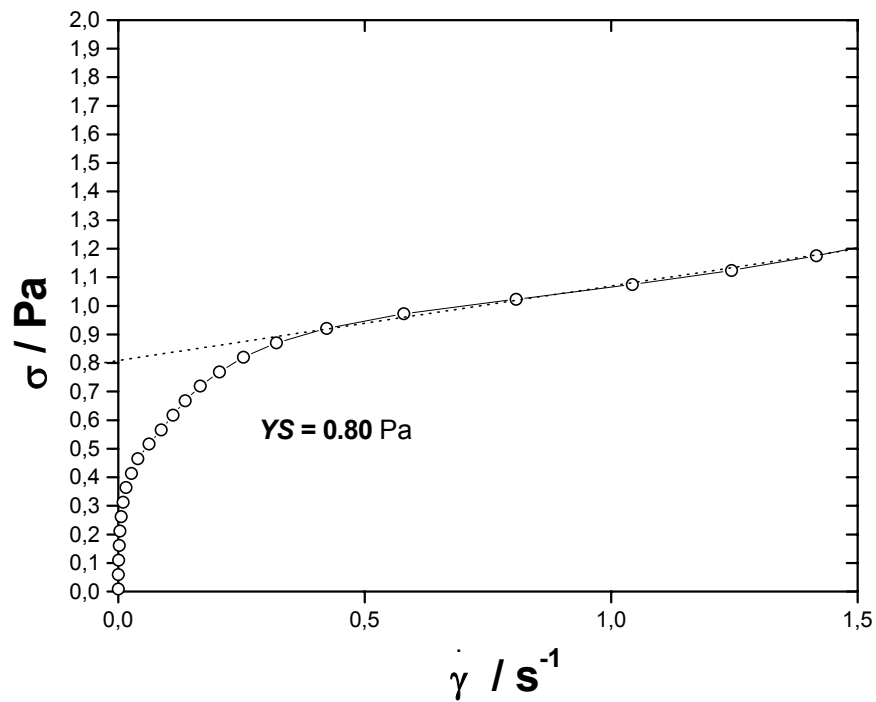


Figure 3.68 : Applied shear stress ( $\sigma$ ) versus shear rate( $\dot{\gamma}$ ) for system with 100 mM  $C_{10}TAOH$  and 100 mM 2,1 HNC at 25 °C.

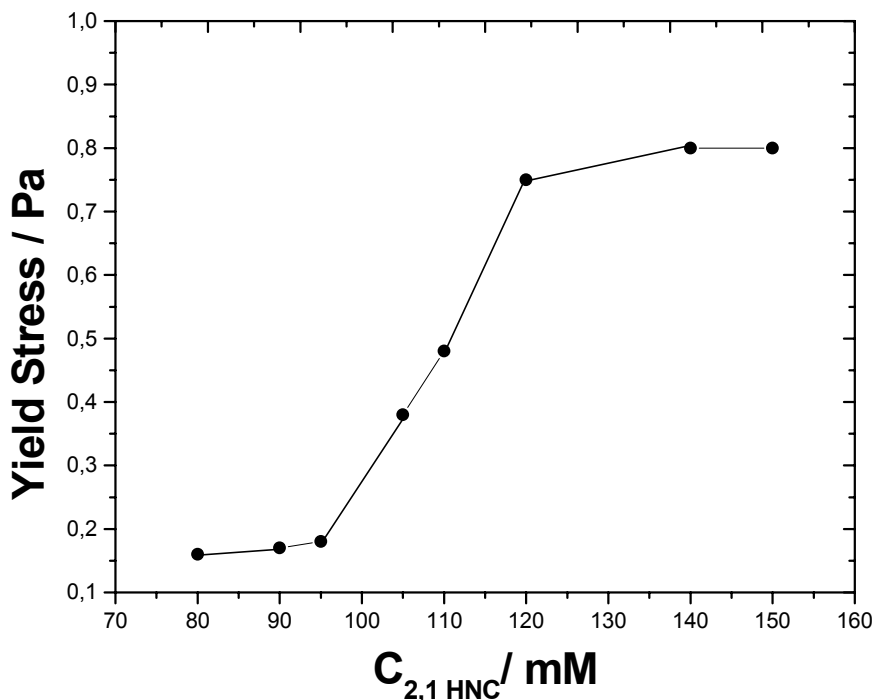


Figure 3.69: Yield stress values versus concentration of 2,1 HNC for systems with 100 mM  $C_{10}\text{TAOH}$  and an increasing amount of 2,1 HNC at 25 °C.

To confirm the knowledge about the relationship between the rheological behavior and phase structure, both sweep and first normal stress difference  $N_1$  measurements were carried out for the solutions in region III. As before for similar viscoelastic solution with similar phase structure, these solutions show a deformation of about 0.1 (10%) and the  $N_1$  is almost negative.  $dN_1/d\dot{\gamma}$  is almost zero. Figure 3.70 shows the sweep measurements for the solutions of 100 mM  $C_{10}\text{TAOH}$  and an increasing amount of 2,1 HNC, while figure 3.71 shows the first normal stress difference measurements for the same solutions. Both results confirm the predictions one can assume for such type of systems.

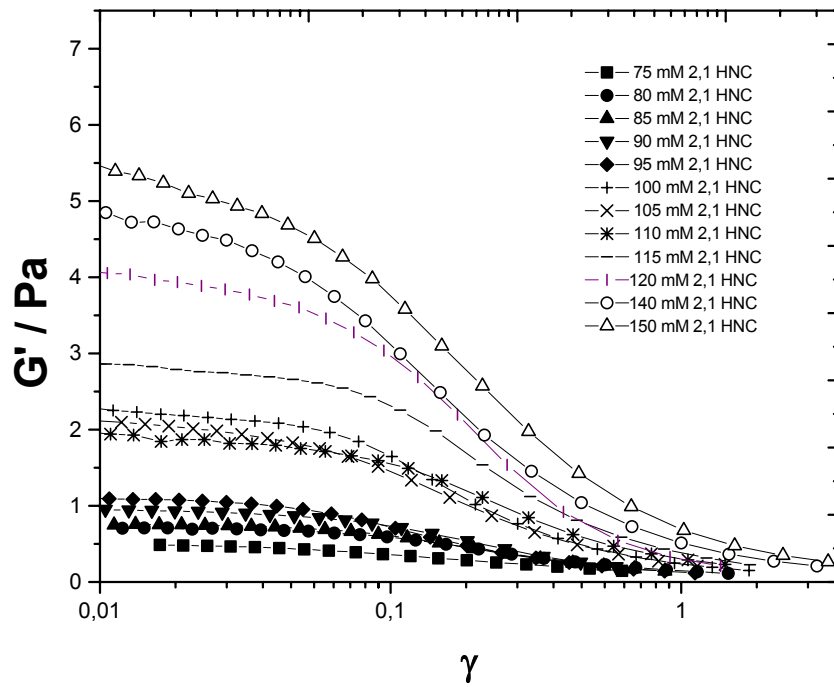


Figure 3.70: Deformation ( $\gamma$ ) versus storage modulus ( $G'$ ) for systems with 100 mM  $C_{10}TAOH$  and different concentrations (mM) of 2,1 HNC at 25 °C.

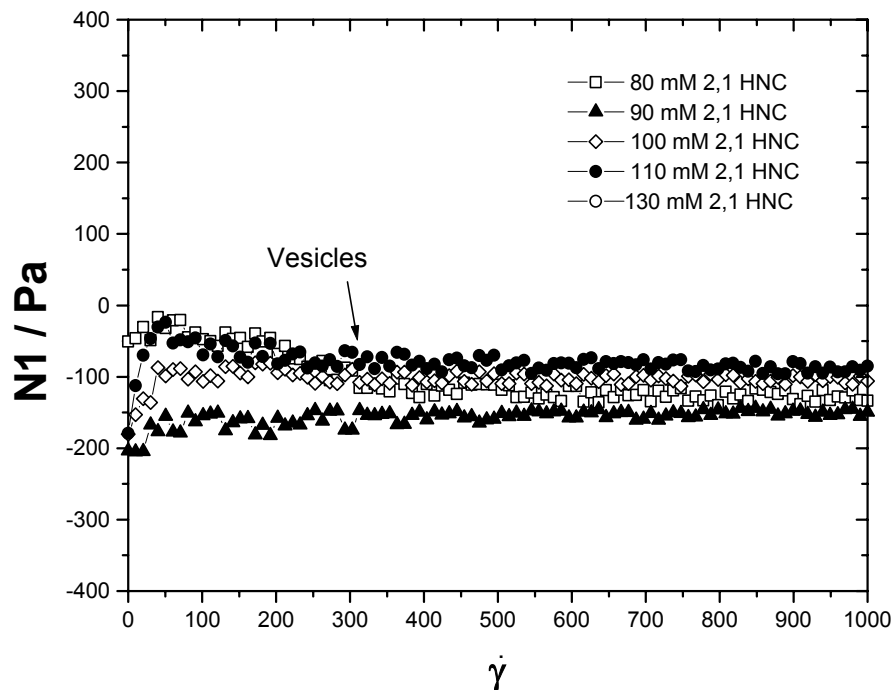


Figure 3.71: First normal stress difference  $N_1$  versus applied shear rate  $\dot{\gamma}$  for system with 100 mM  $C_{10}TAOH$  and various concentrations (mM) of 2,1 HNC at 25 °C.

#### ***Multilamellar vesicles region in the system C<sub>8</sub>TAOH/2,1HNC:***

The rheological behavior of the solution 100 mM C<sub>8</sub>TAOH and increasing amounts of 2,1 HNC was previously shown in figure 3.49 D. Storage modulus is shown in the same figure. At a 2,1 HNC-concentration of higher than 40 mM, the solutions are in two phases, so no viscosity measurements were carried out. The viscosity increases again in the turbid region (two phase region but they look one phase for long time after preparation) then the two phase region appears again, at which no measurements were carried out. The oscillation rheogram of 100 mM C<sub>8</sub>TAOH and 100 mM of 2,1 HNC is shown in figure 3.72. It is a typical rheogram for vesicles, which have a small yield stress value (about 0.12 Pa) as shown in figure 3.73.

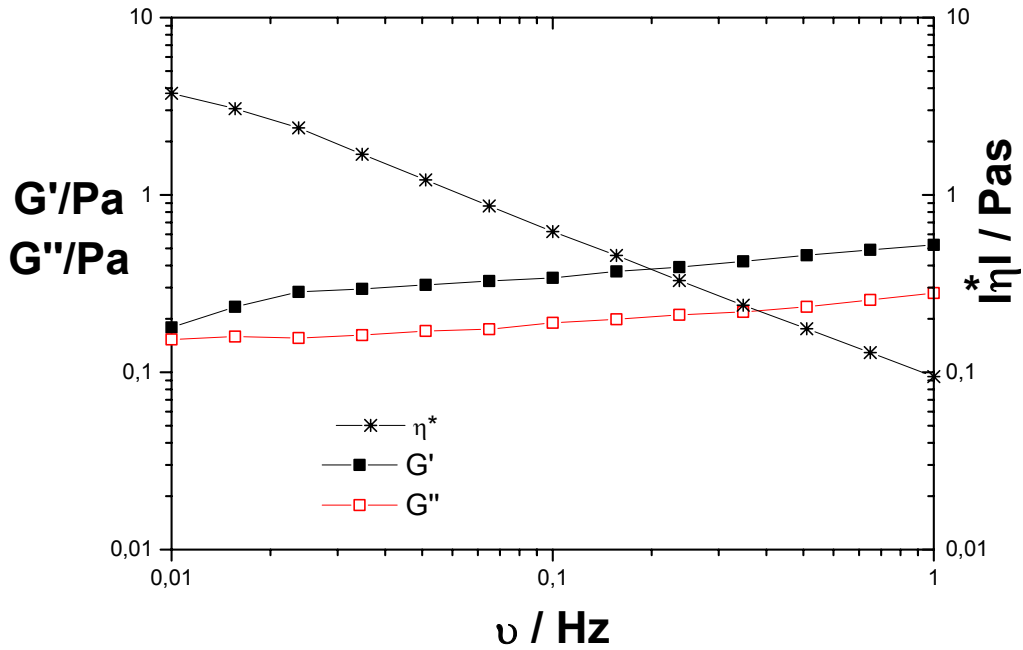


Figure 3.72: Complex viscosity ( $\eta^*$ ), storage modulus  $G'$  and loss modulus  $G''$  versus frequency  $\nu$  for 100 mM  $C_8TAOH$  mixed with 100 mM 2,1 HNC at 25 °C.

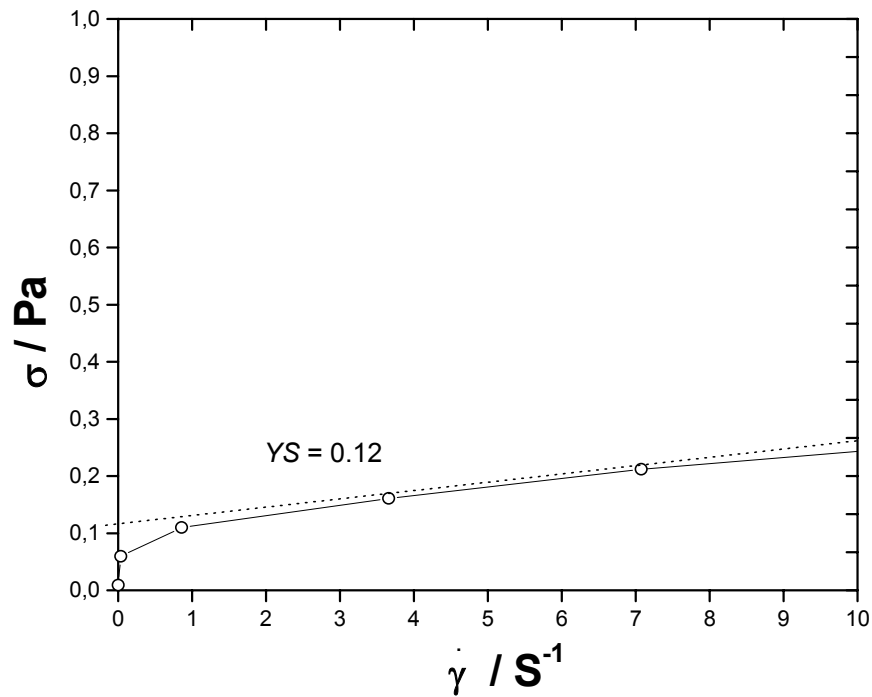


Figure 3.73 : Applied shear stress ( $\sigma$ ) versus shear rate ( $\dot{\gamma}$ ) for system with 100 mM  $C_8TAOH$  and 100 mM 2,1 HNC at 25 °C.

#### 3.4 Comparative Study of Phase and Rheological Behavior in Systems Prepared from Cationic Surfactants with Different Hydrophobic Chain Lengths and Isomeric Structures of $x,y$ HNC.

According to the theory of surfactant aggregation, cationic surfactants form micelle with several microstructure when they are mixed with strongly binding or hydrophobic counterions of suitable geometry. With increasing the concentration of the hydrophobic counterion, the microstructural transition spontaneously goes ahead. The effect of hydrophobic counterion geometry or surfactant's chain lengths control the resulted microstructure, which finally determine the physical properties of the mixed solutions. A comprehensive comparison between the whole studied systems and the agreements to some theoretical models are presented.

##### Phase Behavior

In this work, it has been shown that six new systems show viscoelastic properties. They are the cationic surfactants  $C_{16}$ TAOH,  $C_{14}$ TAOH,  $C_{12}$ TAOH,  $C_{10}$ TAOH and  $C_8$ TAOH mixed with 2,1 HNC or 6,2 HNC. The system  $C_{16}$ TAOH/ 6,2 HNC, and the published system  $C_{16}$ TAOH/ 3,2 HNC also have been studied to find the effect of hydrophobic counterion geometry on the resulted microstructures. The phase behavior of these systems has shown that reducing the chain length of the cationic surfactants  $C_{16}$ TAOH,  $C_{14}$ TAOH,  $C_{12}$ TAOH does not change the phase behavior significantly upon mixing with an increasing amount of **2,1 HNC**. All of these three systems show similar phase transitions upon mixing an increasing amount of 2,1 HNC (0-150 mM) with 100 mM surfactants. The phases are, low viscosity isotropic phase (0 to ~55 mM 2,1 HNC), high viscoelastic isotropic phase consisting of rodlike micelle (~55 to ~80 mM 2,1 HNC), turbid region (two phase region) (~80 to ~90 mM 2,1 HNC), and multilamellar vesicle  $L\alpha$ -Phase (~90 to ~150 mM 2,1 HNC). A very interesting phenomenon in these systems is that their color changes from blue to yellow when they are observed between two crossed polarizers in the multilamellar vesicle region. For the phase behavior of the system  $C_{16}$ TAOH mixed with an increasing amount with **3,2 HNC** almost similar results were obtained as  $C_{16}$ TAOH mixed with 2,1 HNC. They differ in the Krafft point and the solubilization of the hydrophobic counterion capacity. CTAHNC which is resulted from mixing equimolar ratio of  $C_{16}$ TAOH and 3,2 HNC has Krafft point at about 30 °C, while CTAHNC prepared by mixing  $C_{16}$ TAOH and 2,1 HNC has Krafft point of about 22 °C. Both of these systems form multilamellar vesicles at equimolar ratio, however, the excess counterion 2,1 HNC is solubilized in the multilamellar vesicles for the system  $C_{16}$ TAOH/ 2,1 HNC at 25 °C. 3,2 HNC was settled after the equimolar ratio in the system  $C_{16}$ TAOH/ 3,2

HNC at 40 °C. The system of 100 mM C<sub>16</sub>TAOH and an increasing amount of **6,2 HNC** does not form multilamellar vesicles at equimolar ratio, and behave differently in comparison to the previous two systems.

For the system 100 mM C<sub>16</sub>TAOH mixed with an increasing amount of 6,2 HNC one finds, low viscous isotropic phase (0 to ~75 mM 6,2 HNC), isotropic viscoelastic phase consisting of rodlike micelle (75 to ~95 mM 6,2 HNC), and two phase region consisting of rodlike micelles upper phase and un-reacted 6,2 HNC in the lower phase (~95 to ~150 mM 6,2,1 HNC). The systems C<sub>10</sub>TAOH and C<sub>8</sub>TAOH mixed with 2,1 HNC show different phase behavior. For the system 100 mM C<sub>10</sub>TAOH mixed with an increasing amount of 2,1 HNC one finds, low viscous isotropic phase (0 to ~60 mM 2,1 HNC), isotropic two phase region (60 to ~75 mM 2,1 HNC), slight birefringence phase consisting of multilamellar vesicles (75 to ~120 mM 2,1 HNC), and multilamellar vesicle L $\alpha$ -Phase with stronger birefringence (~120 to ~150 mM 2,1 HNC). In the system 100 mM C<sub>8</sub>TAOH mixed with an increasing amount of 2,1 HNC, the two phase region dominates the phase behavior, however, the multilamellar vesicles are formed at equimolar ratio. The phases in the system C<sub>8</sub>TAOH/2,1 HNC are, low viscous isotropic phase (0 to ~40 mM 2,1 HNC), two phase region consisting of isotropic upper phase and precipitated phase (40 to ~85 mM 2,1 HNC), turbid and phase consisting of multilamellar vesicles (85 to ~100 mM 2,1 HNC), and two phase region consisting of isotropic upper phase and precipitated phase (~100 to ~150 mM 2,1 HNC).

#### Conductivity and pH measurements

Conductivity and pH measurements for the whole systems show decreasing in the conductivity of the 100 mM cationic surfactant upon mixing with an increasing amount of 2,1 HNC in the concentration range of 0 to ~85 mM, slight decreasing in the turbid region (~85 to ~90 mM 2,1 HNC), and then the conductivity remains almost constant in the multilamellar vesicles (~90 to ~150 mM 2,1 HNC). This acid-base reaction results in the formation of water and surfactant salts. Instead of free highly hydrated OH<sup>-</sup> counterions, strongly binding HNC<sup>-</sup> is produced and consequently the conductivity decreases. More interesting is that the conductivity remains constant after the neutralization which implies that the excess hydrophobic counterion is in the molecular form instead of in the ionic state. 2,1 HNC is water insoluble when it is in the molecular form, so the only one explanation is that the excess 2,1 HNC is solubilized inside the bilayers of multilamellar vesicles (between the tails). The mobility of the bulky hydrophobic counterion 2,1 HNC<sup>-</sup> is lower than OH<sup>-</sup>, so this

is also a second reason for the decreasing of the conductivity when the two ions are exchanged. The conductivity minimum in the constant region (multilamellar vesicles) decreases as the chain length increases. This is because of increasing the hydrophobicity of the surfactants, which is accompanied with increasing the hydrocarbon part. The conductivity minimums are 800, 130, 80, 70 and 60  $\mu\text{S}/\text{cm}$  for the systems  $\text{C}_8\text{TAOH}$ ,  $\text{C}_{10}\text{TAOH}$ ,  $\text{C}_{12}\text{TAOH}$ ,  $\text{C}_{14}\text{TAOH}$  and  $\text{C}_{14}\text{TAOH}$  (100 mM) mixed with (100-150 mM 2,1 HNC), respectively. The pH measurements have been proven that the neutralization (pH=7) is reached at equal molar ratios (100 mM 2,1 HNC:100 mM CTAOH). This gives more evidence that the turbid phase that has been found in phase behavior was reached before equimolar ratio (neutralization) because of the high viscosity of the solutions and encaging of 2,1 HNC in the molecular form, and not because of concentration deviations of the cationic surfactants.

#### Phase Characterizations

Characterization of the liquid crystalline phases was made firstly with the help of *differential interference contrast microscopy*. The vesicles in the system  $\text{C}_{16}\text{TAOH}/2,1$  HNC were made visible with this technique. These vesicles are polydisperse. Few bigger vesicles with diameter about 30  $\mu\text{m}$  were also seen. An interesting texture was seen for the multilamellar vesicles, at which the membranes were clear and accounted. The vesicle phase in the systems  $\text{C}_{12}\text{TAOH}/2,1$  HNC and  $\text{C}_{10}\text{TAOH}/2,1$  HNC were also made visible using this technique. The vesicles in these two systems were also polydisperse.

Specific details about the structure of the multilamellar vesicle *MLV* phase were made possible with the help of the transmission electron microscopy *TEM* using freeze fracture *FF*- and Cryogenic temperature *Cryo*- techniques. For the system  $\text{C}_{16}\text{TAOH}/2,1$  HNC, multilamellar vesicles have diameters ranging from 100 to 1000 nm, and interlamellar spacing about 60 nm. The vesicles consists of at least ten shells. Mixing the vesicle solutions with 20% wt/wt glycerol leads to similar results. The MLV are polydisperse, and deformed. The MLV phases for the solutions  $\text{C}_{14}\text{TAOH}$ ,  $\text{C}_{12}\text{TAOH}$ ,  $\text{C}_{10}\text{TAOH}$  and  $\text{C}_8\text{TAOH}$  (100 mM) mixed with 100 mM 2,1 HNC was made also visible with FF-TEM. The tabular information about the systems that have been studied by FF-TEM or Cryo-TEM is listed in table 3.3.

Table 3.3 : The systems have been characterized by FF-TEM and cryo-TEM

<i>System</i>	<i>Structure diameter (nm)</i>	<i>Structure type</i>	<i>Interlamellar spacing (nm)</i>	<i>Technique</i>
100 mM C <sub>16</sub> TAOH/100 mM 2,1 HNC	100-1200	Polydisperse MLV	~60	FF-
100 mM C <sub>16</sub> TAOH/110 mM 2,1 HNC /20% wt/wt glycerol	100 -1200	Polydisperse MLV	~60	FF-
100 mM C <sub>16</sub> TAOH/120 mM 2,1 HNC/20% wt/wt glycerol	100-800	Polydisperse MLV	~60-80	FF-
100 mM C <sub>14</sub> TAOH/100 mM 2,1 HNC	100-2200	Polydisperse MLV	~60	FF-
100 mM C <sub>12</sub> TAOH/100 mM 2,1 HNC	100-1000	Polydisperse MLV	~60	FF-
100 mM C <sub>10</sub> TAOH/80 mM 2,1 HNC	100-200	Vesicles	----	FF-
100 mM C <sub>10</sub> TAOH/100 mM 2,1 HNC	100-4000	Polydisperse MLV	~60	FF-
100 mM C <sub>10</sub> TAOH/150 mM 2,1 HNC	100-4000	Polydisperse MLV	~40	FF-
100 mM C <sub>8</sub> TAOH/100 mM 2,1 HNC	100-3500	*MLV	----	FF-
100 mM C <sub>16</sub> TAOH/55 mM 2,1 HNC	10-20	**	---	cryo-
100 mM C <sub>16</sub> TAOH/110 mM 2,1 HNC/10% wt/wt Ethanol	100-1000	Polydisperse MLV	10-100	cryo-

\*Polydisperse precipitated MLV and flat lamella.

\*\*Globular-Rodlike micelle transition structure.

For the system C<sub>10</sub> TAOH/2,1 HNC, the transition from small vesicles to big multilamellar vesicles as detected by FF-TEM, was dependent on 2,1 HNC concentration. At 80 mM 2,1 HNC, vesicles are small as shown in the table 3.3. They become bigger at 100 mM 2,1 HNC with a diameter ranging from 100 nm to 4000 nm.

Based on these information, it seems that the shorting of the chain length of cationic surfactants leads to bigger vesicles. This can be understood by the idea that the hydrophobic

interactions between the tails decreases as they become shorter, so the flexibility of the membrane increases, and they prefer to be with more flat surface. This finding shows somehow a way to control the size of the vesicles by changing the chain length.

For the system 100 mM C<sub>16</sub>TAOH and 55 mM 2,1 HNC, cryo-TEM picture was obtained. The aggregates were with linear dimension of about 10-20 nm. They are not spherically-shaped, but elongated (malleated). Some of them are globular-shaped, but elongated. They are not long enough like rodlike micelles, so it is highly possible that this is the transition structure of globular-rodlike micelle. This result is in agreement with the rheological properties of this solution, at which this solution is with moderate viscosity which is less than the viscosity of rodlike micelles, and higher than Newtonian fluids. Also SANS spectra indicated small aggregate structures for this solution. For the system 100 mM C<sub>16</sub>TAOH and 110 mM 2,1 HNC, cryo-TEM picture showed multilamellar vesicles with interlamellar spacing ranging from 10 nm to about 100 nm. The interlamellar spacing between the internal vesicles is about 100 nm. At the boundaries of the external vesicles, the bilayers are condensed and the interlamellar spacing between them is about 10 nm. The difference between FF-TEM and cryo-TEM could be because of the strong deformation that resulted during the sample preparation conditions at which the solution is placed on the flat narrow-mesh specimen grid, so the vesicle are extended to be flat instead of the spherical-shaped as in the bulk of the solution. Another factor is the evaporation of water which happened during the preparation conditions. The film is also thin, and the surface area of the film is comparably high, so evaporation of water leads to decrease in interlamellar spacing between the bilayers.

The characterization was made also by small angle neutron scattering *SANS*. *SANS* show results similar to that obtained by FF-TEM, and more information about the bilayer thickness is provided. The transition from rodlike micelles to multilamellar vesicles was proven by *SANS*. The results of *SANS* are presented in table 3.4

Table 3.4: SANS characterization data.

System	Spectra-shape	$q_{\max}$	Interlamellar distance (nm)	Bilayer thickness (Å)
100 mM $C_{16}$ TAOH/100 mM 2,1 HNC	MLV	0,010	62	30
100 mM $C_{16}$ TAOH/110 mM 2,1 HNC	MLV	0,011	60	30
100 mM $C_{16}$ TAOH/120 mM 2,1 HNC	MLV	0,011	58	30
100 mM $C_{16}$ TAOH/55 mM 2,1 HNC	Small aggregates	0,030	---	---
100 mM $C_{16}$ TAOH/60 mM 2,1 HNC	Small aggregates	0,030	---	---
100 mM $C_{16}$ TAOH/65 mM 2,1 HNC	Small aggregates	0,030	---	---
100 mM $C_{16}$ TAOH/ 80 mM 6,2 HNC	Small aggregates	0,031	---	---
100 mM $C_{16}$ TAOH/90 mM 6,2 HNC	Small aggregates	0,031	---	---
100 mM $C_{16}$ TAOH/100 mM 6,2 HNC	Small aggregates	0,031	---	---
100 mM $C_{14}$ TAOH/100 mM 2,1 HNC	MLV	0,0103	61	28
100 mM $C_{12}$ TAOH/100 mM 2,1 HNC	MLV	0,0103	60	27
100 mM $C_{10}$ TAOH/100 mM 2,1 HNC	MLV	0,0104	60	26
100 mM $C_8$ TAOH/100 mM 2,1 HNC	---	---	---	--

The effect of hydrophobic counterion geometry on the resulting microstructure was also detected by SANS at which low intensity spectra were measured for the system 6,2 HNC/  $C_{16}$ TAOH, while the correspondent concentrations of the system 2,1 HNC/  $C_{16}$ TAOH show multilamellar vesicles microstructure (see the table for solutions with 100 mM 2,1 HNC or 6,2 HNC with 100 mM  $C_{16}$ TAOH ). The color changes have been seen between two crossed polarizes of the systems  $C_{16}$ TAOH/2,1 HNC,  $C_{14}$ TAOH/2,1 HNC and  $C_{12}$ TAOH/2,1 HNC and this color difference is due to change in the interlamellar distance as calculated from SANS data for the solutions with 100, 110 and 120 mM 2,1 HNC and 100 mM CTAOH.

These different methods of characterizations have been shown clear pictures for the different micelle microstructures, and their relation to the chemical geometry of the hydrophobic counter ion or cationic surfactant's chain length. The second step in this work was to establish the microstructure relation to the viscoelasticity, so the rheological properties of these systems were investigated.

#### The Rheological Behavior

In the present work, the rheological behavior of the whole studied systems was mainly divided into four different regions. They are, the low viscous region (Newtonian), the rodlike micelles (viscoelastic), the turbid region (two phase region), and the multilamellar vesicles (viscoelastic gels) region.

I – low viscosity region: The viscosity of these solutions was low as a result of small volume fractions of the micellar aggregates as described by Einstein's law. For the system  $C_{16}TAOH/2,1$  HNC, the viscosity was mainly independent of shear rate when 2,1 HNC contents were about 0-50 mM, shear induced structure (shear thickening) was observed for the solution with 2,1 HNC content 55 mM, at which the viscosity was rising as a function of applied shear rate. The viscosity of other systems  $C_{14}TAOH/2,1$  HNC,  $C_{12}TAOH/2,1$  HNC,  $C_{10}TAOH/2,1$  HNC, and  $C_8TAOH/2,1$  HNC was independent of the shear rate (when the 2,1 HNC contents were 0 mM to ~40 mM). The viscosity for these systems was about 1 mPa.s. The Newtonian region extends in system  $C_{16}TAOH/6,2$  HNC. It was in 6,2 HNC concentration range from 0 into 70 mM.

#### II – Rodlike micelles region:

For the system  $C_{16}TAOH/2,1$  HNC, the rodlike micelles were present in solutions with 2,1 HNC contents of 60,65 and 70 mM. They exhibit long relaxation time (>1000 seconds). The storage modulus  $G'$  and loss modulus  $G''$  look parallel, and the complex viscosity is rising (from left to right) in the logarithmic scale with slope about -1 in the frequency range (0,001 – 10 Hz). The resulting rheograms were similar to that one for solutions consisting of multilamellar vesicles (type 2). The rodlike micelles are entangled and flexible with long relaxation time in an isotropic micellar phase ( $L_1$  phase, type 1). Rheological measurements were carried out to distinguish type 1 from the second one. The complex viscosity (0.001 Hz) of these systems can differ by at least 6 orders of magnitudes for a 100 mM surfactant solution. Based on rheological measurements, It has been shown that the two types can be distinguished. The rheological measurements made were, firstly, true yield stress measurements (which proved that these solution have no yield stress value). In this measurement the deformation was measured as a function of applied shear stress at two different time intervals, and the shear rate deformation curves deviate even at small

deformation at two interval of time, indicating the absence of true yield stress. This result is different from that one obtains when the yield stress is measured depending on shear rate-shear stress curves, at which the solutions exhibit high yield stress values using this way of determination. For the same solutions, the yield stress is also visually tested. The dispersed small air bubbles rise within ten days or two weeks even they seem stable in short interval of time, indicating the absence of yield stress, and that no energy is required to break the network. On the other hand, the multilamellar vesicles have true value of yield stress, the sample don't flow, if the applied shear stress is below the yield value and dispersed air bubbles don't rise, even after long intervals of time. At small stress values the system behave like true permanent networks, while the system of type 1 behave like temporary networks. Secondly, amplitude sweep measurements were used to distinguish the two phases, at which the flexibility of rodlike micelles in changing their structures and entanglements needs higher deformation compared to multilamellar vesicles. The deformation of type 1 can be about 100% until the modulus breaks down, while in type 2 the modulus starts to decrease already at strain values of about 10%. At higher strains the system starts to flow. Thus, the yield stress is about 10% of the shear modulus (type 2). Thirdly, first normal stress difference measurements  $N_1$  show positive response of  $N_1$  as a function of applied shear rate for rodlike micelle solutions.  $dN_1/d\dot{\gamma}$  is positive for these solutions, and it's magnitude is proportional to the shear modulus of these rodlike micelles. Multilamellar vesicles have zero  $dN_1/d\dot{\gamma}$ . This effect is visually observed for rodlike micelle solutions with 75 mM 2,1 HNC/ 100 mM CTAOH at which the solution climbed on a rotating rod, while no such phenomenon is observed for solution with 130 mM 2,1 HNC and 100 mM CTAOH. An experimental difficulty in measuring  $N_1$  for the rodlike micelle solutions with long relaxation time was faced. For these solution, only the  $N_1$  over a small range of shear rate was measurable. At higher shear rates, the solutions escape out the cone plates. No such difficulty was observed for the solution with shorter relaxation times. The dependence of  $N_1$  on temperature has been studied for rodlike micelles.  $dN_1/d\dot{\gamma}$  decreases as temperature increases. Fourthly, effect of adding electrolyte has proven that storage modulus remains almost constant for rodlike micelles and decreases dramatically for solutions with multilamellar vesicles. Adding electrolyte to rodlike micelles reduces it's relaxation times. As a result of that,  $N_1$  measurements were possible to be made for the rodlike micelle solutions which were unmeasurable due to long relaxation time(> 1000 seconds). Multilamellar vesicles solutions

exhibit  $dN1/d\dot{\gamma}$  slope (almost zero) after adding the electrolyte. Fifthly, relaxation curves for rodlike micelles and multilamellar vesicles are different in shape.

For the system  $C_{16}TAOH/6,2$  HNC the rodlike micelles are with short and single relaxation time (0.02 second). The rheograms resemble to that one can obtain for the Maxwell model. The rodlike micelles show positive normal stress difference after a critical shear rate. A similar result was observed for the whole studied rodlike micellar solutions. This confirms the microstructure-rheological behavior relationship for this viscoelastic system.

The viscoelastic properties and the zero shear viscosity  $\eta^0$  of the rodlike micelles in solutions of  $C_{14}TAOH/2,1$  HNC and  $C_{12}TAOH/2,1$  HNC are resulted from a transient network of entangled rods that is characterized by a shear modulus  $G^0$  and single structural relaxation time according to Maxwell-element :

$$\eta^0 = G^0 \cdot \tau \quad (3.2)$$

For these solutions, the zero shear viscosity  $\eta^0$ , the plateau value of the shear modulus  $G^0$  (calculated from Cole-Cole relation as in figure 3.74 and 3.75) and structural relaxation time  $\tau$  for rodlike micelles in these systems are shown in table 3.5. The experimental results and the theoretically calculated ones are compared. To some extent there is an agreement between the experimental results and the calculated values for the solutions  $100 \text{ mM } C_{14}TAOH/ 65 \text{ mM } 2,1$  HNC and  $100 \text{ mM } C_{14}TAOH/ 70 \text{ mM } 2,1$  HNC.

*Table 3.5 :Hydrophobic counterion concentration dependence of the zero shear viscosity obtained from rheological data and compared to the equation (3.2) for the rodlike micelles in the systems  $C_{14}TAOH/2,1$  HNC and  $C_{12}TAOH/2,1$  HNC at 25 °C*

System	$G^0$ (Pa)	$\tau$ (second)	$\eta^0$ (Pa.s)	$\eta^0$ ,
			Experimental	Theoretical
100 mM $C_{14}TAOH/ 60$ mM 2,1 HNC	15	2,87	101,5	43
100 mM $C_{14}TAOH/ 65$ mM 2,1 HNC	30,5	19,92	543	607
100 mM $C_{14}TAOH/ 70$ mM 2,1 HNC	42,5	1,62	64	69
100 mM $C_{12}TAOH/ 65$ mM 2,1 HNC	30	0,016	1,04	0,47
100 mM $C_{12}TAOH/ 70$ mM 2,1 HNC	72	0,010	,090	0,71

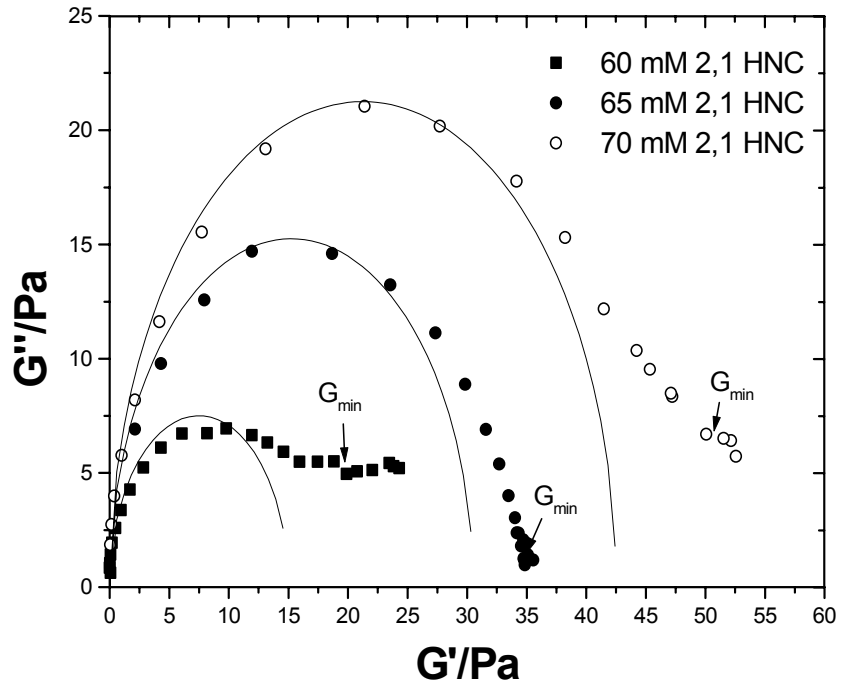


Figure 3.74: Cole-Cole plot for the systems with 60, 65 and 70 mM 2,1 HNC mixed with 100 mM  $C_{14}TAOH$ .

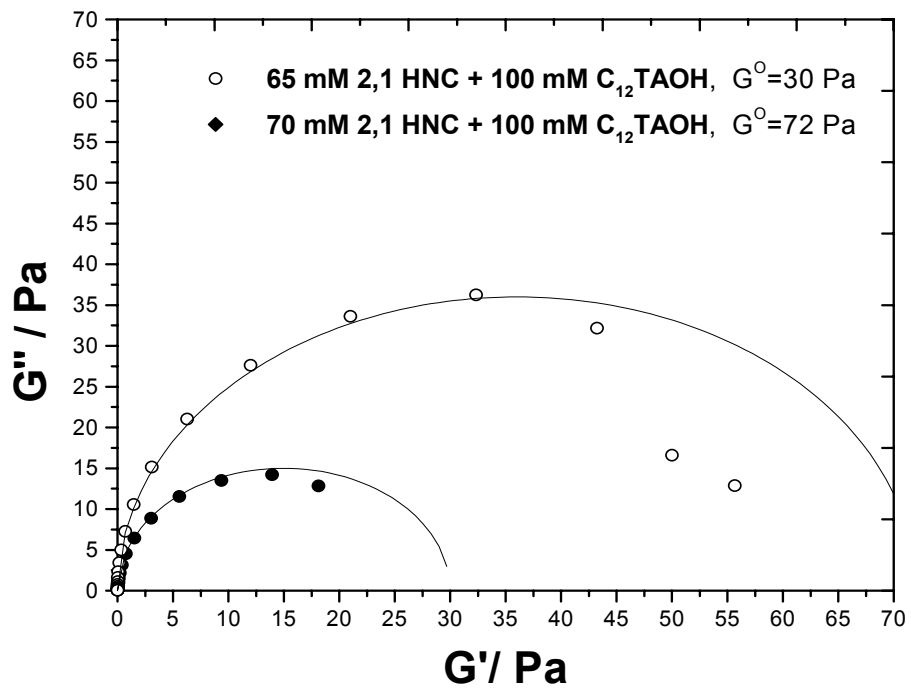


Figure 3.75 : Cole-Cole plot for the systems 65 and 70 mM 2,1 HNC mixed with 100 mM  $C_{12}TAOH$  and

The observed deviations between some experimental and theoretical  $\eta^0$  values are because of under estimation of  $G^0$  as a result of poor fits to the cole-cole representation. It is evident from cole-cole plots that the experimental data fit a semicircle at the left hand side, referring to the low frequency regime. At higher frequencies, there are deviations from the Maxwell behavior for both  $C_{14}TAOH/2,1$  HNC and  $C_{12}TAOH/2,1$  HNC rodlike micellar solutions. As mentioned before, the Maxwell behavior is characterized by a single relaxation time  $\tau$ . According to Maxwell, the shear stress after a rapid deformation relaxes to a stretched exponential function

$$\sigma(t) = \sigma(0) \exp\left(-\frac{t}{\tau}\right)^\alpha \quad (3.3)$$

where  $t$  is the time,  $\sigma(0)$  is the initial applied stress.

In the case of polymer-like micelle or rodlike micelles (Cate's model), relaxation time  $\tau$  is given by

$$\tau = (\tau_b \tau_{rept})^{0.5} \quad (3.4)$$

where  $\tau_b$  is defined as the average time of existence of a micellar chain of the average length  $\bar{L}$  from formation to the disruption into two pieces, while  $\tau_{rept}$  is the time needed for a chain to completely diffuse out of a tubelike environment composed of neighboring micellar chains by the reptation mechanism (i.e., by a snakelike motion along its own contour) along a tube which is constrained by the entanglements from other chains. For  $\tau_{rep} \ll \tau_b$ , the dominant stress relaxation mechanisms is reptation. Then the stress relaxation function indeed obeys the equation:

$$\sigma(t) = \sigma(0) \exp\left(-\frac{t}{\tau_{rept}}\right)^{1/4} \quad (3.5)$$

Under this condition, the stress relaxation is a combination of two processes involving both the scission and reptation of a micellar chain. As long as the oscillation frequency  $\omega$  at which the shear moduli are measured is smaller than the reciprocal value of the relaxation time  $\tau_b$ , the Maxwell behavior is observed for viscoelastic solutions of rodlike micelles. This is

obeyed up to  $\nu \approx 2\pi/\tau_b$ . The minimum in the curves  $G_{\min}$  in cole-cole plots of the system C<sub>14</sub>TAOH/2,1 HNC can be related in accordance with model by Granek and Cates to Rouse motion [134]. The model of Granek and Cates can also be applied to study the regimes involving small time scales where the dominant polymer micelles motion is not reptation but either breathing (which arise from the tube length fluctuations) or local Rouse-like motion (arising from stretches of chain shorter than the entanglement length,  $l_e$  which is defined as the contour length between two consecutive entanglement points ). This regime is characterized by an apparent turn up of both  $G'(\nu)$  and  $G''(\nu)$  at high frequencies. This results in a minimum loss modulus in cole-cole plot. This picture applies when the entanglement length,  $l_e$ , is much larger than the persistence length,  $l_p$  (defined as the length of the stiff part of a cylindrical micelle), and the breaking time is much larger than the Rouse relaxation time,  $\tau_e$ . This regime corresponds to the case  $\tau_{rep} > \tau_b > \tau_e$ , so cole-cole plot obeys the relationship.

$$G''_{\min} = G^o \frac{Al_e}{\bar{L}} \quad (3.6)$$

Where  $A$  is a constant equal to about unity.  $\bar{L}$  is the average length of the rodlike micelles, and  $l_e$  is their entanglement length. The ratio  $\bar{L}/l_e$  was treated as a number of the entanglements per micellar chain. The estimation for the value  $G''_{\min}/G^o$  increases when the concentration of 2,1 HNC increased from 60 to 65 mM and decreased at 70 mM 2,1 HNC in the system C<sub>14</sub>TAOH/2,1 HNC. The same behavior has been seen for the zero shear viscosity of these solutions as in table 3.5. The frequency dependence of the shear modulus can be compared with experimental results providing a direct estimate of the correlation length  $\xi$  and  $l_e/\bar{L}$ . For flexible micelles the entanglement length,  $l_e$  can be estimated from the relation

$$G^o = \frac{k_B T}{\xi^3} = \frac{k_B T}{l_e^{9/5} l_p^{6/5}} \quad (3.7)$$

To estimate the average micellar length from rheological data, it is needed to know the persistence length of the micelle, which could be in principle determined from scattering

techniques. In these calculations, a value of 170 Å is used, as observed in similar wormlike micellar solutions [76]. Table 3.6 shows the hydrophobic counterion concentration dependence of the average micellar length and related parameters obtained from rheological data for one value of persistence length (170 Å).

*Table 3.6: Hydrophobic counterion concentration dependence of the average micellar length and related parameters obtained from rheological data for one value of persistence length (170 Å) for the rodlike micelles in the system C<sub>14</sub>TAOH/2,1 HNC at 25 °C.*

<i>2,1 HNC</i> <i>mM</i>	$G^o$	$G''_{\min}$	$G^o / G''_{\min}$	$\xi$ (Å)	$l_e$ (Å)	$\bar{L}$ (Å)
60	15	5	3	650	1589	4 767
65	30,5	2,1	14,5	513	1071	15 530
70	42,5	5,6	7,6	459	890	6 764

The average micellar length that has been estimated in table 3.6 is related directly to the entanglement points, and it's number density. The shear modulus is independent of the micellar length. It's value is determined by the number density  $\nu$  of the entanglement points in accordance with a relation

$$G^o = \nu k_B T \quad (3.8)$$

In the rodlike micelles region of C<sub>16</sub>TAOH/2,1 HNC, C<sub>14</sub>TAOH/2,1 HNC and C<sub>12</sub>TAOH/2,1 HNC systems, decreasing the chain length leads to lower viscosity. This was explained by the dependence of viscosity on relaxation time, but not on the shear modulus. From Cole-Cole plot, it was shown that the shear moduli of 100 mM C<sub>14</sub>TAOH/ 65 mM 2,1 HNC and 100 mM C<sub>12</sub>TAOH/ 65 mM 2,1 HNC are close to each other, however, their relaxation times are different. The first normal stress difference has also a dependence on the chain length, but this dependence is also because of relaxation time  $\tau_{relaxation}$  and not storage modulus.  $dN1/d\dot{\gamma}$  depends on the chain length as shown in figure 3.76.

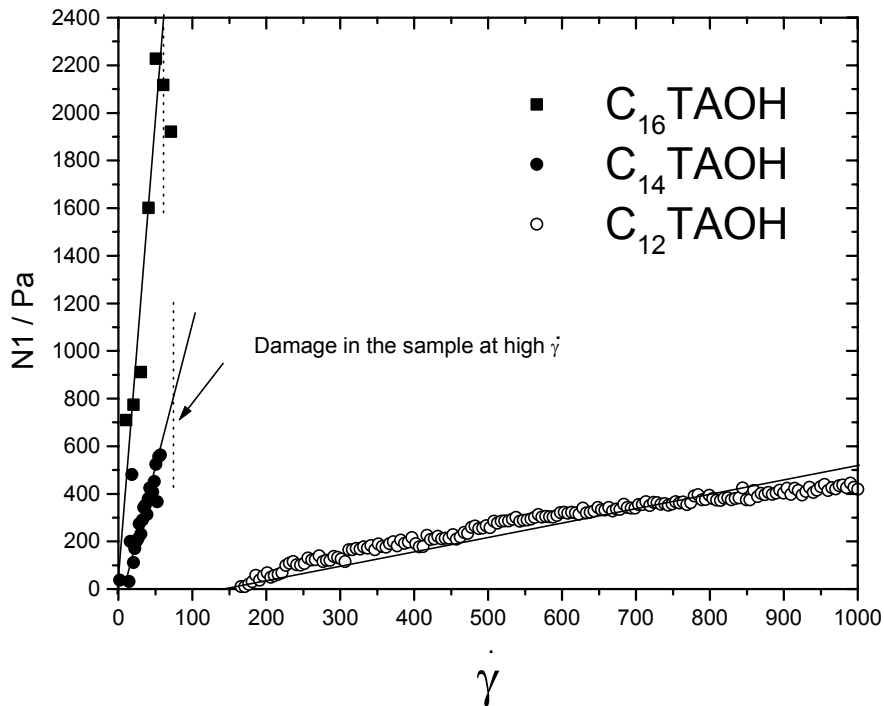


Figure 3.76: Effect of chain length on the first normal stress difference  $N1$  for the systems with 65 mM 2,1 HNC and 100 mM  $C_x$ TAOH.

Dependence of  $dN1/d\dot{\gamma}$  on the relaxation time (controlled by the chain length), and the relation to shear modulus and zero shear viscosity are shown in table 3.7

Table 3.7 :Effect of chain length on  $G^0$ ,  $\tau_{relaxation}$ ,  $dN1/d\dot{\gamma}$ ,  $N1$ , and zero shear viscosity .

System	$G^0$ (Pa)	$\tau_{relaxation}$ (Second)	$dN1/d\dot{\gamma}$ (Pa.s)	zero shear viscosity(Pa.s)
100 mM $C_{12}$ TAOH/ 65 mM 2,1 HNC	31	0,02	2,4	0,785
100 mM $C_{14}$ TAOH/ 65 mM 2,1 HNC	28,5	19	17,4	377,4
100 mM $C_{16}$ TAOH/ 65 mM 2,1 HNC	( $G^0 \sim 20-30$ )	> 1000	34,4	> 3000

On the other hand, in the rodlike micelles region of the C<sub>14</sub>TAOH/ 2,1 HNC system, it was proven that changing the storage modulus changes the  $dN1/d\dot{\gamma}$ . This means that  $dN1/d\dot{\gamma}$  depends on shear modulus. For the systems C<sub>10</sub>TAOH/2,1 HNC and C<sub>8</sub>TAOH/2,1 HNC, no rodlike micelle region was observed. These systems show a two phase region in between the Newtonian and the multilamellar vesicle regions. This is accompanied by the increasing in cmc which is resulted in decreasing the concentration of the surfactant in the micellar form.

After rodlike micelles region, the turbid (two phase region) was reached. No rheological measurements were carried out in this region (III).

IV- Multilamellar vesicles region. FF-TEM pictures have shown that the vesicles are sitting in a cage from which they cannot escape by a simple diffusion process without deformation of its shell, so they have viscoelastic properties. These six new viscoelastic systems assure and generalize the rheological properties of this microstructure. They show a storage modulus which is higher than loss modulus, and both are independent of frequency. The complex viscosity increases in the logarithmic scale (from right to left) with slope equal to -1. For the systems C<sub>16</sub>TAOH/2,1 HNC, C<sub>14</sub>TAOH/2,1 HNC, C<sub>12</sub>TAOH/2,1 HNC, C<sub>10</sub>TAOH/2,1 HNC, C<sub>8</sub>TAOH/2,1 HNC at equimolar compositions, the effect of the chain length on the storage modulus and yield stress is shown in figures 3.77 and 3.78. The storage modulus increases as the chain length increases. Similarly, the yield stress shows the same dependency.

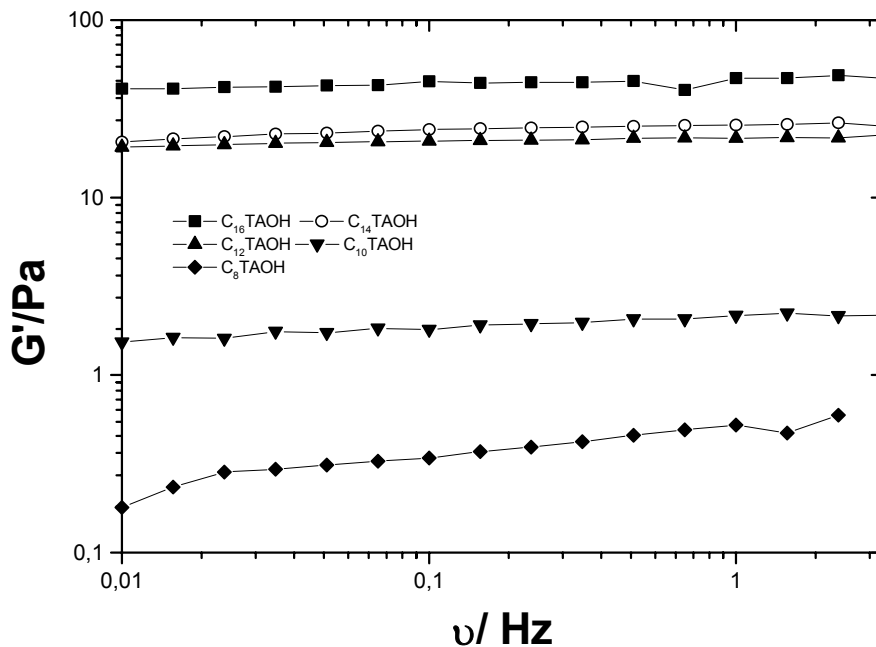


Figure 3.77:  $G'$  against frequency plots for vesicle phases of 100 mM 2,1 HNC and 100 mM  $C_x$ TAOH at 25 °C.

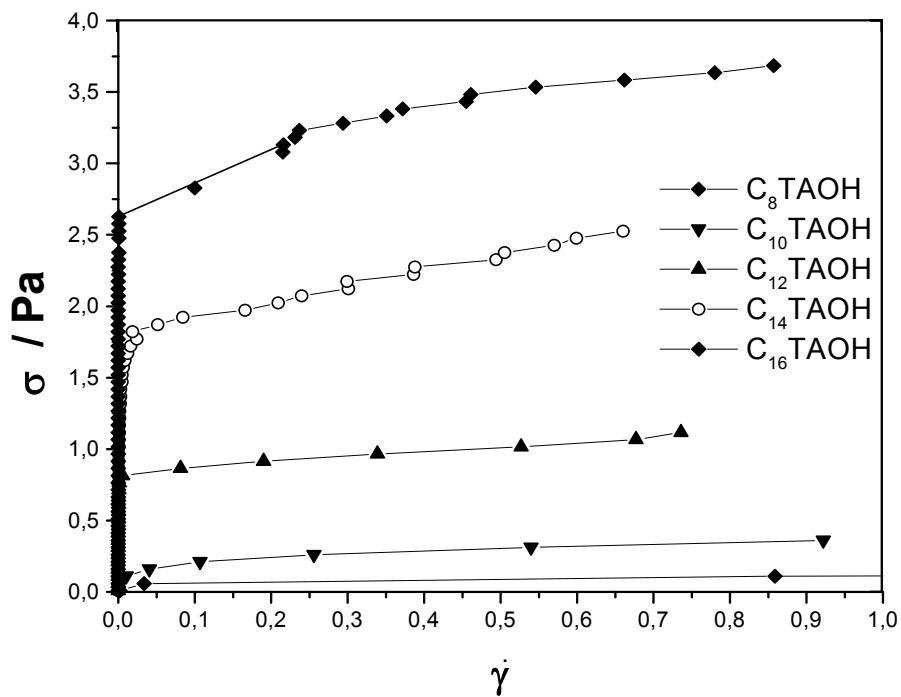


Figure 3.78: shear stress versus shear rate plots for 100 mM 2,1 HNC and 100 mM  $C_x$ TAOH at 25 °C.

The yield stress values have a strong relation to storage moduli. In amplitude sweep measurements, it was proven that the vesicles networks start to move when the deformation is 10%. Accordingly, one can predicate that the value of the yield stress is equal to 10% of the shear modulus. Figures 3.77 and 3.78 show a correspondence between storage moduli and the yield stress values of the systems.

At equimolar ratio of  $C_xTAOH$  ( $x = 8, 10, 12, 14, 16$ ), it is assumed that the vesicle surfaces are still charged, by considering that there are some hydrophobic counterions don't adsorb on the micellar surface. It has been shown (in chapter 3.1) that addition of an electrolyte decreases the storage modulus. This can be understood in the way that the charge density is a function of electrolyte concentration, which means that the modulus is determined by the electrostatic repulsion between the bilayers. Figure 3.79 shows the dependency of storage modulus on the electrolyte concentration for solution with 100 mM CTAOH and 130 mM 2,1 HNC.

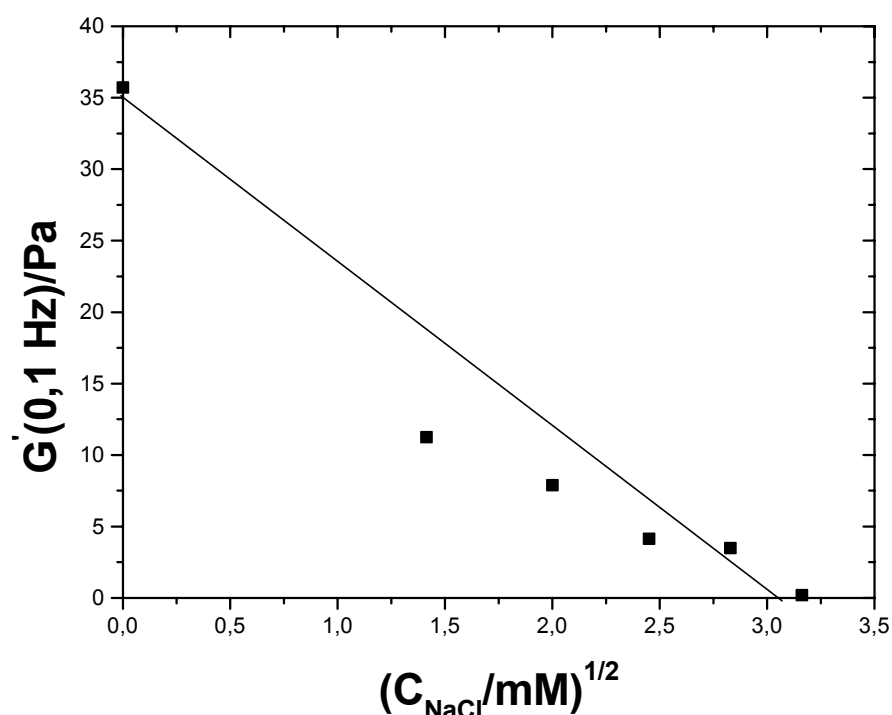


Figure 3.79: The dependency of storage modulus  $G'$  on the electrolyte (NaCl) concentration for solution with 100 mM CTAOH and 130 mM 2,1 HNC.

The results have shown that  $G^o$  of the vesicles decreases with increasing addition of the electrolyte. Excess electrolyte shields the charge on the vesicles. Therefore, it could be assumed that the rheological behavior of the vesicle could be explained by a simple electrostatic model. The published models and some comparison to experimental results are discussed.

Depending on the theory of Princen[127], an established model tries to calculate the moduli of vesicle phases. The model was developed for high internal phase emulsions. For such systems  $G^o$  is expressed by the equation

$$G^o = \frac{2\sigma}{R} \quad (3.9)$$

where  $\sigma$  is the interfacial tension at the surface of an emulsion droplet and  $R$  is the average radius of a droplet.  $\sigma$  can be determined by measuring the interfacial tension between the outer and the inner phase of the emulsion, if this interface is covered by a film of the emulsifier, i.e. the corresponding surfactant. In this model,  $R$  is the outer most radius of a vesicle and  $\sigma$  the interfacial tension of a vesicle phase against a hydrocarbon. The values of  $\sigma$  greatly depend on the charge density and decrease from 10 mN/m to 0.1 mN/m with increasing charge density. Assuming  $\sigma = 0.1$ , one can calculate the following  $G^o$  for the following systems (table 3.8):

*Table 3.8 : Shear modulus  $G^o$  calculated from equation 3.9 for the different systems.*

System	Radii range (nm)	$G^o$ - $G^o$ (Pa) calculated	$G^o$ (Pa) experimentally
100 mM C <sub>16</sub> TAOH/100 mM 2,1 HNC	50-600	333-4000	24
100 mM C <sub>14</sub> TAOH/100 mM 2,1 HNC	50-1100	182-4000	24
100 mM C <sub>12</sub> TAOH/100 mM 2,1 HNC	50-500	400-4000	21
100 mM C <sub>10</sub> TAOH/100 mM 2,1 HNC	50-2000	100-4000	1,8
100 mM C <sub>10</sub> TAOH/150 mM 2,1 HNC	50-2000	100-4000	3,9
100 mM C <sub>8</sub> TAOH/100 mM 2,1 HNC	50-1750	114-3500	0,34

This model shows that the calculated shear modulus don't agree the experimental results . It seems that equation 3.9 is applicable only for vesicles with large sizes ( $R > 3000$  nm).

A second model assumed that if the shear stress is applied to vesicular solution, the vesicle must be deformed and the charged bilayers must be pushed together more closely. The restoring force should then be the compression modulus which is simply given by the osmotic pressure  $\Pi$  of the system.  $\Pi$  is calculated from:

$$\Pi = c_m k_B T, \quad (3.10)$$

Here,  $c_m$  is the number concentration of ions at the midplane between the layers which is obtained by solving the Poissons-Boltzmann equation for given conditions (discussed in details in the introduction of this work). These calculations showed however that  $\Pi$  depends on the charge density in a similar manner as  $G^o$ , but the absolute values of  $\Pi$  are higher by more than two orders of magnitude than  $G^o$  values [135]. Thus, the rheological properties of vesicle phases can not be understood alone on the basis of the simple electrostatic model. In this case  $G^o$  should also not depend on the chain length of the surfactant what is contradictory to the experimental results.

Another model considered that vesicles are dispersed as hard sphere particles. This situation is comparable with a solution containing globular microemulsion droplets. Such systems form cubic phases if the effective volume fraction  $\Phi$  of the droplets is about 0.5. For such a system the compression modulus  $K$  has been calculated by the equation

$$K = \frac{vkT}{S(0)} \quad (3.11)$$

with the number density  $v$  of the particles and the structure factor  $S(0)$  of the system; which can be determined from scattering measurements [127].  $G^o$  is connected with  $K$  by the equation

$$G^o = \frac{3}{2} K \cdot \left( \frac{1 - 2\mu}{1 + \sigma\mu} \right) \quad (3.12)$$

which contains the Poisson number  $\mu$ . In this model each multilamellar vesicle would give the same contribution to the bulk modulus independent of the number of its layer.

Another model for the interpretation of the rheological data could be the formation of networks between the vesicles. As in the case of networks of threadlike micelles.  $G^o$  should then be given by equation (3.8). where  $v$  in this case means the number density of the effective vesicles, i.e. of those vesicles which are in contact with each other.  $G^o$  is given by the equation

$$G^o = \frac{3kT}{4\pi R^3} \quad (3.13)$$

Accordingly, the calculated shear moduli for various systems are listed in table (3.9).

*Table 3.9 : Shear modulus  $G^o$  calculated from equation 3.13 for the different systems.*

System	Radii range (nm)	$G^o$ - $G^o$ (Pa) calculated	$G^o$ (Pa) experimentally
100 mM C <sub>16</sub> TAOH/100 mM 2,1 HNC	50-600	4,5 x 10 <sup>-3</sup> - 7,9	24
100 mM C <sub>14</sub> TAOH/100 mM 2,1 HNC	50-1100	7,4 x 10 <sup>-4</sup> - 7,9	24
100 mM C <sub>12</sub> TAOH/100 mM 2,1 HNC	50-500	7,9 x 10 <sup>-3</sup> - 7,9	21
100 mM C <sub>10</sub> TAOH/100 mM 2,1 HNC	50-2000	1,2 x 10 <sup>-4</sup> - 7,9	1,8
100 mM C <sub>10</sub> TAOH/150 mM 2,1 HNC	50-2000	1,2 x 10 <sup>-4</sup> - 7,9	3,9
100 mM C <sub>8</sub> TAOH/100 mM 2,1 HNC	50-1750	1,8 x 10 <sup>-4</sup> - 7,9	0,34

If one considers the polydispersity of the system, the calculated shear modulus is in agreements for C<sub>x</sub>TAOH (x=8,10)/2,1 HNC and much lower for C<sub>x</sub>TAOH (x=12,14,16)/2,1 HNC. It seems that equation 3.13 is applicable for multilamellar vesicles with lower chain lengths.

## Summary

Anionic hydrophobic counterions with certain geometry adsorb onto the surface of cationic surfactant micelles and they minimize the repulsion between the headgroups, so the charge density on the surface is reduced. As a result of this, the micelle spontaneously changes its morphology due to a new packing for the head groups. The adsorption of 2-hydroxy-1-naphthoic acid 2,1 HNC and 6-hydroxy-2-naphthoic acid 6,2 HNC onto the surface of the cationic surfactant cetyltrimethylammonium hydroxide was studied. The results were compared to the published system 3-hydroxy-2-naphthoic acid 3,2 HNC/CTAOH. When an increasing amount of 2,1 HNC is introduced into a micellar solution of 100 mM CTAOH, one finds low viscous micellar solution, viscoelastic gel (consisting of rod like micelles), turbid region (two phase region), and viscoelastic liquid crystalline gel (consisting of multilamellar vesicles MLV with yield value). The complex viscosity (0.01 Hz) of 100 mM CTAOH rises by six orders of magnitude as the rodlike micelles form. It decreases then to the turbid region, and then rises again approximately six orders of magnitude. The second rising of the complex viscosity is accompanied by the formation of a liquid crystalline phase which consists of multilamellar vesicles. This has been proven by DICM, FF-TEM and Cryo-TEM. The vesicles were polydisperse and ranged from 100 to 1000 nm in diameter. SANS detected the transition in the microstructure which was caused by changing the concentration of 2,1 HNC in the system. SANS calculations show results similar to that obtained by microscopic methods. Surprising rheological behavior was measured in the rodlike micelle region, at which storage modulus was about one order of magnitude higher than loss modulus and both were parallel in the frequency range 0.001-10 Hz. Such behavior usually indicates the presence of vesicles in the liquid crystal phases. It was proved that other rheological measurements can be used to distinguish the two types, namely, amplitude sweep measurements, first normal stress difference  $N_1$  (Weissenberg effect), the effect of adding electrolyte, and stress relaxation curves.

When 6,2 HNC ( new substitution of HNC, the chemical structure is shown in page 75 ) is added with an increasing amount to 100 mM CTAOH, a new phase behavior is observed. Here the structure changes from small micelle aggregates into rodlike micelles, and then a two phase region consisting of  $L_1$ -phase and un-reacted 6,2 HNC is formed. No transition into MLV has been detected. Rheological measurements show viscoelasticity in agreement with the Maxwell model and with short relaxation time for the rodlike solution of this system. SANS spectra also indicated peaks with small intensity which correspond to small micelle aggregates. In the case of 3,2 HNC and 2,1 HNC, the hydroxyl and the carboxyl group are

neighboring, so they can effectively share in reducing the repulsion between the headgroups while the rings are in interaction with hydrocarbon tails. For 6,2 HNC the hydroxyl group is in position number 6 on the aromatic rings (see the chemical structure in page 75), which means that hydroxyl group is distant from the carboxyl group, thereby, less screening for the cationic charge in the micelle surface is obtained. Physical interaction between the hydroxyl groups and the hydrocarbon tails is also not favorable. Both of these reasons prevent the geometrical packing of the heads from reaching a packing parameter value  $\cong 1$ , so no MLV are formed. Substitution of HNC plays a main role in controlling the microstructure and other physical properties such viscosity, Krafft point, ..etc.

In the second part of this work, the hydrophobic counterion is fixed (2,1 HNC), and the length of the cationic surfactant's chain is changed from  $C_{16}$  into  $C_{14}$ ,  $C_{12}$ ,  $C_{10}$  and  $C_8$ . For the system 2,1 HNC/ tetradecyltrimethylammonium hydroxide TTAOH similar phase behavior as 2,1 HNC/CTAOH is observed. At 2,1 HNC/TTAOH ratio  $r \sim 1$ , formation of MLV is observed. After the neutralization addition of excess amount of 2,1 HNC is possible since the insoluble molecular form of 2,1 HNC becomes solublized in the formed MLV. Conductivity measurements prove that 2,1 HNC stays in the molecular form after the neutralization. A difference in the rheological behavior of the system 2,1 HNC/TTAOH compared to 2,1 HNC/CTAOH is seen. In the rodlike micelles region of 2,1 HNC/TTAOH, the solutions exhibit a short relaxation time compared to 2,1 HNC/CTAOH system. FF-TEM and SANS proved the formation of polydisperse MLV in this system with a maximum diameter of about 2000 nm and wall thickness of about 28 nm. The rods are also rheologically detected by their positive value of first normal stress difference  $N_1$  after certain shear rate  $\dot{\gamma}$  or by their positive value of  $dN_1/d\dot{\gamma}$ . The value of  $dN_1/d\dot{\gamma}$  for the rodlike micelle region in the system 2,1 HNC/TTAOH is lower than that one of the same concentration for the system 2,1 HNC/CTAOH. Further reduction in the length of the cationic surfactant is made when the system of 2,1 HNC/ dodecyltrimethylammonium hydroxide DOTAOH was studied. The complex viscosity of rodlike micelles of this system at 0.01 Hz is three orders of magnitude lower than that for the MLV region. The relaxation time becomes much shorter compared to 2,1 HNC/CTAOH.  $dN_1/d\dot{\gamma}$  also becomes less than that for 2,1 HNC/CTAOH and 2,1 HNC/TTAOH. MLV was made visible with DICM and FF-TEM and they have a diameter ranging from 100-1000 nm. SANS proved similar results as FF-TEM.

In the system of 2,1 HNC/ decyltrimethylammonium hydroxide DTAOH at 25°C, one finds with increasing concentration of 2,1 HNC a low viscous solution, a two phase region, and a viscoelastic liquid crystalline  $L_{\alpha}$ -phase which consists of densely packed multilamellar vesicles having a yield stress value. The multilamellar vesicles were made visible by differential contrast microscopy and FF-TEM. The diameter of these vesicles is about 3000 nm. The results of SANS agreed with the microscopic results. In this system, no rodlike micelle behavior is rheologically measured (Maxwell behavior). After the neutralization a turbid phase with slight birefringent consisting of MLV is formed, however, adding further amounts of 2,1 HNC results in solutions with stronger birefringent due to the formation of more organized MLV structures. This has been proved by FF-TEM pictures.  $dN1/d\dot{\gamma}$  for MLV is approximately zero, which is similar to that one for other studied systems in the MLV region.

For 2,1HNC/ octyltrimethylammonium hydroxide OTAOH system at 25°C one finds with increasing concentration of 2,1 HNC a low viscous solution, a turbid region, a precipitated densely packed multilamellar vesicle phase having a small yield stress value. The system begins to form vesicles or bilayers as has been shown from the pictures of FF-TEM. The maximum diameter of these vesicles is about 3000 nm. At around the equal mole ratio of 2,1 HNC and OTAOH, the solutions resist the sedimentation of the vesicles for some months, and after that the two phase region is seen.

As a result of this work, it is concluded that the role of the hydrophobic counterions with certain geometry could be looked upon as a co-surfactant with a shorter chain length which changes the bending rigidity,  $k_c$ , of the bilayer. They are surface active species that bind strongly on the micelle surface and change the packing parameter of the headgroups. It is suggested that the hydrophobicity of the counterion plays an important role in deciding the structure of the supramolecular assemblies such as vesicles, or micelles. As a consequence one can change the morphology of micelle species by changing the ratio of counterion/surfactant ion. These studies also suggest that by mixing cationic surfactant and hydrophobic counterion with varying cationic surfactants chain lengths, one can have a control over the supramolecular structures formed. Long chain cationic surfactants prefer to form multilamellar vesicles with lower diameters compared to the short surfactants.

### Zusammenfassung

Anionische hydrophobe Gegenionen mit bestimmter Geometrie adsorbieren auf der Oberfläche von Mizellen kationischer Tenside und minimieren die Abstoßung zwischen den Kopfgruppen, da die Ladungsdichte auf der Oberfläche reduziert wird. Das Ergebnis ist eine spontane Änderung der Morphologie der Mizelle, da die Kopfgruppen anders gepackt werden. Die Adsorption von 2-Hydroxy-1-Naphthoesäure (2,1 HNC) und von 6-Hydroxy-2-Naphthoesäure (6,2-HNC) auf der Oberfläche des kationischen Tensids Cetyltrimethylammoniumhydroxid wurde untersucht. Die Ergebnisse wurden mit dem bereits veröffentlichten System 3-Hydroxy-2-Naphthoesäure (3,2 HNC)/CTAOH verglichen. Wenn 2,1 HNC in wachsender Menge zu einer mizellaren Lösung von 100mM CTAOH zugegeben wird, findet man eine niedrigviskose mizellare Lösung, ein viskoelastisches Gel (bestehend aus Stäbchenmizellen), eine trübe Region (Zweiphasengebiet) und ein viskoelastisches, flüssigkristallines Gel (bestehend aus multilamellaren Vesikeln, MLV, mit einer Fließgrenze). Die komplexe Viskosität (0,01Hz) von 100mM CTAOH nimmt über sechs Größenordnungen zu, wenn die Stäbchenmizellen gebildet werden. Der zweite Anstieg der komplexen Viskosität wird durch die Bildung einer flüssigkristallinen Phase hervorgerufen, welche aus multilamellaren Vesikeln besteht. Das wurde durch DICM, FF-TEM und Kryo-TEM bestätigt. Die Vesikel waren polydispers und ihre Durchmesser lagen im Bereich zwischen 100 und 1000nm. Mit Hilfe von SANS wurde der Übergang in der Mikrostruktur aufgeklärt, welcher durch die Konzentrationsänderung von 2,1 HNC im System hervorgerufen wurde. SANS Berechnungen ergeben Resultate, die jenen ähnlich sind, welche bei den mikroskopischen Untersuchungen erhalten wurden. Ein überraschendes rheologisches Verhalten wurde im Existenzbereich der Stäbchenmizellen gefunden, in dem der Speichermodul ungefähr eine Größenordnung höher lag als der Verlustmodul und beide im Frequenzbereich zwischen 0,001 und 10Hz parallel verliefen. Ein solches Verhalten zeigt normalerweise das Vorliegen von Vesikeln in flüssigkristallinen Phasen an. Es konnte gezeigt werden, daß andere rheologische Methoden dazu benutzt werden können, die zwei Arten zu unterscheiden, und zwar Amplituden-Sweep-Messungen, die erste Normalspannungsdifferenz  $N_1$  (Weissenberg-Effekt), die Auswirkung von Elektrolytzugabe, und Spannungsrelaxationskurven.

Wenn 6,2 HNC (eine neue Substitution von HNC, die chemische Struktur ist auf Seite gezeigt) in wachsender Menge zu einer 100mM CTAOH-Lösung zugesetzt wird, wird ein neues Phasenverhalten beobachtet. Hier verändert sich die Struktur von kleinen mizellaren

Aggregaten hin zu Stäbchenmizellen und anschließend entsteht ein Zweiphasengebiet, welches aus einer  $L_1$ -Phase und unreaktierter 6,2 HNC besteht. Kein Übergang zu MLV konnte gefunden werden. Rheologische Messungen zeigen viskoelastisches Verhalten, welches durch das Maxwell-Modell mit einer kurzen Relaxationszeit für die Lösung von Stäbchenmizellen in diesem System beschrieben werden kann. SANS-Spektren weisen ebenfalls Peaks mit kleiner Intensität auf, welche kleinen mizellaren Aggregaten zugeordnet werden können. Im Fall von 3,2 HNC und 2,1 HNC sitzen die Hydroxyl- und die Carboxylgruppe in Nachbarschaft, so daß sie gemeinsam dazu beitragen können, die repulsion zwischen den Kopfgruppen zu reduzieren, während die Ringe mit den Kohlenwasserstoff-resten in Wechselwirkung treten. Bei 6,2 HNC sitzt die Hydroxylgruppe in Position Nummer 6 am aromatischen Ring (siehe die chemische Struktur auf Seite 75), was bedeutet, daß die Hydroxylgruppe und die Carboxylgruppe entfernt zueinander angeordnet sind, so daß die kationische Ladung auf der Mizelloberfläche weniger abgeschirmt wird. Eine physikalische Wechselwirkung zwischen der Hydroxylgruppe und den Kohlenwasserstoffresten ist auch unwahrscheinlich. Aus diesen beiden Gründen wird die geometrische Packung der Kopfgruppen nie so dicht werden, daß ein Packungsparameter von ungefähr 1 erreicht wird, so daß keine MLV gebildet werden. Die Substitution von HNC spielt eine wichtige Rolle bei der Kontrolle der Mikrostruktur und anderer physikalischer Eigenschaften wie etwa der Viskosität, des Krafft-Punkts usw..

Im zweiten Teil dieser Arbeit wurde ein bestimmtes hydrophobes Gegenion verwendet (2,1 HNC) und die Kettenlänge des kationischen Tensids von  $C_{16}$  über  $C_{14}$ ,  $C_{12}$ ,  $C_{10}$  bis hin zu  $C_8$  verändert. Für das System 2,1 HNC/Tetradecyltrimethylammoniumhydroxid (TTAOH) wird ein ähnliches Phasenverhalten wie für 2,1 HNC/CTAOH beobachtet. Bei einem molaren Verhältnis von HNC/TTAOH von etwa 1 bilden sich MLV. Nach Neutralisierung ist die Zugabe eines Überschusses an 2,1 HNC möglich, da die unlösliche molekulare Form von 2,1 HNC in den gebildeten MLV solubilisiert wird. Leitfähigkeitsmessungen zeigen, daß 2,1 HNC nach der Neutralisierung in der molekularen Form bleibt. Ein Unterschied im rheologischen Verhalten der Systeme 2,1 HNC/TTAOH und 2,1 HNC/CTAOH konnte beobachtet werden. Im Gebiet der Stäbchenmizellen von 2,1 HNC/TTAOH zeigen die Lösungen kurze Relaxationszeiten im Vergleich zum System 2,1 HNC/CTAOH. Mit Hilfe von FF-TEM und SANS konnte nachgewiesen werden, daß in diesem System polydisperse MLV mit einem maximalen Durchmesser von etwa 2000nm und Wandstärken von etwa 28nm gebildet werden. Die Stäbchen können auch anhand des positiven Werts der ersten

Normalspannungsdifferenz  $N_1$  nach Einwirken einer bestimmten Scherung  $\dot{\gamma}$  oder anhand des positiven Werts von  $dN_1/d\dot{\gamma}$  nachgewiesen werden. Der Wert von  $dN_1/d\dot{\gamma}$  ist für das Gebiet der Stäbchenmizellen im System 2,1 HNC/TTAOH niedriger als derjenige für dieselbe Konzentration beim System 2,1 HNC/CTAOH. Eine weitere Verkürzung der Kettenlänge des kationischen Tensids wird im System 2,1 HNC/Dodecyltrimethylammoniumhydroxid (DOTAOH) erreicht. Die komplexe Viskosität der Stäbchenmizellen dieses Systems bei 0,01Hz ist drei Größenordnungen kleiner als in der MLV-Region. Die Relaxationszeit wird deutlich kürzer im Vergleich zu 2,1 HNC/CTAOH.  $dN_1/d\dot{\gamma}$  ist auch niedriger als der entsprechende Wert für 2,1 HNC/CTAOH und 2,1 HNC/TTAOH. Die MLV wurden mit DICM und FF-TEM sichtbar gemacht und sie haben Durchmesser zwischen 100 und 1000nm. SANS erbrachte ähnliche Resultate wie FF-TEM.

Im System 2,1 HNC/Decyltrimethylammoniumhydroxid (DTAOH) findet man bei 25°C mit zunehmender Konzentration an 2,1 HNC eine niedrigviskose Lösung, ein Zweiphasengebiet und eine viskoelastische, flüssigkristalline  $L_\alpha$ -Phase, welche aus dichtgepackten, multilamellaren Vesikeln mit Fließgrenze besteht. Die multilamellaren Vesikel wurden mit Hilfe von Differentialkontrastmikroskopie und von FF-TEM sichtbar gemacht. Der Durchmesser dieser Vesikel liegt bei etwa 3000nm. Die Ergebnisse aus den SANS-Messungen stimmten mit den mikroskopischen Untersuchungen überein. In diesem System konnte aus der Rheologie kein Hinweis auf das Vorliegen von Stäbchenmizellen abgeleitet werden (Maxwell-Verhalten). Nach Neutralisierung entsteht eine leicht doppelbrechende, trübe Phase, welche aus MLV besteht. Nach einer weiteren Zugabe von 2,1 HNC entstehen jedoch stärker doppelbrechende Lösungen aufgrund der Bildung von stärker organisierten MLV-Strukturen. Dies konnte mit Hilfe von FF-TEM-Bildern untermauert werden. Der Wert von  $dN_1/d\dot{\gamma}$  für die MLV ist ungefähr 0, ähnlich jenen Werten, welche für die anderen untersuchten Systeme im MLV-Bereich gefunden wurden.

Für das System aus 2,1 HNC und Octyltrimethylammoniumhydroxid (OTAOH) findet man bei 25°C mit steigender Konzentration an 2,1 HNC eine niedrigviskose Lösung, eine trübe Region und eine Phase mit einem Niederschlag aus dichtgepackten, multilamellaren Vesikeln mit Fließgrenze. Das System beginnt, Vesikel oder Doppelschichten aufzubauen, was anhand von FF-TEM-Bildern gezeigt wurde. Der maximale Durchmesser dieser Vesikel bewegt sich um 3000nm. Bei einem etwa äquimolaren Verhältnis von 2,1 HNC und OTAOH unterbleibt

die Sedimentation der Vesikel für einige Monate und erst danach wird das Zweiphasensystem beobachtet.

Als Ergebnis dieser Arbeit kann der Schluß gezogen werden, daß das hydrophobe Gegenion mit bestimmter Geometrie die Rolle eines Kationsids spielt, welches eine kürzere Kettenlänge besitzt und die Biegesteifigkeit,  $k_c$ , der Doppelschicht verändert. Es handelt sich um oberflächenaktive Spezies, welche stark an der Mizelloberfläche gebunden werden und den Packungsparameter der Kopfgruppen beeinflussen. Es kann davon ausgegangen werden, daß die Hydrophobie des Gegenions eine wichtige Rolle bei der Festlegung der Struktur der supramolekularen Aggregate, wie etwa Vesikel oder Mizellen, spielt. Daher kann man die Morphologie der mizellaren Spezies durch Veränderung des Verhältnisses Gegenion/Tensidion beeinflussen. Die vorliegenden Untersuchungen deuten auch darauf hin, daß durch Mischen kationischer Tenside unterschiedlicher Kettenlängen mit hydrophoben Gegenionen eine Kontrolle über die Art der gebildeten supramolekularen Strukturen möglich ist. Langkettige kationische Tenside bilden multilamellare Vesikel mit eher niedrigeren Durchmessern im Vergleich zu den kurzkettigen Tensiden.

## References

- 1 Paul C. Hiementz, Raj Rajagopalan, Principles of Colloidal and Surface chemistry, Third edition, 1997.
- 2 H.Hoffmann, Phys. Chem. 98, 1433-1455 (1994) No. 11.
- 3 Paul M. Holland and Donn N. Rubingh, Mixed Surfactants System, ASC symposium series 501, American chemical society, Washington, DC, P1-43, 1992.
- 4 D.Attwood A.T.Florence, Surfactant System, p 1-17, 87-98, Chapman and Hall Ltd. USA, 1985.
- 5 G.Jakobi, A. Lohr, Detergent and Textile Washing, VCH publisher, Germany, P 49-63, 1987.
- 6 Keijhi Kameyama, Ayumu Moroya, and Toshio Takagi, J.Colloid and Interface science.196, P48-57, 1996.
- 7 Sambhav Vora, Alex George, Hemangi Desai, and Pratap Bahadur, Journal of Surfactants and Detergents, 2, P213-221, 1999.
- 8 Md. Emdadul Haque, Akhil Ranjan Das, and Satya Priya Moulik, J.Colloid and Interface science, 217, P 1-7, 1999.
- 9 P. M. Holland and D. N. Rubingh, J. Phys. Chem. 87, P 1984-1990, 1984.  
454-459, 1996.
- 10 Jeffry J.Lopata, Si Thieu, and John F. Scamehorn, J.Colloid and Interface science, 186,  
P 215-224, 1997.
- 11 Hiroki Matsubara, Akio Ohata, Mitsuhiro Kameda, Masum Villeneuve, Norihiro Ikeda,  
and Makoto Aratono, Langmuir, 15, P 5496-5499, 1999.
- 12 Darrell Wells and Calum J. Drummond, Langmuir, 15, 4713-4721, 1999.
- 13 Hiroshi Maeda, Shuichi Muroi, Mami Ishii, Rie Kakehashi, Hideki Kaimoto, Tatsuo  
Nakahara, and Kinsi Motomura, J.Colloid and Interface science, 175, 497-505, 1995.
- 14 Masumi Villeneuve, Hirotomo Sakamoto, Hisanobu Minamizaw, Norihiro Ikeda, Kinsi  
Motomura, and Makoto Aratono, J.Colloid and Interface science, 194, 301-310, 1997.
- 15 Tejas R. Desai and Sharad G. Dexit, J.Colloid and Interface science,177, 471-477, 1996.
- 16 Danuta Goralczyk, J.Colloid and Interface science, 184, 139-146, 1996.
- 17 Hitoshi Matsuki, Makoto Aratono, Shoji Kaneshina, and Kinsi Motomura, J.Colloid and  
Interface science, 191, 120-130, 1997.
- 18 Kathleen L. Herrington and Eric W. Kaler, J.Phys.Chem. 97,13792-13802, 1993.
- 19 Mangnus Bergström and Jan Christer Eriksson, Langmuir, 2000, 16, 7173-7181.

- 20 D. Gräbner, T. Matsuo, E. Hoinkis, C. Thunig, and H. Hoffmann, *Journal of Colloid and Interface Science* 236, 1-13 (2001).
- 21 Reiner Beck, Michael Gradzielski, Klaus Horbaschek, S. Sakhawat Shah, Heinz Hoffmann, and Pavel Strunz, *Journal of Colloid and Interface Science* 221,200-209(2000).
- 22 R. Beck, M. Gradzielski, K. Horbaschek, S. S. Shah, H. Hoffmann, and P. Strunz, *Colloid Polym Sci.* 278:137-142 (2000).
- 23 C.Thunig, G. Platz, and H. Hoffmann, *Springer Proceeding in Physics*, Vol 66, 266-2.
- 24 H. Hoffmann, K. Horbaschek, and F. Witte, , *Journal of Colloid and Interface Science*, 235, 33-45 (2001).
- 25 D. Gräbner, T. Matsuo, E. Hoinkis, C. Thunig and H. Hoffmann, *Journal of Colloid and Interface Science*, 236, 1-13 (2001).
- 26 H. Hoffmann, *Progr Colloid Polym Sci*, 83, 16-28, 1990.
- 27 P. Versluis and J. C. van de Pas, *Langmuir*, Vol. 17, No 16, 2001.
- 28 H. Hoffmann, *Tenside Surf. Det.* 32, (1995), 6.
- 29 Caria Annalisa, Regev Oren, Khan Ali, *Journal of Colloid and Interface Science*, 200 ,19-30 (1998).
- 30 Kopperud, Hilde Molvig, Hansen, Finn Knut, Nystrem, Bo. *Macromolecular Chemistry and Physics*, 99, 11, 2385-2394 (1998).
- 31 William M. Gelbart and Avinoam Ben-Shaul, *J. Phys. Chem.* 1996, 100, 13169-13189.
- 32 Hoffmann, H. and W. Ulbricht, *Recent Res. Devel. in Physical Chem.*, 2 (1998).
- 33 Susanne Nilsson, Krister Thuresson, Per Hansson and Björn Lindman, *J. Phys. Chem. B*, 1998, 102, 7099-7105.
- 34 Toshiyuki Shikata, Hirotaka Hirata and Tadao Kotaka, *Langmuir*, 1987, 3, 1081-1086.
- 35 Lukac, Sava; Harbour, John R. Xerox Res. Cent. Canada, Mississauga, Can. *Journal of the Chemical Society, Chemical Communications* (1982), (3), 154-7.
- 36 Lawrence, M. Jayne. Dep. Pharmacy, King's College London, London, UK. *European Journal of Drug Metabolism and Pharmacokinetics* (1994), 19(3), 257-69.
- 37 Montron Rosoff, *Vesicles. Surfactant Science Series*, Volume 62, New York, 1996.
- 38 Martin Jung, Ph.d thesis, Technische Universiteit Eindhoven, 2000.
- 39 Didier Roux and Fabinne Gauffre, *ECC Research*, P 17-24.(Center de recherc Paul-Pascal, CNRS, Ave Dr Schweizer 33600 Pessac, France).
- 40 Hoffmann, H. *Phys. Chem.* 98, 1433-1455 (1994) No. 11.

- 41 Kathleen L. Herrington, Eric W. Kalar, David D. Miller, Joseph A. Zasadzinski and Shivkumar Chiruvolu, *J. Phys. Chem.* 1993, 97, 13792-13802.
- 42 Heinz Hoffmann and Werner Ulbricht, *Recent Res. Devel. in Physical Chem.*, 2 (1998).
- 43 M.Gradzielski, M. Müllwr, M.Bergmeier, H. Hoffmann and E. Hoinkis, *J. Phys. Chem. B*, 1999, 103, 1416-1424.
- 44 Annalisa Caria and Ali Khan, *Langmuir* 1996, 12, 6282-6290.
- 45 M. Gradzielski, M. Müller, M. Bergmeir, H. Hoffmann and E. Hoinkis, *J. Phys. Chem. B* 1999, 103, 1416-1424.
- 46 Laura L. Brasher and Eric W. Kaler, *Langmuir* 1996, 12, 6270-6276.
- 47 H.Hoffmann, C.Thunig, P. Schmiedel and U.Munkert, *Faraday Discuss.*, 1995,101,319-333.
- 48 P. Panizza, D. Roux, V. Vuillaume, C.-Y.D.Lu, and M.E. Cates, *Langmuir* 1996, 12, 248-252.
- 49 Jihgcheng Hao, Heinz Hoffmann, and Klaus Horbaschek, *J. Phys. Chem. B*, 2000, 104, 10144-10153.
- 50 José Escalante, Ph.D. thesis, Bayreuth University, 2000.
- 51 José Escalante, Heinz Hoffmann, *Rheol Acta*, (2000), 39:209-214.
- 52 Klaus Horbaschek, Heinz Hoffmann, and Jihgcheng Hao, *J. Phys. Chem. B*, Vol. 104, No 13, 2000, 2782-2784.
- 53 Isralelachvili, J. N., Mitchell, D. J. & Ninham, B. W. 1976. *J. Chem. Soc. Faraday Trans II* 72, 1525.
- 54 Robert Lange, *K. Surfactants (A Practical Handbook)*, Hanser Grander Publications, - Inc., Cincinnati.
- 55 J. L. Jones and T. C. B. McLeish, *Langmuir* 1999, 15, 7495-7503.
- 56 W.Helfrich, *Phys.Lett.*,43A (1973)409.
- 57 P.A. Hassan, B. S. Valaulikar, C. Manohar, F. Kern, L. Bourdieu, and S. J. Candau, *Langmuir* 1996, 12, 4350-4357.
- 58 P.A. Hassan , Janaky Narayanan, S. V. G. Menon, R. A. Salkar, and S.D. Samant, C. Monhar, *Colloids and Surfaces A: Physiochemical and Engineering Aspects* 117 (1996)89-94.
- 59 S. A. Safran, F. C. MacKintosh, P. A. Pincus and D. A. Andelman, *Progr Colloid Polym Sci*, 84:3-7,1991.
- 60 D.Fennell Evans and Håkan Wennerström, *The colloidal domain, where physics, chemistry, biology and technology meet*, VCH, 1994.

- 61 Y. Sakaiguchi, T. Shikata, H. Urakami, A. Tamura, H. Hirata, *Colloid and Polymer Science*, (1987), 265(8), 750-3.
- 62 Toshiyuki Shikata, Shin-ichiro Imai, , *Journal of Colloid and Interface Science*, 244(2), 399-404, (2001).
- 63 Toshiyuki Shikata, Shin-ichiro Imai, and Yotaro Morishima, *Langmuir*, 1998, 14, 2020-2026.
- 64 Toshiyuki Shikata and Dale S. Pearson, *Langmuir*, 1994, 10, 4027-4030
- 65 Toshiyuki Shikata and Shin-ichiro Imai, *J. Phys. Chem. B* 1999, 103, 8694-8697.
- 66 Toshiyuki Shikata, Hirotaka Hirata and Tada Kotaka, *J. Phys. Chem. B* 1990, 94, 3702-3706.
- 67 V. K. Aswal, P. Thiyagarajan and P. S. Goyal, *J. Phys. Chem. B* 1998, 102, 2469-2473.
- 68 Rehage, H. and Hoffmann, H. *J. Phys. Chem.* 1988,92,4712.
- 69 Janaky Narayanan, E. Mendes, C. Monohar, *International Journal of Modern Physics B*, Vol. 16, Nos. 1 & 2 (2002) 375-382.
- 70 E. Mendes, R. Oda, C. Monohar, Janaky Narayanan, *J. Phys. Chem. B* 1998, 338-343.
- 71 Sushama Mishra, B. K. Mishra, S. D. Samant, Janaky Narayanaa, and C. Manohar, *Langmuir* 1993, 9, 2804-2807.
- 72 R. Oda, Janaky Narayanaa, P. A. Hassan, C. Manohar, R. A. Salkar, F. Kern and S.J. Candau, , *Langmuir* 1998, 14, 4364-4372.
- 73 P. A. Hassan, S.J. Candau, F. Kern, and C. Manohar, *Langmuir* 1998, 14, 6025-6029.
- 74 Lequeux, F. *Europhys. Lett.* 1992, 19 (8), 675.
- 75 B. K. Mishra, S. D. Samant, P. Pradhan, Sushama B. Mishra, and C. Manohar, *Langmuir*, 1993, 9, 894-898.
- 76 P.A. Hassan, B. S. Valaulikar, C. Monhar, F. Kern, L. Bourdieu, and S. J. Candau, *Langmuir* 1996, 12, 4350-4357.
- 77 Tibor Gilányi, Róbert Mészáros, and Imre Varga, *Langmuir*, 2000, 16, 3200-3205.
- 78 Olle Söderman, Kathleen L. Herrington, Eric W. Kalar and David D. Miller, *Langmuir*, 1997, 13, 5531-5538.
- 79 Kathleen L. Herrington, Eric W. Kalar, David D. Miller, Joseph A. Zasadzinski and Shivkumar Chiruvolu, *J. Phys. Chem.* 1993, 97, 13792-13802.
- 80 Michael T. Yacilla, Kathleen L. Herrington; Laura L. Brasher, Eric W. Kalar, Shivkumar Chiruvolu, and Joseph A. Zasadzinski, *J. Phys. Chem.* 1996, 100, 5874-5879.
- 81 Eric W. Kalar, Kathleen L. Herrington, A. Kamalakara Murthy and Joseph A. Zasadzinski, *J. Phys. Chem.* 1992, 96, 6698-6707.

- 82 Håkan Edlund, Alireza Sadaghiani and Ali Khan, *Langmuir*, 1997, 13, 4953-4963.
- 83 Klaus Horbaschek, Ph.D. thesis, Bayreuth University, 2000.
- 84 Stefan Hoffman, Ph.D. thesis, Bayreuth University, 1994.
- 85 W. H. A. Fincham, M. H. Freeman, *Optics*, P340-355, Ninth edition, 1980.
- 86 Hecht, *Optics*, P 319-345, Third edition, 1999.
- 87 Bass Michael, *Handbook of optics*, volume 1, P 5.1-5.29, 1995.
- 88 P. W. Atkins, *Physical chemistry*, Forth edition, P749-761, 1990.
- 89 Jurgen Meyer, Ph.D thesis, Bayreuth University, 2001.
- 90 Horst Robenek, *Microscopie in Forschung und Praxis*, P 62-64, (GIT VERLAG GMBH), 1995.
- 91 Ludwig Reimer, *Transmission Electron Microscopy, Physics of Image Formation and Microanalysis*, With 264 Figures, Springer-Verlag Berlin Heidelberg NewYork Tokyo 1984.
- 92 Robert J. Hunter, *Introduction to Modern Colloid Science*, Oxford science publications, 1993.
- 93 T. Müller, R. Guggenheim, M. Düggelin and Ch. Scheidegger, *Journal of Microscopy*, vol. 161, Pt 1, January 1991, pp. 73-83.
- 94 David P. Allison, C. Stuart Daw and Marie C. Rorvik, *Journal of Microscopy*, vol. 147, Pt 1, July 1987, pp. 103-108.
- 95 Eijiro Adachi, Toshio Nakatani and Paulo H.Hashimoto, *Journal of Microscopy*, vol. 147, Pt 2, August 1987, pp. 205-208.
- 96 Kissa, Erik, *Dispersions characterization, testing, and Surfactant science series 84*, 1999.
- 97 Hunter, Robert J., *Introduction to modern colloid science*, Oxford Univ. Press, 1993.
- 98 N. W. Ashcoroft and J. Lekner, *Physical Review*, 145, 83-90, 1996.
- 99 Stephen M. King, *Introduction to small angle neutron scattering*, 1995.
- 100 M. Gradzielski, M. Müller, M. Bergmeier, H. Hoffmann, and E. Hoinkis, *J. Phys. Chem. B* 1999, 103, 1416-1424.
- 101 Maurice C. Newstein, Hao Wang, Nitash P. Balsara, Amy A. Lefebvre and Yitzhak Shnidman, *J. Chem. Phys.*, Vol. 111, No. 10, 8, 1999.
- 102 D. V. Boger and K. Waiters (1993) *Rheological Phenomenain Focus*.
- 103 Maik Nowak, *Rheol Acta*, 40, 366-372, 2001.
- 104 H. Rehage and H. Hoffmann, *Molecular Physics*, Vol 74, No. 5, 933-973, 1991.
- 105 N. A. Spenley, M. E. Cates and T. C. B. Mcleish, *Physical Rewiew Letters*, Volume 71, Number 6, 9 August 1993.

- 106 J. W. Goodwin and R. W. Hughes, *Rheology for chemists an introduction*, Royal Society of Chemistry 2000.
- 107 Heinz Hoffmann and Heinz Rehage, *Tenside Detergents*, 22, (1985), 6, 290-298.
- 108 Craig A. Herb and Robert K. Prud'homme, *Structure and Flow in Surfactant Solutions*, American Chemical Society, Washington, DC 1994.
- 109 H.A. Barnes, J.F. Hutton and K. Walters, *An introduction to Rheology*, Rheology serie, 3, Elsevier science publishing company INC, 1989.
- 110 Eberhard Klingbeil, *Tensorrechnung für ingenieure*, B.I. hochschultaschenbücher, 1966, George Arfken, *Mathematical Methods for Physicists*, second edition, 1970.
- 111 P. Panizza, D. Roux, V. Vuillaume, C.-Y. D. Lu, and M. E. Cates, *Langmuir*, 12, 248-252, 1996.
- 112 P. W. Atkins, *Physikalische Chemie*, 2. Auflage, VCH Verlagsgesellschaft mbH, Weinheim, 1996.
- 113 K. Horbaschek, H. Hoffmann, 1 and C. Thunig, *Journal of Colloid & Interfacial Science*, 206, 439-456 (1998)
- 114 Hoffmann, H. , Thunig, C., Munkert, U., Meyer, H. W., and Richter, W., *Langmuir* 8, 2629 (1992).
- 115 Strey, R., *Colloid Polym. Sci.* 272, 1005 (1994).
- 116 J. -B. Huang, B. Y. Zhu, G. -X. Zhao and Z. -Y. Zhang, *langmuir*, 1997, 13, 5759-5761.
- 117 Robert G. Laughlin, *The aqueous phase behavior of surfactants*, (ACADEMIC PRESS), P 261-269, 1994.
- 118 M E Cates, *J. Phys.: Condens. Matter* 8, (1996), 9167-9176.
- 119 N. A. Spenley, M E Cates, and T. C. B. Mcleish, *Physical review letters*, volume 71, number 6, 939-942, 1993.
- 120 M. Valiente, C. Thunig, U. Munkert, U. Lenz, and H. Hoffmann, *Journal of Colloid and Interface Science*, 160, 39-50 (1993).
- 121 H. Hoffmann, C. Thunig, P Schmeidel, V. Munkert, *Langmuir* 10 (1994) 3972.
- 122 H. Hoffmann, D. Gräbner, U. Hornfeck, and G. Platz, *J. Phys. Chem. B*, Vol 103, No. 4, 1999.
- 123 M. Bergmeir, M. Gradzielski, and H. Hoffmann, *J. Phys. Chem. B*, Vol 102, No. 16, 1998.
- 124 Jingcheng Hao, Weimin Liu, and Heinz Hoffmann, *J. Phys. Chem. B* (Submitted).
- 125 S. Haas, H. Hoffmann, C. Thunig, E. Hoinkis, *Colloid Polym Sci*, 277, 865-867, (1999).

- 126 Kunio Esumi and Minoru Ueno, Structure-Performance Relationship in Surfactants, P 285-324, (MARCEL DEKKER, INC), 1997.
- 127 H. Hoffmann, C. Thunig, P Schmeidel, V. Munkert, and W Ulbricht, Tenside Surf. Det. 3 (1994) 389.
- 128 Zs. Németh, L. Halász, J. Pálinkás, A. Bóta and T. Horányi, Colloids and Surface A: Physicochemical and Engineering Aspects 145 (1998) 107-119.
- 129 H. Hoffmann and W. Ulbricht, Tenside Surf. Det. 35, 6, 1998.
- 130 H. Hoffmann, H löbl, H. Rheage and I. Wunderlich W, Tenside Detergent. 22(1985),6.
- 131 Yurii A. Shchipunov, and H. Hoffmann, Rheol Acta, 39, 542-553, (2000).
- 132 Yurii A. Shchipunov, and H. Hoffmann, Langmuir, 14, 6350-6360,(1998).
- 133 Heinz Hoffmann C. Thunig, P. Schmiedel, U. Munkert and W. Ulbricht, Tenside Surf. Det. 31, (1994), 6, 389-400.
- 134 Yurii A. Shchipunov; T. Dürschmidt and H. Hoffmann, Journal of Colloid and Interface Science, 212, 390-401 (1999).
- 135 H. Hoffmann, C. Thunig, P Schmeidel, V. Munkert, IL NUOVO CIMENTO, vol. 16 D, N. 9, 1994.

Hiermit erkläre ich, daß ich die Arbeit selbständig verfaßt und keine anderen als die von mir angegebenen Quellen und Hilfsmittel benutzt habe.

Ferner erkläre ich, daß ich nicht anderweitig mit oder ohne Erfolg versucht habe, diese Dissertation einzureichen. Ich habe keine gleichartige Doktorprüfung an einer anderen Hochschule endgültig nicht bestanden.

Bayreuth, den 14. Juli 2003

Rami Abdel-Rahem

-----